

Answer to Reviewer #1

After reviewing this manuscript, I do not know that weather I should believe the estimated results for the mean annual net ecosystem metabolism (NEM), FCO₂, and CFilt or not, because it is a big issue for air-sea interaction. I am confusing that the authors tried to use a simple 1D model coupled with Global News model in current study. How did they do? Many assumptions should be made to compromise the estimated results for air-sea CO₂ evasion. The authors should clarify many assumptions in their study. In the model, many parameters should be set up to simulate the state variables shown in Table 2. How did the authors select those parameters? The parameters and values should be listed clearly.

We agree with the reviewer that a better representation of carbon dynamics through the quantification of the Net Ecosystem Metabolism, CO₂ outgassing and carbon filtration in estuarine systems is a critical issue for air-sea interaction. This topic is a particularly pressing matter at the regional scale due to the difficulty of deriving consistent regional budgets from the upscaling of rare local measurements performed in morphologically complex and profoundly heterogeneous systems (Borges and Abril, 2011; Laruelle et al., 2013; Regnier et al., 2013). On the modeling side, the set-up of a reliable reactive transport model able to realistically capture the estuarine carbon dynamics generally proves a very costly endeavor in terms of data requirement to constrain the model (i.e. bathymetric data, boundary conditions, climatic forcing...) and in terms of time necessary to develop such model and run it (see e.g. Garnier et al., 2001; Huret et al., 2005; Arndt et al., 2011; Mateus et al., 2012). The model presented here is thus developed as a compromise, as it is currently the only one capable of running regional scale simulations with limited data and computation needs without sacrificing too much to oversimplification (as done when using box models to represent estuarine systems, Gordon et al., 1996). It follows from several studies published over the past few years (Regnier et al., 2013; Volta et al., 2014, 2016a, 2016b) that led to the development of a 1 dimensional generic estuarine model for tidal systems (Volta et al., 2014) forced by a set of generic parameters compiled from an unprecedented literature review (Volta et al., 2016a). This model was successfully applied and validated on several European estuaries (the Scheldt and Elbe, in particular, see Volta et al., 2016a&b) as well as at the regional scale of the North Sea, using a strategy similar to that presented here (Volta et al., 2016b). This strategy involved the use of the same boundary conditions as those used here for the east coast of the US. That is, the outputs of the global river model GLOBALNEWS and the global river carbon database GloRiCH to constrain upstream boundary conditions and the use of the World Ocean Atlas to specify the downstream boundary conditions. In other words, the model described in our

manuscript has precisely been designed to produce regional estuarine carbon budgets using the outputs of GlobalNEWS as boundary conditions and was already successfully used for similar purpose in another region.

As a consequence of the reviewer's skepticism and following numerous precise suggestions from the other reviewer, we have substantially modified the manuscript to better describe and justify our methodology, its underlying assumptions and potential limitations. We have also made the set-up of our simulations more transparent to secure reproducibility of our model results. In particular, the updated version of the manuscript now contains:

- A substantially modified introduction that puts our study into a more precise context and provides an improved description of the structure of the manuscript.
- Numerous additions to the model description section in order to clarify and substantiate all the assumptions on which our model relies on (i.e. calculation of boundary conditions, period of simulation, choice of databases, etc...), and which together, describe in much more detail the set-up of our simulations.
- 6 comprehensive tables (presented in the supplementary information) and which contain all physical forcings (i.e. estuarine geometry, wind speed, temperature...) and boundary conditions (nutrients and carbon concentrations, pH, alkalinity...).
- A new section (3.3. Scope of applicability and model limitations) which reflects on the strengths and weaknesses of our modeling strategy in light of the current state of knowledge available to constrain a model such as ours. In particular, the adequacy of our approach to tackle regional scale modeling, the set-up of boundary condition with available databases and the quantification of the model's uncertainty are addressed in this section.

In 2.6 Model-data comparison, the description of this subsection is very poor. The authors described the model validation for other estuaries in the Europe. How did the authors validate the model for the study areas (U.S. east coast estuaries)? I would like to see the model validation in the study areas to convince me the model is capable and suitable to be used in U.S. east coast estuaries.

We understand the reviewer's concern about the limited validation of our model within the study area. This issue was also pointed out by reviewer #2. We thus expanded extensively section 2.6 to confront the annual CO₂ outgassing predicted by our model with 13 published estimates derived from direct measurements performed in estuaries located along the East coast of the US (Table 1). In addition, we provide a validation of our hydrodynamic model using several seasonal longitudinal salinity profiles in the Delaware Bay as well a validation of our biogeochemical model for two estuaries (the Delaware Bay and the Altamaha estuary). These additional simulations

reveal that C-GEM is able to properly represent a pCO₂ (Delaware Bay) and both pH and pCO₂ longitudinal profiles along the estuarine gradient (Altamaha). Also, in the new section 3.3 (Scope of applicability and model limitations), a paragraph discusses the issue of representativeness of the model's performance through local punctual validations in the case of regional simulations including numerous small systems for which the data that would be required to perform a local validation are simply inexistent.

We hope that all these modifications will convince the reviewer of the usefulness and relevance of our study and modelling strategy.

References:

Arndt, S., Lacroix, G., Gypens, N., Regnier, P., and Lancelot, C.: Nutrient dynamics and phytoplankton development along an estuary-coastal zone continuum: A model study. *Journal of Marine Systems*, 84(3-4), 49-66, 2011.

Borges, A.V., and Abril, G.: Carbon Dioxide and Methane Dynamics in Estuaries. In: E. Wolanski and D.S. McLusky (Editors), *Treatise on Estuarine and Coastal Science*. Academic Press, Waltham, pp. 119–161, 2012.

Garnier, J., Servais, P., Billen, G., Akopian, M., and Brion, N.: Lower Seine River and Estuary (France) Carbon and Oxygen Budgets During Low Flow, *Estuaries*, 24, 964–976, 2001.

Gordon, J. D. C., Boudreau, P. R., Mann, K. H., Ong, J. E., Silvert, W. L., Smith, S. V., Wattayakorn, G., Wulff, F., and Yanagi, T.: LOICZ biogeochemical modelling guidelines. LOICZ reports & studies, 5. Texel: LOICZ, 1996.

Huret, M., Dadou, I., Dumas, F., Lazure, P., and Garçon, V.: Coupling physical and biogeochemical processes in the Rio de la Plata plume, *Cont. Shelf Res.*, 25, 629–653, 2005.

Laruelle, G.G., Dürr, H.H., Lauerwald, R., Hartmann, J., Slomp, C.P., Goossens, N., and Regnier, P.A.G.: Global multi-scale segmentation of continental and coastal waters from the watersheds to the continental margins. *Hydrol. Earth Syst. Sci.*, 17(5), 2029-2051, 2013.

Mateus, M., Vaz, N., and Neves, R.: A process-oriented model of pelagic biogeochemistry for marine systems. Part II: Application to a mesotidal estuary, *J. Mar. Syst.*, 94, 90–101, 2012.

Regnier, P., Arndt, S., Goossens, N., Volta, C., Laruelle, G.G., Lauerwald, R., and Hartmann, J.: Modelling Estuarine Biogeochemical Dynamics: From the Local to the Global Scale. *Aquatic Geochemistry*, 19(5-6), 591-626, 2013.

Volta, C., Arndt, S., Savenije, H.H.G., Laruelle, G.G., and Regnier, P.: C-GEM (v 1.0): a new, cost-efficient biogeochemical model for estuaries and its application to a funnel-shaped system. *Geosci. Model Dev.*, 6(4), 5645-5709, 2014.

Volta, C., Laruelle, G. G., and Regnier, P.: Regional carbon and CO₂ budgets of North Sea tidal estuaries, *Estuarine, Coastal and Shelf Science*, 176, 76-90, 2016a.

Volta, C., Laruelle, G. G., Arndt, S., and Regnier, P.: Linking biogeochemistry to hydro-geometrical variability in tidal estuaries: a generic modeling approach, *Hydrol. Earth Syst. Sci.*, 20, 991-1025, doi:10.5194/hess-20-991-2016, 2016b.

Answer to Reviewer #2

Overall statements

The manuscript "Air-water CO₂ evasion from U.S. East Coast estuaries" by Goossens, N., Gildas, L.G., Arndt, S., Regnier, P. gives valuable estimates on the main biogeochemical fluxes of the estuaries along the US east coast. The authors model 43 tidal estuaries and subdivide the results into 3 different latitudinal zones showing distinct differences which appear reasonable. The problem is that the reader has to accept these "black box results" even though all the details of the different estuaries should be available. I will pinpoint the problems and possible ways to resolve them:

We are grateful for the reviewer's evaluation and the constructive suggestions provided. We understand that the reviewer is mainly concerned about an apparent 'lack of transparency', as well as a seemingly weak validation of the model within the study area. Following the reviewer's recommendations, we thus substantially modified the manuscript to respond to these concerns. More specifically, we added a comparison between model-predicted annual CO₂ outgassing fluxes and 13 published flux estimates, derived from direct measurements in local estuaries to section 2.6 (Model-data comparison). In addition, we also provide new validations of the hydrodynamic and biogeochemical model (section 2.6). Furthermore, we introduced a new section (section 3.4), which critically discusses the scope of applicability and model limitations.

Please find below a detailed answer to each comment. All our answers are written in blue and the modifications within the text are highlighted in bold and italic. In the revised manuscript, changes are tracked via Word's track changes tool.

On behalf of all co-authors,

Goulven Laruelle

* The data preparation for the 43 estuaries is not transparent and reproducible. Please prepare a table in which all details for each estuary are inserted (like Volta et al., 2016a, Tab. 1). If this table appears too large, put it into the Appendix (supplemental data).

In the revised manuscript, we now provide 5 additional, extensive tables as supplementary information, which summarize all key parameters and boundary conditions required to perform the simulations. In addition to table SI1, which already provided the estuarine surface areas, as well as fresh water discharge fluxes for all systems and seasons, these new tables provide:

Table SI2: Geometric properties of the estuary (i.e. length, width at both boundaries, depth and convergence length)

Table SI3: Upstream boundary conditions for nutrients and chlorophyll concentrations

Table SI4: Downstream boundary conditions for nutrients and chlorophyll concentrations

Table SI5: Upstream boundary conditions for the organic carbon and carbonate system (i.e. TOC, DIC, pH...)

Table SI6: Downstream boundary conditions for the organic carbon and carbonate system (i.e. TOC, DIC, pH...)

Please use lat/lon positions of the mouth and estuary names if possible.

As requested, latitudes and longitudes, as well as the names of the largest rivers are provided for each estuary in all aforementioned tables. In addition, within the main text, we now make reference, whenever possible, to the name and coordinates of the estuaries that are being discussed.

* The validation chapter only refers to applications elsewhere. Please validate the model for at least one estuary in each latitudinal zone like Volta et al., 2016a did it for some North Sea estuaries.

The general performance of C-GEM in reproducing and predicting estuarine hydrodynamics and biogeochemical cycling has been extensively tested across a large range of different estuarine systems (e.g. Volta et al., 2014, 2016, see also Savenije 2001 for the estuarine physics). Here, we extended these tests by a number of local model-data comparisons. We added a new comparison between model-predicted annual CO₂ outgassing fluxes and 13 published flux estimates, derived from direct local measurements to section 2.6 (Table 1). In addition, we also evaluated the performance of the hydrodynamic model by comparing simulation results with seasonal, longitudinal salinity profiles in the Delaware Bay. Furthermore, the performance of the biogeochemical model is critically evaluated by comparing simulation results with longitudinal profiles of pCO₂ and pH, in the Delaware Bay and the Altamaha River estuary. These additional model-data comparisons reveal that C-GEM is able to reproduce local measurements of pCO₂ (Delaware Bay), as well as longitudinal pH and pCO₂ profiles (Altamaha). Following what was done in Volta et al. (2016) with the Scheldt and the Elbe in Europe, the choice of using the Delaware Bay and the Altamaha river estuary was motivated by their contrasting geometries: The Delaware Bay is a marine dominated system characterized by a pronounced funnel shape while the Altamaha River ends with a very prismatic estuary characteristic of river dominated systems (Jiang et al., 2008). Thus, selecting these two end-members estuaries reveals the ability of C-GEM to simulate widely differing estuarine dynamics. Although we agree that performing a simulation on a system located in the Northern region would be a valuable addition, we could not find suitable a suitable set of observed nutrient and carbon boundary conditions and their corresponding longitudinal profiles. Note, however, that several flux values reported in Table 1 refer to estuaries located in this region. Finally, within the new section 3.4 (Scope of applicability and model limitations), we critically discuss the difficulties associated with 'validating' regional/global model simulations with a limited set of local, instantaneous observations, as well as the uncertainties that arise from the proposed model approach.

See updated manuscript at the end of this document

* You used some arguable boundary conditions and forcing functions: The Alkalinity near the mouth, DIC and Alkalinity from GLORICH positions closest to the river boundary or older discharge estimates. I know that it is difficult to put this all together in a reasonable way. But the reader should get knowledge about the sensitivities of the model in relation to estimates of boundary or forcing data. Please show how the model reacts on changes in these data. In the detailed statements I will show in which context such studies should be done.

As pointed out by the reviewer, designing realistic and consistent boundary conditions is a critical step in model set-up. In the present study, this task is further complicated by the necessity to find complete sets of boundary conditions for 43 tidal systems located along the eastern coast of the US. C-GEM was specifically designed with this difficulty in mind. Some of the strengths of the model are its comparatively modest data requirement and its transferability from one estuarine system to another, which has already been demonstrated on the estuaries surrounding the North Sea (Volta et al., 2016). C-GEM is also well suited to be operated in conjunction with global databases such as GlobalNEWS (Mayorga et al., 2010) because they share in common the watershed as their fundamental unit, which is essentially what was done in this study. We agree with the reviewer that some of the assumptions and choices of data sources could be better justified and critically discussed in the manuscript. We thus carefully addressed all concerns raised in the answers to the detailed statements of the reviewer. In addition, we also added an entire new section to the manuscript ('Scope of applicability and model limitations') that summarizes the strengths and weaknesses of our regional model approach.

As different input parameters are means over several years, the time span of validity of the results should be defined.

In the present study, simulations are representative for the year 2000 because some of the largest datasets we rely on to constrain boundary conditions or forcings (e.g. GlobalNEWS) are derived from models calibrated for that year. As a consequence, additional data used to constrain boundary conditions and forcing parameters was selected from the same time span. In the revised manuscript, we added a few sentences justifying our data choice and specifying the time period for which simulation results are representative. In addition, we also specify if boundary conditions/forcings are constrained on the basis of punctual measurements or averages of several years.

The introduction reads rather as an advertising text. Give, for example, details about the structure of the ms. A question, which could be tackled, is whether global models miss estuarine processes (Line 39).

In the previous version of our introduction, we tried to emphasize the originality and the potential of our modelling approach. We felt that it was important to stress the novelty of the approach developed here: an explicit simulation of seasonal carbon transformations and fluxes along the land-ocean continuum at a regional scale. This work builds on the study of Volta et al. (2016) which provided the first annually average estimates of estuarine carbon transformations and fluxes focusing on the estuaries surrounding the North Sea. However, we agree with the reviewer that the proportion of the introduction dedicated to the presentation of C-GEM was too long and sometime superfluous. Following the reviewer's advice, we shortened the introduction and emphasized the research questions that can be tackled with the presented model approach. We also provided a better overview of the structure of the manuscript and the studied area. Furthermore, we followed the reviewer's suggestion and shortly discuss the ability of global carbon cycle models to account for the influence of the estuarine modulator.

See updated manuscript at the end of this document

Detailed statements

L14/15 Write 697.000 km²

Done

L19 For which time period?

The sentence has been re-written to state that model simulations are representative of the year 2000.

"Our simulations, performed using conditions representative of the year 2000, suggest that, together, US East coast estuaries emit 1.9 TgC yr⁻¹ in the form of CO₂, which correspond to about 40 % of the carbon inputs from rivers, marshes and mangrove"

L19 Only CO₂, or also other gases including carbon?

Model simulations only account for CO₂ exchange at the air-water interface and the sentence has been modified to clarify this point.

*"..., together, US East coast estuaries emit 1.9 TgC yr⁻¹ **in the form of CO₂**, which correspond to about 40 % of the carbon inputs from rivers, marshes and mangroves."*

L25 the results

Done

*"Finally, **the** results reveal that the ratio of estuarine surface area to the river discharge, S/Q..."*

L100 Make a full sentence: For a review see Laruelle et al. (2013)

We added a sentence.

*"These comprehensive data sets are complemented by local observations of carbon cycling and CO₂ fluxes in selected, individual estuarine systems, making the East coast of the United States an ideal region for a first, fully explicit regional evaluation of CO₂ evasion resolving every major tidal estuary along the selected coastal segment. **An extensive review of published local estimates of CO₂ fluxes in estuarine systems worldwide can be found in Laruelle et al. (2013).**"*

L107/109/124 unify "Fig. x" -> all over the text

On the website of Biogeosciences, the guidelines for authors states: 'The abbreviation "Fig." should be used when it appears in running text and should be followed by a number unless it comes at the beginning of a sentence, e.g.: "The results are depicted in Fig. 5. Figure 9 reveals that...".'

In the updated manuscript, we paid attention to strictly follow these rules.

L125 give lat/lon for these stations or enlarge Fig. 1 and indicate individual stations.

In the paragraph summarizing the published annual mean FCO₂ estimates based on measurements for Atlantic US estuaries, we replaced the reference to Figure 1 by a reference to Table 3, which

provides a list of all the estuaries, as well as their respective coordinates mentioned in that section. Table 3 thus becomes Table 2 in the manuscript.

“A total of thirteen local, annual mean estuarine CO₂ flux estimates across the air-water interface based on measurements are also reported in the literature and are grouped along a latitudinal gradient (**Tab. 2**).”

L146ff 47 stations were simulated. This contradicts the number of 43 (abstract).

Some watersheds flow into the same estuarine system and were merged to calculate boundary conditions for some of the systems (see section 2.4). The sentence the reviewer refers to mistakenly refers to the number of watersheds represented in our simulations rather than the number of estuaries actually represented. Only 43 tidal estuarine systems were simulated and the text was updated in sections 2.2, 2.3 and 3.4. The abstract, which refers to 43 estuaries, is thus still correct. We made the following corrections in the manuscript:

Line 147:

“The National Estuarine Eutrophication Assessment (NEEA) survey (Bricker et al., 2007), which uses geospatial data from the National Oceanic and Atmospheric Administration (NOAA) Coastal Assessment Framework (CAF) (NOAA, 1985), was used to identify and characterize **58** estuarine systems discharging along the Atlantic coast of the United States. From this set, **43** ‘tidal’ estuaries, defined as a river stretch of water that is tidally influenced (Dürr et al., 2011), were retained (fig.1) to be simulated by the C-GEM model, which is designed to represent such systems.”

Line 171:

“The generic 1D Reactive-Transport Model (RTM) C-GEM (Volta et al., 2014) is used to quantify the estuarine carbon cycling in the **43** systems considered in this study.”

Line 278:

“First, **43** coastal cells corresponding to tidal estuaries are identified in the studied area (Fig. 1).”

Line 568:

“The overall carbon filtering capacity of the region thus equals 41% of the total carbon entering the **43** estuarine systems (river + saltmarshes).”

15+47 is not 64 as I would expect from this sentence.

This is indeed a mistake, only 58 estuarine systems are presented (15+43, see comment above).

L151 Do you have a reference for this?

This figure was calculated using the GLOBALNEWS data (Mayorga et al., 2010) for POC and DOC combined with data from Hartmann et al. (2009) for DIC. We modified the sentence in a way that reflects the fact that we performed this calculation ourselves.

“Using outputs from terrestrial models (Hartmann et al., 2009; Mayorga et al., 2010), the cumulated riverine carbon loads for all the non-tidal estuaries that are excluded from the present study amount to 0.9 Tg C yr⁻¹, which represents less than 15% of the total riverine carbon loads of the region. These 15 systems are located in the SAR (10) and in the MAR (5).”

L152 Tab. x not table x (all over the text)

We update the entire manuscript.

L169 2.9 m (use space)

Done

L207 “These parameters were determined through..”?

The geometric parameters we are referring to can be extracted using Geographic Information Systems (GIS). This widely used type of software allows the determination of, for example, a distance such as the width of an estuary at its mouth from a digitalized map. The manuscript has been modified to spell out GIS on its first occurrence and make clear that GIS is the tool that can be used to extract the data from local maps.

“These parameters can be easily determined from local maps or Google Earth using Geographic Information Systems (GIS) or obtained from databases (NASA/NGA, 2003)”.

L210 are described

Corrected

L226 Use C only for concentration

C is the commonly used symbol for Chézy's coefficient but, to avoid any confusion with concentration, we followed the reviewer's advice and use C_z to denote the Chézy's coefficient. We updated equations (6) and the text.

L227 You mean eqs (5) and (6)?

Correct. The text was modified accordingly

L233 You mean eqs (5) and (6)?

Correct. The text was modified accordingly

L239 Use only English peer reviewed references

The original Dutch reference (Van der Burgh, 1972) was replaced by Savenije (1986), which is the oldest English peer reviewed publication using Van der Burgh's equations to calculate the dispersion coefficient in estuarine systems.

“The effective dispersion at the estuarine mouth can be quantified by the following relation (Savenije, 1986):”

L241 Define N by an equation

As stated in the text, the Canter Cremers' estuary number N corresponds to the ratio of the freshwater entering the estuary during a tidal cycle to the volume of salt water entering the estuary over a tidal cycle. We introduced a new equation (new equation 9) to define this parameter.

"...where h_0 (m) is the tidally-averaged water depth at the estuarine mouth and N is the dimensionless Canter Cremers' estuary number defined as the ratio of the freshwater entering the estuary during a tidal cycle to the volume of salt water entering the estuary over a tidal cycle (Simmons, 1955):

$$N = \frac{Q_b \cdot T}{P}$$

In this equation, Q_b is the bankfull discharge ($m^3 s^{-1}$), T is the tidal period (s) and P is the tidal prism (m^3). For each estuary, N can thus be calculated directly from the hydrodynamic model. "

Reference

Simmons, H. B.: Some effects of inland discharge on estuarine hydraulics, Proc. Am. Soc. Civ. Eng.-ASCE, 81, 792, 1955.

L260 Omit brackets

Done

L262 2000 m (use space)

Done

L272 273 please give a more detailed description here

The calculation of the gross primary production in the water column relies on a depth integration of the Platt equation (Platt et al., 1980), which assumes an exponential decrease of the light availability with depth. The article we are referring to (Vanderborght et al., 2007) described a cost efficient algebraic method to perform this integration using a gamma function. A sentence has been added to the text to provide more information about this procedure.

"The primary production dynamics, which requires vertical resolution of the photic depth, is calculated according to the method described in Vanderborght et al. (2007). **This method assumes an exponential decrease of the light in the water column (Platt et al., 1980), which is solved using a Gamma function.**"

L276 For which year? Or are climatological or mean values used?

Boundary conditions for regional simulations that cover a large number of individual and sometimes underexplored systems are notoriously difficult to constrain. Comprehensive, temporally resolved observational data sets that would allow informing boundary conditions are rarely available. Global databases, such as GlobalNEWS, which provide model derived river loads of carbon and nutrients (Seitzinger et al., 2005; Mayorga et al., 2010) are a suitable alternative when direct observations are

not available. Here, we used the GlobalNews database, the GloRich database and the World Ocean Atlas to constrain boundary conditions. GlobalNews model simulations have been calibrated for the year 2000. Boundary conditions for Alkalinity and pH are constrained on the basis of data extracted from the GloRich database. Most of the data compiled in this data base has been collected between 1990 and 2010. Finally, marine boundary conditions and water temperatures are derived the World Ocean Atlas. These values also correspond to climatological means centred on the year 2000. We explicitly paid attention to extracting coherent data sets from the respective databases that are representative of the same time period (around year 2000). We now clearly state in the main text which time period our boundary conditions are representative of:

“Boundary and forcing conditions are extracted from global databases and global model outputs that are available at 0.5° resolution. Therefore, C-GEM simulations are performed at the same resolution according to the following procedure. First, **43** coastal cells corresponding to tidal estuaries are identified in the studied area (**Fig. 1**). If the mouth of an estuary is spread over several 0.5° grid cells, those cells are regrouped in order to represent a single estuary (e.g. Delaware estuary), and subsequently, a single idealized geometry is defined as described above. **The model outputs (Hartmann et al., 2009; Mayorga et al., 2010) and databases (Antonov et al., 2010; Garcia et al., 2010a; Garcia et al., 2010b) used to constrain our boundary conditions are representative of the year 2000.**”

L289 cloud coverage: Which is the origin of this data?

The data comes from ISCCP Cloud Data Products (Rossow and Schiffer, 1999) and the text was updated in order to include this reference:

“Mean daily solar radiation and photoperiods (corrected for cloud coverage **using the ISCCP Cloud Data Products, Rossow and Schiffer, 1999**) are calculated depending on latitude and day of the year using a simple model (Brock, 1981).

Reference:

Rossow, W.B., and Schiffer, R.A., 1999: Advances in Understanding Clouds from ISCCP. Bull. Amer. Meteor. Soc., 80, 2261-2288.”

L293 Are there no recent data available?

The UNH/GRDC runoff dataset of Fekete et al. (2002) is the dataset used in the GlobalNEWS simulations (Mayorga et al., 2010). Although these values are derived from long term averages over the 1960-1990 period, they have been adjusted to represent the year 2000 in the GlobalNEWS simulations. Here, we use the adjusted values to ensure that boundary conditions are representative of the same time period. In addition, while more recent databases exists such as the National Water Information System (NWIS), they do not provide water discharge for all US rivers and, thus, do not provide values for the totality of the systems used in our simulations.

L320 You mean 50 g C (g Chla)-1 ?

Correct. We meant 50 grams of carbon per gram of chlorophyll a and we updated the text with the notation suggested by the reviewer.

“The same source is used for phytoplankton concentrations, using a chlorophyll-a to phytoplankton carbon ratio of 50 gC (gChla)⁻¹ (Riemann et al., 1989) to convert the EPA values to carbon units used in the present study.”

L332 339 W is not consistently defined. Is it percentage or surface area?

W corresponds to the fraction of the estuarine surface area represented by wetlands. The sentence introducing equation (11) has been updated to clarify this point:

“The DOC input of estuarine wetlands (Fig. 5b) scales to their fraction, W, of the total estuarine surface area and is calculated using the GlobalNEWS parameterization”

L341 give definition of “a”

The parameter ‘a’ is a calibration parameter used in the GlobalNEWS models and was first defined in Harrison et al. (2005) as: “unitless coefficient defining how non-point DOC export responds to runoff; for NEWS-DOC ‘a’ was set equal to 0.95.”

In our calculations, we kept the same parametrization and rephrased the sentence as follows:

“W is the percentage of the land area within a watershed that is covered by wetlands, R is the runoff (m y⁻¹) and a is a unit-less calibration coefficient defining how non-point source DOC export responds to runoff. The value of a is set to 0.95, consistent with the original GlobalNEWS -DOC model of Harrison et al. (2005).”

L355 358 It seem that you use this argument twice. Here a sensitivity analysis would help.

The sentences pointed out by reviewer states that our models ignores DIC fluxes from tidal marshes because all the carbon exports from those systems come under the form of organic carbon and then justifies this assumption with the fact that very little degradation of organic matter takes place in the tidal marshes before it reaches the estuary. Considering the relatively small amounts of carbon that can be degraded within tidal marshes (and the lack of data to constrain such process) because of the short time scale of mixing processes, our assumption implicitly means that some biogeochemical processing taking place within tidal marshes may be accounted for by our estuarine model.

L364 I doubt that zero concentration for org C is appropriate at open sea boundary. Often org C is transported from the open sea into the estuaries were it is degraded.

Please substantiate this assumption.

We agree that the assumption that the open ocean is devoid of organic carbon is simplistic and that some organic carbon can enter the estuarine system from the seaward boundary. However, the

focus of our study is to investigate and quantify the fate of the carbon delivered to estuaries by the riverine network. We introduced a sentence to section 2.4.4 to reflect on this limitation.

“This approach also reduces the influence of marine boundary conditions on the simulated estuarine dynamics, especially for all the organic carbon species whose concentrations are fixed at zero at the marine boundary. *This assumption ignores the intrusion of marine organic carbon into the estuary during the tidal cycle but allows focusing on the fate of terrigenous material and its transit through the estuarine filter.*”

In addition, the implications of this assumption are also discussed in a paragraph of the new section 3.4:

“C-GEM places the lower boundary condition 20 km from the estuarine mouth into the coastal ocean and the influence of this boundary condition on simulated biogeochemical dynamics is thus limited. At the lower boundary condition, direct observations for nutrients and oxygen are extracted from databases such as the World Ocean Atlas (Antonov et al., 2014). However, lower boundary conditions for OC and pCO₂ (zero concentration for OC and assumption of pCO₂ equilibrium at the sea side) are simplified. This approach does not allow addressing the additional complexity introduced by biogeochemical dynamics in the estuarine plume (see Arndt et al., 2011). Yet, these dynamics only play a secondary role in the presented study that focuses on the role of the estuarine transition zone in processing terrestrial-derived carbon.”

L374 domain -> boundary

Done

L377 Why longitudinal profiles? You mean at right angles with the river flow?

The term longitudinal profile is commonly used and refers to a concentration profile along the longitudinal (length) axis of the estuary, i.e. from the estuarine mouth to the river. Concentrations are thus representative of the cross-sectional average at the respective longitudinal position.

L383 How large do you estimate the error when neglecting degradation or burial in bottom sediments? A sensitivity test could help.

We agree that neglecting benthic processes is a potential limitation of our model. As the reviewer points out, organic matter degradation and burial may influence the biogeochemical of carbon in some estuaries and affect carbon retention within the system. However, because of the dynamic nature of estuarine sediments and the logistic challenges involved to sample them, direct observations and measurements of benthic processes are even more limited than those available for pelagic processes. Very little is known on the long term fate of organic carbon in estuarine sediments and its burial. Because of this lack of knowledge, benthic processes are not explicitly represented in the model. However, to a certain degree model parameters (such as organic matter degradation, denitrification rate constant) implicitly account for benthic dynamics. We acknowledge that, by ignoring benthic processes and burial in particular, our estimates for the estuarine carbon filtering

may be underestimated. These considerations have been incorporated into a paragraph of the new section 3.4:

“Although the reaction network of C-GEM accounts for all processes that control estuarine FCO_2 (Borges and Abril, 2012; Cai, 2011), several, potentially important processes, such as benthic-pelagic exchange processes, phosphorous sorption/desorption and mineral precipitation, a more complex representation of the local phytoplankton community, grazing by higher trophic levels, or multiple reactive organic carbon pools are not included. Although these processes are difficult to constrain and their importance for FCO_2 is uncertain, the lack of their explicit representations induces uncertainties in C_{filt} . In particular, the exclusion of benthic processes such as organic matter degradation and burial in estuarine sediments could result in an underestimation of C_{filt} . However, because very little is known on the long term fate of organic carbon in estuarine sediments, setting up and calibrating a benthic module proves a difficult task. Furthermore, to a certain degree model parameters (such as organic matter degradation and denitrification rate constant) implicitly account for benthic dynamics. We nonetheless acknowledge that, by ignoring benthic processes and burial in particular, our estimates for the estuarine carbon filtering may be underestimated, particularly in the shallow systems of the SAR.”

In addition, although, the discussion is not centred around the role of benthic processes, a paragraph of the new section 3.4 is also dedicated the difficulty of quantifying the uncertainties of model simulations and an attempt is made using the sensitivity analysis performed by Volta et al. (2014, 2016b).

“Biogeochemical model parameters for regional and global applications are notoriously difficult to constrain (Volta et al., 2016b). Model parameters implicitly account for processes that are not explicitly resolved and their transferability between systems is thus limited. In addition, published parameter values are generally biased towards temperate regions in industrialized countries (Volta et al., 2016b). A first order estimation of the parameter uncertainty associated to the estuarine carbon removal efficiency (C_{filt}) can be extrapolated from the extensive parameter sensitivity analyses carried out by Volta et al. (2014, 2016b). These comprehensive sensitivity studies on end-member systems have shown that the relative variation in C_{filt} when a number of key biogeochemical parameters are varied by two orders of magnitude varies by $\pm 15\%$ in prismatic (short residence time on order of days) to $\pm 25\%$ in funnel-shaped (long residence time) systems. Thus, assuming that uncertainty increases linearly between those bounds as a function of residence time, an uncertainty estimate can be obtained for each of our modelled estuary. With this simple method, the simulated regional C_{filt} of 1.9 Tg C yr^{-1} would be associated with an uncertainty range comprised between 1.5 and 2.2 Tg C yr^{-1} . Our regional estuarine CO_2 evasion estimate is thus reported with moderate confidence. Furthermore, in the future, this uncertainty range could be further constrained using statistical methods such as Monte Carlo simulations (e.g. Lauerwald et al., 2015).”

L408 Fluxes

Done

L430 Boundary conditions and forcings differ from European settings. Show validations for American estuaries.

We added validations for the American estuaries. Section 2.6 (Model-data comparison) now includes a comparison between model-predicted annual CO₂ outgassing fluxes and 13 published flux estimates, derived from direct measurements in local estuaries to section 2.6 (Model-data comparison). In addition, we provide a validation of our hydrodynamic model using several seasonal longitudinal salinity profiles in the Delaware Bay as well a validation of our biogeochemical model on the basis of pH and pCO₂ profiles from two estuaries (the Delaware Bay and the Altamaha estuary). These additional simulations reveal that C-GEM is able to reproduce observed pCO₂ (Delaware Bay) and both pH and pCO₂ longitudinal profiles along the estuarine gradient (Altamaha).

“Although C-GEM has been specifically designed and tested for the type of regional application presented here, its transferability from North Sea to US East Coast estuaries was further evaluated by assessing its performance in two East Coast estuaries. First, the hydrodynamic and transport model was tested for the Delaware Bay (MAR). The model was forced with the monthly, minimal and maximal observed discharge at Trenton over the period between 1912 and 1985 (UNH/GRDC Database). Simulated salinity profiles are compared with salinity observations from January, February, May and June (the months with the highest number of data entries), which were extracted from the UNH/GRDC Database. Fig. 6 shows that the model captures both the salinity intrusion length and the overall shape of the salinity profile well. In addition, the performance of the biogeochemical model and specifically its ability to reproduce pH and pCO₂ profiles was evaluated by a model-data comparison for both the Delaware Bay (MAR) in July 2003 and the Altamaha river estuary (SAR) in October 1995. Similar to Volta et al., 2016a, the test systems were chosen due to their contrasting geometries. The Delaware Bay is a marine dominated system characterized by a pronounced funnel shape, while the Altamaha River has a prismatic estuary characteristic of river dominated systems (Jiang et al., 2008). Monthly upstream boundary conditions for nutrients, as well as observed pH data and calculated pCO₂ are extracted from datasets described in (Sharp, 2010) and (Sharp et al., 2009) for the Delaware and in (Cai and Wang, 1998; Jiang et al., 2008) and (Cai et al., 1998) for the Altamaha river estuary. The additional forcings and boundary conditions are set similarly to the simulation for 2000 (see table 2, 3, 4, 5, 6 in SI). Fig. 7 shows that measured and simulated pH values are in good agreement with observed pH and observation-derived calculations of pCO₂. In the Delaware Bay, a pH minimum is located around km 140 and is mainly caused by intense nitrification sustained by large inputs of NH₄ from the Philadelphia urban area, coupled to an intense heterotrophic activity. Both processes lead to a well-developed pCO₂ increase in this area (Fig. 7b). Although no pCO₂ data were available for validation for the period from which boundary conditions were extracted, the simulated profile agree with pCO₂ measurement from July 2013 presented by Joesoef et al. (2015) with pCO₂ values close to equilibrium with the atmosphere in the widest section of the Delaware Bay (close to the estuarine mouth) and values above 1200 μatm at salinities below 5. For the Altamaha river estuary, pH steadily increases from typical river to typical coastal ocean values (Fig. 7b). In addition, both observations and model results reveal that outgassing is very intense in the low-salinity region with more than a 5 fold decrease in pCO₂ between salinity 0 and 5 (Fig 7d).”

In addition, the new section 3.4 (Scope of applicability and model limitations) critically discusses the difficulties of validating regional/global simulations with local data:

“The generic nature of the applied model approach and, in particular the application of seasonally/annually averaged or model-deduced boundary conditions renders a direct validation of model results on the basis of local and instantaneous observational data (e.g. longitudinal profiles), which is likely not representative of these long-term average conditions, difficult. Therefore, model performance is evaluated on the basis of spatially aggregated estimates (e.g. regional FCO₂ estimates based on local measurements) rather than system-to-system comparisons with longitudinal profile from specific days. However, note that the performance of C-GEM has been intensively tested by specific model-data comparisons for a number of different systems (e.g. Volta et al., 2014, 2016a) and we are thus confident of its predictive capabilities.”

L443 a regional minimum

Done

L440-456 Give these numbers in a table and discuss the most relevant ones.

These results were compiled for all estuaries and seasons in supplementary table SI1 and discussed within the text of section 3.1.

L457-462 The percentages should sum up to 100%

When taking all decimals into account, the percentage values do sum up to 100%. We now provide the exact value in the new manuscript.

“In contrast, the 18 MAR estuaries, with their large relative contribution to the total regional estuarine surface area, account for **as much as 70.1%** of the total outgassing.”

L466 What do you mean with “aspect ratio”?

Aspect ratio refers to the geometry of the estuary (which subsequently affect its biogeochemical behaviour) and more explicitly refers to the ratio between the estuarine width b_0 and convergence length b . A wider, funnel shaped estuary whose dynamics are controlled by a strong marine influence while the dynamics in a narrower prismatic estuary is dominated by the river influence (Savenije, 2001).

In the text, the sentence has been modified and the meaning of the term aspect ratio has been clarified:

“The comparatively larger relative contribution of the NAR to the total NEM as compared to the total FCO₂ can be explained by the importance of the specific aspect ratio for NEM. **A larger ratio of estuarine width b_0 and convergence length b corresponds to a more funnel shaped estuary while a low ratio corresponds to a more prismatic geometry (Savenije, 2001; Volta et al., 2014)'**”

L479ff Why do the small estuaries show higher mean values?

In large systems, the total outgassing of CO₂ extends over a much larger surface area. In small estuaries, the surface area acts as a limiting factor for the gas exchange with the atmosphere.

L485 Give more details about the assumptions made to calculate the partitioning for

In addition to the reference to Regnier et al. (2013), more details regarding the method used to calculate the respective contributions to the estuarine CO₂ outgassing (NEM, nitrification and riverine oversaturated CO₂) is now provided.

*“Following the approach used in Regnier et al. (2013), the contribution of biogeochemical process to FCO₂ is assessed by evaluating their individual contribution to DIC and ALK changes **taking into account the local buffering capacity of an ionic solution when TA and DIC are changing due to internal processes, but ignoring advection and mixing (Zeebe and Wolf-Gladrow 2001). In the present study, we quantify the effect of the NEM on the CO₂ balance, which is almost exclusively controlled by aerobic degradation rates because the contributions of denitrification and NPP to the net ecosystem balance are small. Nitrification, a process triggered by the transport and/or production of NH₄ in oxygenated waters, favors outgassing through its effect on pH, which shifts the acid-base equilibrium of carbonate species and increases the CO₂ concentration. The contribution of supersaturated riverine waters to the overall estuarine CO₂ dynamics is calculated as difference between all the other processes creating or consuming CO₂.”***

Fig. 8a. Were seasonal partitioning combined to overall partitioning?

Indeed, the partitioning presented in figure 8a (and figure 8b) are calculated on the basis of the 4 seasonal fluxes for each estuary. The manuscript was edited to clarify this point:

*“Fig. 8a presents the contribution of the annually integrated NEM, nitrification and evasion of supersaturated, DIC enriched riverine waters to the total outgassing for each system, as well as for individual regions of the domain. **The calculation of these annual values is based on the sum of the seasonal fluxes.**”*

L489 Give more details about the different partitioning in the different zones here

An entire paragraph following L489 fully describes the partitioning of the 3 drivers of FCO₂ (NEM, nitrification and riverine CO₂) in the 3 different zones (i.e. NAR, MAR, SAR). This paragraph used to begin on L496 of the previous version of the manuscript. We now explain and discuss the regional breakdown earlier in the text and moved the description of the influence of nitrification and NEM on CO₂ outgassing to L 485. Now the discussion of the contributions of NEM, nitrification and riverine CO₂ to FCO₂ in each of the 3 sub regions directly follows the sentence in L.489, pointed out by the reviewer.

“Model results reveal that, regionally, the NEM supports about 50% of the estuarine CO₂ outgassing, while nitrification and riverine DIC inputs sustain about 17% and 33% of the CO₂ emissions, respectively. ~~Nitrification, a process triggered by the transport and/or production of NH₄ in oxygenated waters, favors outgassing through its effect on pH, which shifts the acid base equilibrium of carbonate species and increases the CO₂ concentration. In addition, the NEM is almost exclusively controlled by aerobic degradation rates because the contribution of denitrification and NPP to the net ecosystem balance is small.~~The relative significance of the three processes described above shows important spatial variability...”

L508 Where is Table S1?

Table S1 was uploaded as a supplementary table and a link to download it was included on the page from which the manuscript could be downloaded (below the PDF symbol). Attached to this reply, we provide an archive containing the updated manuscript as well as all the supplementary information

L577 budgets

Done

L630 The normalization of NEM by a Q10 value appears reasonable. The normalization of FCO₂ by a Q10 value must be justified. I'm not convinced of the latter normalization.

The rationale for the normalization of FCO₂ by a Q10 value, using the same approach as the one used for NEM, is the fact that, in many systems, NEM and FCO₂ are intimately linked. For instance, Mayer and Eyre (2012) proposed a linear relationship between NEM and FCO₂. Applying the same normalization to both NEM and FCO₂ thus allows testing if a similar relationship can be observed along the entire climatic gradient of the US East Coast.

“In this section, we explore the relationships between such simple physical parameters and indicators of the estuarine carbon processing \overline{NEM} , $\overline{FCO_2}$ and $CFilt$. In order to account for the effect of temperature on C dynamics, \overline{NEM} and $\overline{FCO_2}$ are also normalized to the same temperature (arbitrarily chosen to be 0 degree). These normalized values are obtained by dividing \overline{NEM} and $\overline{FCO_2}$ by a Q₁₀ function $f(T)$ (see Volta et al., 2014). **This procedure allows accounting for the exponential increase in the rate of several temperature dependent processes contributing to the NEM (i.e. photosynthesis, organic carbon degradation...). Applying the same normalization to \overline{NEM} and $\overline{FCO_2}$ is a way of testing how intimately linked NEM and FCO₂ are in estuarine systems. Indeed linear relationships relating one to the other have been reported (Mayer and Eyre, 2012).**”

L660 ff Here it becomes obvious that $f(t)$ cannot be applied to FCO₂.

Indeed, we agree with the reviewer that no clear relationship between Q10-normalized FCO₂ and S/Q can be observed over the entire spectrum of values of S/Q that can be found along the east coast of the US. In fact, our results clearly illustrate that a linear regression between FCO₂ / $f(T)$ and S/Q only provides a good fit using estuaries located in the MAR and SAR regions. The small estuaries from the NAR region, characterized by values of S/Q < 3 d m⁻¹ display a significantly different behaviour. We think that it is important to point out that small estuaries show a different biogeochemical response and establishing a range of values of S/Q within which Mayer and Eyre's relationship can be reproduced justifies the use of this normalization of FCO₂ by a Q10. We modified the text to clarify our approach.

“Thus, the well-documented correlation between \overline{NEM} and $\overline{FCO_2}$ (Maher and Eyre, 2012) does not seem to hold for systems with very short residence times. For systems with S/Q > 3 days m⁻¹, we obtain a regression $FCO_2 = -0.64 \times NEM + 5.96$ with a r^2 of 0.46, which compares well with the relation $FCO_2 = -0.42 \times NEM + 12$ proposed by Maher and Eyre (2012) who used 24 seasonal estimates from small Australian estuaries. **However, our results suggest that this relationship cannot be extrapolated to small systems such as those located in the NAR.**”

“As a consequence of the distinct behavior of short residence time systems, the coefficient of determination of the best-fitted power law function relating $\overline{FCO_2}$ and S/Q is only significant if NAR systems are excluded ($y = 31.64 x^{-0.58}$ with a $r^2 = 0.70$). **This thus suggest that such relationships (as well as that proposed by Maher and Eyre, 2012) cannot be applied to any system but only those for which $S/Q > 3 \text{ day m}^{-1}$.**”

L668 whom -> who

Done

L677 In this case the assumption of pCO₂ in equilibrium with the atmosphere at the lower boundary contradicts the case “still oversaturated waters ..”

In our simulations, the seaward boundary is located 20km away from the estuarine mouth and estuarine waters close to the mouths can thus be still oversaturated.

At the beginning of section 2.4.4, we state that ‘For each estuary, the downstream boundary is located 20 km beyond the mouth to minimize the bias introduced by the choice of a fixed concentration boundary condition to characterize the ocean water masses (e.g. Regnier et al., 1998).’

This assumption is also discussed in a paragraph of the new section 3.4:

“C-GEM places the lower boundary condition 20 km from the estuarine mouth into the coastal ocean and the influence of this boundary condition on simulated biogeochemical dynamics is thus limited. At the lower boundary condition, direct observations for nutrients and oxygen are extracted from databases such as the World Ocean Atlas (Antonov et al., 2014). However, lower boundary conditions for OC and pCO₂ (zero concentration for OC and assumption of pCO₂ equilibrium at the sea side) are simplified. This approach does not allow addressing the additional complexity introduced by biogeochemical dynamics in the estuarine plume (see Arndt et al., 2011). Yet, these dynamics only play a secondary role in the presented study that focuses on the role of the estuarine transition zone in processing terrestrial-derived carbon.”

L682 No link to Fig. 10d ?

We added a reference to Fig. 10d (now Fig.12d), as well as a brief discussion of the non-normalized results to the text.

“Figure 12d, which reports non-normalized FCO₂ reveals a monotonous increase of FCO₂ with S/Q. This suggests that, unlike the NEM for which the normalization by a temperature function allowed explaining most of the variability; FCO₂ is mostly controlled by the water residence time within the system. Discharge is the main FCO₂ driver in riverine dominated systems, while interactions with marshes are driving the outgassing in marine dominated systems surrounded by marshes.”

L739 You really mean “prediction”? Not “projection”?

We agree that term projection is better suited and the text was updated accordingly.

“In regions with better data coverage, such as the one investigated here, our study highlights that the regional-scale quantification, attribution, and **projection** of estuarine biogeochemical cycling are now at reach.”

L740 As your model is rather based on empirical relations than on first principles, I expect that changed systems due to climate shifts and consequences can change your basic relationship. Please include this aspect in a more careful outlook.

We agree with the remark of the reviewer stating that the domain of applicability of the relationship we found between NEM, temperature and the depth normalized estuarine residence is bound within the range of values observed within our study area. Some of these aspects are tackled in the new section ‘Scope of applicability and model limitations’.

Additionally, following the reviewer’s recommendation, a sentence was added in the outlook section to account for the limitations of the applicability of the relationships we designed. We would like however, to draw the attention of the reviewer on the mechanistic nature of our model. Thus, while the relationships presented in section 3.5 are indeed empirical, they stem from results produced by a model that is actually largely based on first principles.

“In the future, such simple relationships, relying on readily available geometric and hydraulic parameters could be used to quantify carbon processing in areas of the world devoid of direct measurements. **However, it is important to note that such simple relationships are only valid over the range of boundary conditions and forcings explored and may not be applicable to conditions that fall outside of this range.** In regions with better data coverage, such as the one investigated here, our study highlights that the regional-scale quantification, attribution, and **projection** of estuarine biogeochemical cycling are now at reach.”

L1021 7(4), 1271-1295

The reference was updated:

“Volta, C., Arndt, S., Savenije, H. H. G., Laruelle, G. G., and Regnier, P.: C-GEM (v 1.0): a new, cost-efficient biogeochemical model for estuaries and its application to a funnel-shaped system, *Geosci. Model Dev.*, **7**, **1271-1295**, [doi:10.5194/gmd-7-1271-2014](https://doi.org/10.5194/gmd-7-1271-2014), 2014.”

L1045 give units and if possible your own values.

Following the reviewer’s advice, table 3 (now table 2) has been updated to include the unit of the values in the caption and the values calculated by our simulations for the selected estuaries.

“Table 2: Published local annually averaged estimates of $\overline{FCO_2}$ in mol C m⁻² yr⁻¹ for estuaries along the East coast of the US.”

Name	Lon	Lat	$\overline{FCO_2}$		Reference
			Observed.	Modeled	
Altamaha Sound	-81.3	31.3	32.4	72.7	Jiang et al. (2008)
Bellamy	-70.9	43.2	3.6	3.9	Hunt et al. (2010)
Cocheco	-70.9	43.2	3.1	3.9	Hunt et al. (2010)
Doboy Sound	-81.3	31.4	13.9	25.7	Jiang et al. (2008)
Great Bay	-70.9	43.1	3.6	3.9	Hunt et al. (2011)
Little Bay	-70.9	43.1	2.4	3.9	Hunt et al. (2011)
Oyster Bay	-70.9	43.1	4	3.9	Hunt et al. (2011)
Parker River estuary	-70.8	42.8	1.1	3.9	Raymond and Hopkinson (2003)
Sapelo Sound	-81.3	31.6	13.5	20.6	Jiang et al. (2008)
Satilla River	-81.5	31	42.5	25.7	Cai and Wang (1998)
York River	-76.4	37.2	6.2	8.1	Raymond et al. (2000)
Hudson River	-74	40.6	13.5	15.5	Raymond et al. (1997)
Florida Bay	-80.68	24.96	1.4	n.a.	Dufore (2012)

In addition, the text of the section 2.6 (Model-data comparison) has also been updated to compare observed and simulated FCO_2 in these 13 systems.

“While such local validations allow assessing the performance of the model for a specific set of conditions, the purpose of this study is to capture the average biogeochemical behaviour of the estuaries of the eastern coast of the US. Therefore, in addition to the system-specific validation, published annually averaged FCO_2 estimates for 13 tidal systems located within the study area collected over the 1994-2006 period are compared to simulated FCO_2 for conditions representative of the year 2000. Overall, simulated FCO_2 are comparable to values reported in the literature (Tab. 2). Although discrepancies, which sometimes can be significant, are observed at the level of individual systems, the model captures remarkably well the overall trend in CO_2 evasion rate across estuaries. The model simulates low CO_2 efflux ($< 5 \text{ mol C m}^{-2} \text{ yr}^{-1}$) for the 7 systems where such conditions have been observed, while the 6 systems for which the CO_2 evasion exceeds $10 \text{ mol C m}^{-2} \text{ yr}^{-1}$ are the same in the observations and in the model runs. The discrepancy at the individual system level likely result from a combination of factors, including the choice of model processes and their parametrization, the uncertainties in constraining boundary conditions and the limited representability of instantaneous and local observed.”

L1052 definition of winter (DJF)?

We define winter in section 2.4 as January, February and March. The definitions of the seasons are now reiterated in the table caption of table 5 to avoid any confusion:

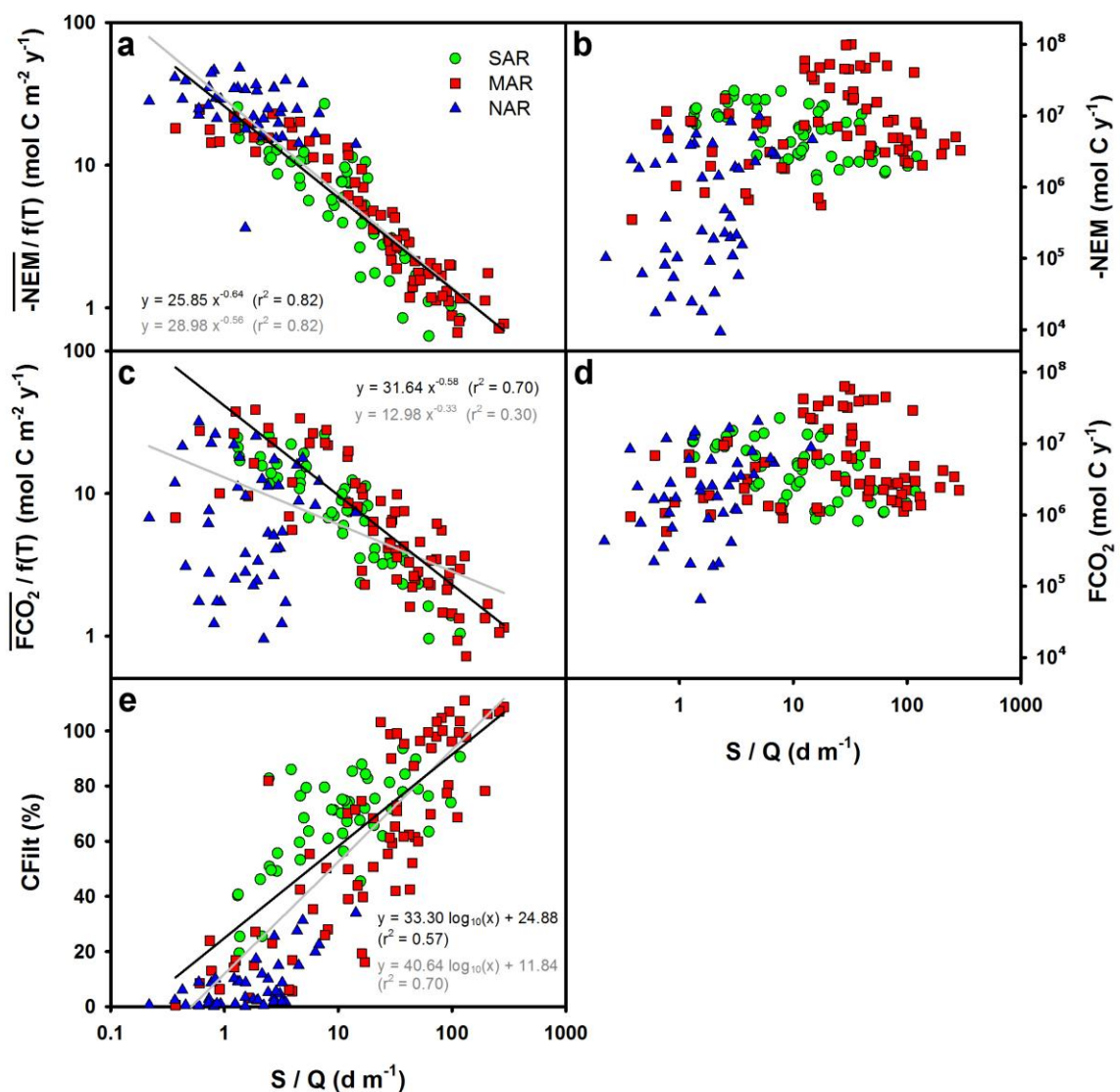
“Table 5: Seasonal contribution to FCO_2 and NEM in each the sub-region. The seasons displaying the highest percentages are indicated in bold. **Winter is defined as January, February and March, Spring as April, May and June and so on...**”

L1103 The caption must be understandable alone. & L1105 Separate: “black lines .. using all points” “ grey lines are best fit only for ..”

The caption was rewritten taking into account the suggestion of the reviewer:

“Figure 10: System scale integrated biogeochemical indicators expressed as a function of the depth normalized residence time expressed as the ratio of the estuarine surface S and the river discharge Q for all seasons. Panels b, d and e represent NEM, -FCO₂ and CFilt, respectively. Panels a and c represent NEM, -FCO₂ normalized by a temperature Q₁₀ function. Black lines are the best fitted linear regressions obtained using all the point. Grey lines are best fit using only the estuaries from the MAR and SAR regions.”

In addition, the y axis of panels b and d were updated.



References:

- Antonov, J.I., Seidov, D., Boyer, T.P., Locarnini, R.A., Mishonov, A.V., Garcia, H.E., Baranova, O.K., Zweng, M.M., and Johnson, D.R.: World Ocean Atlas 2009, Volume 2: Salinity. S., 2010.
- Arndt, S., Regnier, P., and Vanderborght, J.P.: Seasonally-resolved nutrient export fluxes and filtering capacities in a macrotidal estuary. *Journal of Marine Systems*, 78(1), 42-58, 2009.
- Arndt, S., Lacroix, G., Gypens, N., Regnier, P., and Lancelot, C.: Nutrient dynamics and phytoplankton development along an estuary-coastal zone continuum: A model study. *Journal of Marine Systems*, 84(3-4), 49-66, 2011.
- Bauer, J.E., Cai, W.J., Raymond, P.A., Bianchi, T.S., Hopkinson, C.S., and Regnier, P.A.G.: The changing carbon cycle of the coastal ocean. *Nature*, 504(7478), 61-70, 2013.
- Billen, G., Thieu, V., Garnier, J., and Silvestre, M.: Modelling the N cascade in regional waters: The case study of the Seine, Somme and Scheldt rivers, *Agr. Ecosyst. Environ.*, 133, 234–246, 2009.
- Borges, A.V., and Abril, G.: Carbon Dioxide and Methane Dynamics in Estuaries. In: E. Wolanski and D.S. McLusky (Editors), *Treatise on Estuarine and Coastal Science*. Academic Press, Waltham, pp. 119–161, 2012.
- Bricker, S., Longstaff, B., Dennison, W., Jones, A., Boicourt, K., Wicks, C., and Woerner, J.: *Effects of Nutrient Enrichment In the Nation's Estuaries: A Decade of Change*, NOAA, MD, 2007.
- Brock, T.D.: Calculating solar radiation for ecological studies. *Ecological Modelling*, 14(1-2), 1-19, 1981.
- Cai, W.J., and Wang, Y.: The chemistry, fluxes, and sources of carbon dioxide in the estuarine waters of the Satilla and Altamaha Rivers, Georgia. *Limnology and Oceanography*, 43(4), 657-668, 1998.
- Cai, W.J., Wang, Y., and Hodson, R. E.: Acid-base properties of dissolved organic matter in the estuarine waters of Georgia, USA. *Geochimica et Cosmochimica Acta*, 62(3), 473-483, 1998.
- Cai, W.J.: Estuarine and coastal ocean carbon paradox: CO₂ sinks or sites of terrestrial carbon incineration? *Ann. Rev. Mar. Sci.*, 3, 123-145, 2011.
- Chen, C.-T. A., Huang, T.-H., Chen, Y.-C., Bai, Y., He, X., and Kang, Y.: Air-sea exchanges of CO₂ in the world's coastal seas, *Biogeosciences*, 10, 6509–6544, doi:10.5194/bg-10-6509-2013, 2013.
- Dufore, C. M.: *Spatial and Temporal Variations in the Air-Sea Carbon Dioxide Fluxes of Florida Bay*, Graduate School Thesis, University of South Florida, 2012.
- Dürr, H.H., Laruelle, G.G., van Kempen, C.M., Slomp, C.P., Meybeck, M., and Middelkoop, H.: Worldwide Typology of Nearshore Coastal Systems: Defining the Estuarine Filter of River Inputs to the Oceans. *Estuaries and Coasts*, 34(3), 441-458, 2011.
- Fekete, B.M., Vörösmarty, C.J., and Grabs, W.: High-resolution fields of global runoff combining observed river discharge and simulated water balances. *Global Biogeochemical Cycles*, 16(3), 15-1, 2002.
- Garcia, H.E., Locarnini, R.A., Boyer, E.W., Antonov, A., Baranova, O.K., Zweng, M.M., and Johnson, D.R.: World Ocean Atlas 2009, Volume 3: Dissolved Oxygen, Apparent Oxygen Utilization, and Oxygen Saturation, 2010a.
- Garcia, H.E., Locarnini, R.A., Boyer, E.W., Antonov, J.I., Baranova, O.K., Zweng, M.M., and Johnson, D.R.: World Ocean Atlas 2009, Volume 4: Nutrients (phosphate, nitrate, silicate), 2010b.
- Garnier, J., Servais, P., Billen, G., Akopian, M., and Brion, N.: Lower Seine River and Estuary (France) Carbon and Oxygen Budgets During Low Flow, *Estuaries*, 24, 964–976, 2001.
- Harrison, J.A., Caraco, N., and Seitzinger, S.P.: Global patterns and sources of dissolved organic matter export to the coastal zone: Results from a spatially explicit, global model. *Global Biogeochemical Cycles*, 19(4), GB4S03, doi:10.1029/2004GB002357, 2005.
- Hartmann, J., Jansen, N., Dürr, H.H., Kempe, S., and Köhler, P.: Global CO₂ consumption by chemical weathering: What is the contribution of highly active weathering regions? *Global Planet. Change*, 69(4), 185-194, 2009.

- Hofmann, A.F., Soetaert, K., and Middelburg, J.J.: Present nitrogen and carbon dynamics in the Scheldt estuary using a novel 1-D model. *Biogeosciences*, 5(4), 981-1006, 2008.
- Hofmann, E.E., Cahill, B., Fennel, K., Friedrichs, M.A.M., Hyde, K., Lee, C., Mannino, A., Najjar, R.G., O'Reilly, J.E., Wilkin, J., and Xue, J.: Modeling the dynamics of continental shelf carbon. *Ann Rev Mar Sci*. 3, 93-122, 2011.
- Hunt, C. W., Salisbury, J. E., Vandemark, D., and McGillis, W.: Contrasting Carbon Dioxide Inputs and Exchange in Three Adjacent New England Estuaries. *Estuar. Coast.*, 34, 68–77, doi:10.1007/s12237-010-9299-9, 2010.
- Hunt, C.W., Salisbury, J.E., Vandemark, D., and McGillis, W.: Contrasting Carbon Dioxide Inputs and Exchange in Three Adjacent New England Estuaries. *Estuaries and Coasts*, 34(1), 68-77, 2011.
- Jiang, L.Q., Cai, W.J., and Wang, Y.: A comparative study of carbon dioxide degassing in river- and marine-dominated estuaries. *Limnology and Oceanography*, 53(6), 2603-2615, 2008.
- Joesoef, A., Huang, W.-J., Gao, Y., and Cai, W.-J.: Air–water fluxes and sources of carbon dioxide in the Delaware Estuary: spatial and seasonal variability, *Biogeosciences*, 12, 6085-6101, doi:10.5194/bg-12-6085-2015, 2015.
- Laruelle, G. G., Regnier, P., Ragueneau, O., Kempa, M., Moriceau, B., Ni Longphuir, S., Leynaert, A., Thouzeau, G., and Chauvaud, L.: Benthic-pelagic coupling and the seasonal silica cycle in the Bay of Brest (France): new insights from a coupled physical-biological model, *Mar. Ecol.-Prog. Ser.*, 385, 15–32, 2009.
- Laruelle, G.G., Dürr, H.H., Slomp, C.P., and Borges, A.V.: Evaluation of sinks and sources of CO₂ in the global coastal ocean using a spatially-explicit typology of estuaries and continental shelves. *Geophys. Res. Lett.*, 37(15), L15607, doi:10.1029/2010GL043691, 2010.
- Laruelle, G.G., Dürr, H.H., Lauerwald, R., Hartmann, J., Slomp, C.P., Goossens, N., and Regnier, P.A.G.: Global multi-scale segmentation of continental and coastal waters from the watersheds to the continental margins. *Hydrol. Earth Syst. Sci.*, 17(5), 2029-2051, 2013.
- Laruelle, G.G., Lauerwald, R., Rotschi, J. Raymond, P.A., and Regnier, P.: Seasonal response of air-water CO₂ exchange along the land-ocean aquatic continuum of the northeast North American coast. *Biogeosci.* 12, 1447-1458, 2015.
- Lauerwald, R., Hartmann, J., Moosdorf, N., Kempe, S., and Raymond, P.A.: What controls the spatial patterns of the riverine carbonate system? — A case study for North America. *Chemical Geology*, 337–338, 114-127, 2013.
- Lauerwald, R., Laruelle, G. G., Hartmann, J., Ciais, P., and Regnier, P. A. G.: Spatial patterns in CO₂ evasion from the global river network, *Global Biogeochem. Cy.*, 29, 534–554, doi:10.1002/2014GB004941, 2015.
- Le Quéré, C., Peters, G. P., Andres, R. J., Andrew, R. M., Boden, T. A., Ciais, P., Friedlingstein, P., Houghton, R. A., Marland, G., Moriarty, R., Sitch, S., Tans, P., Arneeth, A., Arvanitis, A., Bakker, D. C. E., Bopp, L., Canadell, J. G., Chini, L. P., Doney, S. C., Harper, A., Harris, I., House, J. I., Jain, A. K., Jones, S. D., Kato, E., Keeling, R. F., Klein Goldewijk, K., Körtzinger, A., Koven, C., Lefèvre, N., Maignan, F., Omar, A., Ono, T., Park, G.-H., Pfeil, B., Poulter, B., Raupach, M. R., Regnier, P., Rödenbeck, C., Saito, S., Schwinger, J., Segschneider, J., Stocker, B. D., Takahashi, T., Tilbrook, B., van Heuven, S., Viovy, N., Wanninkhof, R., Wiltshire, A., and Zaehle, S.: Global carbon budget 2013, *Earth Syst. Sci. Data*, 6, 235-263, doi:10.5194/essd-6-235-2014, 2014.
- Le Quéré, C., Moriarty, R., Andrew, R. M., Canadell, J. G., Sitch, S., Korsbakken, J. I., Friedlingstein, P., Peters, G. P., Andres, R. J., Boden, T. A., Houghton, R. A., House, J. I., Keeling, R. F., Tans, P., Arneeth, A., Bakker, D. C. E., Barbero, L., Bopp, L., Chang, J., Chevallier, F., Chini, L. P., Ciais, P., Fader, M., Feely, R. A., Gkritzalis, T., Harris, I., Hauck, J., Ilyina, T., Jain, A. K., Kato, E., Kitidis, V., Klein Goldewijk, K., Koven, C., Landschützer, P., Lauvset, S. K., Lefèvre, N., Lenton, A., Lima, I. D., Metzl, N., Millero, F., Munro, D. R., Murata, A., Nabel, J. E. M. S., Nakaoka, S., Nojiri, Y., O'Brien, K., Olsen, A., Ono, T., Pérez, F. F., Pfeil, B., Pierrot, D., Poulter, B., Rehder, G., Rödenbeck, C., Saito, S., Schuster, U., Schwinger, J., Séférian, R., Steinhoff, T., Stocker, B.

- D., Sutton, A. J., Takahashi, T., Tilbrook, B., van der Laan-Luijkx, I. T., van der Werf, G. R., van Heuven, S., Vandemark, D., Viovy, N., Wiltshire, A., Zaehle, S., and Zeng, N.: Global Carbon Budget 2015, *Earth Syst. Sci. Data*, 7, 349-396, doi:10.5194/essd-7-349-2015, 2015.
- Maher, D.T., and Eyre, B.D.: Carbon budgets for three autotrophic Australian estuaries: Implications for global estimates of the coastal air-water CO₂ flux. *Global Biogeochem. Cycles*, 26(1), GB1032, 2012.
- Mayorga, E., Seitzinger, S.P., Harrison, J.A., Dumont, E., Beusen, A.H.W., Bouwman, A.F., Fekete, B.M., Kroeze, C., and Van Drecht, G.: Global Nutrient Export from WaterSheds 2 (NEWS 2): Model development and implementation. *Environmental Modelling and Software*, 25(7), 837-853, 2010.
- NASA/NGA: SRTM Water Body Data Product Specific Guidance, Version 2.0, 2003.
- NOAA: National Estuarine Inventory Data Atlas, Volume 1: Physical and Hydrologic Characteristics, National Oceanic and Atmospheric Administration, MD, 1985.
- Paerl, H.W., Valdes, L.M., Peierls, B.L., Adolf, J.E., and Harding Jr, L.W.: Anthropogenic and climatic influences on the eutrophication of large estuarine ecosystems. *Limnology and Oceanography*, 51(1 II), 448-462, 2006.
- Platt, T., Gallegos, C. L., and Harrison, W. G.: Photoinhibition of photosynthesis in natural assemblages of marine phytoplankton. *J. Mar. Res.*, 38, 687-701, 1980.
- Raymond, P.A., Caraco, N.F., and Cole, J.J.: Carbon dioxide concentration and atmospheric flux in the Hudson River. *Estuaries*, 20(2), 381-390, 1997.
- Raymond, P.A., Bauer, J.E., and Cole, J.J.: Atmospheric CO₂ evasion, dissolved inorganic carbon production, and net heterotrophy in the York River estuary. *Limnology and Oceanography*, 45(8), 1707-1717, 2000.
- Raymond, P.A., and Hopkinson, C.S.: Ecosystem Modulation of Dissolved Carbon Age in a Temperate Marsh-Dominated Estuary. *Ecosystems*, 6(7), 694-705, 2003.
- Rossow, W.B., and Schiffer, R.A.: Advances in understanding clouds from ISCCP. *Bull. Amer. Meteorol. Soc.*, 80, 2261-2288, doi:10.1175/1520-0477(1999)080<2261:AIUCFI>2.0.CO;2, 1999.
- Regnier, P., Mouchet, A., Wollast, R., and Roday, F.: A discussion of methods for estimating residual fluxes in strong tidal estuaries, *Cont. Shelf Res.*, 18, 1543-1571, 1998.
- Regnier, P., Friedlingstein, P., Ciais, P., Mackenzie, F.T., Gruber, N., Janssens, I.A., Laruelle, G.G., Lauerwald, R., Luysaert, S., Andersson, A.J., Arndt, S., Arnosti, C., Borges, A.V., Dale, A.W., Gallego-Sala, A., Godderis, Y., Goossens, N., Hartmann, J., Heinze, C., Ilyina, T., Joos, F., LaRowe, D.E., Leifeld, J., Meysman, F.J.R., Munhoven, G., Raymond, P.A., Spahni, R., Suntharalingam, P., and Thullner, M.: Anthropogenic perturbation of the carbon fluxes from land to ocean. *Nature Geosci*, 6(8), 597-607, 2013.
- Regnier, P., Arndt, S., Goossens, N., Volta, C., Laruelle, G.G., Lauerwald, R., and Hartmann, J.: Modelling Estuarine Biogeochemical Dynamics: From the Local to the Global Scale. *Aquatic Geochemistry*, 19(5-6), 591-626, 2013b.
- Riemann, B., Simonsen, P., and Stensgaard, L.: The carbon and chlorophyll content of phytoplankton from various nutrient regimes. *Journal of Plankton Research*, 11 (5), 1037-1045, 1989.
- Savenije, H.H.G.: A one-dimensional model for salinity intrusion in alluvial estuaries. *Journal of Hydrology*, 85(1-2), 87-109, 1986.
- Savenije, H. H. G.: A simple analytical expression to describe tidal damping or amplification, *J. Hydrol.*, 243, 205-215, 2001.
- Schwarz, G.E., Hoos, A.B., Alexander, R.B., and Smith, R.A.: The SPARROW Surface Water-Quality Model: Theory, Application and User Documentation. U.S. Geological Survey, Techniques and Methods Report, Book 6, Chapter B3, Reston, Virginia, 2006.
- Seitzinger, S. P., Harrison, J. A., Dumont, E., Beusen, A. H. W., and Bouwman, A. F.: Sources and delivery of carbon, nitrogen, and phosphorus to the coastal zone: An overview of Global

- Nutrient Export from Watersheds (NEWS) models and their application, *Global Biogeochem. Cycles*, 19, GB4S01, doi:10.1029/2005GB002606, 2005.
- Signorini, S.R., Mannino, A., Najjar Jr, R.G., Friedrichs, M.A.M., Cai, W.J., Salisbury, J., Wang, Z.A., Thomas, H., and Shadwick, E.: Surface ocean pCO₂ seasonality and sea-air CO₂ flux estimates for the North American east coast. *Journal of Geophysical Research C: Oceans*, 118(10), 5439-5460, 2013.
- Simmons, H. B.: Some effects of inland discharge on estuarine hydraulics, *Proc. Am. Soc. Civ. Eng.-ASCE*, 81, 792, 1955.
- Sharp, J. H., Yoshiyama, K., Parker, Schwartz, M. C., Curless, S. E., Bearegard, A. Y., Ossolinski, J. E., and Davis, A. R.: A Biogeochemical View of Estuarine Eutrophication: Seasonal and Spatial Trends and Correlations in the Delaware Estuary. *Estuaries and Coasts*, 32, 1023-1043, doi:10.1007/s12237-009-9210-8, 2009.
- Sharp, J. H.: Estuarine oxygen dynamics: What can we learn about hypoxia from long-time records in the Delaware Estuary? *Limnol. Oceanogr.*, 55(2), 2010, 535–548, 2010.
- Soetaert, K., and Herman, P.M.J.: Nitrogen dynamics in the Westerschelde estuary (SW Netherlands) estimated by means of the ecosystem model MOSES. *Hydrobiologia*, 311(1-3), 225-246, 1995.
- Thieu, V., Mayorga, E., Billen, G., and Garnier, J.: Subregional and downscaled global scenarios of nutrient transfer in river basins: Seine-Somme-Scheldt case study. *Global Biogeochemical Cycles*, 24(2) , 2010.
- Vanderborgh, J.P., Wollast, R., Loijens, M., and Regnier, P.: Application of a transport-reaction model to the estimation of biogas fluxes in the Scheldt Estuary. *Biogeochemistry*, 59(1-2), 207-237, 2002.
- Vanderborgh, J.P., Folmer, I., Aguilera, D.R., Uhrenholdt, T., and Regnier, P.: Reactive-transport modelling of a river-estuarine-coastal zone system: application to the Scheldt estuary. *Mar. Chem.* 106, 92-110, 2007.
- Van der Burgh, P.: Ontwikkeling van een methode voor het voorspellen van zoutverdelingen in estuaria, kanalen and zeeen, Rijkswaterstaat Rapport, The Netherlands, 1972.
- Volta, C., Arndt, S., Savenije, H.H.G., Laruelle, G.G., and Regnier, P.: C-GEM (v 1.0): a new, cost-efficient biogeochemical model for estuaries and its application to a funnel-shaped system. *Geosci. Model Dev.*, 7, 1271-1295, doi:10.5194/gmd-7-1271-2014, 2014.
- Volta, C., Laruelle, G. G., and Regnier, P.: Regional carbon and CO₂ budgets of North Sea tidal estuaries, *Estuarine, Coastal and Shelf Science*, 176, 76-90, 2016.
- Volta, C., Laruelle, G. G., Arndt, S., and Regnier, P.: Linking biogeochemistry to hydro-geometrical variability in tidal estuaries: a generic modeling approach, *Hydrol. Earth Syst. Sci.*, 20, 991-1030, doi:10.5194/hess-20-991-2016, 2016.
- Zeebe, R. E. and Wolf-Gladrow, D. (Eds.): CO₂ in seawater: equilibrium, kinetics, isotopes, Elsevier, Amsterdam, 2001.

1 **Updated Manuscript with track changes**

2

3

Air-water CO₂ evasion from U.S. East Coast estuaries

4 Goossens, Nicolas¹, Laruelle, Goulven Gildas^{1*}, Arndt, Sandra², Cai, Wei-Jun³ & Regnier, Pierre¹

5

6 1 Department Geosciences, Environment and Society, Université Libre de Bruxelles, Brussels,
7 Belgium

8 2 School of Geographical Sciences, University of Bristol, Bristol, UK

9 3 School of Marine Science and Policy, University of Delaware, Newark, Delaware, USA

10

11 *corresponding author: goulven.gildas.laruelle@ulb.ac.be

12

13

14 **Abstract:**

15 This study presents the first regional-scale assessment of estuarine CO₂ evasion along the East coast
16 of the US (25 – 45 °N). The focus is on 43 tidal estuaries, which together drain a catchment of
17 697~~000~~ km² or 76 % of the total area within this latitudinal band. The approach is based on the
18 Carbon – Generic Estuarine Model (C-GEM) that allows simulating hydrodynamics, transport and
19 biogeochemistry for a wide range of estuarine systems using readily available geometric parameters
20 and global databases of seasonal climatic, hydraulic, and riverine biogeochemical information. ~~Our~~
21 ~~simulations, performed using conditions representative of the year 2000, suggest that, together,~~ US
22 East coast estuaries emit 1.9 TgC yr⁻¹ ~~in the form of CO₂,~~ which correspond to about 40 % of the
23 carbon inputs from rivers, marshes and mangroves. Carbon removal within estuaries results from a
24 combination of physical (outgassing of supersaturated riverine waters) and biogeochemical
25 processes (net heterotrophy and nitrification). The CO₂ evasion and its underlying drivers show
26 important variations across individual systems, but reveal a clear latitudinal pattern characterized by
27 a decrease in the relative importance of physical over biogeochemical processes along a North-South
28 gradient. Finally, ~~the~~ results reveal that the ratio of estuarine surface area to the river discharge, S/Q
29 (which has a scale of per meter discharged water per year), could be used as a predictor of the
30 estuarine carbon processing in future regional and global scale assessments.

Deleted: 10³

Formatted: Superscript

Deleted: Together

Formatted: Subscript

33 **1 Introduction**

34 Carbon fluxes along the land-ocean aquatic continuum are currently receiving increasing attention
35 because of their recently recognized role in the global carbon cycle and anthropogenic CO₂ budget
36 (Bauer et al., 2013; Regnier et al., 2013a; LeQuéré et al., 2014, 2015). Estuaries are important
37 reactive conduits along this continuum, which links the terrestrial and marine global carbon cycles
38 (Cai, 2011). Large amounts of terrestrial carbon transit through these systems, where they mix with
39 carbon from autochthonous, as well as marine sources. During estuarine transit, heterotrophic
40 processes degrade a fraction of the allochthonous and autochthonous organic carbon inputs,
41 supporting a potentially significant, yet poorly quantified CO₂ evasion flux to the atmosphere. Recent
42 estimates suggest that 0.15-0.25 PgC yr⁻¹ is emitted from estuarine systems worldwide (Borges and
43 Abril, 2012; Cai, 2011; Laruelle et al., 2010; Regnier et al., 2013a; Laruelle et al., 2013, Bauer et al.,
44 2013). Thus, in absolute terms the global estuarine CO₂ evasion corresponds to about 15% of the
45 open ocean CO₂ uptake despite the much smaller total surface area.

46 Currently, estimates of regional and global estuarine CO₂ emissions are mainly derived on the basis
47 of data-driven approaches that rely on the extrapolation of a small number of local measurements
48 (Cai, 2011; Chen et al., 2013; Laruelle et al., 2013). These approaches fail to capture the spatial and
49 temporal heterogeneity of the estuarine environment (Bauer et al., 2013) and are biased towards
50 anthropogenically influenced estuarine systems located in industrialized countries (Regnier et al.,
51 2013a). Even in the best surveyed regions of the world (e.g. Australia, Western Europe, North
52 America or China), observations are merely available for a small number of estuarine systems. In
53 addition, if available, data sets are generally of low spatial and temporal resolution. As a
54 consequence, data-driven approaches can only provide first-order estimates of regional and global
55 estuarine CO₂ emissions.

56 Integrated model-data approaches can help here, as models provide the means to extrapolate over
57 temporal and spatial scales and allow disentangling the complex and very dynamic network of

Deleted: few

Deleted: While these approaches provide useful first-order estimates, they

Deleted: . In addition, these global estimates

Deleted: .

Deleted: and e

Deleted: surveyed

Deleted: such as

Deleted: ,

Deleted: only

Deleted: fraction

Deleted:

71 physical and biogeochemical processes that controls estuarine CO₂ emissions. Over the past
 72 decades, increasingly complex process-based models have been applied, in combination with local
 73 data, to elucidate the coupled carbon-nutrient cycles on the scale of individual estuaries (e.g.,
 74 O’Kane, 1980; Soetaert and Herman, 1995; Vanderborgh et al., 2002; Lin et al., 2007; Arndt et al.,
 75 2009; Cerco et al., 2010; Baklouti et al., 2011). However, the application of such model approaches
 76 remains limited to the local scale due to their high data requirements for calibration and validation
 77 (e.g. bathymetric and geometric information and boundary conditions), as well as the high
 78 computational demand associated with resolving the complex interplay of physical and
 79 biogeochemical processes on the relevant temporal and spatial scales (Regnier et al., 2013b).
 80 Complex process-based models are thus not suitable for the application on a regional or global scale
 81 and, as a consequence, the estuarine carbon filter is, despite its increasingly recognized role in
 82 regional and global carbon cycling (e.g. Bauer et al., 2013), typically not taken into account in model-
 83 derived regional or global carbon budgets (Bauer et al., 2013). The lack of regional and global model
 84 approaches that could be used as stand-alone applications or that could be coupled to regional
 85 terrestrial river network models (e.g. GLOBALNEWS: Seitzinger et al., 2005; Mayorga et al., 2010;
 86 SPARROW: Schwarz et al., 2006) and continental shelf models (e.g. Hofmann et al., 2011) is thus
 87 critical.

88 The Carbon-Generic Estuary Model (C-GEM (v1.0); Volta et al., 2014) has been developed with the
 89 aim of providing such a regional/global modeling tool that can help improve existing, observationally
 90 derived first order estimates of estuarine CO₂ emissions. C-GEM (v1.0) has been specifically designed
 91 to reduce data requirements and computational demand and, thus, tackles the main impediments
 92 for the application of estuarine models on a regional or global scale. The approach takes advantage
 93 of the mutual dependency between estuarine geometry and hydrodynamics in alluvial estuaries
 94 and uses an idealized representation of the estuarine geometry to support the hydrodynamic
 95 calculations. It thus allows running steady state or fully transient annual to multi-decadal simulations
 96 for a large number of estuarine systems, using geometric information readily available through maps

- Deleted:** located in the study area, often with limited spatial and temporal coverage.
- Deleted:** Furthermore, data alone Furthermore, observation-based approaches and do not provide sufficient insights into the complex and dynamic interplay of biogeochemical and physical processes that controls estuarine carbon and CO₂ fluxes. ¶
- Formatted:** English (U.K.)
- Deleted:** increasingly
- Formatted:** Font:
- Formatted:** English (U.K.), Not Highlight
- Formatted:** English (U.K.), Not Highlight
- Deleted:** these
- Deleted:** a
- Formatted:** English (U.K.), Not Highlight
- Deleted:** by
- Deleted:** procedures
- Formatted:** Not Highlight
- Formatted:** English (U.K.), Not Highlight
- Deleted:** by
- Deleted:** required
- Deleted:** to address the
- Deleted:** complex
- Formatted:** English (U.K.)
- Formatted:** English (U.K.), Not Highlight
- Formatted:** Not Highlight
- Formatted:** Adjust space between Latin and Asian text, Adjust space between Asian text and numbers
- Deleted:** These models are thus not suitable for regional or global applications (Bauer et al., 2013), which require simplifications to afford the treatment of a large number of estuaries, including those for which morphological, hydrodynamic and biogeochemical data are incomplete or absent. Therefore, the regional and global quantification of the estuarine filter thus remains ignored is not considered in modelling efforts because terrestrial models representing the river network typically do not account for the estuaries (i.e. GLOBALNEWS: Seitzinger et al., 2005)
- Moved (insertion) [1]**
- Formatted:** French (France), Highlight
- Moved (insertion) [2]**
- Deleted:** a

166 [or remote sensing images. Although the development of such a regional/global tool inevitably](#)
 167 [requires simplification, careful model evaluations have shown that, despite the geometric](#)
 168 [simplification, C-GEM provides an accurate description of the hydrodynamics, transport and](#)
 169 [biogeochemistry in tidal estuaries \(Volta et al., 2014\). In addition, the model approach was](#)
 170 [successfully used to quantify the contribution of different biogeochemical processes for CO₂ air-](#)
 171 [water fluxes in an idealized, funnel-shaped estuary forced by typical summer conditions](#)
 172 [characterizing a temperate Western European climate \(Regnier et al., 2013b\). Volta et al. \(2016b\)](#)
 173 [further investigated the effect of estuarine geometry on the CO₂ outgassing using three idealized](#)
 174 [systems and subsequently established the first regional carbon budget for estuaries surrounding the](#)
 175 [North Sea by explicitly simulating the six largest systems of the area \(Volta et al., 2016a\), including](#)
 176 [the Scheldt and the Elbe for which detailed validation was performed.](#)

177 Here, [we extend the domain of application of C-GEM \(v1.0\) to quantify CO₂ exchange fluxes, as well](#)
 178 as the overall organic and inorganic carbon budgets for the full suite of estuarine systems located
 179 along the entire East coast of the United States, [one of the most intensively monitored regions in the](#)
 180 world. A unique set of regional data, including [partial pressure of CO₂ in riverine](#) and continental
 181 shelf [waters](#) (pCO₂; Signorini et al., 2013; Laruelle et al., 2015), riverine biogeochemical
 182 [characteristics](#) (Lauerwald et al., 2013), estuarine eutrophication status (Bricker et al., 2007) and
 183 estuarine morphology (NOAA, 1985) are available. These comprehensive data sets are
 184 complemented by local observations of carbon cycling and CO₂ fluxes in selected, individual
 185 estuarine systems (see Laruelle et al., 2013 for a review), making the East coast of the United States
 186 an ideal region for a first, fully explicit regional evaluation of CO₂ evasion resolving every major tidal
 187 estuary along the selected coastal segment. The scale addressed in the present study is
 188 unprecedented so far (> 3000 km of coastline) and covers a wide range of estuarine morphological
 189 features, climatic conditions, land-use and land cover types, as well as urbanization levels. [The](#)
 190 [presented study will not only allow a further evaluation of C-GEM \(v1.0\), but will also provide the](#)
 191 [first regional-scale assessment of estuarine CO₂ evasion along the East coast of the US \(25 – 45 °N\)](#)

- Formatted:** English (U.K.), Not Highlight
- Deleted:** careful
- Deleted:** enabling the quantification of biogeochemical dynamics in estuaries on a regional and global scale. The focus is on tidal systems as defined by Dürr et al. (2011) and the approach is based on a one-dimensional, time-dependent representation of hydrodynamic, transport and reaction processes within an estuary.
- Deleted:** C-GEM is computationally efficient and reduces data requirements by using an idealized representation of the geometry to support the hydrodynamic calculations and, subsequently, transport and biogeochemical reaction processes. The C-GEM modeling platform thus enables hundreds to thousands of steady state or fully transient simulations spanning years to decades for a multitude of estuarine systems, using geometric information readily available through maps or remote sensing images. Despite the geometric simplification, C-GEM resolves the most (...)
- Deleted:** first
- Deleted:** successfully
- Formatted:** ...
- Deleted:** is applied
- Formatted:** Font: Not Bold, Not Italic, No underline
- Moved up [1]:** The global quantification filter thus remains ignored in modelling (...)
- Formatted:** Font: Not Bold, Not Italic, No underline
- Moved up [2]:** The lack of regional or global evaluations of the estuarine carb (...)
- Deleted:** In this respect, integrated model-data approaches provide a suitab (...)
- Formatted:** Font: Not Bold, Not Italic, No underline
- Deleted:** ¶
- Deleted:** an extended version of
- Deleted:** . The applied RTM approach allows to evaluate the relative significan (...)
- Deleted:**
- Deleted:** sea partial pressure of CO₂
- Deleted:** properties
- Deleted:** characteristics
- Moved (insertion) [3]**
- Deleted:** An extensive review of published local estimates of CO₂ fluxes i (...)
- Moved up [3]:** An extensive review of published local estimates of CO₂ fluxes i (...)
- Formatted:** Font: Not Bold, Not Italic, No underline

400 [and will help explore general relationships between carbon cycling and CO₂ evasion, and readily](#)
401 [available estuarine geometrical parameters.](#)

402 ~~After a description of the model itself and of the dataset used to set up the simulations, a local~~
403 ~~validation is presented which includes salinity, pCO₂ and pH longitudinal profiles for two well~~
404 ~~monitored systems (the Delaware Bay and the Altamaha River Estuary). The yearly averaged rates of~~
405 ~~CO₂ exchange at the air-water interface simulated by the model for 13 individual estuaries are also~~
406 ~~compared with observed values reported in the literature. Next, regional scale simulations for 43~~
407 ~~tidal estuaries of the eastern US coast provide seasonal and yearly integrated estimates of the Net~~
408 ~~Ecosystem Metabolism (NEM), CO₂ evasion and carbon filtering capacity, C_{filt}. Model results are~~
409 ~~then used to elucidate the estuarine biogeochemical behavior along the latitudinal transect~~
410 ~~encompassed by the present study (30-45° N). Finally, our results are used to derive general~~
411 ~~relationships between carbon cycling and CO₂ evasion, and readily available estuarine geometrical~~
412 ~~parameters.~~

Deleted: ¶
Formatted: Font: Not Bold, Not Italic,
No underline

Formatted: Font: Not Bold, Not Italic,
No underline

414 2. Regional description and model approach

415 2.1 Observation-based carbon budget for the East coast of the United States

416 The study area covers the Atlantic coast of the United States (Fig.1), from the southern tip of Florida
417 (25°N) to Cobscook Bay (45°N) at the US-Canada boundary. This area encompasses distinct climatic
418 zones and land cover types and exhibits a variety of morphologic features (Fig. 1). The region can be
419 subdivided into several sub-regions following a latitudinal gradient (Signorini et al., 2013). In this
420 study, we define three sub-regions following the boundaries suggested by the COSCAT segmentation
421 (Meybeck et al., 2006; Laruelle et al., 2013) and the further subdivision described in Laruelle et al.
422 (2015). From North to South, the regions are called North Atlantic, Mid Atlantic and South Atlantic
423 Regions (Fig. 1). Total carbon inputs from watersheds to US East coast estuaries (Tab. 1) have been

Deleted: Figure

Deleted: ure

Deleted: Table

428 estimated to range from 4.0 to 10.7 Tg C yr⁻¹ (Mayorga et al., 2010; Shih et al., 2010; Stets and Strieg,
429 2012; Tian et al., 2010; Tian et al., 2012), consisting of dissolved organic carbon (DOC; ~50%),
430 dissolved inorganic carbon (DIC; ~40%) and particulate organic carbon (POC; ~10%). In addition, a
431 statistical approach has been applied to estuaries of the region to quantify organic carbon budgets
432 and Net Ecosystem Productivity (NEP) using empirical models (Herrmann et al., 2015).

433 Recent studies estimated that, along the East coast of the United States, rivers emit 11.4 TgC yr⁻¹ of
434 CO₂ to the atmosphere (Raymond et al., 2013), while continental shelf waters absorb between 3.4
435 and 5.4 TgC yr⁻¹ of CO₂ from the atmosphere (Signorini et al., 2013). A total of thirteen local, annual
436 mean estuarine CO₂ flux estimates across the air-water interface based on measurements are also
437 reported in the literature and are grouped along a latitudinal gradient (Tab. 2). Four of these
438 estimates are located in the South Atlantic region (SAR): Sapelo Sound, Doboy Sound, Altamaha
439 Sound (Jiang et al., 2008), and the Satilla River estuary (Cai and Wang, 1998). Three studies
440 investigate CO₂ fluxes in the mid-Atlantic Region (MAR): the York River Estuary (Raymond et al.,
441 2000) and the Hudson River (Raymond et al., 1997). There is also a comprehensive CO₂ flux study for
442 the Delaware Estuary published after the completion of this work (Joeseof et al., 2015). Six systems
443 are located in the North Atlantic region (NAR): The Great Bay, the Little Bay, the Oyster estuary, the
444 Bellamy estuary, the Cocheco estuary (Hunt et al., 2010; 2011), and the Parker River estuary
445 (Raymond and Hopkinson, 2003). The mean annual flux per unit area from these local studies is
446 11.7±13.1 mol C m⁻² yr⁻¹ and its extrapolation to the total estuarine surface leads to a regional CO₂
447 evasion estimate of 3.8 Tg C y⁻¹. This estimate is in line with that of Laruelle et al. (2013) for the same
448 region which proposes an average CO₂ emission rate of 10.8 mol C m⁻² yr⁻¹. Thus, CO₂ outgassing
449 could remove 35% to 95% of the riverine carbon loads during estuarine transit. About 75 % of the
450 air-water exchange occurs in tidal estuaries (2.8 Tg C y⁻¹) while lagoons and small deltas contribute to
451 the remaining 25 %. Although these simple extrapolations from limited observational data are
452 associated with large uncertainties, they highlight the potentially significant contribution of estuaries
453 to the CO₂ outgassing in the region. However, process-based quantifications of regional organic and

Deleted: fig

Deleted: 1

456 inorganic C budgets including air-water CO₂ fluxes for the estuarine systems along the East coast are
457 not available.

458 2.2 Selection of estuaries

459 The National Estuarine Eutrophication Assessment (NEEA) survey (Bricker et al., 2007), which uses
460 geospatial data from the National Oceanic and Atmospheric Administration (NOAA) Coastal

461 Assessment Framework (CAF) (NOAA, 1985), was used to identify and characterize 58 estuarine

Deleted: 64

462 systems discharging along the Atlantic coast of the United States. From this set, 43 'tidal' estuaries,

Deleted: 47

463 defined as a river stretch of water that is tidally influenced (Dürr et al., 2011), were retained (Fig. 1)

Deleted:

464 to be simulated by the C-GEM model, which is designed to represent such systems. Using outputs

Deleted: fig

465 from terrestrial models (Hartmann et al., 2009; Mayorga et al., 2010), the cumulated riverine carbon

Formatted: Font: Not Bold, Not Italic, No underline

466 loads for all the non-tidal estuaries that are excluded from the present study amount to 0.9 Tg C yr⁻¹,

Deleted: The 15

467 which represents less than 15% of the total riverine carbon loads of the region. These 15 systems are

Formatted: Font: Not Bold, Not Italic, No underline

468 located in the SAR (10) and in the MAR (5),

Formatted: Font: Not Bold, Not Italic, No underline

469 The northeastern part of the domain (NAR, Fig. 1; Tab. 1) includes 20 estuaries along the Gulf of

Deleted: and account for less than 15% of the total riverine carbon loads of the region

470 Maine and the Scotian shelf, covering a cumulative surface area of ~5300 km². It includes drowned

Deleted: table

471 valleys, rocky shores and a few tidal marshes. The climate is relatively cold (annual mean= 8°C) and

472 the human influence is relatively limited because of low population density and low freshwater

473 inputs. The mean estuarine water depth is 12.9 m and the mean tidal range is 2.8 m.

474 The central zone (MAR) includes 17 tidal estuaries accounting for a total surface area of 14500 km².

475 The Chesapeake Bay and the Delaware estuaries alone contribute more than 60% to the surface area

476 of the region. In this region, estuaries are drowned valleys with comparatively high river discharge

477 and intense exchange with the ocean. Several coastal lagoons, characterized by a limited exchange

478 with the ocean are located here, but are not included in our analysis. The Mid-Atlantic Region (MAR)

479 is characterized by a mean annual temperature of 13°C and is strongly impacted by human activities,

489 due to the presence of several large cities (e.g. New York, Washington, Philadelphia, Baltimore) and
490 intense agriculture. The mean water depth is about 4.7 m and the tidal range is 0.8 m.

491 The southern Atlantic region (SAR) includes 10 tidal estuaries covering a total surface area of 12182
492 km². These systems are generally dendritic and surrounded by extensive salt marshes. The climate is
493 subtropical with an average annual temperature of 19°C. Land use includes agriculture and industry,
494 but the population density is generally low. Estuarine systems in the SAR are characterized by a
495 shallow mean water depth of 2.9 m and a tidal range of 1.2 m.

496 **2.3 Model set-up**

497 The generic 1D Reactive-Transport Model (RTM) C-GEM (Volta et al., 2014) is used to quantify the
498 estuarine carbon cycling in the 43 systems considered in this study. The approach is based on
499 idealized geometries (Savenije, 2005; Volta et al., 2014) and is designed for regional and global scale
500 applications (Regnier et al., 2013b; Volta et al., 2014, 2016a). The model approach builds on the
501 premise that hydrodynamics exerts a first-order control on estuarine biogeochemistry (Arndt et al.,
502 2007; Friedrichs and Hofmann, 2001) and CO₂ fluxes (Regnier et al., 2013a). The method takes
503 advantage of the mutual dependence between geometry and hydrodynamics in tidal estuaries
504 (Savenije, 1992) and the fact that, as a consequence, transport and mixing can be easily quantified
505 from readily available geometric data (Regnier et al., 2013a; Savenije, 2005; Volta et al., 2016b).

Deleted: 47

506 **2.3.1 Description of idealized geometries for tidally-averaged conditions**

507 Although tidal estuaries display a wide variety of shapes, they nevertheless share common
508 geometric characteristics that are compatible with an idealized representation (Fig. 2, Savenije,
509 1986; Savenije, 2005). For tidally-averaged conditions, their width B (or cross-sectional area A) can
510 be described by an exponential decrease as a function of distance, x, from the mouth (Savenije,
511 1986; Savenije, 2005):

$$B = B0 * \exp\left(-\frac{x}{b}\right) \quad (1)$$

513 where B (m) is the tidally averaged width, B0 (m) the width at the mouth, x (m) the distance from
 514 the mouth (x=0) and b (m) the width convergence length (Fig. 2). The width convergence length, b, is
 515 defined as the distance between the mouth and the point at which the width is reduced to B0 e⁻¹. It
 516 is directly related to the dominant hydrodynamic forcing. A high river discharge typically results in a
 517 prismatic channel with long convergence length (river dominated estuary), while a large tidal range
 518 results in a funnel-shaped estuary with short convergence length (marine dominated estuary). At the
 519 upstream boundary, the estuarine width is given by:

$$B_L = B0 * \exp\left(-\frac{L}{b}\right) \quad (2)$$

520 Where L denotes the total estuarine length (m) along the estuarine longitudinal axis.

521 The total estuarine surface S (m²) can be estimated by integrating equation (1) over the estuarine
 522 length:

$$S = \int_0^L B dx = b * B0 * \left(1 - \exp\left(-\frac{L}{b}\right)\right) \quad (3)$$

523

524 The width convergence length is then calculated from B0, B_L, L and the real estuarine surface area
 525 (SR) by inserting equation (2) in equation (3):

$$b = \frac{SR}{B0 - B_L} \quad (4)$$

526 SR is calculated for each system using the SRTM water body data (Fig. 3a), a geographical dataset
 527 encoding high-resolution worldwide coastal outlines in a vector format (NASA/NGA, 2003). While
 528 such a database exists for a well monitored region such as the East coast of the US, resorting to
 529 using the idealized estuarine surface area (S) is necessary in many other regions. The longitudinal

Deleted: fig

531 mean, tidally averaged, depth h (m), is obtained from the National Estuarine Eutrophication
 532 Assessment database (Bricker et al., 2007).

533 Using this idealized representation, the estuarine geometry can be defined by a limited number of
 534 parameters: the width at the mouth (B_0), the estuarine length (L), the estuarine width at the
 535 upstream limit (B_L) and the mean depth h . These parameters can be easily determined from local
 536 maps or Google Earth using Geographic Information Systems (GIS), or obtained from databases
 537 (NASA/NGA, 2003).

Formatted: Font: Not Bold, Not Italic, No underline

Formatted: Font: Not Bold, Not Italic, No underline

Deleted: through GIS, local maps, Google Earth

538 2.3.2 Hydrodynamics, transport and biogeochemistry

539 Estuarine hydrodynamics are described by the one-dimensional barotropic, cross-sectionally
 540 integrated mass and momentum conservation equations for a channel with arbitrary geometry
 541 (Nihoul and Ronday, 1976; Regnier et al., 1998; Regnier and Steefel, 1999):

Deleted: is

$$542 \quad r_s \frac{\partial A}{\partial t} + \frac{\partial Q}{\partial x} = 0 \quad (5)$$

$$543 \quad \frac{\partial U}{\partial t} + U \frac{\partial U}{\partial x} = -g \frac{\partial \zeta}{\partial x} - g \frac{U|U|}{C_z^2 H} \quad (6)$$

Deleted: $\frac{\partial U}{\partial t} + U \frac{\partial U}{\partial x} = -$

Formatted: Lowered by 10 pt

544 where:

545	t	time	[s]
546	x	distance along the longitudinal axis	[m]
547	A	cross-section area $A = H \cdot B$	[m ²]
548	Q	cross-sectional discharge $Q = A \cdot U$	[m ³ s ⁻¹]
549	U	flow velocity Q/A	[m s ⁻¹]
550	r_s	storage ratio $r_s = B_s / B$	[-]

555	B_s	storage width	[m]
556	g	gravitational acceleration	[m s ⁻²]
557	ξ	elevation	[m]
558	H	total water depth $H = h + \xi(x, t)$	[m]

559 C_z Chézy coefficient [m^{1/2} s⁻¹]

Formatted: Subscript

560 The coupled partial differential equations (Eqs. [5](#)) and [6](#)) are solved by specifying the elevation
561 $\xi_0(t)$ at the estuarine mouth and the river discharge $Q_r(t)$ at the upstream limit of the model domain.

Deleted: 6

Deleted: 7

562 The one-dimensional, tidally-resolved, advection-dispersion equation for a constituent of
563 concentration $C(x, t)$ in an estuary can be written as (e.g. Pritchard, 1958):

$$564 \quad \frac{\partial C}{\partial t} + \frac{Q}{A} \frac{\partial C}{\partial x} = \frac{1}{A} \frac{\partial}{\partial x} \left(AD \frac{\partial C}{\partial x} \right) + P \quad (7)$$

565 where $Q(x, t)$ and $A(x, t)$ denote the cross-sectional discharge and area, respectively and are provided
566 by the hydrodynamic model (eq. [5](#) and [6](#)). $P(x, t)$ is the sum of all production and consumption
567 process rates affection the concentration of the constituent. The effective dispersion coefficient D
568 (m² s⁻¹) implicitly accounts for dispersion mechanisms associated to sub-grid scale processes (Fischer,
569 1976; Regnier et al., 1998). In general, D is maximal near the sea, decreases upstream and becomes
570 virtually zero near the tail of the salt intrusion curve (Preddy, 1954; Kent, 1958; Ippen and Harleman,
571 1961; Stigter and Siemons, 1967). The effective dispersion at the estuarine mouth can be quantified
572 by the following relation ([Savenije, 1986](#)):

Deleted: 6

Deleted: 7

Deleted: Van der Burgh

Deleted: 1972

$$573 \quad D_0 = 26 \cdot (h_0)^{1.5} \cdot (N \cdot g)^{0.5} \quad (8)$$

574 where h_0 (m) is the tidally-averaged water depth at the estuarine mouth and N is the dimensionless
575 Canter Cremers' estuary number defined as the ratio of the freshwater entering the estuary during a

582 tidal cycle to the volume of salt water entering the estuary over a tidal cycle (Simmons, 1955).

583
$$N = \frac{Q_b \cdot T}{P} \quad (9)$$

584 In this equation, Q_b is the bankfull discharge ($m^3 s^{-1}$), T is the tidal period (s) and P is the tidal prism
585 (m^3). For each estuary, N can thus be calculated directly from the hydrodynamic model. The

Formatted: Font: Not Bold, Not Italic, No underline

586 variation in D along the estuarine gradient can be described by Van der Burgh's equation (Savenije,
587 1986):

588
$$\frac{\partial D}{\partial x} = -K \frac{Q_r}{A} \quad (10)$$

Deleted: 9

589 where K is the dimensionless Van der Burgh's coefficient and the minus sign indicates that D
590 increases in downstream direction (Savenije, 2012). The Van der Burgh's coefficient is a shape factor
591 that has values between 0 and 1 (Savenije, 2012), and is a function of estuarine geometry for tidally
592 average conditions. Therefore, each estuarine system has its own characteristic K value, which
593 correlates with geometric and hydraulic scales (Savenije, 2005). Based on a regression analysis
594 covering a set of 15 estuaries, it has been proposed to constrain K from the estuarine geometry
595 (Savenije, 1992):

596
$$K = 4.32 \cdot \frac{h_0^{0.36}}{B_0^{0.21} \cdot b^{0.14}} \quad \text{with } 0 < K < 1 \quad (11)$$

Deleted: 10

597 Reaction processes P considered in C-GEM comprise aerobic degradation, denitrification,
598 nitrification, primary production, phytoplankton mortality and air-water gas exchange for O_2 and CO_2
599 (Fig. 4 and Tab. 3). These processes and their mathematical formulation are described in detail in
600 Volta et al. (2014) and Volta et al. (2016a).

Deleted: Table

Deleted: 2

601 The non-linear partial differential equations for the hydrodynamics are solved by a finite difference
602 scheme following the approach of (Regnier et al., 1997; Regnier and Steefel, 1999) and
603 (Vanderborcht et al., 2002). The timestep Δt is 150s and the grid size Δx is constant along the

Deleted:)

Deleted: ,

Deleted: (

611 longitudinal axis of the estuary. The grid size default value is 2000_m, but can be smaller for short
612 length estuaries to guarantee a minimum of 20 grid points within the computational domain.
613 Transport and reaction terms are solved in sequence within a single timestep using an operator
614 splitting approach (Regnier et al., 1997). The advection term in the transport equation is integrated
615 using a third-order accurate total variation diminishing (TVD) algorithm with flux limiters (Regnier et
616 al., 1998), ensuring monotonicity (Leonard, 1984), while a semi-implicit Crank-Nicholson algorithm is
617 used for the dispersion term (Press et al., 1992). These schemes have been extensively tested using
618 the CONTRASTE estuarine model (e.g. Regnier et al., 1998; Regnier and Steefel, 1999; Vanderborght
619 et al., 2002) and guarantee mass conservation to within <1%. The reaction network (including
620 erosion-deposition terms when the constituent is a solid species), is numerically integrated using the
621 Euler method (Press et al., 1992). The primary production dynamics, which requires vertical
622 resolution of the photic depth, is calculated according to the method described in Vanderborght et
623 al. (2007). This method assumes an exponential decrease of the light in the water column (Platt et
624 al., 1980), which is solved using a Gamma function.

625 **2.4 Boundary and forcing conditions**

626 Boundary and forcing conditions are extracted from global databases and global model outputs that
627 are available at 0.5° resolution. Therefore, C-GEM simulations are performed at the same resolution
628 according to the following procedure. First, 43 coastal cells corresponding to tidal estuaries are
629 identified in the studied area (Fig. 1). If the mouth of an estuary is spread over several 0.5° grid cells,
630 those cells are regrouped in order to represent a single estuary (e.g. Delaware estuary), and
631 subsequently, a single idealized geometry is defined as described above. The model outputs
632 (Hartmann et al., 2009; Mayorga et al., 2010) and databases (Antonov et al., 2010; Garcia et al.,
633 2010a; Garcia et al., 2010b) used to constrain our boundary conditions are representative of the
634 year 2000.

Deleted: 47

Deleted: fig

637 For each resulting cell, boundary and forcing conditions are calculated for the following periods:
638 January-March; April-June; July-September and October-December. This allows for an explicit
639 representation of the seasonal variability in the simulations.

640 **2.4.1 External forcings**

641 Transient physical forcings are calculated for each season and grid cell using monthly mean values of
642 water temperature (World Ocean Atlas, 2009) and seasonal averaged values for wind speed (Cross-
643 Calibrated-Multi-Platform (CCMP) Ocean Surface Wind Vector Analyses project (Atlas et al., 2011)).

644 Mean daily solar radiation and photoperiods (corrected for cloud coverage using the ISCCP Cloud
645 Data Products, Rossow and Schiffer, 1999) are calculated depending on latitude and day of the year
646 using a simple model (Brock, 1981).

Formatted: Font: Not Bold, Not Italic,
No underline

647 **2.4.2 Riverine discharge, concentrations and fluxes**

648 River discharges are extracted from the UNH/GRDC runoff dataset (Fekete et al., 2002). These
649 discharges represent long-term averages (1960-1990) of monthly and annual runoff at 0.5 degree
650 resolution. The dataset is a composite of long-term gauging data, which provides average runoff for
651 the largest river basins, and a climate driven water balance model (Fekete et al., 2002). Total runoff
652 values are then aggregated for each watershed at the coarser 0.5 degree resolution (Fig. 3b). Next,
653 seasonal mean values (in $\text{m}^3 \text{s}^{-1}$) are derived in order to account for the intra-annual variability in
654 water fluxes. Based on annual carbon and nutrients inputs from the watersheds (Mg y^{-1}), mean
655 annual concentrations (mmol m^{-3}) are estimated for each watershed using the UNH/GRDC annual
656 runoff ($\text{km}^3 \text{y}^{-1}$). Mean seasonal concentrations are then calculated from the seasonally resolved
657 river water fluxes of a given sub-region.

Deleted: fig

658 Annual inputs of dissolved organic carbon (DOC), particulate organic carbon (POC) and inorganic
659 nutrients are derived from the globalNEWS2 model (Mayorga et al., 2010). Global NEWS is a spatially
660 explicit, multi-element (N, P, Si, C) and multi-form global model of nutrient exports by rivers. In a

662 nutshell, DOC exports are a function of runoff, wetland area, and consumptive water use (Harrison
663 et al., 2005). No distinction is made between agricultural and natural landscapes, since they appear
664 to have similar DOC export coefficients (Harrison et al., 2005). Sewage inputs of OC are ignored in
665 GlobalNEWS, because their inclusion did not improve model fit to data (Harrison et al., 2005). POC
666 exports from watersheds are estimated using an empirical relationship with Suspended Particulate
667 Matter (SPM; Ludwig et al., 1996). Inorganic nitrogen (DIN) and phosphorus (DIP) fluxes calculated
668 by GlobalNEWS depend on agriculture and tropical forest coverage, fertilizer application, animal
669 grazing, sewage input, atmospheric N deposition and biological N fixation (Mayorga et al., 2010). The
670 inputs of dissolved silica (DSi) are controlled by soil bulk density, precipitation, slope, and presence
671 of volcanic lithology (Beusen et al., 2009).

672 The DIN speciation is not provided by the GlobalNEWS2 model. The NH_4 and NO_3 concentrations are
673 therefore determined independently on the basis of an empirical relationship between ammonium
674 fraction (NH_4/DIN ratio) and DIN loads (Meybeck, 1982). Dissolved Oxygen (DO) concentrations are
675 extracted from the water quality criteria recommendations published by the United States
676 Environmental Protection Agency (EPA, 2009). The same source is used for phytoplankton
677 concentrations, using a chlorophyll-a to phytoplankton carbon ratio of $50 \text{ gC (gChla)}^{-1}$ (Riemann et
678 al., 1989) to convert the EPA values to carbon units used in the present study.

679 Inputs of dissolved inorganic carbon (DIC) and total Alkalinity (ALK) are calculated from values
680 reported in the GLORICH database (Hartmann et al., 2009). For each watershed, seasonal mean
681 values of DIC and ALK concentrations are estimated from measurements performed at the sampling
682 locations that are closest to the river-estuary boundary. The spatial distribution of annual inputs of
683 $\text{TOC}=\text{DOC}+\text{POC}$, DIC, and $\text{TC}=\text{TOC}+\text{DIC}$ from continental watersheds to estuaries are reported in Fig.
684 5a, 5c and 5d, respectively. The contribution of tidal wetlands to the TOC inputs is also shown (Fig.
685 5b). Overall, the TC input over the entire model domain is estimated at 4.6 Tg C yr^{-1} , which falls in
686 the lower end of previous reported estimations (Najjar et al. 2012).

Deleted: fig

688

689 2.4.3 Inputs from tidal wetlands

690 The DOC input of estuarine wetlands (Fig. 5b) scales to their fraction, W, of the total estuarine and is
691 calculated using the GlobalNEWS parameterization:

Formatted: Font: Not Bold, Not Italic, No underline

Deleted: their surface area W

$$Y_{DOC} = \frac{[(E_{C_{wet}} * W) + E_{C_{dry}} * (1 - W)] * R^a * Q_{act}}{Q_{nat}}$$

(12)

Deleted: 11

692

$$\frac{Y_{DOC_{wet}}}{Y_{DOC}} = \frac{E_{C_{wet}} * W}{E_{C_{wet}} * W + E_{C_{dry}} * (1 - W)}$$

(13)

Deleted: 12

693

694 where Y_{DOC} is the DOC yield ($\text{kg C km}^{-2} \text{y}^{-1}$) calculated for the entire watershed, $Y_{DOC_{wet}}$ is the
695 estimated DOC yield from wetland areas ($\text{kg C km}^{-2} \text{y}^{-1}$), Q_{act}/Q_{nat} is the ratio between the measured
696 discharge after dam construction and before dam construction, $E_{C_{wet}}$ and $E_{C_{dry}}$ ($\text{kg C km}^{-2} \text{y}^{-1}$) are
697 the export coefficients of DOC from wetland and non-wetland soils, respectively. W is the
698 percentage of the land area within a watershed that is covered by wetlands, R is the runoff (m y^{-1})
699 and a is a unit-less calibration coefficient defining how non-point source DOC export responds to
700 runoff. The value of a is set to 0.95, consistent with the original GlobalNEWS -DOC model of Harrison
701 et al. (2005). The carbon load $Y_{DOC_{wet}}$ is then exported as a diffuse source along the relevant
702 portions of estuary. The estuarine segments receiving carbon inputs from tidal wetlands are
703 identified using the National Wetlands Inventory of the U.S. Fish and Wildlife Service (U.S. Fish and
704 Wildlife Service, 2014). The inputs from those systems are then allocated to the appropriate grid cell
705 of the model domain using GIS. The flux calculated is an annual average that is subsequently
706 partitioned between the four seasons as a function of the mean seasonal temperature, assumed to
707 be the main control of the wetland-estuarine exchange. This procedure reflects the observation that

711 in spring and early summer, DOC export is small as a result of its accumulation in the salt marshes
712 induced by the high productivity (Dai and Wiegert, 1996), (Jiang et al., 2008). In late summer and fall,
713 the higher water temperature and greater availability of labile DOC contribute to higher bacterial
714 remineralization rates in the intertidal marshes (Cai et al., 1999; Middelburg et al., 1996; Wang and
715 Cai, 2004), which induce an important export. This marsh production-recycle-export pattern is
716 consistent with the observed excess DIC signal in the offshore water (Jiang et al. 2013). DIC export
717 from tidal wetlands is neglected here because it is assumed that OC is not degraded before reaching
718 the estuarine realm. Although this assumption may lead to an overestimation of OC export from
719 marshes and respiration in estuarine water, it will not significantly affect the water $p\text{CO}_2$ and
720 degassing in the estuarine waters because mixing is faster than respiration.

721 **2.4.4 Concentrations at the estuarine mouth**

722 For each estuary, the downstream boundary is located 20 km beyond the mouth to minimize the
723 bias introduced by the choice of a fixed concentration boundary condition to characterize the ocean
724 water masses (e.g. Regnier et al., 1998). This approach also reduces the influence of marine
725 boundary conditions on the simulated estuarine dynamics, especially for all organic carbon species
726 whose concentrations are fixed at zero at the marine boundary. This assumption ignores the
727 intrusion of marine organic carbon into the estuary during the tidal cycle but allows focusing on the
728 fate of terrigenous material and its transit through the estuarine filter. DIC concentrations are
729 extracted from the GLODAP dataset (Key et al., 2004), from which ALK and pH are calculated
730 assuming CO_2 equilibrium between coastal waters and the atmosphere. The equilibrium value is
731 computed using temperature (WOA2009, Locarnini et al., 2010) and salinity (WOA2009, Antonov et
732 al. (2010)) data which vary both spatially and temporally. The equilibrium approach is a reasonable
733 assumption because differences in partial pressure $\Delta p\text{CO}_2$ between coastal waters and the
734 atmosphere are generally much smaller (0-250 μatm (Signorini et al., 2013)) than those reported for
735 estuaries ($\Delta p\text{CO}_2$ in the range 0-10000 μatm (Borges and Abril, 2012)). Salinity, DO, NO_3 , DIP and DSI

Deleted:

737 concentrations are derived from the World Ocean Atlas (Antonov et al., 2010; Garcia et al., 2010a;
738 Garcia et al., 2010b). NH_4 concentrations are set to zero in marine waters. For all variables, seasonal
739 means are calculated for each grid cell of the boundary.

Deleted: domain

740

741 2.5 Biogeochemical indicators

742 The model outputs (longitudinal profiles of concentration and reaction rates) are integrated in time
743 over the entire volume or surface of each estuary to produce the following indicators of the
744 estuarine biogeochemical functioning (Regnier et al., 2013b): the mean annual Net Ecosystem
745 Metabolism (*NEM*), the air-water CO_2 flux (*FCO₂*), the carbon and nitrogen filtering capacity (*CFilt*
746 and *NFilt*) and their corresponding element budgets. The *NEM* (molC y^{-1}) (Caffrey, 2004; Odum,
747 1956) is defined as the difference between net primary production (*NPP*) and total heterotrophic
748 respiration (*HR*) at the system scale:

$$NEM = \int_0^{365} \int_0^L [NPP(x, t) - R_{aer}(x, t) - R_{den}(x, t)] * B(x) * H(x, t) dx dt$$

(14)

Deleted: 13

749

750 where *NPP* is the Net Primary Production ($\text{mol C m}^{-3} \text{y}^{-1}$), R_{aer} the aerobic degradation of organic
751 matter (in $\text{mol C m}^{-3} \text{y}^{-1}$) and R_{den} the denitrification (in $\text{mol C m}^{-3} \text{y}^{-1}$) (see Volta et al., 2014 for
752 detailed formulations). *NEM* is thus controlled by the production and decomposition of
753 autochthonous organic matter, by the amount and degradability of organic carbon delivered by
754 rivers and tidal wetlands and by the export of terrestrial and in-situ produced organic matter to the
755 adjacent coastal zone. Following the definition of *NEM*, the trophic status of estuaries can be net
756 heterotrophic ($NEM < 0$) when *HR* exceeds *NPP* or net autotrophic ($NEM > 0$), when *NPP* is larger than
757 *HR* because the burial and export of autochthonous organic matter exceeds the decomposition of
758 river-borne material.

761 The FCO_2 (mol C γ^{-1}) is defined as:

$$FCO_2 = \int_0^{365} \int_0^L RCO_2(x, t) * B(x) dx dt$$

(15)

Deleted: 14

762

$$RCO_2(x, t) = -v_p(x, t) ([CO_2(aq)](x, t) - K_0(x, t) * P_{CO_2}(x, t))$$

(16)

Deleted: 15

763

764 where RCO_2 (molC $m^{-2} \gamma^{-1}$) is the rate of exchange in CO_2 at the air-water interface per unit surface
765 area, v_p is the piston velocity ($m \gamma^{-1}$) and is calculated according to Regnier et al. (2002) to account
766 for the effect of current velocity and wind speed, $[CO_2(aq)]$ is the concentration of CO_2 in the
767 estuary ($mol m^{-3}$), K_0 is Henry's constant of CO_2 in sea water ($mol m^{-3} atm^{-1}$) and P_{CO_2} is the
768 atmospheric partial pressure in CO_2 (atm).

769 The carbon filtering capacity (in %) corresponds to the fraction of the river-borne supply that is lost
770 to the atmosphere and is defined here as the ratio of the net outgassing flux of CO_2 and the total
771 inputs of C, e.g. total carbon expressed as the sum of inorganic and organic carbon species, both in
772 the dissolved and particulate phases.

$$CFilt = \frac{FCO_2}{\int_0^{365} Q * [TC]_{riv} dt} * 100$$

(17)

Deleted: 16

774 where $[TC]_{riv}$ denote the total concentrations of C in the riverine inputs.

775 Fluxes per unit area for FCO_2 and NEM , noted $\overline{FCO_2}$ and \overline{NEM} , respectively, are defined in $mol C m^{-2}$
776 γ^{-1} and are calculated by dividing the integrated values calculated above by the (idealized) estuarine
777 surface S :

$$\overline{NEM} = \frac{NEM}{S} * 1000$$

(18)

Deleted: 17

$$\overline{FCO_2} = \frac{FCO_2}{S} * 1000$$

(19)

Deleted: 18

785 Seasonal values for the biogeochemical indicators are calculated using the same formula as above,
786 but calculate the integral over a seasonal rather than annual timescale (i.e. 3 months).

787

788

789 2.6 Model-data comparison

790 ~~C-GEM has been specifically designed for an application on a global/regional scale requiring the~~
791 ~~representation of a large number of individual and often data-poor systems. Maximum model~~
792 ~~transferability and minimum validation requirements were thus central to the model design process~~
793 ~~and the ability of the underlying approach in reproducing observed dynamics with minimal~~
794 ~~calibration effort has been extensively tested.~~ The performance ~~C-GEM's one-dimensional~~

Formatted: Font: Not Bold, Not Italic,
No underline

795 hydrodynamic and transport models using idealized geometries have been evaluated for a number
796 of estuarine systems exhibiting a wide variety of shapes (Savenije, 2012). In particular, it has been
797 shown that the estuarine salt intrusion can be successfully reproduced using the proposed modeling
798 approach (Savenije 2005; Volta et al., 2014; 2016b). ~~In addition,~~ C-GEM's biogeochemistry has also
799 been carefully validated for geometrically contrasting estuarine system in temperate climate zones.

Deleted: of 1D

Formatted: Font: Not Bold, Not Italic,
No underline

800 Simulations for the Scheldt Estuary (Belgium and the Netherlands), a typical funnel-shaped estuary,
801 were validated through model-data and model-model comparison (Volta et al., 2014; Volta et al.,

802 2016a). ~~Furthermore, simulations~~ for the Elbe estuary (Germany), a typical prismatic shape estuary

Deleted: Simulations

803 ~~that drains~~ carbonate terrains ~~and, thus, exhibits~~ very high pH was validated against field data (Volta
804 et al., 2016a). In addition, C-GEM carbon budgets have been compared ~~budget derived from~~

Deleted: draining

Deleted: resulting in

Deleted: to

805 observations for 6 European estuaries discharging in the North Sea (Volta et al., 2016a). ~~Although C-~~

Deleted: -based estimations

806 ~~GEM has been specifically designed and tested for the type of regional application presented here,~~

Formatted: Font: Not Bold, Not Italic,
No underline

807 ~~its transferability from North Sea to US East Coast estuaries was further evaluated by assessing its~~

808 ~~performance in two East Coast estuaries. First, the hydrodynamic and transport model was tested~~

815 for the Delaware Bay (MAR). The model was forced with the monthly, minimal and maximal
816 observed discharge at Trenton over the period between 1912 and 1985 (UNH/GRDC Database,
817 Fekete et al., 2000). Simulated salinity profiles are compared with salinity observations from January,
818 February, May and June (the months with the highest number of data entries), which were extracted
819 from the UNH/GRDC Database. Figure 6 shows that the model captures both the salinity intrusion
820 length and the overall shape of the salinity profile well. In addition, the performance of the
821 biogeochemical model and specifically its ability to reproduce pH and pCO₂ profiles was evaluated by
822 a model-data comparison for both the Delaware Bay (MAR) in July 2003 and the Altamaha river
823 estuary (SAR) in October 1995. Similar to Volta et al., 2016a, the test systems were chosen due to
824 their contrasting geometries. The Delaware Bay is a marine dominated system characterized by a
825 pronounced funnel shape, while the Altamaha River has a prismatic estuary characteristic of river
826 dominated systems (Jiang et al., 2008). Monthly upstream boundary conditions for nutrients, as well
827 as observed pH data and calculated pCO₂ are extracted from datasets described in (Sharp, 2010) and
828 (Sharp et al., 2009) for the Delaware and in (Cai and Wang, 1998; Jiang et al., 2008) and (Cai et al.,
829 1998) for the Altamaha river estuary. The additional forcings and boundary conditions are set
830 similarly to the simulation for 2000 (see Tab. 2, 3, 4, 5, 6 in SI). Figure 7 shows that measured and
831 simulated pH values are in good agreement with observed pH and observation-derived calculations
832 of pCO₂. In the Delaware Bay, a pH minimum is located around km 140 and is mainly caused by
833 intense nitrification sustained by large inputs of NH₄ from the Philadelphia urban area, coupled to an
834 intense heterotrophic activity. Both processes lead to a well-developed pCO₂ increase in this area
835 (Fig. 7b). Although no pCO₂ data were available for validation for the period from which boundary
836 conditions were extracted, the simulated profile agree with pCO₂ measurement from July 2013
837 presented by Joesoef et al. (2015) with pCO₂ values close to equilibrium with the atmosphere in the
838 widest section of the Delaware Bay (close to the estuarine mouth) and values above 1200 μatm at
839 salinities below 5. For the Altamaha river estuary, pH steadily increases from typical river to typical
840 coastal ocean values (Fig. 7b). In addition, both observations and model results reveal that

Formatted: Font: Not Bold, Not Italic, No underline

Formatted: Font: Not Bold, Not Italic

Formatted: Font: Not Bold, Not Italic, No underline

Formatted: Font: Not Bold, Not Italic, No underline

Formatted: Font: Not Bold, Not Italic, No underline

Formatted: Font: Not Bold, Not Italic, No underline

841 outgassing is very intense in the low-salinity region with more than a 5 fold decrease in pCO_2
842 between salinity 0 and 5 (Fig. 7d).

Formatted: Font: Not Bold, Not Italic,
No underline

843 While such local validations allow assessing the performance of the model for a specific set of
844 conditions, the purpose of this study is to capture the average biogeochemical behavior of the
845 estuaries of the eastern coast of the US. Therefore, in addition to the system-specific validation,
846 published annually averaged FCO_2 estimates for 13 tidal systems located within the study area
847 collected over the 1994-2006 period are compared to simulated FCO_2 for conditions representative
848 of the year 2000. Overall, simulated FCO_2 are comparable to values reported in the literature (Tab,
849 2). Although discrepancies, which sometimes can significant, are observed at the level of individual
850 systems, the model captures remarkably well the overall trend in CO_2 evasion rate across estuaries.
851 The model simulates low CO_2 efflux ($< 5 \text{ mol C m}^{-2} \text{ yr}^{-1}$) for the 7 systems were such conditions have
852 been observed, while the 6 systems for which the CO_2 evasion exceeds $10 \text{ mol C m}^{-2} \text{ yr}^{-1}$ are the same
853 in the observations and in the model runs. The discrepancy at the individual system level likely result
854 from a combination of factors, including the choice of model processes and there parametrization,
855 the uncertainties in constraining boundary conditions and the limited representability of
856 instantaneous and local observed.

Formatted: Font: Not Bold, Not Italic,
No underline

Formatted: Font: Not Bold, Not Italic,
No underline

Deleted: This analysis is pursued here by
evaluating our model results in the context
of estuarine CO_2 evasion estimates along
the East coast of the US.

857 **3 Results and discussion**

858 **3.1 Spatial variability of estuarine carbon dynamics**

859 Figure 8 presents the spatial distribution of simulated mean annual $\overline{FCO_2}$ and $-\overline{NEM}$ (Fig. 8a), as well
860 as FCO_2 and $-NEM$ (Fig. 8b). In general, mean annual $\overline{FCO_2}$ are about 30% larger than mean annual
861 \overline{NEM} , with the exception of six estuaries situated in the North of the coastal segment. Overall, the
862 \overline{NEM} is characterized by smaller system to system variability compared to the $\overline{FCO_2}$ in all regions. In
863 addition, Fig. 8 reveals distinct differences across the three coastal segments and highlights the

Deleted: 6

Deleted: 6a

Deleted: 6

Deleted: Figure

Deleted: 6

873 important influence of the estuarine geometry and residence time, as well as the latitudinal
874 temperature gradient on estuarine carbon cycling.

875 Overall, $\overline{FCO_2}$ values are the lowest in the NAR (mean flux = $17.3 \pm 16.4 \text{ mol C m}^{-2} \text{ y}^{-1}$; surface
876 weighted average = $23.1 \text{ mol C m}^{-2} \text{ y}^{-1}$), consistent with previously reported very low values for small

877 estuaries surrounding the Gulf of Maine (Hunt et al., 2010; 2011; [Tab. 2](#)). In contrast, \overline{NEM} reveals a
878 regional minimum in the NAR ($-51.2 \pm 16.6 \text{ mol C m}^{-2} \text{ y}^{-1}$; surface weighted average = $-52.8 \text{ mol C m}^{-2}$
879 y^{-1}). The MAR is characterized by intermediate values for $\overline{FCO_2}$, with a mean flux of $26.3 \pm 34.6 \text{ mol}$

880 $\text{C m}^{-2} \text{ y}^{-1}$ (surface weighted average = $11.1 \text{ mol C m}^{-2} \text{ y}^{-1}$) and lowest values for \overline{NEM} ($-15.1 \pm 14.2 \text{ mol}$
881 $\text{C m}^{-2} \text{ y}^{-1}$; surface weighted average = $-7.4 \text{ mol C m}^{-2} \text{ y}^{-1}$). This region also shows the largest variability

882 in CO_2 outgassing compared to the NAR and SAR, with the standard deviation exceeding the mean

883 $\overline{FCO_2}$, and individual estimates ranging from $3.9 \text{ mol C m}^{-2} \text{ y}^{-1}$ to $150.8 \text{ mol C m}^{-2} \text{ y}^{-1}$. This variability

884 is mainly the result of largely variable estuarine surface areas and volumes. Some of the largest East
885 coast estuaries (e.g. Chesapeake and Delaware Bays), as well as some of smallest estuaries (e.g. York

886 River and Hudson River estuaries, Raymond et al., 1997; 2000), are located in this region ([Tab. 2](#) and

887 4). The maximum values of $150.8 \text{ mol C m}^{-2} \text{ y}^{-1}$ simulated in the MAR are similar to the highest FCO_2
888 reported in the literature ($132.3 \text{ mol C m}^{-2} \text{ y}^{-1}$ for the Tapti estuary in India; Sarma et al., 2012). The

889 SAR is characterized by the highest mean $\overline{FCO_2}$ ($46.7 \pm 33.0 \text{ mol C m}^{-2} \text{ y}^{-1}$; surface weighted average

890 = $40.0 \text{ mol C m}^{-2} \text{ y}^{-1}$) and intermediate \overline{NEM} ($-36.8 \pm 24.7 \text{ mol C m}^{-2} \text{ y}^{-1}$; surface weighted average = -

891 $31.2 \text{ mol C m}^{-2} \text{ y}^{-1}$).

892 The NAR is characterized by a regional minimum in $\overline{FCO_2}$, and only contributes 4.6% to the total

893 FCO_2 of the East coast of the US, owing to the small cumulative surface area available for gas

894 exchange in its 10 estuarine systems. In contrast, the 18 MAR estuaries, with their large relative

895 contribution to the total regional estuarine surface area, account for as much as 70.1% of the total

896 outgassing. Because of their smaller cumulated surface area compared to those of the MAR, the 14

897 SAR estuaries account for merely 25.3% of the total outgassing despite their regional maximal $\overline{FCO_2}$.

Deleted: table

Deleted: 3

Deleted: maximum

Deleted: table

Deleted: 3

Formatted: Font: Not Bold, Not Italic,
No underline

Deleted: more than 70%

904 A similar, yet slightly less pronounced pattern emerges for the \overline{NEM} . The NAR, MAR and SAR
905 respectively contribute 13.7%, 60.7% and 25.6% to the total regional net ecosystem metabolism. The
906 comparatively larger relative contribution of the NAR to the total NEM as compared to the total
907 FCO_2 can be explained by the importance of the specific aspect ratio for NEM . A larger ratio of
908 estuarine width b_0 and convergence length b corresponds to a more funnel shaped estuary while a
909 low ratio corresponds to a more prismatic geometry (Savenije, 2000; Volta et al., 2014). In the NAR,
910 estuaries are generally characterized by relatively narrow widths and deep-water depths, thus
911 limiting the potential surface area for gas exchange with the atmosphere. However, the relative
912 contribution of each region to the total regional NEM and FCO_2 is largely controlled by estuarine
913 surface area. Figure 9 illustrates the cumulative NEM (a) and FCO_2 (b) as a function of the cumulative
914 estuarine surface areas. The disproportionate contribution of large estuaries from the MAR
915 translates into a handful of systems (Chesapeake and Delaware Bays and the main tributaries of the
916 former, in particular) contributing to roughly half of the regional NEM and FCO_2 , in spite of relatively
917 low individual rates per unit surface area. However, the smallest systems (mostly located in the NAR
918 and SAR) nevertheless still contribute a significant fraction to the total regional NEM and FCO_2 . The
919 27 smallest systems merely account for less than 10% of the total regional estuarine surface area,
920 yet contribute 38% and 29% to the total regional NEM and FCO_2 , respectively (Fig. 9). This
921 disproportioned contribution can be mainly attributed to their high individual $\overline{FCO_2}$ and \overline{NEM} . This
922 is illustrated by the average simulated $\overline{FCO_2}$ for all 27 smallest systems (calculated as the sum of
923 each estuarine CO_2 outgassing per unit surface area divided by the total number of estuarine
924 systems) which is significantly higher ($30.2 \text{ mol C m}^{-2} \text{ y}^{-1}$) than its surface weighted average (14 mol C
925 $\text{m}^{-2} \text{ y}^{-1}$). Thereby accounting for the disproportionate contribution of very large systems (calculated
926 as the sum of each estuarine CO_2 outgassing divided by the total estuarine surface area across the
927 region).

Formatted: Font: Not Bold, Not Italic,
No underline

Deleted: 7

Deleted: Figure

Deleted: 7

931 Following the approach used in Regnier et al. (2013), the contribution of each biogeochemical
932 process to FCO_2 is assessed by evaluating their individual contribution to DIC and ALK changes taking
933 into account the local buffering capacity of an ionic solution when TA and DIC are changing due to
934 internal processes, but ignoring advection and mixing (Zeebe and Wolf-Gladrow 2001). In the
935 present study, we quantify the effect of the NEM on the CO_2 balance, which is almost exclusively
936 controlled by aerobic degradation rates because the contributions of denitrification and NPP to the
937 net ecosystem balance are small. Nitrification, a process triggered by the transport and/or
938 production of NH_4 in oxygenated waters, favors outgassing through its effect on pH, which shifts the
939 acid-base equilibrium of carbonate species and increases the CO_2 concentration. The contribution of
940 supersaturated riverine waters to the overall estuarine CO_2 dynamics is calculated as difference
941 between all the other processes creating or consuming CO_2 . Figure 10a presents the contribution of
942 the annually integrated *NEM*, nitrification and evasion of supersaturated, DIC enriched riverine
943 waters to the total outgassing for each system, as well as for individual regions of the domain. The
944 calculation of these annual values is based on the sum of the seasonal fluxes. Model results reveal
945 that, regionally, the *NEM* supports about 50% of the estuarine CO_2 outgassing, while nitrification and
946 riverine DIC inputs sustain about 17% and 33% of the CO_2 emissions, respectively. The relative
947 significance of the three processes described above shows important spatial variability. In the NAR,
948 oversaturated riverine waters and NEM respectively sustain 50% and 44% of the outgassing within
949 the sub-region, while nitrification is of minor importance (6%). In the MAR, the contribution of
950 riverine DIC inputs is significantly lower (~30%) and the main contribution to the outgassing is *NEM*
951 (~50%); nitrification accounting for slightly less than 20% of the outgassing. In the SAR, the riverine
952 contribution is even lower (~20%), and the outgassing is mainly attributed to the *NEM* (~55%) and
953 nitrification (~25%). Therefore, although the model results reveal significant variability across
954 individual systems, a clear latitudinal trend in the contribution to the total FCO_2 emerge from the
955 analysis; the importance of oversaturated riverine water decreasing from North to South, while *NEM*
956 and nitrification increase along the same latitudinal gradient. The increasing relative importance of

Formatted: Font: Not Bold, Not Italic, No underline

Deleted: T

Formatted: Font: Not Bold, Not Italic, No underline

Formatted: Font: Not Bold, Not Italic, No underline

Deleted: (see Regnier et al., 2013b)

Deleted: .

Deleted: 8a

Formatted: Font: Not Bold, Not Italic, No underline

Deleted: Nitrification, a process triggered by the transport and/or production of NH_4 in oxygenated waters, favors outgassing through its effect on pH, which shifts the acid-base equilibrium of carbonate species and increases the CO_2 concentration. In addition, the *NEM* is almost exclusively controlled by aerobic degradation rates because the contribution of denitrification and NPP to the net ecosystem balance is small. ¶

972 estuarine biogeochemical processes over riverine DIC inputs as drivers of FCO_2 along the North-
973 South gradient is largely driven by increasing temperatures from North to South, especially in the
974 SAR region (Tab. S1.1).

Deleted: Table

975 Contrasting patterns across the 3 regions can also be observed with respect to carbon filtering
976 capacities, $CFilt$ (Fig. 10b). In the NAR, over 90% of the riverine carbon flux is exported to the coastal
977 ocean. However, in the MAR, the high efficiency of the largest systems in processing organic carbon
978 results in a regional $CFilt$ that exceeds 50%. This contrast between the NAR and the MAR and its
979 potential implication for the carbon dynamics of the adjacent continental shelf waters has already
980 been discussed by Laruelle et al. (2015). In the NAR, short estuarine residence results in a much
981 lower removal of riverine carbon by degassing compared to the MAR. Laruelle et al. (2015)
982 suggested that this process could contribute to the weaker continental shelf carbon sink adjacent to
983 the NAR, compared to the MAR. In the SAR, most estuaries remove between 40% and 65% of the
984 carbon inputs. The high temperatures observed and resulting accelerated biogeochemical process
985 rates in this region favor the degradation of organic matter and contribute to increase the estuarine
986 filtering capacity for carbon. However, in the SAR, a large fraction of the OC loads is derived from
987 adjacent salt marshes located along the estuarine salinity gradients, thereby reducing the overall
988 residence time of OC within the systems. The filtering capacity of the riverine OC alone, which
989 transits through the entire estuary, would thus be higher than the one calculated here. As a
990 consequence, highest C retention rates are expected in warm tidal estuaries devoid of salt marshes
991 or mangroves (Cai, 2011).

Deleted: 8b

992 **3.2 Seasonal variability of estuarine carbon dynamics**

993 Carbon dynamics in estuaries of the US East coast not only show a marked spatial variability, but also
994 vary on the seasonal timescale. Table 5 presents the seasonal distribution of NEM and FCO_2 for each
995 sub-region. In the NAR, a strong seasonality is simulated for the NEM and the summer period
996 contributes more than a third to the annually integrated value. The outgassing reveals a lower

999 seasonal variability and is only slightly higher than summer outgassing during fall and lower during
1000 spring. In the MAR, summer contributes more to the *NEM* (>28% of the yearly total) than any other
1001 season, but seasonality is less pronounced than in the NAR. Here, FCO_2 is largest in winter and
1002 particularly low during summer. In the SAR, summer accounts for 30 % of the *NEM*, while spring
1003 contributes 21 %. FCO_2 is relatively constant throughout the year suggesting that seasonal variations
1004 in carbon processing decrease towards the lower latitudes in the SAR. This is partly related to the
1005 low variability in river discharge throughout the year in lower latitudes (Tab. S1). In riverine
1006 dominated systems with low residence times, such as, for instance, the Altamaha River estuary, the
1007 CO_2 exchange at the air-water interface is mainly controlled by the river discharge because the time
1008 required to degrade the entire riverine organic matter flux exceeds the transit time of OC through
1009 the estuary. Therefore, the riverine sustained outgassing is highest during the spring peak discharge
1010 periods. In contrast, the seasonal variability in FCO_2 in long-residence, marine-dominated systems
1011 with large marsh areas (e.g. Sapelo and Doboy Sound) is essentially controlled by seasonal
1012 temperature variations. Its maximum is reached during summer when marsh plants are dying and
1013 decomposing, as opposed to spring when marshes are in their productive stage (Jiang et al., 2008).
1014 These contrasting seasonal trends have already been reported for different estuarine systems in
1015 Georgia, such as the Altamaha Sound, the Sapelo Sound and the Doboy Sound (Cai, 2011). At the
1016 scale of the entire East coast of the US, the seasonal trends in *NEM* reveal a clear maximum in
1017 summer and minimal values during autumn and winter. The seasonality of FCO_2 is much less
1018 pronounced because the outgassing of oversaturated riverine waters throughout the year
1019 contributes to a large fraction of the FCO_2 and dampens the effect of the temperature dependent
1020 processes (*NEM* and denitrification). In our simulations, the competition between temperature and
1021 river discharge is the main driver of the seasonal estuarine carbon dynamics is. When discharge
1022 increases, the carbon loads increase proportionally and the residence time within the system
1023 decreases, consequently limiting an efficient degradation of organic carbon input fluxes. In warm

Deleted: Table

1025 regions like the SAR, the temperature is sufficiently high all year round to sustain high C processing
1026 rates and this explains the reduced seasonal variability in NEM.

1027

1028 3.3 Regional carbon budget: a comparative analysis

1029 The annual carbon budget for the entire East coast of the US is summarized in [Fig. 11a](#). The total
1030 carbon input to estuaries along the East coast of the US is 4.6 Tg C y^{-1} , of which 42% arrives in
1031 organic form and 58% in inorganic form. Of this total input, saltmarshes contribute 0.6 Tg C yr^{-1} ,
1032 which corresponds to about 14% of the total carbon loads and 32% of the organic loads in the
1033 region. The relative contribution of the saltmarshes to the total carbon input increases towards low
1034 latitudes and is as high as 60% in the SAR region. Model results suggest that 2.7 Tg C y^{-1} is exported
1035 to the continental shelf (25% as TOC and 75% as DIC), while 1.9 Tg C y^{-1} is emitted to the
1036 atmosphere. The overall carbon filtering capacity of the region thus equals 41% of the total carbon

Deleted: fig

Deleted: 9a

1037 entering the [43](#) estuarine systems (river + saltmarshes). Because of the current lack of a benthic
1038 module in C-GEM, the water column carbon removal occurs entirely in the form of CO_2 outgassing
1039 and does not account for the potential contribution of carbon burial in sediments. The estimated
1040 estuarine carbon retention presented here is thus likely a lower bound estimate. Reported to the
1041 modeled surface area of the region, the total FCO_2 of 1.9 Tg C y^{-1} translates into a mean air water
1042 CO_2 flux of about 14 mol C $\text{m}^{-2} \text{y}^{-1}$. This value is slightly higher than the estimate of 10.8 mol C $\text{m}^{-2} \text{y}^{-1}$
1043 calculated by Laruelle et al., (2013) on the basis of local $\overline{\text{FCO}_2}$ estimates assumed to be
1044 representative of yearly averaged conditions (see section 2.1). The latter was calculated as the
1045 average of 13 annual $\overline{\text{FCO}_2}$ values reported in the literature ([Tab. 2](#)), irrespective of the size of the
1046 systems. This approach is useful and widely used to derive regional and global carbon budgets
1047 (Borges et al., 2005; Laruelle et al., 2010; Chen et al., 2013). However, it may lead to potentially
1048 significant errors (Volta et al., 2016a) due to the uncertainty introduced by the spatial interpolation

Deleted: 47

Deleted: table

Deleted: 3

1054 of local measurements to large regional surface areas, while useful and widely used to derive
1055 regional and global carbon budgets.

1056 Regional C budgets are sparse. To our knowledge, the only other published regional assessment of
1057 the estuarine carbon and CO₂ dynamics comes from a relatively well studied region: the estuaries
1058 flowing into the North Sea in Western Europe (Fig. [11b](#)). This budget was calculated using a similar
1059 approach (Volta 2016a) and thus provides an ideal opportunity for a comparative assessment of C
1060 cycling in these regions. However, it is important to note that there are also important differences in
1061 the applied model approaches and those differences should be taken into account when comparing
1062 the derived budgets. In particular, the NW European study is based on a simulation of the 6 largest
1063 systems only (Elbe, Scheldt, Thames, Ems, Humber and Weser), accounting for about 40% for the
1064 riverine carbon loads of the region. It assumes that the intensity of carbon processing and evasion in
1065 all other smaller estuaries discharging into the North Sea (16 % of the carbon loads) can be
1066 represented by the average of the 6 largest system simulation results. In addition, the Rhine-Meuse
1067 system, which alone accounts for 44% of the carbon riverine inputs of the region, was treated as a
1068 passive conduit with respect to carbon due to its very short freshwater residence time (Abril et al.,
1069 2002). The contribution of saltmarshes to the regional carbon budget was also ignored because their
1070 total surface area is much smaller than along the US East coast (Regnier et al., 2013b). Another
1071 important difference is the inclusion of seasonality in the present study while the budget calculated
1072 for the North Sea is derived from yearly average conditions (Volta et al., 2016a).

1073 Overall, although both regions receive similar amounts of C from rivers (4.6 Tg C y⁻¹ and 5.9 Tg C y⁻¹
1074 for the East coast of the US and the North Sea, respectively), they reveal significantly different C
1075 filtering capacities. While the estuaries of the East coast of the US filter 41% of the riverine TC loads,
1076 those from the North Sea only remove 8% of the terrestrial-derived material. This is partly due to the
1077 large amounts of carbon transiting through the 'passive' Rhine-Meuse system. The regional filtering
1078 capacity is higher (15%) when this system is excluded from the analysis. However, even when

Deleted: 9b

1080 neglecting this system, significant differences in filtering efficiencies between both regions remain.
1081 FCO_2 from the North Sea estuaries (0.5 Tg C y^{-1}) is significantly lower than the 1.9 Tg C y^{-1} computed
1082 for the East coast of the US. The reason for the lower evasion rate in NW European estuaries is
1083 essentially twofold. First, the total cumulative surface area available for gas exchange is significantly
1084 lower along the North Sea, in spite of comparable flux densities calculated using the entire estuarine
1085 surface areas of both regions ($14 \text{ mol C m}^{-2} \text{ y}^{-1}$ and $23 \text{ mol C m}^{-2} \text{ y}^{-1}$ for the East coast of the US and
1086 the North Sea, respectively). Second, although the overall riverine carbon loads are comparable in
1087 both regions (Fig. [11](#)), the ratio of organic to inorganic matter input is much lower in the North Sea
1088 area because of the regional lithology is dominated by carbonate rocks and mixed sediments that
1089 contain carbonates (Dürr et al., 2005; Hartmann et al., 2012). As a consequence, TOC represents less
1090 than 20% of the riverine loads and only 10% of the carbon exported to the North Sea. In both
1091 regions, however, the increase of the inorganic to organic carbon ratio between input and output is
1092 sustained by a negative NEM (Fig. [11](#)). Although the ratios themselves may significantly vary from a
1093 region of the world to the other as evidenced by these two studies, a NEM driven increase of the
1094 inorganic fraction within carbon load along the estuarine axis is consistent with the global estuarine
1095 carbon budget proposed by Bauer et al. (2013). In the East coast of the US, the respiration of riverine
1096 OC within the estuarine filter is partly compensated by OC inputs from marshes and mangroves in
1097 such a way that the input and export IC/OC ratios are closer than in the North Sea region.

Deleted: 9

Deleted: 9

1098 **3.4 Scope of applicability and model limitations**

1099 Complex multidimensional models are now increasingly applied to quantitatively explore carbon and
1100 nutrient dynamics along the land-ocean transition zone over seasonal and even annual timescales
1101 (Garnier et al., 2001; Arndt et al., 2007, 2009; Arndt and Regnier, 2007; Mateus et al., 2012).
1102 However, the application of such complex models remains limited to individual, well-constrained
1103 systems due their high data requirements and computational demand resulting from the need to
1104 resolve important physical, biogeochemical and geological processes on relevant temporal and

1107 spatial scales. The one-dimensional, computationally efficient model C-GEM has been specifically
1108 designed to reduce data requirements and computational demand and to enable regional/global
1109 scale applications (Volta et al., 2014, 2016a). However, such a low data demand and computational
1110 efficiency inevitably requires simplification. The following paragraphs critically discuss these
1111 simplifications and their implications.

1112 *Spatial resolution*

1113 Here, C-GEM is used with a 0.5° spatial resolution. While this resolution captures the features of
1114 large systems, it is still very coarse for relatively small watershed, such as those of the St. Francis
1115 River, Piscataqua River, May River or the Sapelo River. For instance, the 5 estuaries reported by Hunt
1116 et al. (2010, 2011, see section 2.6) are all small systems contained by the same watershed at a 0.5°
1117 resolution. Only watersheds whose area spans several grid cells can be properly identified and
1118 represented (i.e. Merrimack or Penobscot with 6 and 9 cells, respectively).

1120 *Hydrodynamic and Transport Model*

1121 C-GEM is based on a theoretical framework that uses idealized geometries and significantly reduces
1122 data requirements. These idealized geometries are fully described by three, easily obtainable
1123 geometrical parameters (B, b_0 , H). The model thus approximates the variability of estuarine width
1124 and cross-section along the longitudinal axis through a set of exponential functions. A
1125 comprehensive sensitivity study (Volta et al., 2014) has shown that integrated process rates are
1126 generally sensitive to changes in these geometrical parameters because of their control on estuarine
1127 residence times. For instance, Volta et al. (2014) demonstrated that the NEM, is particularly sensitive
1128 to the convergence length. Similarly, the use of constant depth profile may lead to variations of
1129 about 10% in NEM (Volta et al., 2014). Nevertheless, geometrical parameters are generally easy to
1130 constrain, especially well-monitored regions such as the US east coast. Here, all geometrical
1131 parameters are constrained on the basis of observed estuarine surface areas and average water

1132 depths. In addition, the model also accounts for the slope of the estuarine channel. This approach
1133 ensures that simulated estuarine surface areas, volumes and, thus, residence times are in good
1134 agreement with those of the real systems and minimizes uncertainties associated to the physical set-
1135 up.

1136 In addition, the one-dimensional representation of the idealized estuarine systems does not resolve
1137 two- or three-dimensional circulation features induced by complex topography and density driven
1138 circulation. While C-GEM performs well in representing the dominant longitudinal gradients, its
1139 applicability to branched systems or those with aspect ratios for which a dominant axis is difficult to
1140 identify (e.g. Blackwater estuary, UK; Pearl River estuary, China; Tagus estuary, Portugal; Bay of
1141 Brest, France) is limited.

1142 *Biogeochemical Model*

1143 Although the reaction network of C-GEM accounts for all processes that control estuarine FCO_2
1144 (Borges and Abril, 2012; Cai, 2011), several, potentially important processes, such as benthic-pelagic
1145 exchange processes, phosphorous sorption/desorption and mineral precipitation, a more complex
1146 representation of the local phytoplankton community, grazing by higher trophic levels, or multiple
1147 reactive organic carbon pools are not included. Although these processes are difficult to constrain
1148 and their importance for FCO_2 is uncertain, the lack of their explicit representations induces
1149 uncertainties in C_{filt} . In particular, the exclusion of benthic processes such as organic matter
1150 degradation and burial in estuarine sediments could result in an underestimation of C_{filt} . However,
1151 because very little is known on the long term fate of organic carbon in estuarine sediments, setting
1152 up and calibrating a benthic module proves a difficult task. Furthermore, to a certain degree model
1153 parameters (such as organic matter degradation and denitrification rate constant) implicitly account
1154 for benthic dynamics. We nonetheless acknowledge that, by ignoring benthic processes and burial in
1155 particular, our estimates for the estuarine carbon filtering may be underestimated, particularly in
1156 the shallow systems of the SAR.

1157 Biogeochemical model parameters for regional and global applications are notoriously difficult to
1158 constrain (Volta et al., 2016b). Model parameters implicitly account for processes that are not
1159 explicitly resolved and their transferability between systems is thus limited. In addition, published
1160 parameter values are generally biased towards temperate regions in industrialized countries (Volta
1161 et al., 2016b). A first order estimation of the parameter uncertainty associated to the estuarine
1162 carbon removal efficiency (C_{filt}) can be extrapolated from the extensive parameter sensitivity
1163 analyses carried out by Volta et al. (2014, 2016b). These comprehensive sensitivity studies on end-
1164 member systems have shown that the relative variation in C_{filt} when a number of key
1165 biogeochemical parameters are varied by two orders of magnitude varies by is ±15 % in prismatic
1166 (short residence time on order of days) to ±25 % in funnel-shaped (long residence time) systems.
1167 Thus, assuming that uncertainty increases linearly between those bounds as a function of residence
1168 time, an uncertainty estimate can be obtained for each of our modelled estuary. With this simple
1169 method, the simulated regional C_{filt} of 1.9 Tg C yr⁻¹ would be associated with an uncertainty range
1170 comprised between 1.5 and 2.2 Tg C yr⁻¹. Our regional estuarine CO₂ evasion estimate is thus
1171 reported with moderate confidence. Furthermore, in the future, this uncertainty range could be
1172 further constrained using statistical methods such as Monte Carlo simulations (e.g. Lauerwald et al.,
1173 2015).

1174 *Boundary Conditions and Forcings*

1175 In addition, simulations are only performed for climatological means over the period 1990-2010
1176 without resolving interannual and secular variability. Boundary conditions and forcings are critical as
1177 they place the modelled system in its environmental context and drive transient dynamics. However,
1178 for regional applications, temporally resolved boundary conditions and forcings are difficult to
1179 constrain. C-GEM places the lower boundary condition 20 km from the estuarine mouth into the
1180 coastal ocean and the influence of this boundary condition on simulated biogeochemical dynamics is
1181 thus limited. At the lower boundary condition, direct observations for nutrients and oxygen are

1182 extracted from databases such as the World Ocean Atlas (Antonov et al., 2014). However, lower
1183 boundary conditions for OC and pCO₂ (zero concentration for OC and assumption of pCO₂
1184 equilibrium at the sea side) are simplified. This approach does not allow addressing the additional
1185 complexity introduced by biogeochemical dynamics in the estuarine plume (see Arndt et al., 2011).
1186 Yet, these dynamics only play a secondary role in the presented study that focuses on the role of the
1187 estuarine transition zone in processing terrestrial-derived carbon.

1188 Constraining upper boundary conditions and forcings is thus more critical. Here, C-GEM is forced by
1189 seasonally-averaged conditions for Q, T, and radiation. To date, GlobalNEWS only provide yearly-
1190 averaged conditions for a number of upper boundary conditions (Seitzinger et al., 2005; Mayorga et
1191 al., 2010), representative of the year 2000. Simulations are thus only partly transient (induced by
1192 seasonality in Q, T and radiation) and do not resolve short-lived events such as storms or extreme
1193 drought conditions. In addition, direct observations of upper boundary conditions are rarely
1194 available- in particular over seasonal or annual timescales. For the US East Coast estuaries, direct
1195 observations are only available for O₂, chlorophyll a, DIC and Alk. For DIC and alkalinity and boundary
1196 conditions are constrained by calculating the average concentration over a period of about three
1197 decades. In addition, observational data is extracted at the station closest to the model's upper
1198 boundary, which might be still located several kilometres upstream or downstream of the model
1199 boundary. Upper boundary conditions of POC, DOC, DIN, DIP, DSi are extracted from GlobalNews
1200 and thus model-derived. As a consequence, our results are thus intimately dependent on the
1201 robustness of the GlobalNEWS predictions. These values are usually only considered robust
1202 estimates for watersheds larger than ~10 cells (Beusen et al., 2005), which only correspond to 13 of
1203 the 43 estuaries modelled in this study.

1204 *Model-data comparison*

1205 The generic nature of the applied model approach and, in particular the application of
1206 seasonally/annually averaged or model-deduced boundary conditions renders a direct validation of

1207 model results on the basis of local and instantaneous observational data (e.g. longitudinal profiles),
1208 which is likely not representative of these long-term average conditions, difficult. Therefore, model
1209 performance is evaluated on the basis of spatially aggregated estimates (e.g. regional $\overline{FCO_2}$ estimates
1210 based on local measurements) rather than system-to-system comparisons with longitudinal profile
1211 from specific days. However, note that the performance of C-GEM has been intensively tested by
1212 specific model-data comparisons for a number of different systems (e.g. Volta et al., 2014, 2016a)
1213 and we are thus confident of its predictive capabilities.

1214 Despite the numerous simplifying assumptions inevitably required for such a regional assessment of
1215 carbon fluxes along the land-ocean continuum, the presented approach does nevertheless provide
1216 an important step forward in evaluating the role of land-ocean transition systems in the global
1217 carbon cycle. It provides a first robust estimate of carbon dynamics based on a theoretically well-
1218 founded and carefully tested, spatially and temporally resolved model approach. This approach
1219 provides novel insights that go beyond those gained through traditionally applied zero-salinity
1220 method or box model approaches. In addition, it also highlights critical variables and data gaps and
1221 thus helps guide efficient monitoring strategies.

1222 **3.5 Towards predictors of the estuarine carbon processing**

Deleted: 4

1223 The mutual dependence between geometry and transport in tidal estuaries and, ultimately, their
1224 biogeochemical functioning (Savenije, 1992; Volta et al., 2014) allows relating easily extractable
1225 parameters linked to their shape or their hydraulic properties to biogeochemical indicators. In this
1226 section, we explore the relationships between such simple physical parameters and indicators of the
1227 estuarine carbon processing \overline{NEM} , $\overline{FCO_2}$ and $CFilt$. In order to account for the effect of temperature
1228 on C dynamics, $-\overline{NEM}$ and $\overline{FCO_2}$ are also normalized to the same temperature (arbitrarily chosen to
1229 be 0 degree). These normalized values are obtained by dividing $-\overline{NEM}$ and $\overline{FCO_2}$ by a Q_{10} function
1230 $f(T)$ (see Volta et al., 2014). This procedure allows accounting for the exponential increase in the rate
1231 of several temperature dependent processes contributing to the NEM (i.e. photosynthesis, organic

Deleted:

1234 carbon degradation...). Applying the same normalization to \overline{NEM} and $\overline{FCO_2}$ is a way of testing how
1235 intimately linked \overline{NEM} and $\overline{FCO_2}$ are in estuarine systems. Indeed linear relationships relating one to
1236 the other have been reported (Mayer and Eyre, 2012). The three indicators are then investigated as
1237 a function of the ratio between the estuarine surface S and the seasonal river discharge Q . The
1238 surface area is calculated from the estuarine width and length, as described by equation 2, in order
1239 to use a parameter which is potentially applicable to other regions for which direct estimates of the
1240 real estuarine surface area is not available. Since the fresh water residence time of a system is
1241 obtained by dividing volume by river discharge, the S/Q ratio is also intimately linked to residence
1242 time. Here, we choose to exclude the estuarine depth from the analysis because this variable cannot
1243 be easily quantified from maps or remote sensing images and would thus compromise the
1244 applicability of a predictive relationship on the global scale. However, from dimensional analysis, S/Q
1245 can be viewed as a water residence time normalized to meter depth of water. As shown by equation
1246 3, S only requires constraining BO and width convergence length b , two parameters that can readily
1247 be extracted from the Google Earth engine. Global database of river discharges, as for instance
1248 RivDIS (Vörösmarty et al., 1996) are also available in such a way that the S/Q ratio can potentially be
1249 extracted for all estuaries around the globe.

Formatted: Font: Italic
Formatted: Font: Italic
Formatted: Font: Italic, Subscript

1250 Figure [12a](#) reveals that small values of S/Q are associated with the most negative $\overline{NEM} / f(T)$. The
1251 magnitude of the \overline{NEM} then exponentially decreases with increasing values of S/Q . Estuaries
1252 characterized by small values of S/Q are mainly located in the NAR sub-region and correspond to
1253 small surface area, and thus short residence time systems. It is possible to quantitatively relate -
1254 $\overline{NEM} / f(T)$ and S/Q through a power law function ($y = 25.85 x^{-0.64}$ with a $r^2 = 0.82$). The coefficient
1255 of determination remains the same when excluding estuaries from the NAR region and the equation
1256 itself is not significantly different, although those estuaries on their own do not display any
1257 statistically significant trend ([Tab. 6](#)). The decrease in the intensity of the net ecosystem metabolism
1258 in larger estuaries (Fig [8](#)), characterized by high S/Q ratios, can be related to the extensive

Deleted: 10a

Deleted: table

Deleted: 6

1262 consumption of the organic matter pool during its transit through the estuarine filter. However,
1263 when reported to the entire surface area of the estuary, larger systems (with high values of S/Q) still
1264 reveal the most negative surface integrated NEM (Fig. 12b). It can also be noted that some estuaries
1265 from the NAR region display very low values of $-NEM$. These data points correspond to fall and
1266 winter simulations for which the temperature was relatively cold (<5 °C) and biogeochemical
1267 processing was very low.

Deleted: fig

Deleted: 10b

1268 The overall response of $\overline{FCO_2}/f(T)$ to S/Q is comparable to that of $-\overline{NEM}/f(T)$ (Fig. 12c), with
1269 lower values of $\overline{FCO_2}$ observed for high values of S/Q. However, for $S/Q < 3$ days m^{-1} , the $\overline{FCO_2}$
1270 values are very heterogeneous and contain many, low $\overline{FCO_2}$ outliers from the NAR region. These
1271 data points generally correspond to low water temperature conditions which keep pCO_2 low, even if
1272 the system generates enough CO_2 internally via NEM. Thus, the well-documented correlation
1273 between \overline{NEM} and $\overline{FCO_2}$ (Maher and Eyre, 2012) does not seem to hold for systems with very short
1274 residence times. For systems with $S/Q > 3$ days m^{-1} , we obtain a regression $FCO_2 = -0.64 \times NEM + 5.96$
1275 with a r^2 of 0.46, which compares well with the relation $FCO_2 = -0.42 \times NEM + 12$ proposed by Maher
1276 and Eyre (2012) who used 24 seasonal estimates from small Australian estuaries. However, our
1277 results suggest that this relationship cannot be extrapolated to small systems such as those located
1278 in the NAR. Figure 12d, which reports non-normalized FCO_2 reveals a monotonous increase of FCO_2
1279 with S/Q. This suggests that, unlike the NEM for which the normalization by a temperature function
1280 allowed explaining most of the variability; FCO_2 is mostly controlled by the water residence time
1281 within the system. Discharge is the main FCO_2 driver in riverine dominated systems, while
1282 interactions with marshes are driving the outgassing in marine dominated systems surrounded by
1283 marshes. Net aquatic biological production (NEM being negative or near 0) in large estuaries (with
1284 large S/Q) is another important reason for low FCO_2 in such systems. For example, despite the higher
1285 CO_2 degassing flux in the upper estuary of the Delaware, strong biological CO_2 uptake in the mid-bay
1286 and near zero NEM in the lower bay result in a much lower FCO_2 for the entire estuary (Joesoef et al.

Deleted: 10c

Deleted: m

Formatted: Font: Italic

1291 2015). In systems with $S/Q < 3 \text{ days m}^{-1}$, the short residence time prevents the excess CO_2 of
1292 oversaturated water from being entirely exchanged with the atmosphere and simulations reveal that
1293 the estuarine waters are still oversaturated in CO_2 at the estuarine mouth. Thus, the inorganic
1294 carbon, produced by the decomposition of organic matter, is not outgassed within the estuary but
1295 exported to the adjacent continental shelf waters. This result is consistent with the observation-
1296 based hypothesis of Laruelle et al. (2015) for the NAR estuaries. As a consequence of the distinct
1297 behavior of short residence time systems, the coefficient of determination of the best-fitted power
1298 law function relating $\overline{FCO_2}$ and S/Q is only significant if NAR systems are excluded ($y = 31.64 x^{-0.58}$

1299 with a $r^2 = 0.70$). This thus suggest that such relationships (as well as that proposed by Maher and
1300 Eyre, 2012) cannot be applied to any system but only those for which $S/Q > 3 \text{ day m}^{-1}$.

Formatted: Superscript

1301 Finally, Fig. 12e reports the simulated mean seasonal carbon filtering capacities as a function of the
1302 depth normalized residence time. Not surprisingly, and in overall agreement with previous studies
1303 on nutrient dynamics in estuaries (Nixon et al., 1996), the carbon filtering capacity increases with
1304 S/Q . The best statistical relation between $CFilt$ and S/Q is obtained when including all 3 regions,
1305 resulting in $r^2 = 0.70$ ($y = 40.64 \log_{10}(x) + 11.84$). Very little C removal occurs in systems with $S/Q < 1$
1306 day m^{-1} . For systems characterized by longer depth-normalized residence times, $CFilt$ increases
1307 regularly, and reaches 100% for $S/Q > 100 \text{ day m}^{-1}$. Such high values are only observed for very large
1308 estuaries from the MAR region (Delaware and Chesapeake Bays); the majority of our systems had an
1309 S/Q range between 1 and 100 day m^{-1} . The quantitative assessment of estuarine filtering capacities
1310 is further complicated by the complex interplay of estuarine and coastal processes. Episodically,
1311 marked spatial variability in concentration gradients near the estuarine mouth may lead to a reversal
1312 of net material fluxes from coastal waters into the estuary (Regnier et al., 1998; Arndt et al. 2011).
1313 Our results show that this feature is particularly significant for estuaries with a large width at the
1314 mouth and short convergence length (funnel shaped or 'Bay type' systems). These coastal nutrient
1315 and carbon inputs influence the internal estuarine C dynamics and lead to filtering capacities that

Deleted: Figure

Deleted: 10e

1318 can exceed 100%. This feature is particularly significant in summer, when riverine inputs are low and
1319 the marine material is intensively processed inside the estuary.

1320 Previous work investigated the relationship between fresh water residence time and nutrient
1321 retention (Nixon et al., 1996; Arndt et al., 2011; Laruelle, 2009). These studies, however, were
1322 constrained by the scarcity of data. For instance, the pioneering work of Nixon et al. (1996) only
1323 relied on a very limited number (<10) of quite heterogeneous coastal systems, all located along the
1324 North Atlantic. Here, our modeling approach allows us to generate 172 (43 x 4) data points, each
1325 representing a system-scale biogeochemical behavior. Together, this database spans the entire
1326 spectrum of estuarine settings and climatic conditions found along the East coast of the US. In
1327 addition, the ratio S/Q used as master variable for predicting temperature normalized $\overline{-NEM}$, $\overline{FCO_2}$
1328 and $CFilt$ only requires a few easily accessible geometric parameters (B_0 , b and L) and an estimate of
1329 the river discharge. While it is difficult to accurately predict $\overline{FCO_2}$ for small systems such as those
1330 located in the NAR region, the relationships found are quite robust for systems in which $S/Q > 3$ days
1331 m^{-1} . Most interestingly, $CFilt$ values reveal a significant correlation with S/Q and could be used in
1332 combination with global riverine carbon delivery estimates such as GlobalNews 2 (Mayorga et al.,
1333 2010) to constrain the estuarine CO_2 evasion and the carbon export to the coastal ocean at the
1334 continental and global scales.

1335 **4. Conclusions**

1336 This study presents the first complete estuarine carbon budget for the East coast of the US using a
1337 modeling approach. The structure of the model C-GEM relies on a restricted number of readily
1338 available global datasets to constrain boundary conditions and limits the number of geometrical and
1339 physical parameters to be constrained. Our simulations predict a total CO_2 outgassing of $1.9 \text{ Tg C } \gamma^{-1}$
1340 for all tidal estuaries of the East coast of the US. This quantification accounts for the seasonality in
1341 estuarine carbon processing as well as for distinct individual behaviors among estuarine types
1342 (marine or river dominated). The total carbon output to the coastal ocean is estimated at $2.7 \text{ TgC } \gamma^{-1}$,

1343 and the carbon filtering capacity with respect to riverine, marshes and mangrove inputs is thus on
1344 the order of 40%. This value is significantly higher than the recently estimated C filtering capacity for
1345 estuaries surrounding the North Sea using a similar approach (Volta et al., 2016a), mainly because
1346 the surface area available for gas exchange and the draining lithology limits the CO₂ evasion in the
1347 NW European systems. At the regional scale of the US East coast estuaries, net heterotrophy is the
1348 main driver (50%) of the CO₂ outgassing, followed by the ventilation of riverine supersaturated
1349 waters entering the estuarine systems (32%) and nitrification (18%). The dominant mechanisms for
1350 the gas exchange and the resulting carbon filtering capacities nevertheless reveal a clear latitudinal
1351 pattern, which reflects the shapes of estuarine systems, climatic conditions and dominant land-use
1352 characteristics.

1353 Our model results are used to derive predictive relationships relating the intensity of the area-based
1354 Net Ecosystem Metabolism (\overline{NEM}), air-water CO₂ exchange ($\overline{FCO_2}$) and the carbon filtering capacity
1355 ($CFilt$) to the depth normalized residence time, expressed as the ratio of the estuarine surface area
1356 to the river discharge. In the future, such simple relationships relying on readily available geometric
1357 and hydraulic parameters could be used to quantify carbon processing in areas of the world devoid
1358 of direct measurements. However, it is important to note that such simple relationships are only
1359 valid over the range of boundary conditions and forcings explored and may not be applicable to
1360 conditions that fall outside of this range. In regions with better data coverage, such as the one
1361 investigated here, our study highlights that the regional-scale quantification, attribution, and
1362 projection of estuarine biogeochemical cycling are now at reach.

Formatted: Font: Not Bold, Not Italic,
No underline

Deleted: prediction

1363 5. Acknowledgements

1364 G. G. Laruelle is Chargé de recherches du F.R.S.-FNRS at the Université Libre de Bruxelles. The
1365 research leading to these results has received funding from the European Union's Horizon 2020
1366 research and innovation programme under the Marie Skłodowska-Curie grant agreement No 643052

1368 (C-CASCADES project). The authors thank V. L. Mulder for her thorough reading of the manuscript
1369 upon submission.

1370 |

1371 **References:**

- 1372 Abril, G., Nogueira, M., Etcheber, H., Cabeçadas, G., Lemaire, E., and Brogueira, M.J.: Behaviour of
1373 organic carbon in nine contrasting European estuaries. *Estuar. Coast. Shelf Sci.*, 54, 241-262,
1374 2002.
- 1375 Antonov, J.I., Seidov, D., Boyer, T.P., Locarnini, R.A., Mishonov, A.V., Garcia, H.E., Baranova, O.K.,
1376 Zweng, M.M., and Johnson, D.R.: *World Ocean Atlas 2009, Volume 2: Salinity*. S., 2010.
- 1377 Arndt, S., Vanderborght, J.P., and Regnier, P.: Diatom growth response to physical forcing in a
1378 macrotidal estuary: Coupling hydrodynamics, sediment transport, and biogeochemistry.
1379 *Journal of Geophysical Research C: Oceans*, 112(5), 2007.
- 1380 [Arndt, S. and Regnier, P.: A model for the benthic-pelagic coupling of silica in estuarine ecosystems:
1381 sensitivity analysis and system scale simulation, *Biogeosciences*, 4, 331–352, doi:10.5194/bg-
1382 4-331-2007, 2007.](#)
- 1383 Arndt, S., Regnier, P., and Vanderborght, J.P.: Seasonally-resolved nutrient export fluxes and filtering
1384 capacities in a macrotidal estuary. *Journal of Marine Systems*, 78(1), 42-58, 2009.
- 1385 Arndt, S., Lacroix, G., Gypens, N., Regnier, P., and Lancelot, C.: Nutrient dynamics and phytoplankton
1386 development along an estuary-coastal zone continuum: A model study. *Journal of Marine
1387 Systems*, 84(3-4), 49-66, 2011.
- 1388 Atlas, R., Hoffman, R.N., Ardizzone, J., Leidner, S.M., Jusem, J.C., Smith, D.K. and Gombos, D.: A
1389 cross-calibrated, multiplatform ocean surface wind velocity product for meteorological and
1390 oceanographic applications. *Bulletin of the American Meteorological Society*, 92(2), 157-174,
1391 2011.
- 1392 [Baklouti, M., Chevalier, C., Bouvy, M., Corbin, D., Pagano, M., Troussellier, M., and Arfi, R.: A study of
1393 plankton dynamics under osmotic stress in the Senegal River Estuary, West Africa, using a 3D
1394 mechanistic model, *Ecol. Model.*, 222, 2704–2721, 2011.](#)
- 1395 Bauer, J.E., Cai, W.J., Raymond, P.A., Bianchi, T.S., Hopkinson, C.S., and Regnier, P.A.G.: The changing
1396 carbon cycle of the coastal ocean. *Nature*, 504(7478), 61-70, 2013.
- 1397 [Beusen, A. H.W., Dekkers, A. L. M., Bouwman, A. F., Ludwig, W., and Harrison, J.: Estimation of global
1398 river transport of sediments and associated particulate C, N, and P, *Global Biogeochem. Cy.*,
1399 19, GB4S05, doi:10.1029/2005GB002453, 2005.](#)
- 1400 Beusen, A.H.W., Bouwman, A.F., Dürr, H.H., Dekkers, A.L.M., and Hartmann, J.: Global patterns of
1401 dissolved silica export to the coastal zone: Results from a spatially explicit global model.
1402 *Global Biogeochemical Cycles*, 23, GB0A02, doi:10.1029/2008GB003281, 2009.
- 1403 Billen, G., Thieu, V., Garnier, J., and Silvestre, M.: Modelling the N cascade in regional waters: The
1404 case study of the Seine, Somme and Scheldt rivers, *Agr. Ecosyst. Environ.*, 133, 234–246,
1405 2009.
- 1406 Borges, A.V., Delille, B., and Frankignoulle, M.: Budgeting sinks and sources of CO₂ in the coastal
1407 ocean: Diversity of ecosystems counts. *Geophys. Res. Lett.*, 32(14), L14601, 2005.
- 1408 Borges, A.V., and Abril, G.: Carbon Dioxide and Methane Dynamics in Estuaries. In: E. Wolanski and
1409 D.S. McLusky (Editors), *Treatise on Estuarine and Coastal Science*. Academic Press, Waltham,
1410 pp. 119–161, 2012.
- 1411 Bricker, S., Longstaff, B., Dennison, W., Jones, A., Boicourt, K., Wicks, C., and Woerner, J.: Effects of
1412 Nutrient Enrichment In the Nation's Estuaries: A Decade of Change, NOAA, MD, 2007.
- 1413 Brock, T.D.: Calculating solar radiation for ecological studies. *Ecological Modelling*, 14(1-2), 1-19,
1414 1981.
- 1415 Caffrey, J.: Factors controlling net ecosystem metabolism in U.S. estuaries. *Estuaries*, 27(1), 90-101,
1416 2004.
- 1417 Cai, W.J., and Wang, Y.: The chemistry, fluxes, and sources of carbon dioxide in the estuarine waters
1418 of the Satilla and Altamaha Rivers, Georgia. *Limnology and Oceanography*, 43(4), 657-668,
1419 1998.
- 1420 [Cai, W.J., Wang, Y., and Hodson, R. E.: Acid-base properties of dissolved organic matter in the
1421 estuarine waters of Georgia, USA. *Geochimica et Cosmochimica Acta*, 62\(3\), 473-483, 1998.](#)

Deleted: ¶

Formatted: English (U.K.)

Formatted: English (U.K.)

Deleted: ¶

Formatted: English (U.K.)

Formatted: English (U.K.)

1424 Cai, W.J., Pomeroy, L.R., Moran, M.A., and Wang, Y.: Oxygen and carbon dioxide mass balance for
1425 the estuarine-intertidal marsh complex of five rivers in the southeastern U.S. *Limnology and*
1426 *Oceanography*, 44, 639-649, 1999.

1427 Cai, W.J.: Estuarine and coastal ocean carbon paradox: CO₂ sinks or sites of terrestrial carbon
1428 incineration? *Ann. Rev. Mar. Sci.*, 3, 123-145, 2011.

1429 [Cercio, C., Kim, S.-C., and Noel, M.: The 2010 Chesapeake Bay eutrophication model. US](#)
1430 [Environmental Protection Agency Chesapeake Bay Program, Annapolis, MD, 2010.](#)

1431 Chen, C.-T.A., Huang, T.-H., Fu, Y.-H., Bai, Y., and He, X.: Strong sources of CO₂ in upper estuaries
1432 become sinks of CO₂ in large river plumes. *Current Opinion in Environmental Sustainability*,
1433 4(2), 179-185, 2012.

1434 Chen, C.-T. A., Huang, T.-H., Chen, Y.-C., Bai, Y., He, X., and Kang, Y.: Air-sea exchanges of CO₂ in the
1435 world's coastal seas, *Biogeosciences*, 10, 6509–6544, doi:10.5194/bg-10-6509-2013, 2013.

1436 Dai, T., and Wiegert, R.G.: Estimation of the primary productivity of *Spartina alterniflora* using a
1437 canopy model. *Ecography*, 19(4), 410-423, 1996.

1438 [Dufore, C. M.: Spatial and Temporal Variations in the Air-Sea Carbon Dioxide Fluxes of Florida Bay,](#)
1439 [Graduate School Thesis, University of South Florida, 2012.](#)

1440 Dürr, H.H., Meybeck, M., and Dürr, S.H.: Lithological composition of the Earth's continental surfaces
1441 derived from a new digital map emphasizing riverine material transfer. *Glob. Biogeochem.*
1442 *Cycles* 19 (4), GB4S10, 2005.

1443 Dürr, H.H., Laruelle, G.G., van Kempen, C.M., Slomp, C.P., Meybeck, M., and Middelkoop, H.:
1444 Worldwide Typology of Nearshore Coastal Systems: Defining the Estuarine Filter of River
1445 Inputs to the Oceans. *Estuaries and Coasts*, 34(3), 441-458, 2011.

1446 EPA (2009). "1970 - 2008 Average annual emissions, all criteria pollutants in MS Excel." National
1447 Emissions Inventory (NEI) Air Pollutant Emissions Trends Data. Office of Air Quality Planning
1448 and Standards. Available online at <<http://www.epa.gov/ttn/chieftrends/index.html>>

1449 Fekete, B.M., Vörösmarty, C.J., and Grabs, W.: High-resolution fields of global runoff combining
1450 observed river discharge and simulated water balances. *Global Biogeochemical Cycles*, 16(3),
1451 15-1, 2002.

1452 Fischer, H. B.: Mixing and Dispersion in Estuaries, *Annu. Rev. Fluid Mech.*, 8, 107–133,
1453 1976. Friedrichs, M.A.M., and Hofmann, E.E.: Physical control of biological processes in the
1454 central equatorial Pacific Ocean. *Deep-Sea Research Part I: Oceanographic Research Papers*,
1455 48(4), 1023-1069, 2001.

1456 Garcia, H.E., Locarnini, R.A., Boyer, E.W., Antonov, A., Baranova, O.K., Zweng, M.M., and Johnson,
1457 D.R.: *World Ocean Atlas 2009, Volume 3: Dissolved Oxygen, Apparent Oxygen Utilization,*
1458 *and Oxygen Saturation, 2010a.*

1459 Garcia, H.E., Locarnini, R.A., Boyer, E.W., Antonov, J.I., Baranova, O.K., Zweng, M.M., and Johnson,
1460 D.R.: *World Ocean Atlas 2009, Volume 4: Nutrients (phosphate, nitrate, silicate), 2010b.*

1461 [Garnier, J., Servais, P., Billen, G., Akopian, M., and Brion, N.: Lower Seine River and Estuary \(France\)](#)
1462 [Carbon and Oxygen Budgets During Low Flow, *Estuaries*, 24, 964–976, 2001.](#)

1463 Harrison, J.A., Caraco, N., and Seitzinger, S.P.: Global patterns and sources of dissolved organic
1464 matter export to the coastal zone: Results from a spatially explicit, global model. *Global*
1465 *Biogeochemical Cycles*, 19(4), GB4S03, doi:10.1029/2004GB002357, 2005.

1466 Hartmann, J., Jansen, N., Dürr, H.H., Kempe, S., and Köhler, P.: Global CO₂ consumption by chemical
1467 weathering: What is the contribution of highly active weathering regions? *Global Planet.*
1468 *Change*, 69(4), 185-194, 2009.

1469 Hartmann, J., Dürr, H.H., Moosdorf, N., Meybeck, M., and Kempe, S.: The geochemical composition
1470 of the terrestrial surface (without soils) and comparison with the upper continental crust.
1471 *Int. J. Earth Sci.* 101, 365-376, 2012.

1472 Herrmann, M., Najjar, R.G., Kemp, W.M., Alexander, R.B., Boyer, E.W., Cai, W.-J., Griffith, P.C.,
1473 Kroeger, K.D., McCallister, S.L., and Smith, R.A.: Net ecosystem production and organic

Deleted: F

1475 carbon balance of U.S. East Coast estuaries: A synthesis approach, *Global Biogeochem.*
1476 *Cycles*, 29, doi:10.1002/2013GB004736, 2015.

1477 Hofmann, A.F., Soetaert, K., and Middelburg, J.J.: Present nitrogen and carbon dynamics in the
1478 Scheldt estuary using a novel 1-D model. *Biogeosciences*, 5(4), 981-1006, 2008.

1479 [Hofmann, E.E., Cahill, B., Fennel, K., Friedrichs, M.A.M., Hyde, K., Lee, C., Mannino, A., Najjar, R.G.,
1480 O'Reilly, J.E., Wilkin, J., and Xue, J.: Modeling the dynamics of continental shelf carbon. *Ann
1481 Rev Mar Sci.* 3, 93-122, 2011.](#)

1482 Hunt, C. W., Salisbury, J. E., Vandemark, D., and McGillis, W.: Contrasting Carbon Dioxide Inputs and
1483 Exchange in Three Adjacent New England Estuaries. *Estuar. Coast.*, 34, 68–77,
1484 doi:10.1007/s12237-010-9299-9, 2010.

1485 Hunt, C.W., Salisbury, J.E., Vandemark, D., and McGillis, W.: Contrasting Carbon Dioxide Inputs and
1486 Exchange in Three Adjacent New England Estuaries. *Estuaries and Coasts*, 34(1), 68-77, 2011.

1487 Ippen, A.T., and Harleman, D.R.F.: One-dimensional Analysis of Salinity Intrusion in Estuaries,
1488 Technical Bulletin No. 5, Committee on Tidal Hydraulics, Corps of Engineers, US Army,
1489 Vicksburg, 1961.

1490 Jiang, L.Q., Cai, W.J., and Wang, Y.: A comparative study of carbon dioxide degassing in river- and
1491 marine-dominated estuaries. *Limnology and Oceanography*, 53(6), 2603-2615, 2008.

1492 Jiang, L.-Q., Cai, W.-J., Wang, Y., and Bauer, J. E.: Influence of terrestrial inputs on continental shelf
1493 carbon dioxide, *Biogeosciences*, 10, 839–849, doi:10.5194/bg-10-839-2013, 2013.

1494 Joesoef, A., Huang, W.-J., Gao, Y., and Cai, W.-J.: Air–water fluxes and sources of carbon dioxide in
1495 the Delaware Estuary: spatial and seasonal variability, *Biogeosciences*, 12, 6085-6101,
1496 doi:10.5194/bg-12-6085-2015, 2015.

1497 Kent, B.H.: Turbulent diffusion in a Sectionally Homogeneous Estuary, Technical Report 16,
1498 Chesapeake Bay Institute, John Hopkins, University, Baltimore, 1958.

1499 Key, R.M., Kozyr, A., Sabine, C.L., Lee, K., Wanninkhof, R., Bullister, J.L., Feely, R.A., Millero, F.J.,
1500 Mordy, C., and Peng, T.H.: A global ocean carbon climatology: Results from Global Data
1501 Analysis Project (GLODAP). *Global Biogeochemical Cycles*, 18(4), 1-23, 2004.

1502 Laruelle, G.G.: Quantifying nutrient cycling and retention in coastal waters at the global scale, Ph D
1503 dissertation, Utrecht University, 2009.

1504 Laruelle, G. G., Regnier, P., Ragueneau, O., Kempa, M., Moriceau, B., Ni Longphuiert, S., Leynaert, A.,
1505 Thouzeau, G., and Chauvaud, L.: Benthic-pelagic coupling and the seasonal silica cycle in the
1506 Bay of Brest (France): new insights from a coupled physical-biological model, *Mar. Ecol.-
1507 Prog. Ser.*, 385, 15–32, 2009.

1508 Laruelle, G.G., Dürr, H.H., Slomp, C.P., and Borges, A.V.: Evaluation of sinks and sources of CO₂ in the
1509 global coastal ocean using a spatially-explicit typology of estuaries and continental shelves.
1510 *Geophys. Res. Lett.*, 37(15), L15607, doi:10.1029/2010GL043691, 2010.

1511 Laruelle, G.G., Dürr, H.H., Lauerwald, R., Hartmann, J., Slomp, C.P., Goossens, N., and Regnier, P.A.G.:
1512 Global multi-scale segmentation of continental and coastal waters from the watersheds to
1513 the continental margins. *Hydrol. Earth Syst. Sci.*, 17(5), 2029-2051, 2013.

1514 Laruelle, G.G., Lauerwald, R., Rotschi, J. Raymond, P.A., and Regnier, P.: Seasonal response of air-
1515 water CO₂ exchange along the land-ocean aquatic continuum of the northeast North
1516 American coast. *Biogeosci.* 12, 1447-1458, 2015.

1517 Lauerwald, R., Hartmann, J., Moosdorf, N., Kempe, S., and Raymond, P.A.: What controls the spatial
1518 patterns of the riverine carbonate system? — A case study for North America. *Chemical
1519 Geology*, 337–338, 114-127, 2013.

1520 [Lauerwald, R., Laruelle, G. G., Hartmann, J., Clais, P., and Regnier, P. A. G.: Spatial patterns in CO₂
1521 evasion from the global river network, *Global Biogeochem. Cy.*, 29, 534–554,
1522 doi:10.1002/2014GB004941, 2015.](#)

1523 Leonard, B.: Third-Order Upwinding as a Rational Basis for Computational Fluid Dynamics, in:
1524 *Computational Techniques and Applications: CTAC-83*, edited by: Noye J. and Fletcher C. A.
1525 J., Elsevier, North-Holland, 1984.

- 1526 Le Quéré, C., Peters, G. P., Andres, R. J., Andrew, R. M., Boden, T. A., Ciais, P., Friedlingstein, P.,
 1527 Houghton, R. A., Marland, G., Moriarty, R., Sitch, S., Tans, P., Arneeth, A., Arvanitis, A., Bakker,
 1528 D. C. E., Bopp, L., Canadell, J. G., Chini, L. P., Doney, S. C., Harper, A., Harris, I., House, J. I.,
 1529 Jain, A. K., Jones, S. D., Kato, E., Keeling, R. F., Klein Goldewijk, K., Körtzinger, A., Koven, C.,
 1530 Lefèvre, N., Maignan, F., Omar, A., Ono, T., Park, G.-H., Pfeil, B., Poulter, B., Raupach, M. R.,
 1531 Regnier, P., Rödenbeck, C., Saito, S., Schwinger, J., Segschneider, J., Stocker, B. D., Takahashi,
 1532 T., Tilbrook, B., van Heuven, S., Viovy, N., Wanninkhof, R., Wiltshire, A., and Zaehle, S.:
 1533 Global carbon budget 2013, *Earth Syst. Sci. Data*, 6, 235-263, doi:10.5194/essd-6-235-2014,
 1534 2014.
- 1535 Le Quéré, C., Moriarty, R., Andrew, R. M., Canadell, J. G., Sitch, S., Korsbakken, J. I., Friedlingstein, P.,
 1536 Peters, G. P., Andres, R. J., Boden, T. A., Houghton, R. A., House, J. I., Keeling, R. F., Tans, P.,
 1537 Arneeth, A., Bakker, D. C. E., Barbero, L., Bopp, L., Chang, J., Chevallier, F., Chini, L. P., Ciais, P.,
 1538 Fader, M., Feely, R. A., Gkritzalis, T., Harris, I., Hauck, J., Ilyina, T., Jain, A. K., Kato, E., Kitidis,
 1539 V., Klein Goldewijk, K., Koven, C., Landschützer, P., Lauvset, S. K., Lefèvre, N., Lenton, A.,
 1540 Lima, I. D., Metzl, N., Millero, F., Munro, D. R., Murata, A., Nabel, J. E. M. S., Nakaoka, S.,
 1541 Nojiri, Y., O'Brien, K., Olsen, A., Ono, T., Pérez, F. F., Pfeil, B., Pierrot, D., Poulter, B., Rehder,
 1542 G., Rödenbeck, C., Saito, S., Schuster, U., Schwinger, J., Séférian, R., Steinhoff, T., Stocker, B.
 1543 D., Sutton, A. J., Takahashi, T., Tilbrook, B., van der Laan-Luijckx, I. T., van der Werf, G. R., van
 1544 Heuven, S., Vandemark, D., Viovy, N., Wiltshire, A., Zaehle, S., and Zeng, N.: Global Carbon
 1545 Budget 2015, *Earth Syst. Sci. Data*, 7, 349-396, doi:10.5194/essd-7-349-2015, 2015.
- 1546 [Lin, J., Xie, L., Pietrafesa, L. J., Ramus, J. S., and Paerl, H.W.: Water Quality Gradients across](#)
 1547 [Albemarle-Pamlico Estuarine System: Seasonal Variations and Model Applications, *J. Coast.*](#)
 1548 [Res., 23, 213–229, 2007.](#)
- 1549 Locarnini, R.A., Mishonov, A.V., Antonov, J.I., Boyer, T.P., Garcia, H.E., Baranova, O.K., Zweng, M.M.,
 1550 and Johnson, D.R.: World Ocean Atlas 2009, Volume 1: Temperature, 2010.
- 1551 Ludwig, W., Probst, J. L., and Kempe, S.: predicting the oceanic input of organic carbon by
 1552 continental erosion, *Global Biogeochem. Cy.*, 10, 23–41, 1996.
- 1553 Maher, D.T., and Eyre, B.D.: Carbon budgets for three autotrophic Australian estuaries: Implications
 1554 for global estimates of the coastal air-water CO₂ flux. *Global Biogeochem. Cycles*, 26(1),
 1555 GB1032, 2012.
- 1556 [Mateus, M., Vaz, N., and Neves, R.: A process-oriented model of pelagic biogeochemistry for marine](#)
 1557 [systems. Part II: Application to a mesotidal estuary, *J. Mar. Syst.*, 94, 90–101, 2012.](#)
- 1558 Mayorga, E., Seitzinger, S.P., Harrison, J.A., Dumont, E., Beusen, A.H.W., Bouwman, A.F., Fekete,
 1559 B.M., Kroeze, C., and Van Drecht, G.: Global Nutrient Export from WaterSheds 2 (NEWS 2):
 1560 Model development and implementation. *Environmental Modelling and Software*, 25(7),
 1561 837-853, 2010.
- 1562 Meybeck, M.: Carbon, nitrogen, and phosphorus transport by world rivers. *Am. J. Sci.*, 282(4), 401-
 1563 450, 1982.
- 1564 Meybeck, M., Dürr, H. H., and Vörosmary, C. J.: Global coastal segmentation and its river catchment
 1565 contributors: A new look at land-ocean linkage, *Global Biogeochem. Cy.*, 20, GB1S90,
 1566 doi:10.1029/2005GB002540, 2006.
- 1567 Middelburg, J.J., Klaver, G., Nieuwenhuize, J., Wielemaker, A., De Haas, W., Vlug, T., and Van Der
 1568 Nat, J.F.W.A.: Organic matter mineralization in intertidal sediments along an estuarine
 1569 gradient. *Marine Ecology Progress Series*, 132(1-3), 157-168, 1996.
- 1570 NASA/NGA: SRTM Water Body Data Product Specific Guidance, Version 2.0, 2003.
- 1571 Najjar, R.G., Friedrichs, M., and Cai, W.-J. (Editors): Report of The U.S. East Coast Carbon Cycle
 1572 Synthesis Workshop, January 19-20, 2012. Ocean Carbon and Biogeochemistry Program and
 1573 North American Carbon Program, 34 pp, 2012.
- 1574 Nihoul, J. C. J., and Runday, F.: Modèles d'estuaires partiellement stratifiés, *Projet Mer*, Vol. 10,
 1575 Service de la Programmation Scientifique, Bruxelles, Belgium, 71–98, 1976.

- 1576 Nixon, S.W., J.W. Ammerman, L.P. Atkinson, V.M. Berounsky, G. Billen, W.C. Boicourt, W.R. Boynton,
 1577 T.M. Church, D.M. Ditoro, R. Elmgren, J.H. Garber, A.E. Giblin, R.A. Jahnke, N.J. P. Owens,
 1578 M.E.Q. Pilson, and Seitzinger, S.P.: The fate of nitrogen and phosphorus at the land–sea
 1579 margin of the North Atlantic Ocean. *Biogeochemistry* 3, 141–180, 1996.
- 1580 NOAA: National Estuarine Inventory Data Atlas, Volume 1: Physical and Hydrologic Characteristics,
 1581 National Oceanic and Atmospheric Administration, MD, 1985.
- 1582 Odum, H.T.: Primary Production in Flowing Waters. *Limnol. Oceanogr.*, 1, 102-117, 1956.
- 1583 O'Kane, J. P.: Estuarine Water Quality Management. Pitman, London, U.K, 1980.
- 1584 Paerl, H.W., Valdes, L.M., Peierls, B.L., Adolf, J.E., and Harding Jr, L.W.: Anthropogenic and climatic
 1585 influences on the eutrophication of large estuarine ecosystems. *Limnology and*
 1586 *Oceanography*, 51(1 II), 448-462, 2006.
- 1587 Platt, T., Gallegos, C. L., and Harrison, W. G.: Photoinhibition of photosynthesis in natural
 1588 assemblages of marine phytoplankton. *J. Mar. Res.*, 38, 687-701, 1980.
- 1589 Preddy, W. S.: The mixing and movement of water in the estuary of the Thames, *J. Mar. biol. Ass. UK*,
 1590 33, 645–662, 1954.
- 1591 Press, W. H., Teukolosky, S. A., Vetterling, W. T., and Flannery, B.P.: Numerical Recipes in C: The Art
 1592 of Scientific Programming, 2nd Edn., Cambridge University Press, USA, 1992.
- 1593 Pritchard, D. W.: The Equations of Mass Continuity and Salt Continuity in Estuaries, *J. Marine Res.*,
 1594 15, 33–42, 1958.
- 1595 Raymond, P.A., Caraco, N.F., and Cole, J.J.: Carbon dioxide concentration and atmospheric flux in the
 1596 Hudson River. *Estuaries*, 20(2), 381-390, 1997.
- 1597 Raymond, P.A., Bauer, J.E., and Cole, J.J.: Atmospheric CO₂ evasion, dissolved inorganic carbon
 1598 production, and net heterotrophy in the York River estuary. *Limnology and Oceanography*,
 1599 45(8), 1707-1717, 2000.
- 1600 Raymond, P.A., and Hopkinson, C.S.: Ecosystem Modulation of Dissolved Carbon Age in a Temperate
 1601 Marsh-Dominated Estuary. *Ecosystems*, 6(7), 694-705, 2003.
- 1602 Raymond, P.A., Hartmann, J., Lauerwald, R., Sobek, S., McDonald, C., Hoover, M., Butman, D., Striegl,
 1603 R., Mayorga, E., Humborg, C., Kortelainen, P., Dürr, H., Meybeck, M., Ciais, P., and Guth, P.:
 1604 Global carbon dioxide emissions from inland waters. *Nature*, 503(7476), 355-359, 2013.
- 1605 Regnier, P., Wollast, R., and Steefel, C.I.: Long-term fluxes of reactive species in macrotidal estuaries:
 1606 Estimates from a fully transient, multicomponent reaction-transport model. *Marine*
 1607 *Chemistry*, 58(1-2), 127-145, 1997.
- 1608 Regnier, P., Mouchet, A., Wollast, R., and Ronday, F.: A discussion of methods for estimating residual
 1609 fluxes in strong tidal estuaries, *Cont. Shelf Res.*, 18, 1543–1571, 1998.
- 1610 Regnier, P., and Steefel, C.I.: A high resolution estimate of the inorganic nitrogen flux from the
 1611 Scheldt estuary to the coastal North Sea during a nitrogen-limited algal bloom, spring 1995.
 1612 *Geochimica et Cosmochimica Acta*, 63(9), 1359-1374, 1999.
- 1613 Regnier, P., Vanderborght, J. P., Steefel, C. I., and O'Kane, J. P.: Modeling complex multi-component
 1614 reactive-transport systems: Towards a simulation environment based on the concept of a
 1615 Knowledge Base, *Appl. Math. Model.*, 26, 913–927, 2002.
- 1616 Regnier, P., Friedlingstein, P., Ciais, P., Mackenzie, F.T., Gruber, N., Janssens, I.A., Laruelle, G.G.,
 1617 Lauerwald, R., Luyssaert, S., Andersson, A.J., Arndt, S., Arnosti, C., Borges, A.V., Dale, A.W.,
 1618 Gallego-Sala, A., Godderis, Y., Goossens, N., Hartmann, J., Heinze, C., Ilyina, T., Joos, F.,
 1619 LaRowe, D.E., Leifeld, J., Meysman, F.J.R., Munhoven, G., Raymond, P.A., Spahni, R.,
 1620 Suntharalingam, P., and Thullner, M.: Anthropogenic perturbation of the carbon fluxes from
 1621 land to ocean. *Nature Geosci*, 6(8), 597-607, 2013a.
- 1622 Regnier, P., Arndt, S., Goossens, N., Volta, C., Laruelle, G.G., Lauerwald, R., and Hartmann, J.:
 1623 Modelling Estuarine Biogeochemical Dynamics: From the Local to the Global Scale. *Aquatic*
 1624 *Geochemistry*, 19(5-6), 591-626, 2013b.
- 1625 Riemann, B., Simonsen, P., and Stensgaard, L.: The carbon and chlorophyll content of phytoplankton
 1626 from various nutrient regimes. *Journal of Plankton Research*, 11 (5), 1037-1045, 1989.

Deleted: .

1628 [Rossow, W.B., and Schiffer, R.A.: Advances in understanding clouds from ISCCP. Bull. Amer.](#)
1629 [Meteorol. Soc., 80, 2261-2288, doi:10.1175/1520-0477\(1999\)080<2261:AIUCFI>2.0.CO;2,](#)
1630 [1999.](#)

1631 Sarma, V.V.S.S., Viswanadham, R., Rao, G.D., Prasad, V.R., Kumar, B.S.K., Naidu, S.A., Kumar, N.A.,
1632 Rao, D.B., Sridevi, T., Krishna, M.S., Reddy, N.P.C., Sadhuram, Y., and Murty, T.V.R.: Carbon
1633 dioxide emissions from Indian monsoonal estuaries. *Geophysical Research Letters*, 39(3),
1634 L03602, 2012.

1635 Savenije, H.H.G.: A one-dimensional model for salinity intrusion in alluvial estuaries. *Journal of*
1636 *Hydrology*, 85(1-2), 87-109, 1986.

1637 Savenije, H.H.G.: Lagrangian solution of St. Venant's equations for alluvial estuary. *Journal of*
1638 *Hydraulic Engineering*, 118(8), 1153-1163, 1992.

1639 Savenije, H. H. G. (Ed.): *Salinity and Tides in Alluvial Estuaries*, 1st Edn., Elsevier, Amsterdam, 2005.

1640 Savenije, H. H. G. (Ed.): *Salinity and Tides in Alluvial Estuaries*, 2nd Edn., available at:
1641 <http://salinityandtides.com> (last access: 8 March 2015), 2012.

1642 [Seitzinger, S. P., Harrison, J. A., Dumont, E., Beusen, A. H. W., and Bouwman, A. F.: Sources and](#)
1643 [delivery of carbon, nitrogen, and phosphorus to the coastal zone: An overview of Global](#)
1644 [Nutrient Export from Watersheds \(NEWS\) models and their application, *Global Biogeochem.*](#)
1645 [Cycles, 19, GB4S01, doi:10.1029/2005GB002606, 2005.](#)

1646 [Schwarz, G.E., Hoos, A.B., Alexander, R.B., and Smith, R.A.: The SPARROW Surface Water-Quality](#)
1647 [Model: Theory, Application and User Documentation. U.S. Geological Survey, Techniques](#)
1648 [and Methods Report, Book 6, Chapter B3, Reston, Virginia, 2006](#)

1649 [Sharp, J. H., Yoshiyama, K., Parker, Schwartz, M. C., Curless, S. E., Beauregard, A. Y., Ossolinski, J. E.,](#)
1650 [and Davis, A. R.: A Biogeochemical View of Estuarine Eutrophication: Seasonal and Spatial](#)
1651 [Trends and Correlations in the Delaware Estuary. *Estuaries and Coasts*, 32, 1023-1043.,](#)
1652 [doi:10.1007/s12237-009-9210-8, 2009.](#)

1653 [Sharp, J. H.: Estuarine oxygen dynamics: What can we learn about hypoxia from long-time records in](#)
1654 [the Delaware Estuary? *Limnol. Oceanogr.*, 55\(2\), 2010, 535-548, 2010.](#)

1655 Shih, J.-S., Alexander, R.B., Smith, R.A., Boyer, E.W., Schwarz, G.E., and Chung, S.: An initial SPARROW
1656 model of land use and in-stream controls on total organic carbon in streams of the
1657 conterminous United States, U. S. Geological Survey, Reston, Virginia, 2010.

1658 Signorini, S.R., Mannino, A., Najjar Jr, R.G., Friedrichs, M.A.M., Cai, W.J., Salisbury, J., Wang, Z.A.,
1659 Thomas, H., and Shadwick, E.: Surface ocean pCO₂ seasonality and sea-air CO₂ flux
1660 estimates for the North American east coast. *Journal of Geophysical Research C: Oceans*,
1661 118(10), 5439-5460, 2013.

1662 [Simmons, H. B.: Some effects of inland discharge on estuarine hydraulics, *Proc. Am. Soc. Civ. Eng.-*](#)
1663 [ASCE, 81, 792, 1955.](#)

1664 Soetaert, K., and Herman, P.M.J.: Nitrogen dynamics in the Westerschelde estuary (SW Netherlands)
1665 estimated by means of the ecosystem model MOSES. *Hydrobiologia*, 311(1-3), 225-246,
1666 1995.

1667 Stets, E.G., and Strieg, R.G.: Carbon export by rivers draining the conterminous united states. *Inland*
1668 *Waters*, 2(4), 177-184, 2012.

1669 Stigter, C., and Siemons, J.: Calculation of longitudinal salt distribution in estuaries as function of
1670 time, Publication Delft Hydraulics Laboratory, 52, The Netherlands, 1967.

1671 Thieu, V., Mayorga, E., Billen, G., and Garnier, J.: Subregional and downscaled global scenarios of
1672 nutrient transfer in river basins: Seine-Somme-Scheldt case study. *Global Biogeochemical*
1673 *Cycles*, 24(2), 2010.

1674 Tian, H., Chen, G., Liu, M., Zhang, C., Sun, G., Lu, C., Xu, X., Ren, W., Pan, S., and Chappelka, A.: Model
1675 estimates of net primary productivity, evapotranspiration, and water use efficiency in the
1676 terrestrial ecosystems of the southern United States during 1895-2007. *Forest Ecology and*
1677 *Management*, 259(7), 1311-1327, 2010.

1678 Tian, H., Chen, G., Zhang, C., Liu, M., Sun, G., Chappelka, A., Ren, W., Xu, X., Lu, C., Pan, S., Chen, H.,
 1679 Hui, D., McNulty, S., Lockaby, G., and Vance, E.: Century-Scale Responses of Ecosystem
 1680 Carbon Storage and Flux to Multiple Environmental Changes in the Southern United States.
 1681 *Ecosystems*, 15(4), 674-694, 2012.

1682 U. S. Fish and Wildlife Service. 2014. National Wetlands Inventory website. U.S. Department of the
 1683 Interior, Fish and Wildlife Service, Washington, D.C. <http://www.fws.gov/wetlands/>, last
 1684 accessed: February 2015.

1685 Vanderborght, J.P., Wollast, R., Loijens, M., and Regnier, P.: Application of a transport-reaction
 1686 model to the estimation of biogas fluxes in the Scheldt Estuary. *Biogeochemistry*, 59(1-2),
 1687 207-237, 2002.

1688 Vanderborght, J.P., Folmer, I., Aguilera, D.R., Uhrenholdt, T., and Regnier, P.: Reactive-transport
 1689 modelling of a river-estuarine-coastal zone system: application to the Scheldt estuary. *Mar.*
 1690 *Chem.* 106, 92-110, 2007.

1691 Van der Burgh, P.: Ontwikkeling van een methode voor het voorspellen van zoutverdelingen in
 1692 estuaria, kanalen and zeeen, Rijkswaterstaat Rapport, The Netherlands, 1972.

1693 Volta, C., Arndt, S., Savenije, H.H.G., Laruelle, G.G., and Regnier, P.: C-GEM (v 1.0): a new, cost-
 1694 efficient biogeochemical model for estuaries and its application to a funnel-shaped system.
 1695 *Geosci. Model Dev.*, [7, 1271-1295, doi:10.5194/gmd-7-1271-2014](#), 2014.

1696 Volta, C., Laruelle, G. G., and Regnier, P.: Regional carbon and CO₂ budgets of North Sea tidal
 1697 estuaries, *Estuarine, Coastal and Shelf Science*, 176, 76-90, 2016a.

1698 Volta, C., Laruelle, G. G., Arndt, S., and Regnier, P.: Linking biogeochemistry to hydro-geometrical
 1699 variability in tidal estuaries: a generic modeling approach, *Hydrol. Earth Syst. Sci.*, 20, 991-
 1700 1030, doi:10.5194/hess-20-991-2016, 2016b.

1701 Vörösmarty, C.J., Fekete, B., and Tucker, B.A.: River Discharge Database, Version 1.0 (RivDIS v1.0),
 1702 Volumes 0 through 6. A contribution to IHP-V Theme 1. Technical Documents in Hydrology
 1703 Series. UNESCO, Paris, 1996.

1704 Wang, Z.A., and Cai, W.J.: Carbon dioxide degassing and inorganic carbon export from a marsh-
 1705 dominated estuary (the Duplin River): A marsh CO₂ pump. *Limnology and Oceanography*,
 1706 49(2), 341-354, 2004.

Deleted: 6(4), 5645-5709,

Deleted: ¶

1707

1710 **Table 1:** Estimates of total annual riverine input from watersheds to estuaries (Tg C yr⁻¹). The ranges
 1711 are based on Stets and Striegl (2012), Global NEWS (Mayorga et al. 2010), Hartmann et al. (2009),
 1712 SPARROW (Shih et al. 2010) and DLEM (Tian et al. 2010, 2012). Modified from Najjar et al. 2012.

	DIC	DOC	POC	TOTAL
NAR	0.2-0.8	0.3-2.1	0.1-0.2	0.6-3.1
MAR	1.4-1.8	0.5-2.3	0.1-0.3	2.0-4.4
SAR	0.4-1.4	0.9-1.6	0.1-0.2	1.4-3.2
TOTAL	2.0-4.0	1.7-6.0	0.3-0.7	4.0-10.7

1713

1714

1715

1716
1717

Table 2: Published local annually averaged estimates of $\overline{FCO_2}$ in mol C m⁻² yr⁻¹ for estuaries along the East coast of the US."

Name	Lon	Lat	$\overline{FCO_2}$		Reference
			Observed.	Modeled	
Altamaha Sound	-81.3	31.3	32.4	72.7	Jiang et al. (2008)
Bellamy	-70.9	43.2	3.6	3.9	Hunt et al. (2010)
Cocheco	-70.9	43.2	3.1	3.9	Hunt et al. (2010)
Doboy Sound	-81.3	31.4	13.9	25.7	Jiang et al. (2008)
Great Bay	-70.9	43.1	3.6	3.9	Hunt et al. (2011)
Little Bay	-70.9	43.1	2.4	3.9	Hunt et al. (2011)
Oyster Bay	-70.9	43.1	4	3.9	Hunt et al. (2011)
Parker River estuary	-70.8	42.8	1.1	3.9	Raymond and Hopkinson (2003)
Sapelo Sound	-81.3	31.6	13.5	20.6	Jiang et al. (2008)
Satilla River	-81.5	31	42.5	25.7	Cai and Wang (1998)
York River	-76.4	37.2	6.2	8.1	Raymond et al. (2000)
Hudson River	-74	40.6	13.5	15.5	Raymond et al. (1997)
Florida Bay	-80.68	24.96	1.4	n.a.	Dufore (2012)

1718

1719

1720

Table 3: State variables and processes explicitly implemented in CGEM.

Deleted: 2

State variables

Name	Symbol	Unit
Suspended Particulate Mater	SPM	g L^{-1}
Total Organic Carbon	TOC	$\mu\text{M C}$
Nitrate	NO_3	$\mu\text{M N}$
Ammonium	NH_4	$\mu\text{M N}$
Phosphate	DIP	$\mu\text{M P}$
Dissolved Oxygen	DO	$\mu\text{M O}_2$
Phytoplankton	Phy	$\mu\text{M C}$
Dissolved Silica	dSi	$\mu\text{M Si}$
Dissolved Inorganic Carbon	DIC	$\mu\text{M C}$


Biogeochemical reactions

Name	Symbol	Unit
Gross primary production	GPP	$\mu\text{M C s}^{-1}$
Net primary production	NPP	$\mu\text{M C s}^{-1}$
Phytoplankton mortality	M	$\mu\text{M C s}^{-1}$
Aerobic degradation	R	$\mu\text{M C s}^{-1}$
Denitrification	D	$\mu\text{M C s}^{-1}$
Nitrification	N	$\mu\text{M N s}^{-1}$
O_2 exchange with the atmosphere	FO_2	$\mu\text{M O}_2 \text{ s}^{-1}$
CO_2 exchange with the atmosphere	FCO_2	$\mu\text{M C s}^{-1}$
SPM erosion	E_{SPM}	$\text{g L}^{-1} \text{ s}^{-1}$
SPM deposition	D_{SPM}	$\text{g L}^{-1} \text{ s}^{-1}$

1721

1722

1725 **Table 4:** Yearly averaged surface area (*S*), fresh water discharge (*Q*), residence time (*Rt*), *FCO₂* and
 1726 *NEM* of all simulated estuaries.

Deleted: Table 3: Published local annually averaged estimates of *FCO₂* for estuaries along the East coast of the US. 

long degrees	lat degrees	<i>S</i> km ²	<i>Q</i> m ³ s ⁻¹	<i>Rt</i> days	$\overline{FCO_2}$ mol C m ⁻² yr ⁻¹	\overline{NEM} mol C m ⁻² yr ⁻¹	<i>FCO₂</i> 10 ⁶ mol C yr ⁻¹	<i>NEM</i> 10 ⁶ mol C yr ⁻¹
NAR								
-67.25	44.75	7	38.5	15	3.7	-37.4	27	-270
-67.25	45.25	12	73.6	15	6.0	-56.7	71	-666
-67.25	45.25	12	73.6	15	13.8	-56.6	162	-666
-67.75	44.75	3	68.5	4	6.7	-63.5	23	-221
-68.25	44.75	14	69.5	19	4.1	-56.2	58	-791
-68.75	44.75	89	309.9	23	27.4	-58.2	2431	-5163
-69.75	44.25	50	626.6	5	32.3	-74.4	1607	-3703
-70.25	43.75	3	25.8	10	2.1	-21.0	7	-71
-70.75	41.75	288	103.6	958	5.0	-4.0	1428	-1146
-70.75	42.25	63	210.7	40	16.2	-32.9	1025	-2081
-70.75	42.75	17	105.8	3	56.3	-69.0	943	-1155
MAR								
-70.75	43.25	31	29.9	11	21.6	-37.4	662	-1146
-71.25	41.75	257	28.2	808	3.9	-2.5	997	-650
-71.75	41.25	21	112.4	4	35.2	-32.6	726	-672
-72.75	40.75	20	25.4	62	30.7	-21.1	623	-430
-72.75	41.25	10	142.5	2	150.8	-36.9	1578	-386
-72.75	41.75	55	476.6	3	55.9	-45.7	3088	-2523
-73.25	40.75	19	26.8	56	31.4	-28.4	608	-550
-74.25	40.75	1192	608.2	126	15.5	-11.8	18432	-14047
-75.25	38.25	399	80.5	172	13.9	-5.0	5558	-2016
-75.25	38.75	354	31.8	357	7.5	-3.0	2659	-1076
-75.25	39.75	1716	499.0	221	10.0	-7.8	17072	-13439
-75.75	39.25	224	18.3	434	7.5	-2.9	1685	-640
-76.25	39.25	3427	717.1	352	8.1	-5.1	27646	-17352
-76.75	37.25	586	272.3	74	15.0	-10.4	8810	-6084
-76.75	37.75	154	36.3	163	10.7	-6.6	1654	-1023
-76.75	39.25	59	71.2	29	48.6	-34.6	2862	-2038
-77.25	38.25	206	30.2	268	6.1	-3.3	1265	-676
-77.25	38.75	568	259.2	118	16.7	-10.8	9488	-6134
SAR								
-78.25	34.25	48	167.4	7	122.5	-62.4	5916	-3015
-79.25	33.25	47	56.3	42	43.4	-36.5	2056	-1728
-79.25	33.75	45	291.4	8	85.1	-78.7	3843	-3551
-79.75	33.25	25	33.8	15	37.9	-32.8	956	-828
-80.25	32.75	25	31.0	50	48.8	-42.5	1214	-1057
-80.25	33.25	92	75.5	61	62.7	-61.2	5769	-5625
-80.75	32.25	71	21.1	182	12.9	-7.0	918	-501
-80.75	32.75	164	63.1	95	20.6	-11.5	3372	-1879
-81.25	31.75	92	71.7	45	25.7	-20.9	2361	-1926
-81.25	32.25	130	379.8	11	51.7	-39.2	6732	-5097
-81.75	30.75	34	18.7	61	17.5	-14.7	602	-505
-81.75	31.25	130	17.7	294	5.5	-4.0	713	-523
-81.75	31.75	56	350.5	4	72.7	-67.4	4068	-3770

1727

1732 **Table 5:** Seasonal contribution to FCO_2 and NEM in each the sub-region. The seasons displaying the
 1733 highest percentages are indicated in bold. [Winter is defined as January, February and March, Spring](#)
 1734 [as April, May and June and so on...](#)

Region	NEM mol C y^{-1}	winter %	spring %	summer %	fall %	FCO_2 mol C y^{-1}	winter %	spring %	summer %	fall %
NAR	$-16.3 \cdot 10^9$	14.7	21.2	37.0	27.2	$7.2 \cdot 10^9$	26.3	18.9	26.5	28.3
MAR	$-72.2 \cdot 10^9$	21.9	25.9	28.8	23.4	$108.3 \cdot 10^9$	29.8	23.3	20.7	26.2
SAR	$-30.5 \cdot 10^9$	24.6	20.9	30.3	24.2	$39.2 \cdot 10^9$	26	23.4	27	23.6

1735

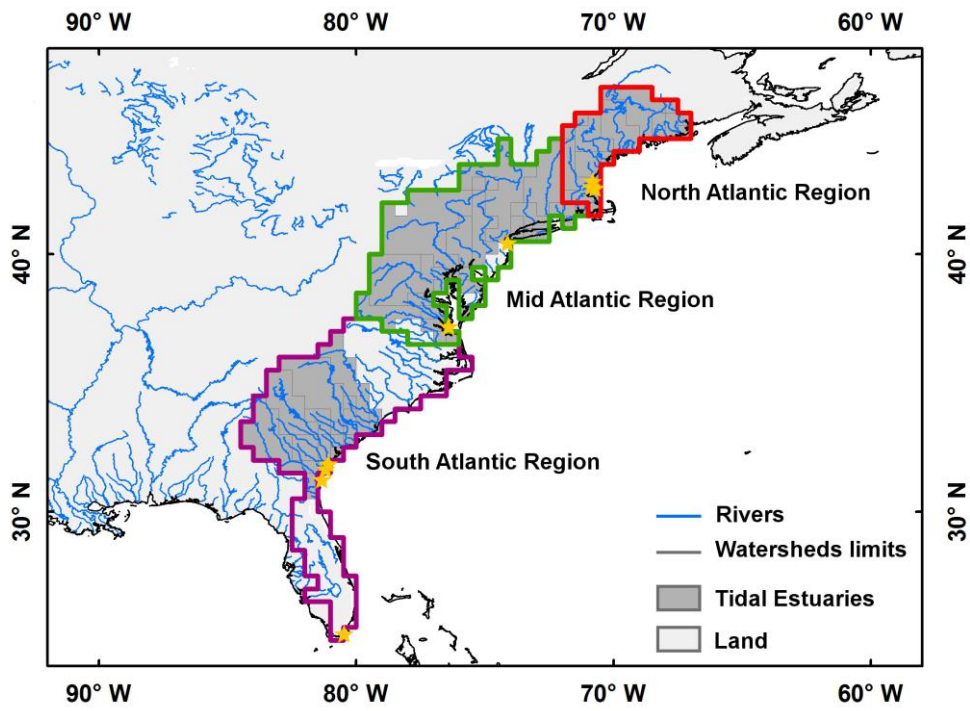
1736

1737 **Table 6:** Regressions and associated coefficient of determination between the depth normalized
 1738 residence time (S/Q) and $\overline{-NEM}/f(T)$, $\overline{FCO_2}/f(T)$ and $CFilt$.

Region	$\overline{-NEM}/f(T)$	$\overline{FCO_2}/f(T)$	$CFilt$
NAR	$y = 27.84 x^{-0.17}$ $r^2 = 0.11$	$y = 6.07 x^{0.00}$ $r^2 = 0.00$	$y = 15.08 \log_{10}(x) + 4.86$ $r^2 = 0.40$
MAR	$y = 26.03 x^{-0.63}$ $r^2 = 0.86$	$y = 34.36 x^{-0.58}$ $r^2 = 0.68$	$y = 40.46 \log_{10}(x) + 9.60$ $r^2 = 0.70$
SAR	$y = 28.36 x^{-0.71}$ $r^2 = 0.76$	$y = 32.82 x^{-0.66}$ $r^2 = 0.80$	$y = 23.19 \log_{10}(x) + 43.71$ $r^2 = 0.46$
MAR + SAR	$y = 25.85 x^{-0.64}$ $r^2 = 0.82$	$y = 31.64 x^{-0.58}$ $r^2 = 0.70$	$y = 33.30 \log_{10}(x) + 24.88$ $r^2 = 0.57$
NAR + MAR + SAR	$y = 28.98 x^{-0.66}$ $r^2 = 0.82$	$y = 12.98 x^{-0.33}$ $r^2 = 0.30$	$y = 40.64 \log_{10}(x) + 11.84$ $r^2 = 0.70$

1739

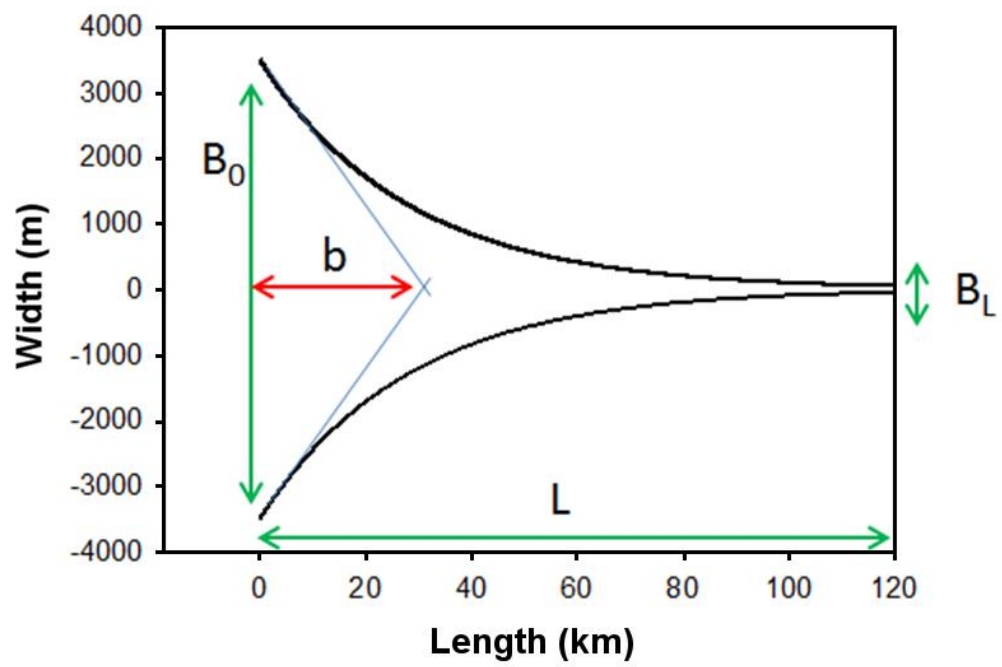
1740



1741

1742 **Figure 1:** Limits of the 0.5 degrees resolution watersheds corresponding to tidal estuaries of the East
 1743 coast of the US. 3 sub-regions are delimited with colors and orange stars represent the location of
 1744 previous studies.

1745

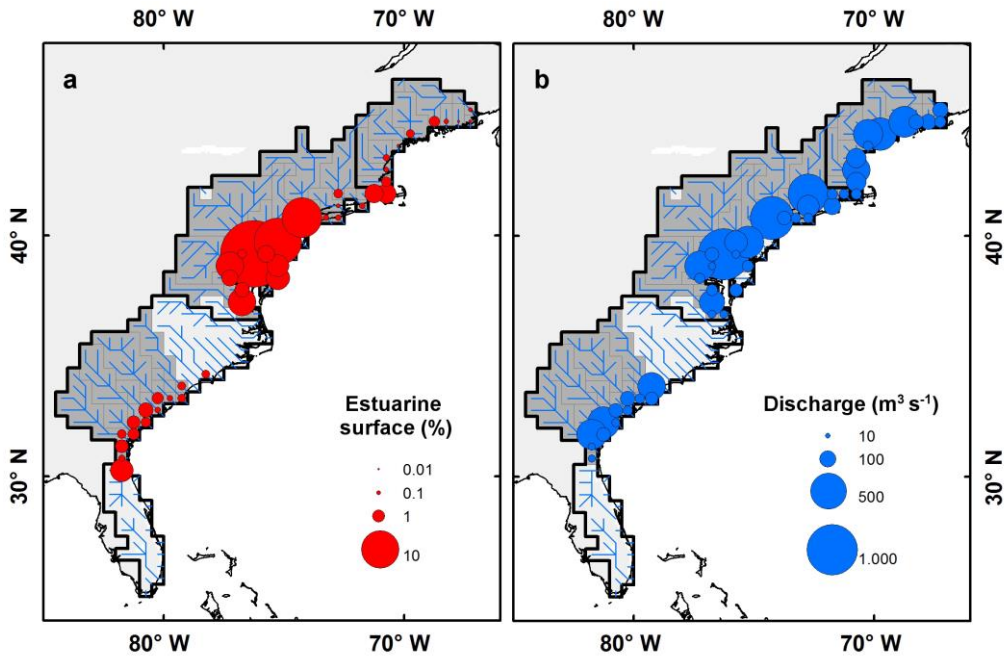


1746

1747 **Figure 2:** Idealized estuarine geometry and main parameters. Parameters indicated by green arrows
 1748 are measured, b is calculated. See section 2.3.1 for further details.

1749

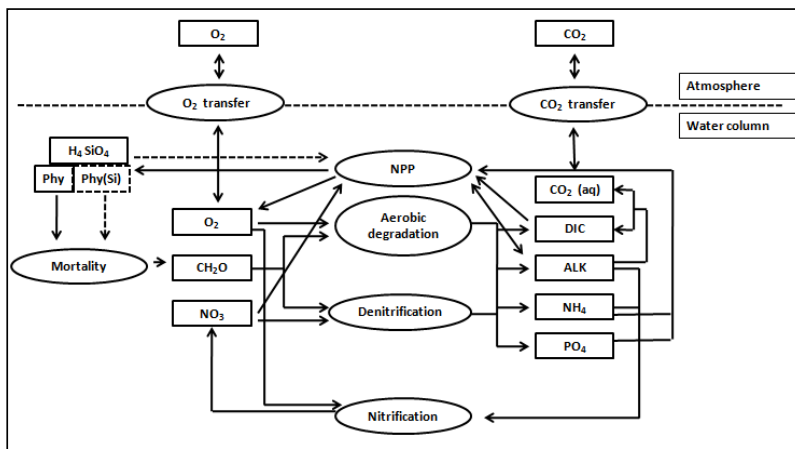
1750



1751

1752 **Figure 3:** Estuarine surface area (a) and mean annual freshwater discharge (b) for each tidal estuary
1753 of the East coast of the US. Estuarine surface area are expressed as percentage of the entire surface
1754 area of the region (19830 km²)

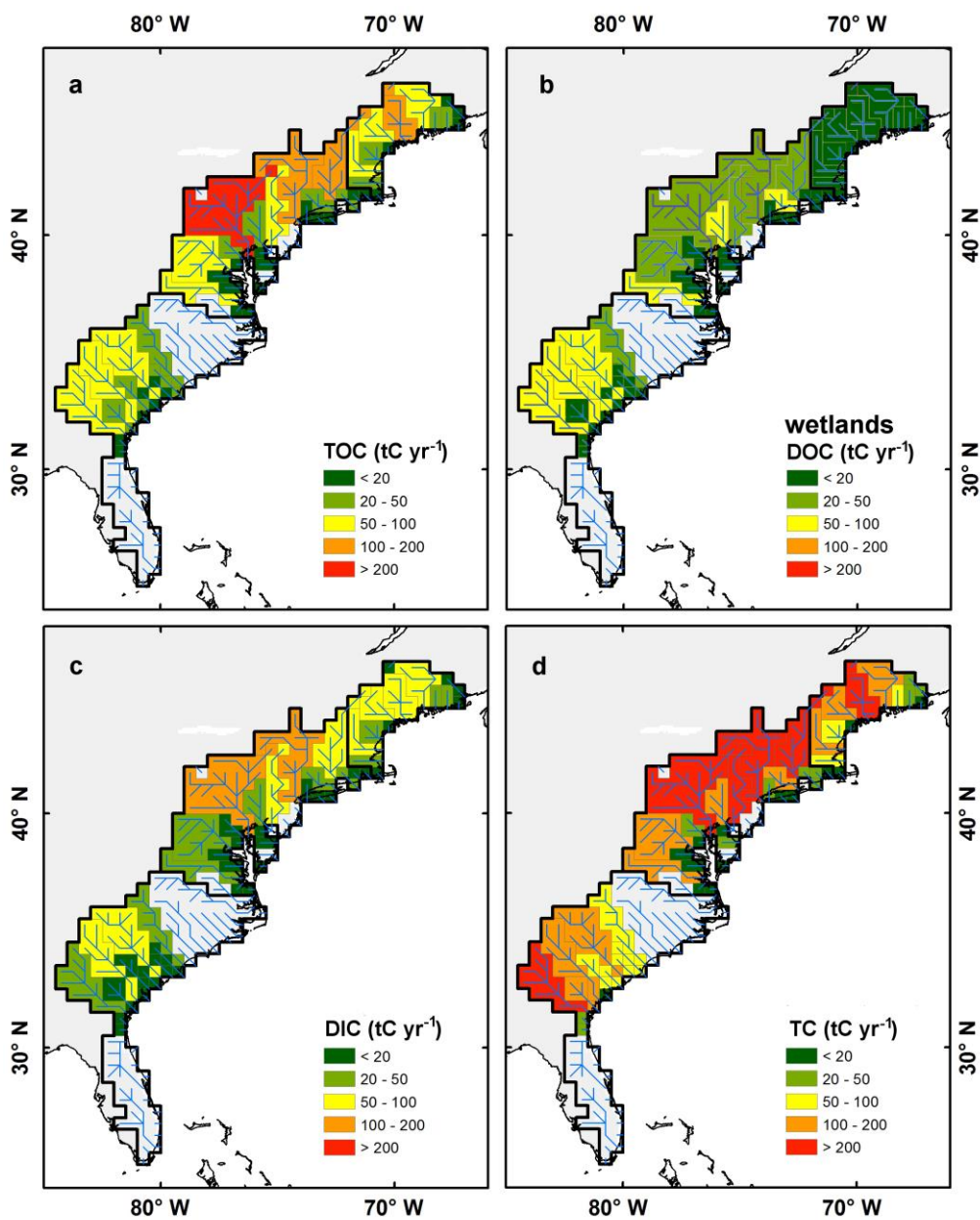
1755



1756

1757 **Figure 4:** Conceptual scheme of the biogeochemical module of C-GEM used in this study. State-
 1758 variables and processes are represented by boxes and oval shapes, respectively. Modified from Volta
 1759 et al., 2014.

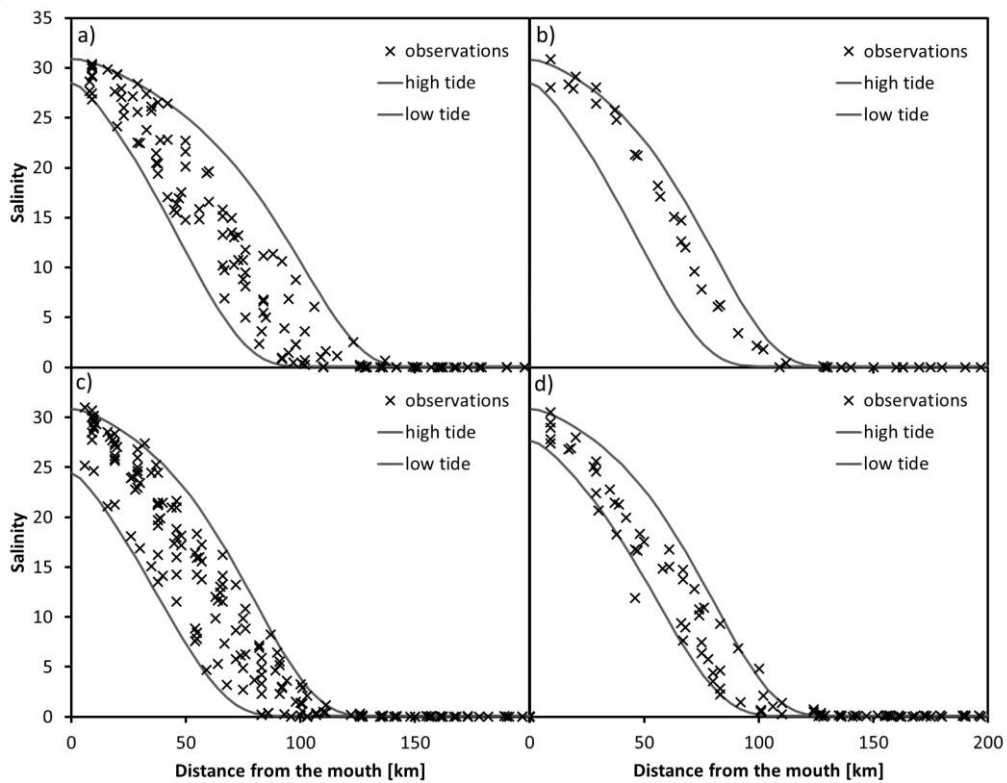
1760



1761

1762 **Figure 5:** Annual river carbon loads of TOC (a), annual DOC fluxes from wetlands (b), annual river
 1763 carbon loads of DIC (c) and annual TC fluxes (d). All fluxes are indicated per watershed.

1764



Formatted: Font color: Blue

1765

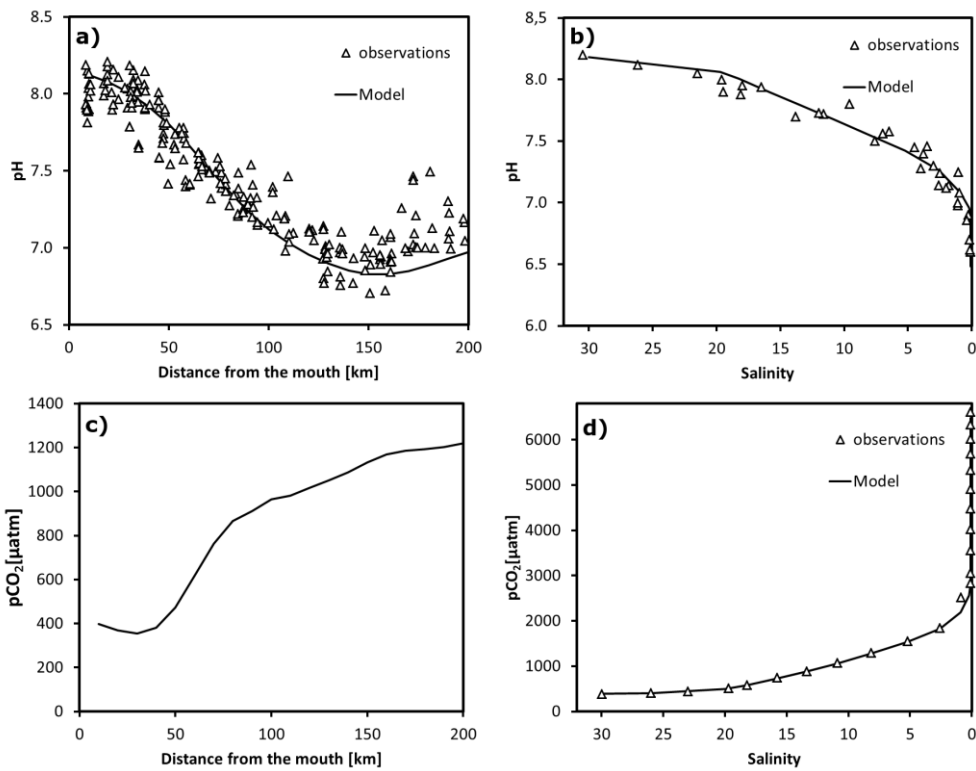
1766 **Figure 6.** Modeled (lines) and measured (crosses) salinities in the Delaware Bay estuary for January

Formatted: Font: Bold, Not Italic

1767 (a), February (b), May (c), June (d). The two lines correspond to high and low tides.

Formatted: Font: Not Italic

1768



Formatted: Font: Bold, Font color: Blue

1769

1770 Figure 7. Longitudinal profiles of pH (top) and pCO₂ (bottom) for the Delaware Bay (left) and
 1771 Altamaha river estuary (right).

1772

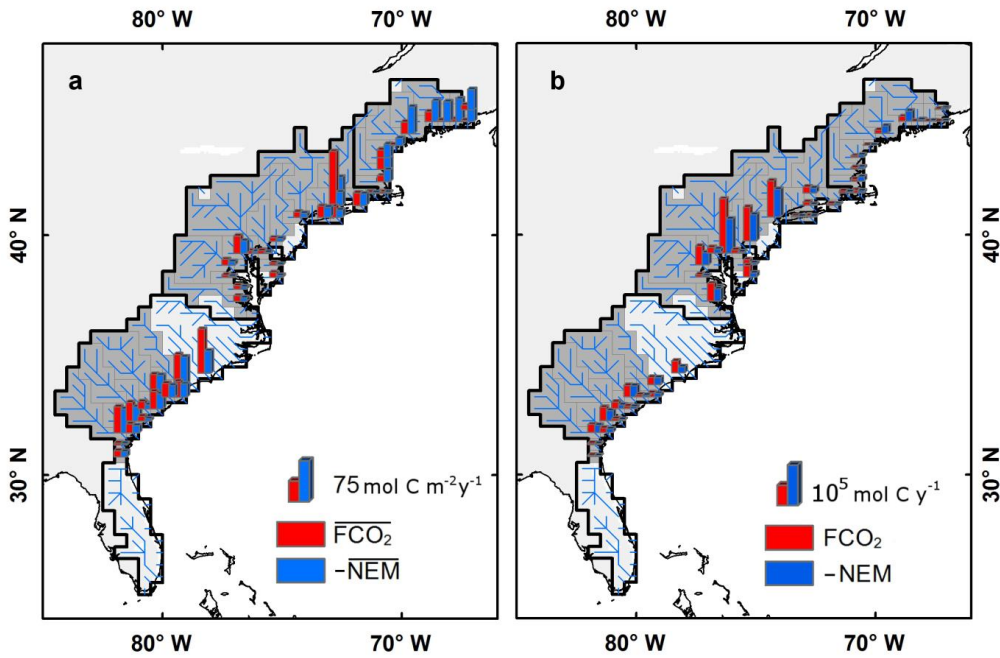
Formatted: Font: Not Italic, No underline

Formatted: Font: Not Italic, No underline

Formatted: Font: Not Bold, Not Italic, No underline

Formatted: Font: Not Italic, No underline

1773



1774

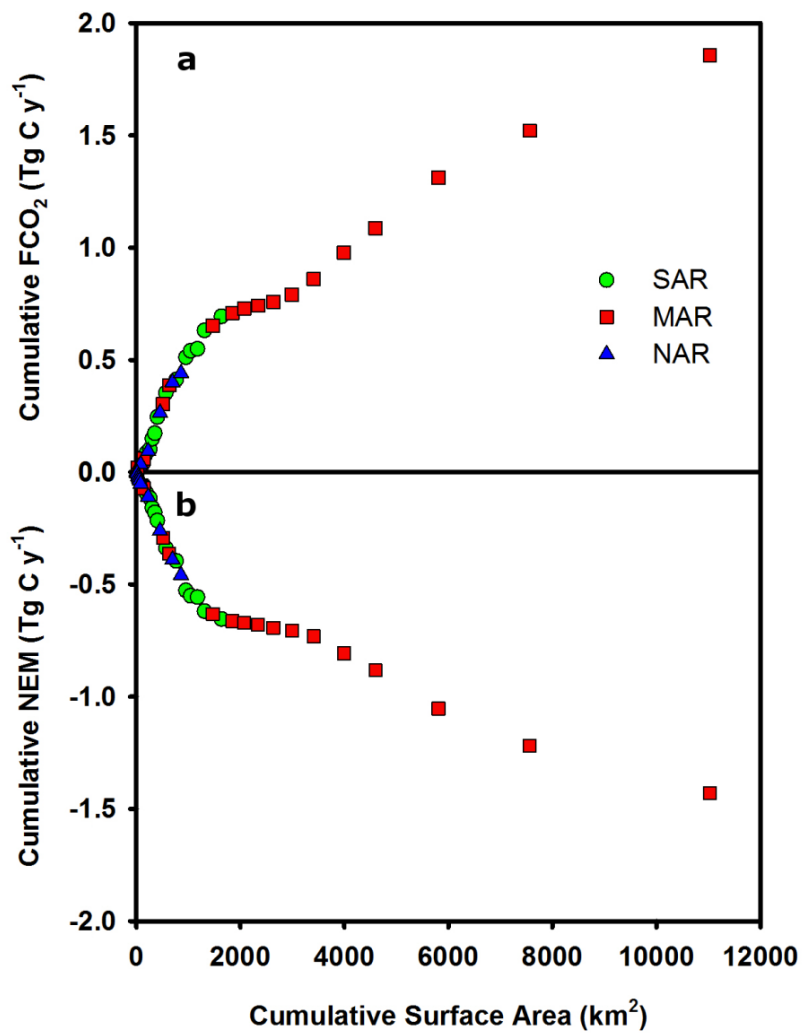
1775 | **Figure 8:** Spatial distribution of spatially averaged value (a) and integrated value (b) of mean annual
1776 FCO_2 (red) and $-NEM$ (blue) along the East coast of the US. On panel a, the notation with overbars
1777 ($\overline{FCO_2}$ and $-\overline{NEM}$) represents rates per unit surface. For the sake of the comparison with $\overline{FCO_2}$, **Fig.**
1778 **8** displays $-\overline{NEM}$ because the model predicts that all estuaries in this region are net heterotrophic.

Deleted: 6

Deleted: figure

Deleted: 6

1779

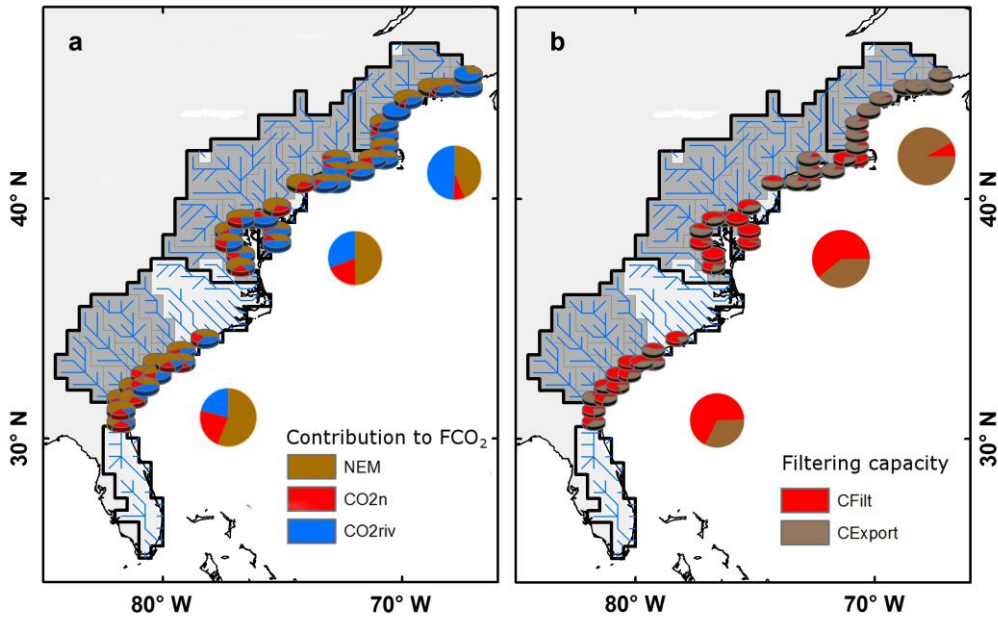


1783

1784 | **Figure 9:** The Cumulative FCO_2 (a) and NEM (b) as functions of the cumulative estuarine surface area.
 1785 Systems are sorted by increasing surface area.

Deleted: 7

1786



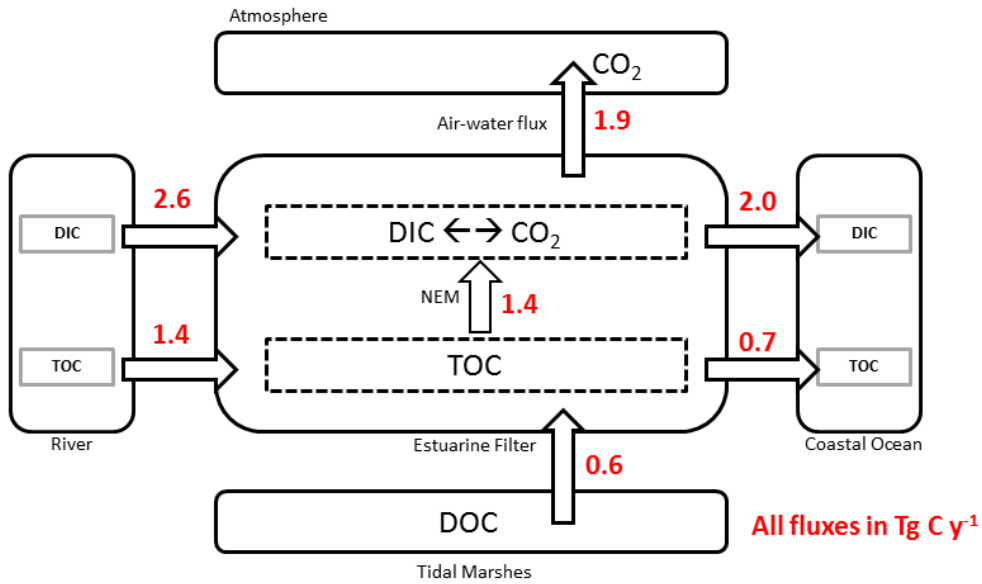
1788

1789 | **Figure 10:** Contribution of *NEM*, nitrification and riverine waters super-saturated waters to the mean
 1790 annual FCO_2 (a). Spatial distribution of mean annual carbon filtration capacities ($CFilt$) and export
 1791 ($CExport$) along the East coast of the US (b).

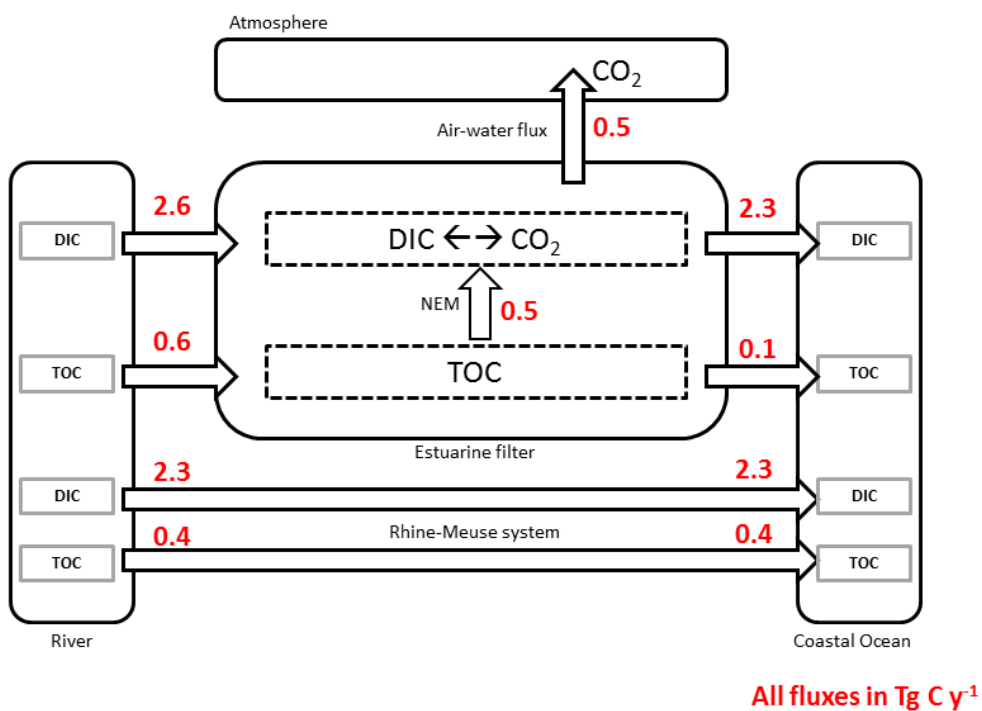
Deleted: 8

1792

a) Eastern US coast



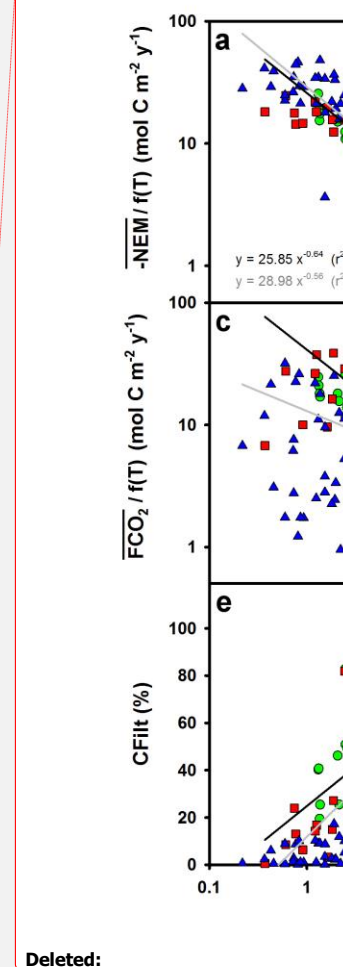
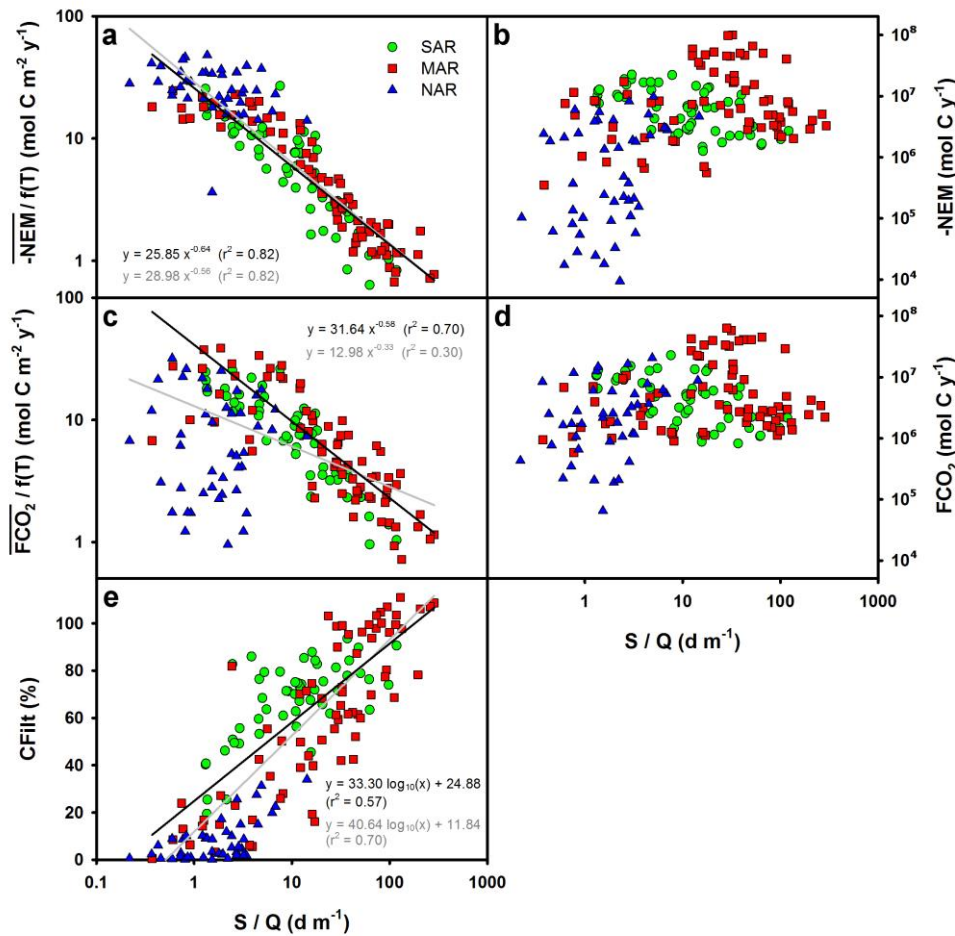
b) North Sea coast



1794

1795 | **Figure 11:** Annual carbon budget of the estuaries of the East coast of the US (a) and of the coast of
 1796 the North Sea (b, modified from Volta et al., 2016a).

Deleted: 9



1798
 1799 **Figure 12:** System scale integrated biogeochemical indicators expressed as functions of the depth
 1800 normalized residence time expressed as the ratio of the estuarine surface S and the river discharge Q
 1801 for all seasons. Panels b, d and e represent NEM, -FCO₂ and CFilt, respectively. Panels a and c
 1802 represent NEM, -FCO₂ normalized by a temperature Q₁₀ function. Black lines are the best fitted linear
 1803 regressions obtained using all the point. Grey lines are best fit using only the estuaries from the MAR
 1804 and SAR regions.
 1805

- Deleted:** 10
- Deleted:** $\overline{-NEM} / f(T)$ (a), $-NEM$ (b), $\overline{FCO_2} / f(T)$ (c), FCO_2 (d) and $CFilt$ (e)
- Formatted:** Font: Not Bold, Not Italic, No underline
- Formatted:** Font: Not Bold, Not Italic, No underline
- Formatted:** Font: Not Bold, Not Italic, No underline
- Formatted:** Font: Not Bold, Not Italic, No underline
- Formatted:** Font: Not Bold, Not Italic, No underline
- Formatted:** Font: Not Bold, Not Italic, No underline
- Deleted:** The grey and black lines are the best fitted regressions obtained using all the point or only the estuaries from the MAR and SAR regions, respectively.

1
2
3
4
5
6
7
8
9
10
11

Air-water CO₂ evasion from U.S. East Coast estuaries

Goossens, Nicolas¹, Laruelle, Goulven Gildas^{1*}, Arndt, Sandra², Cai, Wei-Jun³ & Regnier, Pierre¹

1 Department Geosciences, Environment and Society, Université Libre de Bruxelles, Brussels, Belgium

2 School of Geographical Sciences, University of Bristol, Bristol, UK

3 School of Marine Science and Policy, University of Delaware, Newark, Delaware, USA

*corresponding author: goulven.gildas.laruelle@ulb.ac.be

12 **Abstract:**

13 This study presents the first regional-scale assessment of estuarine CO₂ evasion along the East coast
14 of the US (25 – 45 °N). The focus is on 43 tidal estuaries, which together drain a catchment of
15 697~~000~~ km² or 76 % of the total area within this latitudinal band. The approach is based on the
16 Carbon – Generic Estuarine Model (C-GEM) that allows simulating hydrodynamics, transport and
17 biogeochemistry for a wide range of estuarine systems using readily available geometric parameters
18 and global databases of seasonal climatic, hydraulic, and riverine biogeochemical information. ~~Our~~
19 ~~simulations, performed using conditions representative of the year 2000, suggest that, together,~~ US
20 East coast estuaries emit 1.9 TgC yr⁻¹ ~~in the form of CO₂,~~ which correspond to about 40 % of the
21 carbon inputs from rivers, marshes and mangroves. Carbon removal within estuaries results from a
22 combination of physical (outgassing of supersaturated riverine waters) and biogeochemical
23 processes (net heterotrophy and nitrification). The CO₂ evasion and its underlying drivers show
24 important variations across individual systems, but reveal a clear latitudinal pattern characterized by
25 a decrease in the relative importance of physical over biogeochemical processes along a North-South
26 gradient. Finally, ~~the~~ results reveal that the ratio of estuarine surface area to the river discharge, S/Q
27 (which has a scale of per meter discharged water per year), could be used as a predictor of the
28 estuarine carbon processing in future regional and global scale assessments.

Deleted: 10³

Formatted: Superscript

Deleted: Together

Formatted: Subscript

31 **1 Introduction**

32 Carbon fluxes along the land-ocean aquatic continuum are currently receiving increasing attention
33 because of their recently recognized role in the global carbon cycle and anthropogenic CO₂ budget
34 (Bauer et al., 2013; Regnier et al., 2013a; LeQuéré et al., 2014, 2015). Estuaries are important
35 reactive conduits along this continuum, which links the terrestrial and marine global carbon cycles
36 (Cai, 2011). Large amounts of terrestrial carbon transit through these systems, where they mix with
37 carbon from autochthonous, as well as marine sources. During estuarine transit, heterotrophic
38 processes degrade a fraction of the allochthonous and autochthonous organic carbon inputs,
39 supporting a potentially significant, yet poorly quantified CO₂ evasion flux to the atmosphere. Recent
40 estimates suggest that 0.15-0.25 PgC yr⁻¹ is emitted from estuarine systems worldwide (Borges and
41 Abril, 2012; Cai, 2011; Laruelle et al., 2010; Regnier et al., 2013a; Laruelle et al., 2013, Bauer et al.,
42 2013). Thus, in absolute terms the global estuarine CO₂ evasion corresponds to about 15% of the
43 open ocean CO₂ uptake despite the much smaller total surface area.

44 Currently, estimates of regional and global estuarine CO₂ emissions are mainly derived on the basis
45 of data-driven approaches that rely on the extrapolation of a small number of local measurements
46 (Cai, 2011; Chen et al., 2013; Laruelle et al., 2013). These approaches fail to capture the spatial and
47 temporal heterogeneity of the estuarine environment (Bauer et al., 2013) and are biased towards
48 anthropogenically influenced estuarine systems located in industrialized countries (Regnier et al.,
49 2013a). Even in the best surveyed regions of the world (e.g. Australia, Western Europe, North
50 America or China), observations are merely available for a small number of estuarine systems. In
51 addition, if available, data sets are generally of low spatial and temporal resolution. As a
52 consequence, data-driven approaches can only provide first-order estimates of regional and global
53 estuarine CO₂ emissions.

54 Integrated model-data approaches can help here, as models provide the means to extrapolate over
55 temporal and spatial scales and allow disentangling the complex and very dynamic network of

Deleted: few

Deleted: While these approaches provide useful first-order estimates, they

Deleted: . In addition, these global estimates

Deleted: .

Deleted: and e

Deleted: surveyed

Deleted: such as

Deleted: ,

Deleted: only

Deleted: fraction

Deleted:

69 physical and biogeochemical processes that controls estuarine CO₂ emissions. Over the past
70 decades, increasingly complex process-based models have been applied, in combination with local
71 data, to elucidate the coupled carbon-nutrient cycles on the scale of individual estuaries (e.g.,
72 O’Kane, 1980; Soetaert and Herman, 1995; Vanderborght et al., 2002; Lin et al., 2007; Arndt et al.,
73 2009; Cerco et al., 2010; Baklouti et al., 2011). However, the application of such model approaches
74 remains limited to the local scale due to their high data requirements for calibration and validation
75 (e.g. bathymetric and geometric information and boundary conditions), as well as the high
76 computational demand associated with resolving the complex interplay of physical and
77 biogeochemical processes on the relevant temporal and spatial scales (Regnier et al., 2013b).
78 Complex process-based models are thus not suitable for the application on a regional or global scale
79 and, as a consequence, the estuarine carbon filter is, despite its increasingly recognized role in
80 regional and global carbon cycling (e.g. Bauer et al., 2013), typically not taken into account in model-
81 derived regional or global carbon budgets (Bauer et al., 2013). The lack of regional and global model
82 approaches that could be used as stand-alone applications or that could be coupled to regional
83 terrestrial river network models (e.g. GLOBALNEWS: Seitzinger et al., 2005; Mayorga et al., 2010;
84 SPARROW: Schwarz et al., 2006) and continental shelf models (e.g. Hofmann et al., 2011) is thus
85 critical.

86 The Carbon-Generic Estuary Model (C-GEM (v1.0); Volta et al., 2014) has been developed with the
87 aim of providing such a regional/global modeling tool that can help improve existing, observationally
88 derived first order estimates of estuarine CO₂ emissions. C-GEM (v1.0) has been specifically designed
89 to reduce data requirements and computational demand and, thus, tackles the main impediments
90 for the application of estuarine models on a regional or global scale. The approach takes advantage
91 of the mutual dependency between estuarine geometry and hydrodynamics in alluvial estuaries
92 and uses an idealized representation of the estuarine geometry to support the hydrodynamic
93 calculations. It thus allows running steady state or fully transient annual to multi-decadal simulations
94 for a large number of estuarine systems, using geometric information readily available through maps

- Deleted:** located in the study area, often with limited spatial and temporal coverage.
- Deleted:** Furthermore, data alone Furthermore, observation-based approaches and do not provide sufficient insights into the complex and dynamic interplay of biogeochemical and physical processes that controls estuarine carbon and CO₂ fluxes. ¶
- Formatted:** English (U.K.)
- Deleted:** increasingly
- Formatted:** Font:
- Formatted:** English (U.K.), Not Highlight
- Formatted:** English (U.K.), Not Highlight
- Deleted:** these
- Deleted:** a
- Formatted:** English (U.K.), Not Highlight
- Deleted:** by
- Deleted:** procedures
- Formatted:** Not Highlight
- Formatted:** English (U.K.), Not Highlight
- Deleted:** by
- Deleted:** required
- Deleted:** to address the
- Deleted:** complex
- Formatted:** English (U.K.)
- Formatted:** English (U.K.), Not Highlight
- Formatted:** Not Highlight
- Formatted:** Adjust space between Latin and Asian text, Adjust space between Asian text and numbers
- Deleted:** These models are thus not suitable for regional or global applications (Bauer et al., 2013), which require simplifications to afford the treatment of a large number of estuaries, including those for which morphological, hydrodynamic and biogeochemical data are incomplete or absent. Therefore, the regional and global quantification of the estuarine filter thus remains ignored is not considered in modelling efforts because terrestrial models representing the river network typically do not account for the estuaries (i.e. GLOBALNEWS: Seitzinger et al., 2005)
- Moved (insertion) [1]**
- Formatted:** French (France), Highlight
- Moved (insertion) [2]**
- Deleted:** a

164 [or remote sensing images. Although the development of such a regional/global tool inevitably](#)
 165 [requires simplification, careful model evaluations have shown that, despite the geometric](#)
 166 [simplification, C-GEM provides an accurate description of the hydrodynamics, transport and](#)
 167 [biogeochemistry in tidal estuaries \(Volta et al., 2014\). In addition, the model approach was](#)
 168 [successfully used to quantify the contribution of different biogeochemical processes for CO₂ air-](#)
 169 [water fluxes in an idealized, funnel-shaped estuary forced by typical summer conditions](#)
 170 [characterizing a temperate Western European climate \(Regnier et al., 2013b\). Volta et al. \(2016b\)](#)
 171 [further investigated the effect of estuarine geometry on the CO₂ outgassing using three idealized](#)
 172 [systems and subsequently established the first regional carbon budget for estuaries surrounding the](#)
 173 [North Sea by explicitly simulating the six largest systems of the area \(Volta et al., 2016a\), including](#)
 174 [the Scheldt and the Elbe for which detailed validation was performed.](#)

175 Here, [we extend the domain of application of C-GEM \(v1.0\) to quantify CO₂ exchange fluxes, as well](#)
 176 as the overall organic and inorganic carbon budgets for the full suite of estuarine systems located
 177 along the entire East coast of the United States, [one of the most intensively monitored regions in the](#)
 178 world. A unique set of regional data, including [partial pressure of CO₂ in riverine](#) and continental
 179 shelf [waters](#) (pCO₂; Signorini et al., 2013; Laruelle et al., 2015), riverine biogeochemical
 180 [characteristics](#) (Lauerwald et al., 2013), estuarine eutrophication status (Bricker et al., 2007) and
 181 estuarine morphology (NOAA, 1985) are available. These comprehensive data sets are
 182 complemented by local observations of carbon cycling and CO₂ fluxes in selected, individual
 183 estuarine systems (see Laruelle et al., 2013 for a review), making the East coast of the United States
 184 an ideal region for a first, fully explicit regional evaluation of CO₂ evasion resolving every major tidal
 185 estuary along the selected coastal segment. [The scale addressed in the present study is](#)
 186 unprecedented so far (> 3000 km of coastline) and covers a wide range of estuarine morphological
 187 features, climatic conditions, land-use and land cover types, as well as urbanization levels. [The](#)
 188 [presented study will not only allow a further evaluation of C-GEM \(v1.0\), but will also provide the](#)
 189 [first regional-scale assessment of estuarine CO₂ evasion along the East coast of the US \(25 – 45 °N\)](#)

- Formatted:** English (U.K.), Not Highlight
- Deleted:** careful
- Deleted:** enabling the quantification of biogeochemical dynamics in estuaries on a regional and global scale. The focus is on tidal systems as defined by Dürr et al. (2011) and the approach is based on a one-dimensional, time-dependent representation of hydrodynamic, transport and reaction processes within an estuary.
- Deleted:** C-GEM is computationally efficient and reduces data requirements by using an idealized representation of the geometry to support the hydrodynamic calculations and, subsequently, transport and biogeochemical reaction processes. The C-GEM modeling platform thus enables hundreds to thousands of steady state or fully transient simulations spanning years to decades for a multitude of estuarine systems, using geometric information readily available through maps or remote sensing images. Despite the geometric simplification, C-GEM resolves the most (...)
- Deleted:** first
- Deleted:** succesfully
- Formatted:** (...)
- Deleted:** is applied
- Formatted:** Font: Not Bold, Not Italic, No underline
- Moved up [1]:** The global quantification filter thus remains ignored in modelling (...)
- Formatted:** Font: Not Bold, Not Italic, No underline
- Moved up [2]:** The lack of regional or global evaluations of the estuarine carb (...)
- Deleted:** In this respect, integrated model-data approaches provide a suitab (...)
- Formatted:** Font: Not Bold, Not Italic, No underline
- Deleted:** ¶
- Deleted:** an extended version of
- Deleted:** . The applied RTM approach allows to evaluate the relative significan (...)
- Deleted:**
- Deleted:** sea partial pressure of CO₂
- Deleted:** properties
- Deleted:** characteristics
- Moved (insertion) [3]**
- Deleted:** An extensive review of published local estimates of CO₂ fluxes i (...)
- Moved up [3]:** An extensive review of published local estimates of CO₂ fluxes i (...)
- Formatted:** Font: Not Bold, Not Italic, No underline

398 [and will help explore general relationships between carbon cycling and CO₂ evasion, and readily](#)
399 [available estuarine geometrical parameters.](#)

400 ~~After a description of the model itself and of the dataset used to set up the simulations, a local~~
401 ~~validation is presented which includes salinity, pCO₂ and pH longitudinal profiles for two well~~
402 ~~monitored systems (the Delaware Bay and the Altamaha River Estuary). The yearly averaged rates of~~
403 ~~CO₂ exchange at the air-water interface simulated by the model for 13 individual estuaries are also~~
404 ~~compared with observed values reported in the literature. Next, regional scale simulations for 43~~
405 ~~tidal estuaries of the eastern US coast provide seasonal and yearly integrated estimates of the Net~~
406 ~~Ecosystem Metabolism (NEM), CO₂ evasion and carbon filtering capacity, C_{filt}. Model results are~~
407 ~~then used to elucidate the estuarine biogeochemical behavior along the latitudinal transect~~
408 ~~encompassed by the present study (30-45° N). Finally, our results are used to derive general~~
409 ~~relationships between carbon cycling and CO₂ evasion, and readily available estuarine geometrical~~
410 ~~parameters.~~

Deleted: ¶
Formatted: Font: Not Bold, Not Italic,
No underline

Formatted: Font: Not Bold, Not Italic,
No underline

412 2. Regional description and model approach

413 2.1 Observation-based carbon budget for the East coast of the United States

414 The study area covers the Atlantic coast of the United States (Fig.1), from the southern tip of Florida
415 (25°N) to Cobscook Bay (45°N) at the US-Canada boundary. This area encompasses distinct climatic
416 zones and land cover types and exhibits a variety of morphologic features (Fig. 1). The region can be
417 subdivided into several sub-regions following a latitudinal gradient (Signorini et al., 2013). In this
418 study, we define three sub-regions following the boundaries suggested by the COSCAT segmentation
419 (Meybeck et al., 2006; Laruelle et al., 2013) and the further subdivision described in Laruelle et al.
420 (2015). From North to South, the regions are called North Atlantic, Mid Atlantic and South Atlantic
421 Regions (Fig. 1). Total carbon inputs from watersheds to US East coast estuaries (Tab. 1) have been

Deleted: Figure

Deleted: ure

Deleted: Table

426 estimated to range from 4.0 to 10.7 Tg C yr⁻¹ (Mayorga et al., 2010; Shih et al., 2010; Stets and Strieg,
427 2012; Tian et al., 2010; Tian et al., 2012), consisting of dissolved organic carbon (DOC; ~50%),
428 dissolved inorganic carbon (DIC; ~40%) and particulate organic carbon (POC; ~10%). In addition, a
429 statistical approach has been applied to estuaries of the region to quantify organic carbon budgets
430 and Net Ecosystem Productivity (NEP) using empirical models (Herrmann et al., 2015).

431 Recent studies estimated that, along the East coast of the United States, rivers emit 11.4 TgC yr⁻¹ of
432 CO₂ to the atmosphere (Raymond et al., 2013), while continental shelf waters absorb between 3.4
433 and 5.4 TgC yr⁻¹ of CO₂ from the atmosphere (Signorini et al., 2013). A total of thirteen local, annual
434 mean estuarine CO₂ flux estimates across the air-water interface based on measurements are also
435 reported in the literature and are grouped along a latitudinal gradient (Tab. 2). Four of these
436 estimates are located in the South Atlantic region (SAR): Sapelo Sound, Doboy Sound, Altamaha
437 Sound (Jiang et al., 2008), and the Satilla River estuary (Cai and Wang, 1998). Three studies
438 investigate CO₂ fluxes in the mid-Atlantic Region (MAR): the York River Estuary (Raymond et al.,
439 2000) and the Hudson River (Raymond et al., 1997). There is also a comprehensive CO₂ flux study for
440 the Delaware Estuary published after the completion of this work (Joeseof et al., 2015). Six systems
441 are located in the North Atlantic region (NAR): The Great Bay, the Little Bay, the Oyster estuary, the
442 Bellamy estuary, the Cocheco estuary (Hunt et al., 2010; 2011), and the Parker River estuary
443 (Raymond and Hopkinson, 2003). The mean annual flux per unit area from these local studies is
444 11.7±13.1 mol C m⁻² yr⁻¹ and its extrapolation to the total estuarine surface leads to a regional CO₂
445 evasion estimate of 3.8 Tg C y⁻¹. This estimate is in line with that of Laruelle et al. (2013) for the same
446 region which proposes an average CO₂ emission rate of 10.8 mol C m⁻² yr⁻¹. Thus, CO₂ outgassing
447 could remove 35% to 95% of the riverine carbon loads during estuarine transit. About 75 % of the
448 air-water exchange occurs in tidal estuaries (2.8 Tg C y⁻¹) while lagoons and small deltas contribute to
449 the remaining 25 %. Although these simple extrapolations from limited observational data are
450 associated with large uncertainties, they highlight the potentially significant contribution of estuaries
451 to the CO₂ outgassing in the region. However, process-based quantifications of regional organic and

Deleted: fig

Deleted: 1

454 inorganic C budgets including air-water CO₂ fluxes for the estuarine systems along the East coast are
455 not available.

456 2.2 Selection of estuaries

457 The National Estuarine Eutrophication Assessment (NEEA) survey (Bricker et al., 2007), which uses
458 geospatial data from the National Oceanic and Atmospheric Administration (NOAA) Coastal

459 Assessment Framework (CAF) (NOAA, 1985), was used to identify and characterize 58 estuarine

Deleted: 64

460 systems discharging along the Atlantic coast of the United States. From this set, 43 'tidal' estuaries,

Deleted: 47

461 defined as a river stretch of water that is tidally influenced (Dürr et al., 2011), were retained (Fig. 1)

Deleted:

462 to be simulated by the C-GEM model, which is designed to represent such systems. Using outputs

Deleted: fig

463 from terrestrial models (Hartmann et al., 2009; Mayorga et al., 2010), the cumulated riverine carbon

Formatted: Font: Not Bold, Not Italic, No underline

464 loads for all the non-tidal estuaries that are excluded from the present study amount to 0.9 Tg C yr⁻¹,

Deleted: The 15

465 which represents less than 15% of the total riverine carbon loads of the region. These 15 systems are

Formatted: Font: Not Bold, Not Italic, No underline

466 located in the SAR (10) and in the MAR (5),

Formatted: Font: Not Bold, Not Italic, No underline

467 The northeastern part of the domain (NAR, Fig. 1; Tab. 1) includes 20 estuaries along the Gulf of

Deleted: and account for less than 15% of the total riverine carbon loads of the region

468 Maine and the Scotian shelf, covering a cumulative surface area of ~5300 km². It includes drowned

Deleted: table

469 valleys, rocky shores and a few tidal marshes. The climate is relatively cold (annual mean= 8°C) and

470 the human influence is relatively limited because of low population density and low freshwater

471 inputs. The mean estuarine water depth is 12.9 m and the mean tidal range is 2.8 m.

472 The central zone (MAR) includes 17 tidal estuaries accounting for a total surface area of 14500 km².

473 The Chesapeake Bay and the Delaware estuaries alone contribute more than 60% to the surface area

474 of the region. In this region, estuaries are drowned valleys with comparatively high river discharge

475 and intense exchange with the ocean. Several coastal lagoons, characterized by a limited exchange

476 with the ocean are located here, but are not included in our analysis. The Mid-Atlantic Region (MAR)

477 is characterized by a mean annual temperature of 13°C and is strongly impacted by human activities,

487 due to the presence of several large cities (e.g. New York, Washington, Philadelphia, Baltimore) and
488 intense agriculture. The mean water depth is about 4.7 m and the tidal range is 0.8 m.

489 The southern Atlantic region (SAR) includes 10 tidal estuaries covering a total surface area of 12182
490 km². These systems are generally dendritic and surrounded by extensive salt marshes. The climate is
491 subtropical with an average annual temperature of 19°C. Land use includes agriculture and industry,
492 but the population density is generally low. Estuarine systems in the SAR are characterized by a
493 shallow mean water depth of 2.9 m and a tidal range of 1.2 m.

494 **2.3 Model set-up**

495 The generic 1D Reactive-Transport Model (RTM) C-GEM (Volta et al., 2014) is used to quantify the
496 estuarine carbon cycling in the 43 systems considered in this study. The approach is based on
497 idealized geometries (Savenije, 2005; Volta et al., 2014) and is designed for regional and global scale
498 applications (Regnier et al., 2013b; Volta et al., 2014, 2016a). The model approach builds on the
499 premise that hydrodynamics exerts a first-order control on estuarine biogeochemistry (Arndt et al.,
500 2007; Friedrichs and Hofmann, 2001) and CO₂ fluxes (Regnier et al., 2013a). The method takes
501 advantage of the mutual dependence between geometry and hydrodynamics in tidal estuaries
502 (Savenije, 1992) and the fact that, as a consequence, transport and mixing can be easily quantified
503 from readily available geometric data (Regnier et al., 2013a; Savenije, 2005; Volta et al., 2016b).

Deleted: 47

504 **2.3.1 Description of idealized geometries for tidally-averaged conditions**

505 Although tidal estuaries display a wide variety of shapes, they nevertheless share common
506 geometric characteristics that are compatible with an idealized representation (Fig. 2, Savenije,
507 1986; Savenije, 2005). For tidally-averaged conditions, their width B (or cross-sectional area A) can
508 be described by an exponential decrease as a function of distance, x, from the mouth (Savenije,
509 1986; Savenije, 2005):

$$B = B0 * \exp\left(-\frac{x}{b}\right) \quad (1)$$

511 where B (m) is the tidally averaged width, B0 (m) the width at the mouth, x (m) the distance from
 512 the mouth (x=0) and b (m) the width convergence length (Fig. 2). The width convergence length, b, is
 513 defined as the distance between the mouth and the point at which the width is reduced to B0 e⁻¹. It
 514 is directly related to the dominant hydrodynamic forcing. A high river discharge typically results in a
 515 prismatic channel with long convergence length (river dominated estuary), while a large tidal range
 516 results in a funnel-shaped estuary with short convergence length (marine dominated estuary). At the
 517 upstream boundary, the estuarine width is given by:

$$B_L = B0 * \exp\left(-\frac{L}{b}\right) \quad (2)$$

518 Where L denotes the total estuarine length (m) along the estuarine longitudinal axis.

519 The total estuarine surface S (m²) can be estimated by integrating equation (1) over the estuarine
 520 length:

$$S = \int_0^L B dx = b * B0 * \left(1 - \exp\left(-\frac{L}{b}\right)\right) \quad (3)$$

521

522 The width convergence length is then calculated from B0, B_L, L and the real estuarine surface area
 523 (SR) by inserting equation (2) in equation (3):

$$b = \frac{SR}{B0 - B_L} \quad (4)$$

524 SR is calculated for each system using the SRTM water body data (Fig. 3a), a geographical dataset
 525 encoding high-resolution worldwide coastal outlines in a vector format (NASA/NGA, 2003). While
 526 such a database exists for a well monitored region such as the East coast of the US, resorting to
 527 using the idealized estuarine surface area (S) is necessary in many other regions. The longitudinal

Deleted: fig

529 mean, tidally averaged, depth h (m), is obtained from the National Estuarine Eutrophication
 530 Assessment database (Bricker et al., 2007).

531 Using this idealized representation, the estuarine geometry can be defined by a limited number of
 532 parameters: the width at the mouth (B_0), the estuarine length (L), the estuarine width at the
 533 upstream limit (B_L) and the mean depth h . These parameters can be easily determined from local
 534 maps or Google Earth using Geographic Information Systems (GIS), or obtained from databases
 535 (NASA/NGA, 2003).

Formatted: Font: Not Bold, Not Italic, No underline

Formatted: Font: Not Bold, Not Italic, No underline

Deleted: through GIS, local maps, Google Earth

536 2.3.2 Hydrodynamics, transport and biogeochemistry

537 Estuarine hydrodynamics are described by the one-dimensional barotropic, cross-sectionally
 538 integrated mass and momentum conservation equations for a channel with arbitrary geometry
 539 (Nihoul and Ronday, 1976; Regnier et al., 1998; Regnier and Steefel, 1999):

Deleted: is

$$540 \quad r_s \frac{\partial A}{\partial t} + \frac{\partial Q}{\partial x} = 0 \quad (5)$$

$$541 \quad \frac{\partial U}{\partial t} + U \frac{\partial U}{\partial x} = -g \frac{\partial \zeta}{\partial x} - g \frac{U|U|}{C_z^2 H} \quad (6)$$

Deleted: $\frac{\partial U}{\partial t} + U \frac{\partial U}{\partial x} = -$

Formatted: Lowered by 10 pt

542 where:

543	t	time	[s]
544	x	distance along the longitudinal axis	[m]
545	A	cross-section area $A = H \cdot B$	[m ²]
546	Q	cross-sectional discharge $Q = A \cdot U$	[m ³ s ⁻¹]
547	U	flow velocity Q / A	[m s ⁻¹]
548	r_s	storage ratio $r_s = B_s / B$	[-]

553	B_s	storage width	[m]
554	g	gravitational acceleration	[m s ⁻²]
555	ξ	elevation	[m]
556	H	total water depth $H = h + \xi(x, t)$	[m]

557 C_z Chézy coefficient [m^{1/2} s⁻¹]

Formatted: Subscript

558 The coupled partial differential equations (Eqs. [5](#) and [6](#)) are solved by specifying the elevation
559 $\xi_0(t)$ at the estuarine mouth and the river discharge $Q_0(t)$ at the upstream limit of the model domain.

Deleted: 6

Deleted: 7

560 The one-dimensional, tidally-resolved, advection-dispersion equation for a constituent of
561 concentration $C(x, t)$ in an estuary can be written as (e.g. Pritchard, 1958):

$$562 \quad \frac{\partial C}{\partial t} + \frac{Q}{A} \frac{\partial C}{\partial x} = \frac{1}{A} \frac{\partial}{\partial x} \left(AD \frac{\partial C}{\partial x} \right) + P \quad (7)$$

563 where $Q(x, t)$ and $A(x, t)$ denote the cross-sectional discharge and area, respectively and are provided
564 by the hydrodynamic model (eq. [5](#) and [6](#)). $P(x, t)$ is the sum of all production and consumption
565 process rates affection the concentration of the constituent. The effective dispersion coefficient D
566 (m² s⁻¹) implicitly accounts for dispersion mechanisms associated to sub-grid scale processes (Fischer,
567 1976; Regnier et al., 1998). In general, D is maximal near the sea, decreases upstream and becomes
568 virtually zero near the tail of the salt intrusion curve (Preddy, 1954; Kent, 1958; Ippen and Harleman,
569 1961; Stigter and Siemons, 1967). The effective dispersion at the estuarine mouth can be quantified
570 by the following relation ([Savenije, 1986](#)):

Deleted: 6

Deleted: 7

Deleted: Van der Burgh

Deleted: 1972

$$571 \quad D_0 = 26 \cdot (h_0)^{1.5} \cdot (N \cdot g)^{0.5} \quad (8)$$

572 where h_0 (m) is the tidally-averaged water depth at the estuarine mouth and N is the dimensionless
573 Canter Cremers' estuary number defined as the ratio of the freshwater entering the estuary during a

580 tidal cycle to the volume of salt water entering the estuary over a tidal cycle (Simmons, 1955).

581
$$N = \frac{Q_b \cdot T}{P} \quad (9)$$

582 In this equation, Q_b is the bankfull discharge ($m^3 s^{-1}$), T is the tidal period (s) and P is the tidal prism
583 (m^3). For each estuary, N can thus be calculated directly from the hydrodynamic model. The

Formatted: Font: Not Bold, Not Italic,
No underline

584 variation in D along the estuarine gradient can be described by Van der Burgh's equation (Savenije,
585 1986):

586
$$\frac{\partial D}{\partial x} = -K \frac{Q_r}{A} \quad (10)$$

Deleted: 9

587 where K is the dimensionless Van der Burgh's coefficient and the minus sign indicates that D
588 increases in downstream direction (Savenije, 2012). The Van der Burgh's coefficient is a shape factor
589 that has values between 0 and 1 (Savenije, 2012), and is a function of estuarine geometry for tidally
590 average conditions. Therefore, each estuarine system has its own characteristic K value, which
591 correlates with geometric and hydraulic scales (Savenije, 2005). Based on a regression analysis
592 covering a set of 15 estuaries, it has been proposed to constrain K from the estuarine geometry
593 (Savenije, 1992):

594
$$K = 4.32 \cdot \frac{h_0^{0.36}}{B_0^{0.21} \cdot b^{0.14}} \quad \text{with } 0 < K < 1 \quad (11)$$

Deleted: 10

595 Reaction processes P considered in C-GEM comprise aerobic degradation, denitrification,
596 nitrification, primary production, phytoplankton mortality and air-water gas exchange for O_2 and CO_2
597 (Fig. 4 and Tab. 3). These processes and their mathematical formulation are described in detail in
598 Volta et al. (2014) and Volta et al. (2016a).

Deleted: Table

Deleted: 2

599 The non-linear partial differential equations for the hydrodynamics are solved by a finite difference
600 scheme following the approach of (Regnier et al., 1997; Regnier and Steefel, 1999) and
601 (Vanderborcht et al., 2002). The timestep Δt is 150s and the grid size Δx is constant along the

Deleted:)

Deleted: ,

Deleted: (

609 longitudinal axis of the estuary. The grid size default value is 2000_m, but can be smaller for short
610 length estuaries to guarantee a minimum of 20 grid points within the computational domain.
611 Transport and reaction terms are solved in sequence within a single timestep using an operator
612 splitting approach (Regnier et al., 1997). The advection term in the transport equation is integrated
613 using a third-order accurate total variation diminishing (TVD) algorithm with flux limiters (Regnier et
614 al., 1998), ensuring monotonicity (Leonard, 1984), while a semi-implicit Crank-Nicholson algorithm is
615 used for the dispersion term (Press et al., 1992). These schemes have been extensively tested using
616 the CONTRASTE estuarine model (e.g. Regnier et al., 1998; Regnier and Steefel, 1999; Vanderborght
617 et al., 2002) and guarantee mass conservation to within <1%. The reaction network (including
618 erosion-deposition terms when the constituent is a solid species), is numerically integrated using the
619 Euler method (Press et al., 1992). The primary production dynamics, which requires vertical
620 resolution of the photic depth, is calculated according to the method described in Vanderborght et
621 al. (2007). This method assumes an exponential decrease of the light in the water column (Platt et
622 al., 1980), which is solved using a Gamma function.

623 **2.4 Boundary and forcing conditions**

624 Boundary and forcing conditions are extracted from global databases and global model outputs that
625 are available at 0.5° resolution. Therefore, C-GEM simulations are performed at the same resolution
626 according to the following procedure. First, 43 coastal cells corresponding to tidal estuaries are
627 identified in the studied area (Fig. 1). If the mouth of an estuary is spread over several 0.5° grid cells,
628 those cells are regrouped in order to represent a single estuary (e.g. Delaware estuary), and
629 subsequently, a single idealized geometry is defined as described above. The model outputs
630 (Hartmann et al., 2009; Mayorga et al., 2010) and databases (Antonov et al., 2010; Garcia et al.,
631 2010a; Garcia et al., 2010b) used to constrain our boundary conditions are representative of the
632 year 2000.

Deleted: 47

Deleted: fig

635 For each resulting cell, boundary and forcing conditions are calculated for the following periods:
636 January-March; April-June; July-September and October-December. This allows for an explicit
637 representation of the seasonal variability in the simulations.

638 **2.4.1 External forcings**

639 Transient physical forcings are calculated for each season and grid cell using monthly mean values of
640 water temperature (World Ocean Atlas, 2009) and seasonal averaged values for wind speed (Cross-
641 Calibrated-Multi-Platform (CCMP) Ocean Surface Wind Vector Analyses project (Atlas et al., 2011)).

642 Mean daily solar radiation and photoperiods (corrected for cloud coverage using the ISCCP Cloud
643 Data Products, Rossow and Schiffer, 1999) are calculated depending on latitude and day of the year
644 using a simple model (Brock, 1981).

Formatted: Font: Not Bold, Not Italic,
No underline

645 **2.4.2 Riverine discharge, concentrations and fluxes**

646 River discharges are extracted from the UNH/GRDC runoff dataset (Fekete et al., 2002). These
647 discharges represent long-term averages (1960-1990) of monthly and annual runoff at 0.5 degree
648 resolution. The dataset is a composite of long-term gauging data, which provides average runoff for
649 the largest river basins, and a climate driven water balance model (Fekete et al., 2002). Total runoff

650 values are then aggregated for each watershed at the coarser 0.5 degree resolution (Fig. 3b). Next,
651 seasonal mean values (in $\text{m}^3 \text{s}^{-1}$) are derived in order to account for the intra-annual variability in
652 water fluxes. Based on annual carbon and nutrients inputs from the watersheds (Mg y^{-1}), mean
653 annual concentrations (mmol m^{-3}) are estimated for each watershed using the UNH/GRDC annual
654 runoff ($\text{km}^3 \text{y}^{-1}$). Mean seasonal concentrations are then calculated from the seasonally resolved
655 river water fluxes of a given sub-region.

Deleted: fig

656 Annual inputs of dissolved organic carbon (DOC), particulate organic carbon (POC) and inorganic
657 nutrients are derived from the globalNEWS2 model (Mayorga et al., 2010). Global NEWS is a spatially
658 explicit, multi-element (N, P, Si, C) and multi-form global model of nutrient exports by rivers. In a

660 nutshell, DOC exports are a function of runoff, wetland area, and consumptive water use (Harrison
661 et al., 2005). No distinction is made between agricultural and natural landscapes, since they appear
662 to have similar DOC export coefficients (Harrison et al., 2005). Sewage inputs of OC are ignored in
663 GlobalNEWS, because their inclusion did not improve model fit to data (Harrison et al., 2005). POC
664 exports from watersheds are estimated using an empirical relationship with Suspended Particulate
665 Matter (SPM; Ludwig et al., 1996). Inorganic nitrogen (DIN) and phosphorus (DIP) fluxes calculated
666 by GlobalNEWS depend on agriculture and tropical forest coverage, fertilizer application, animal
667 grazing, sewage input, atmospheric N deposition and biological N fixation (Mayorga et al., 2010). The
668 inputs of dissolved silica (DSi) are controlled by soil bulk density, precipitation, slope, and presence
669 of volcanic lithology (Beusen et al., 2009).

670 The DIN speciation is not provided by the GlobalNEWS2 model. The NH_4 and NO_3 concentrations are
671 therefore determined independently on the basis of an empirical relationship between ammonium
672 fraction (NH_4/DIN ratio) and DIN loads (Meybeck, 1982). Dissolved Oxygen (DO) concentrations are
673 extracted from the water quality criteria recommendations published by the United States
674 Environmental Protection Agency (EPA, 2009). The same source is used for phytoplankton
675 concentrations, using a chlorophyll-a to phytoplankton carbon ratio of $50 \text{ gC (gChla)}^{-1}$ (Riemann et
676 al., 1989) to convert the EPA values to carbon units used in the present study.

677 Inputs of dissolved inorganic carbon (DIC) and total Alkalinity (ALK) are calculated from values
678 reported in the GLORICH database (Hartmann et al., 2009). For each watershed, seasonal mean
679 values of DIC and ALK concentrations are estimated from measurements performed at the sampling
680 locations that are closest to the river-estuary boundary. The spatial distribution of annual inputs of
681 $\text{TOC}=\text{DOC}+\text{POC}$, DIC, and $\text{TC}=\text{TOC}+\text{DIC}$ from continental watersheds to estuaries are reported in Fig.
682 5a, 5c and 5d, respectively. The contribution of tidal wetlands to the TOC inputs is also shown (Fig.
683 5b). Overall, the TC input over the entire model domain is estimated at 4.6 Tg C yr^{-1} , which falls in
684 the lower end of previous reported estimations (Najjar et al. 2012).

Deleted: fig

686

687 2.4.3 Inputs from tidal wetlands

688 The DOC input of estuarine wetlands (Fig. 5b) scales to their fraction, W, of the total estuarine and is
689 calculated using the GlobalNEWS parameterization:

Formatted: Font: Not Bold, Not Italic, No underline

Deleted: their surface area W

$$Y_{DOC} = \frac{[(E_{C_{wet}} * W) + E_{C_{dry}} * (1 - W)] * R^a * Q_{act}}{Q_{nat}}$$

(12)

Deleted: 11

690

$$\frac{Y_{DOC_{wet}}}{Y_{DOC}} = \frac{E_{C_{wet}} * W}{E_{C_{wet}} * W + E_{C_{dry}} * (1 - W)}$$

(13)

Deleted: 12

691

692 where Y_{DOC} is the DOC yield ($\text{kg C km}^{-2} \text{y}^{-1}$) calculated for the entire watershed, $Y_{DOC_{wet}}$ is the
693 estimated DOC yield from wetland areas ($\text{kg C km}^{-2} \text{y}^{-1}$), Q_{act}/Q_{nat} is the ratio between the measured
694 discharge after dam construction and before dam construction, $E_{C_{wet}}$ and $E_{C_{dry}}$ ($\text{kg C km}^{-2} \text{y}^{-1}$) are
695 the export coefficients of DOC from wetland and non-wetland soils, respectively. W is the
696 percentage of the land area within a watershed that is covered by wetlands, R is the runoff (m y^{-1})
697 and a is a unit-less calibration coefficient defining how non-point source DOC export responds to
698 runoff. The value of a is set to 0.95, consistent with the original GlobalNEWS -DOC model of Harrison
699 et al. (2005). The carbon load $Y_{DOC_{wet}}$ is then exported as a diffuse source along the relevant
700 portions of estuary. The estuarine segments receiving carbon inputs from tidal wetlands are
701 identified using the National Wetlands Inventory of the U.S. Fish and Wildlife Service (U.S. Fish and
702 Wildlife Service, 2014). The inputs from those systems are then allocated to the appropriate grid cell
703 of the model domain using GIS. The flux calculated is an annual average that is subsequently
704 partitioned between the four seasons as a function of the mean seasonal temperature, assumed to
705 be the main control of the wetland-estuarine exchange. This procedure reflects the observation that

709 in spring and early summer, DOC export is small as a result of its accumulation in the salt marshes
710 induced by the high productivity (Dai and Wiegert, 1996), (Jiang et al., 2008). In late summer and fall,
711 the higher water temperature and greater availability of labile DOC contribute to higher bacterial
712 remineralization rates in the intertidal marshes (Cai et al., 1999; Middelburg et al., 1996; Wang and
713 Cai, 2004), which induce an important export. This marsh production-recycle-export pattern is
714 consistent with the observed excess DIC signal in the offshore water (Jiang et al. 2013). DIC export
715 from tidal wetlands is neglected here because it is assumed that OC is not degraded before reaching
716 the estuarine realm. Although this assumption may lead to an overestimation of OC export from
717 marshes and respiration in estuarine water, it will not significantly affect the water $p\text{CO}_2$ and
718 degassing in the estuarine waters because mixing is faster than respiration.

719 **2.4.4 Concentrations at the estuarine mouth**

720 For each estuary, the downstream boundary is located 20 km beyond the mouth to minimize the
721 bias introduced by the choice of a fixed concentration boundary condition to characterize the ocean
722 water masses (e.g. Regnier et al., 1998). This approach also reduces the influence of marine
723 boundary conditions on the simulated estuarine dynamics, especially for all organic carbon species
724 whose concentrations are fixed at zero at the marine boundary. This assumption ignores the
725 intrusion of marine organic carbon into the estuary during the tidal cycle but allows focusing on the
726 fate of terrigenous material and its transit through the estuarine filter. DIC concentrations are
727 extracted from the GLODAP dataset (Key et al., 2004), from which ALK and pH are calculated
728 assuming CO_2 equilibrium between coastal waters and the atmosphere. The equilibrium value is
729 computed using temperature (WOA2009, Locarnini et al., 2010) and salinity (WOA2009, Antonov et
730 al. (2010)) data which vary both spatially and temporally. The equilibrium approach is a reasonable
731 assumption because differences in partial pressure $\Delta p\text{CO}_2$ between coastal waters and the
732 atmosphere are generally much smaller (0-250 μatm (Signorini et al., 2013)) than those reported for
733 estuaries ($\Delta p\text{CO}_2$ in the range 0-10000 μatm (Borges and Abril, 2012)). Salinity, DO, NO_3 , DIP and DSI

Deleted:

735 concentrations are derived from the World Ocean Atlas (Antonov et al., 2010; Garcia et al., 2010a;
736 Garcia et al., 2010b). NH_4 concentrations are set to zero in marine waters. For all variables, seasonal
737 means are calculated for each grid cell of the boundary.

Deleted: domain

738

739 2.5 Biogeochemical indicators

740 The model outputs (longitudinal profiles of concentration and reaction rates) are integrated in time
741 over the entire volume or surface of each estuary to produce the following indicators of the
742 estuarine biogeochemical functioning (Regnier et al., 2013b): the mean annual Net Ecosystem
743 Metabolism (*NEM*), the air-water CO_2 flux (*FCO₂*), the carbon and nitrogen filtering capacity (*CFilt*
744 and *NFilt*) and their corresponding element budgets. The *NEM* (molC y^{-1}) (Caffrey, 2004; Odum,
745 1956) is defined as the difference between net primary production (*NPP*) and total heterotrophic
746 respiration (*HR*) at the system scale:

$$NEM = \int_0^{365} \int_0^L [NPP(x, t) - R_{aer}(x, t) - R_{den}(x, t)] * B(x) * H(x, t) dx dt$$

(14)

Deleted: 13

747

748 where *NPP* is the Net Primary Production ($\text{mol C m}^{-3} \text{y}^{-1}$), R_{aer} the aerobic degradation of organic
749 matter (in $\text{mol C m}^{-3} \text{y}^{-1}$) and R_{den} the denitrification (in $\text{mol C m}^{-3} \text{y}^{-1}$) (see Volta et al., 2014 for
750 detailed formulations). *NEM* is thus controlled by the production and decomposition of
751 autochthonous organic matter, by the amount and degradability of organic carbon delivered by
752 rivers and tidal wetlands and by the export of terrestrial and in-situ produced organic matter to the
753 adjacent coastal zone. Following the definition of *NEM*, the trophic status of estuaries can be net
754 heterotrophic ($NEM < 0$) when *HR* exceeds *NPP* or net autotrophic ($NEM > 0$), when *NPP* is larger than
755 *HR* because the burial and export of autochthonous organic matter exceeds the decomposition of
756 river-borne material.

759 The FCO_2 (mol C γ^{-1}) is defined as:

$$FCO_2 = \int_0^{365} \int_0^L RCO_2(x, t) * B(x) dx dt$$

(15)

Deleted: 14

760

$$RCO_2(x, t) = -v_p(x, t) ([CO_2(aq)](x, t) - K_0(x, t) * P_{CO_2}(x, t))$$

(16)

Deleted: 15

761

762 where RCO_2 (molC $m^{-2} \gamma^{-1}$) is the rate of exchange in CO_2 at the air-water interface per unit surface
763 area, v_p is the piston velocity ($m \gamma^{-1}$) and is calculated according to Regnier et al. (2002) to account
764 for the effect of current velocity and wind speed, $[CO_2(aq)]$ is the concentration of CO_2 in the
765 estuary ($mol m^{-3}$), K_0 is Henry's constant of CO_2 in sea water ($mol m^{-3} atm^{-1}$) and P_{CO_2} is the
766 atmospheric partial pressure in CO_2 (atm).

767 The carbon filtering capacity (in %) corresponds to the fraction of the river-borne supply that is lost
768 to the atmosphere and is defined here as the ratio of the net outgassing flux of CO_2 and the total
769 inputs of C, e.g. total carbon expressed as the sum of inorganic and organic carbon species, both in
770 the dissolved and particulate phases.

$$CFilt = \frac{FCO_2}{\int_0^{365} Q * [TC]_{riv} dt} * 100$$

(17)

Deleted: 16

772 where $[TC]_{riv}$ denote the total concentrations of C in the riverine inputs.

773 Fluxes per unit area for FCO_2 and NEM , noted $\overline{FCO_2}$ and \overline{NEM} , respectively, are defined in $mol C m^{-2}$
774 γ^{-1} and are calculated by dividing the integrated values calculated above by the (idealized) estuarine
775 surface S :

$$\overline{NEM} = \frac{NEM}{S} * 1000$$

(18)

Deleted: 17

$$\overline{FCO_2} = \frac{FCO_2}{S} * 1000$$

(19)

Deleted: 18

783 Seasonal values for the biogeochemical indicators are calculated using the same formula as above,
784 but calculate the integral over a seasonal rather than annual timescale (i.e. 3 months).

785

786

787 2.6 Model-data comparison

788 ~~C-GEM has been specifically designed for an application on a global/regional scale requiring the~~
789 ~~representation of a large number of individual and often data-poor systems. Maximum model~~
790 ~~transferability and minimum validation requirements were thus central to the model design process~~
791 ~~and the ability of the underlying approach in reproducing observed dynamics with minimal~~
792 ~~calibration effort has been extensively tested.~~ The performance ~~C-GEM's one-dimensional~~

Formatted: Font: Not Bold, Not Italic,
No underline

793 hydrodynamic and transport models using idealized geometries have been evaluated for a number
794 of estuarine systems exhibiting a wide variety of shapes (Savenije, 2012). In particular, it has been
795 shown that the estuarine salt intrusion can be successfully reproduced using the proposed modeling
796 approach (Savenije 2005; Volta et al., 2014; 2016b). ~~In addition,~~ C-GEM's biogeochemistry has also
797 been carefully validated for geometrically contrasting estuarine system in temperate climate zones.
798 Simulations for the Scheldt Estuary (Belgium and the Netherlands), a typical funnel-shaped estuary,
799 were validated through model-data and model-model comparison (Volta et al., 2014; Volta et al.,

Deleted: of 1D

Formatted: Font: Not Bold, Not Italic,
No underline

800 2016a). ~~Furthermore, simulations~~ for the Elbe estuary (Germany), a typical prismatic shape estuary
801 ~~that drains~~ carbonate terrains ~~and, thus, exhibits~~ very high pH was validated against field data (Volta

Deleted: Simulations

802 et al., 2016a). In addition, C-GEM carbon budgets have been compared ~~budget derived from~~
803 observations for 6 European estuaries discharging in the North Sea (Volta et al., 2016a). ~~Although C-~~

Deleted: draining

Deleted: resulting in

Deleted: to

804 ~~GEM has been specifically designed and tested for the type of regional application presented here,~~
805 ~~its transferability from North Sea to US East Coast estuaries was further evaluated by assessing its~~
806 ~~performance in two East Coast estuaries. First, the hydrodynamic and transport model was tested~~

Deleted: -based estimations

Formatted: Font: Not Bold, Not Italic,
No underline

813 for the Delaware Bay (MAR). The model was forced with the monthly, minimal and maximal
814 observed discharge at Trenton over the period between 1912 and 1985 (UNH/GRDC Database,
815 Fekete et al., 2000). Simulated salinity profiles are compared with salinity observations from January,
816 February, May and June (the months with the highest number of data entries), which were extracted
817 from the UNH/GRDC Database. Figure 6 shows that the model captures both the salinity intrusion
818 length and the overall shape of the salinity profile well. In addition, the performance of the
819 biogeochemical model and specifically its ability to reproduce pH and pCO₂ profiles was evaluated by
820 a model-data comparison for both the Delaware Bay (MAR) in July 2003 and the Altamaha river
821 estuary (SAR) in October 1995. Similar to Volta et al., 2016a, the test systems were chosen due to
822 their contrasting geometries. The Delaware Bay is a marine dominated system characterized by a
823 pronounced funnel shape, while the Altamaha River has a prismatic estuary characteristic of river
824 dominated systems (Jiang et al., 2008). Monthly upstream boundary conditions for nutrients, as well
825 as observed pH data and calculated pCO₂ are extracted from datasets described in (Sharp, 2010) and
826 (Sharp et al., 2009) for the Delaware and in (Cai and Wang, 1998; Jiang et al., 2008) and (Cai et al.,
827 1998) for the Altamaha river estuary. The additional forcings and boundary conditions are set
828 similarly to the simulation for 2000 (see Tab. 2, 3, 4, 5, 6 in SI). Figure 7 shows that measured and
829 simulated pH values are in good agreement with observed pH and observation-derived calculations
830 of pCO₂. In the Delaware Bay, a pH minimum is located around km 140 and is mainly caused by
831 intense nitrification sustained by large inputs of NH₄ from the Philadelphia urban area, coupled to an
832 intense heterotrophic activity. Both processes lead to a well-developed pCO₂ increase in this area
833 (Fig. 7b). Although no pCO₂ data were available for validation for the period from which boundary
834 conditions were extracted, the simulated profile agree with pCO₂ measurement from July 2013
835 presented by Joesoef et al. (2015) with pCO₂ values close to equilibrium with the atmosphere in the
836 widest section of the Delaware Bay (close to the estuarine mouth) and values above 1200 μatm at
837 salinities below 5. For the Altamaha river estuary, pH steadily increases from typical river to typical
838 coastal ocean values (Fig. 7b). In addition, both observations and model results reveal that

Formatted: Font: Not Bold, Not Italic, No underline

Formatted: Font: Not Bold, Not Italic

Formatted: Font: Not Bold, Not Italic, No underline

Formatted: Font: Not Bold, Not Italic, No underline

Formatted: Font: Not Bold, Not Italic, No underline

Formatted: Font: Not Bold, Not Italic, No underline

839 outgassing is very intense in the low-salinity region with more than a 5 fold decrease in pCO₂
840 between salinity 0 and 5 (Fig. 7d).

Formatted: Font: Not Bold, Not Italic,
No underline

841 While such local validations allow assessing the performance of the model for a specific set of
842 conditions, the purpose of this study is to capture the average biogeochemical behavior of the
843 estuaries of the eastern coast of the US. Therefore, in addition to the system-specific validation,
844 published annually averaged FCO₂ estimates for 13 tidal systems located within the study area
845 collected over the 1994-2006 period are compared to simulated FCO₂ for conditions representative
846 of the year 2000. Overall, simulated FCO₂ are comparable to values reported in the literature (Tab.
847 2). Although discrepancies, which sometimes can significant, are observed at the level of individual
848 systems, the model captures remarkably well the overall trend in CO₂ evasion rate across estuaries.
849 The model simulates low CO₂ efflux (< 5 mol C m⁻² yr⁻¹) for the 7 systems were such conditions have
850 been observed, while the 6 systems for which the CO₂ evasion exceeds 10 mol C m⁻² yr⁻¹ are the same
851 in the observations and in the model runs. The discrepancy at the individual system level likely result
852 from a combination of factors, including the choice of model processes and there parametrization,
853 the uncertainties in constraining boundary conditions and the limited representability of
854 instantaneous and local observed.

Formatted: Font: Not Bold, Not Italic,
No underline

Formatted: Font: Not Bold, Not Italic,
No underline

Deleted: This analysis is pursued here by
evaluating our model results in the context
of estuarine CO₂ evasion estimates along
the East coast of the US.

855 **3 Results and discussion**

856 **3.1 Spatial variability of estuarine carbon dynamics**

857 Figure 8 presents the spatial distribution of simulated mean annual $\overline{FCO_2}$ and $-\overline{NEM}$ (Fig. 8a), as well
858 as FCO_2 and $-NEM$ (Fig. 8b). In general, mean annual $\overline{FCO_2}$ are about 30% larger than mean annual
859 \overline{NEM} , with the exception of six estuaries situated in the North of the coastal segment. Overall, the
860 \overline{NEM} is characterized by smaller system to system variability compared to the $\overline{FCO_2}$ in all regions. In
861 addition, Fig. 8 reveals distinct differences across the three coastal segments and highlights the

Deleted: 6

Deleted: 6a

Deleted: 6

Deleted: Figure

Deleted: 6

871 important influence of the estuarine geometry and residence time, as well as the latitudinal
872 temperature gradient on estuarine carbon cycling.

873 Overall, $\overline{FCO_2}$ values are the lowest in the NAR (mean flux = $17.3 \pm 16.4 \text{ mol C m}^{-2} \text{ y}^{-1}$; surface
874 weighted average = $23.1 \text{ mol C m}^{-2} \text{ y}^{-1}$), consistent with previously reported very low values for small

875 estuaries surrounding the Gulf of Maine (Hunt et al., 2010; 2011; [Tab. 2](#)). In contrast, \overline{NEM} reveals a
876 regional minimum in the NAR ($-51.2 \pm 16.6 \text{ mol C m}^{-2} \text{ y}^{-1}$; surface weighted average = $-52.8 \text{ mol C m}^{-2}$
877 y^{-1}). The MAR is characterized by intermediate values for $\overline{FCO_2}$, with a mean flux of $26.3 \pm 34.6 \text{ mol}$

878 $\text{C m}^{-2} \text{ y}^{-1}$ (surface weighted average = $11.1 \text{ mol C m}^{-2} \text{ y}^{-1}$) and lowest values for \overline{NEM} ($-15.1 \pm 14.2 \text{ mol}$
879 $\text{C m}^{-2} \text{ y}^{-1}$; surface weighted average = $-7.4 \text{ mol C m}^{-2} \text{ y}^{-1}$). This region also shows the largest variability

880 in CO_2 outgassing compared to the NAR and SAR, with the standard deviation exceeding the mean

881 $\overline{FCO_2}$, and individual estimates ranging from $3.9 \text{ mol C m}^{-2} \text{ y}^{-1}$ to $150.8 \text{ mol C m}^{-2} \text{ y}^{-1}$. This variability

882 is mainly the result of largely variable estuarine surface areas and volumes. Some of the largest East
883 coast estuaries (e.g. Chesapeake and Delaware Bays), as well as some of smallest estuaries (e.g. York

884 River and Hudson River estuaries, Raymond et al., 1997; 2000), are located in this region ([Tab. 2](#) and

885 4). The maximum values of $150.8 \text{ mol C m}^{-2} \text{ y}^{-1}$ simulated in the MAR are similar to the highest FCO_2
886 reported in the literature ($132.3 \text{ mol C m}^{-2} \text{ y}^{-1}$ for the Tapti estuary in India; Sarma et al., 2012). The

887 SAR is characterized by the highest mean $\overline{FCO_2}$ ($46.7 \pm 33.0 \text{ mol C m}^{-2} \text{ y}^{-1}$; surface weighted average

888 = $40.0 \text{ mol C m}^{-2} \text{ y}^{-1}$) and intermediate \overline{NEM} ($-36.8 \pm 24.7 \text{ mol C m}^{-2} \text{ y}^{-1}$; surface weighted average = -

889 $31.2 \text{ mol C m}^{-2} \text{ y}^{-1}$).

890 The NAR is characterized by a regional minimum in $\overline{FCO_2}$, and only contributes 4.6% to the total

891 FCO_2 of the East coast of the US, owing to the small cumulative surface area available for gas

892 exchange in its 10 estuarine systems. In contrast, the 18 MAR estuaries, with their large relative

893 contribution to the total regional estuarine surface area, account for as much as 70.1% of the total

894 outgassing. Because of their smaller cumulated surface area compared to those of the MAR, the 14

895 SAR estuaries account for merely 25.3% of the total outgassing despite their regional maximal $\overline{FCO_2}$.

Deleted: table

Deleted: 3

Deleted: maximum

Deleted: table

Deleted: 3

Formatted: Font: Not Bold, Not Italic,
No underline

Deleted: more than 70%

902 A similar, yet slightly less pronounced pattern emerges for the \overline{NEM} . The NAR, MAR and SAR
903 respectively contribute 13.7%, 60.7% and 25.6% to the total regional net ecosystem metabolism. The
904 comparatively larger relative contribution of the NAR to the total NEM as compared to the total
905 FCO_2 can be explained by the importance of the specific aspect ratio for NEM . A larger ratio of
906 estuarine width b_0 and convergence length b corresponds to a more funnel shaped estuary while a
907 low ratio corresponds to a more prismatic geometry (Savenije, 2000; Volta et al., 2014). In the NAR,
908 estuaries are generally characterized by relatively narrow widths and deep-water depths, thus
909 limiting the potential surface area for gas exchange with the atmosphere. However, the relative
910 contribution of each region to the total regional NEM and FCO_2 is largely controlled by estuarine
911 surface area. Figure 9 illustrates the cumulative NEM (a) and FCO_2 (b) as a function of the cumulative
912 estuarine surface areas. The disproportionate contribution of large estuaries from the MAR
913 translates into a handful of systems (Chesapeake and Delaware Bays and the main tributaries of the
914 former, in particular) contributing to roughly half of the regional NEM and FCO_2 , in spite of relatively
915 low individual rates per unit surface area. However, the smallest systems (mostly located in the NAR
916 and SAR) nevertheless still contribute a significant fraction to the total regional NEM and FCO_2 . The
917 27 smallest systems merely account for less than 10% of the total regional estuarine surface area,
918 yet contribute 38% and 29% to the total regional NEM and FCO_2 , respectively (Fig. 9). This
919 disproportioned contribution can be mainly attributed to their high individual $\overline{FCO_2}$ and \overline{NEM} . This
920 is illustrated by the average simulated $\overline{FCO_2}$ for all 27 smallest systems (calculated as the sum of
921 each estuarine CO_2 outgassing per unit surface area divided by the total number of estuarine
922 systems) which is significantly higher ($30.2 \text{ mol C m}^{-2} \text{ y}^{-1}$) than its surface weighted average (14 mol C
923 $\text{m}^{-2} \text{ y}^{-1}$). Thereby accounting for the disproportionate contribution of very large systems (calculated
924 as the sum of each estuarine CO_2 outgassing divided by the total estuarine surface area across the
925 region).

Formatted: Font: Not Bold, Not Italic,
No underline

Deleted: 7

Deleted: Figure

Deleted: 7

929 Following the approach used in Regnier et al. (2013), the contribution of each biogeochemical
930 process to FCO_2 is assessed by evaluating their individual contribution to DIC and ALK changes taking
931 into account the local buffering capacity of an ionic solution when TA and DIC are changing due to
932 internal processes, but ignoring advection and mixing (Zeebe and Wolf-Gladrow 2001). In the
933 present study, we quantify the effect of the NEM on the CO_2 balance, which is almost exclusively
934 controlled by aerobic degradation rates because the contributions of denitrification and NPP to the
935 net ecosystem balance are small. Nitrification, a process triggered by the transport and/or
936 production of NH_4 in oxygenated waters, favors outgassing through its effect on pH, which shifts the
937 acid-base equilibrium of carbonate species and increases the CO_2 concentration. The contribution of
938 supersaturated riverine waters to the overall estuarine CO_2 dynamics is calculated as difference
939 between all the other processes creating or consuming CO_2 . Figure 10a presents the contribution of
940 the annually integrated *NEM*, nitrification and evasion of supersaturated, DIC enriched riverine
941 waters to the total outgassing for each system, as well as for individual regions of the domain. The
942 calculation of these annual values is based on the sum of the seasonal fluxes. Model results reveal
943 that, regionally, the *NEM* supports about 50% of the estuarine CO_2 outgassing, while nitrification and
944 riverine DIC inputs sustain about 17% and 33% of the CO_2 emissions, respectively. The relative
945 significance of the three processes described above shows important spatial variability. In the NAR,
946 oversaturated riverine waters and *NEM* respectively sustain 50% and 44% of the outgassing within
947 the sub-region, while nitrification is of minor importance (6%). In the MAR, the contribution of
948 riverine DIC inputs is significantly lower (~30%) and the main contribution to the outgassing is *NEM*
949 (~50%); nitrification accounting for slightly less than 20% of the outgassing. In the SAR, the riverine
950 contribution is even lower (~20%), and the outgassing is mainly attributed to the *NEM* (~55%) and
951 nitrification (~25%). Therefore, although the model results reveal significant variability across
952 individual systems, a clear latitudinal trend in the contribution to the total FCO_2 emerge from the
953 analysis; the importance of oversaturated riverine water decreasing from North to South, while *NEM*
954 and nitrification increase along the same latitudinal gradient. The increasing relative importance of

Formatted: Font: Not Bold, Not Italic, No underline

Deleted: T

Formatted: Font: Not Bold, Not Italic, No underline

Formatted: Font: Not Bold, Not Italic, No underline

Deleted: (see Regnier et al., 2013b)

Deleted: .

Deleted: 8a

Formatted: Font: Not Bold, Not Italic, No underline

Deleted: Nitrification, a process triggered by the transport and/or production of NH_4 in oxygenated waters, favors outgassing through its effect on pH, which shifts the acid-base equilibrium of carbonate species and increases the CO_2 concentration. In addition, the *NEM* is almost exclusively controlled by aerobic degradation rates because the contribution of denitrification and NPP to the net ecosystem balance is small. ¶

970 estuarine biogeochemical processes over riverine DIC inputs as drivers of FCO_2 along the North-
971 South gradient is largely driven by increasing temperatures from North to South, especially in the
972 SAR region (Tab. S1.1).

Deleted: Table

973 Contrasting patterns across the 3 regions can also be observed with respect to carbon filtering
974 capacities, $CFilt$ (Fig. 10b). In the NAR, over 90% of the riverine carbon flux is exported to the coastal
975 ocean. However, in the MAR, the high efficiency of the largest systems in processing organic carbon
976 results in a regional $CFilt$ that exceeds 50%. This contrast between the NAR and the MAR and its
977 potential implication for the carbon dynamics of the adjacent continental shelf waters has already
978 been discussed by Laruelle et al. (2015). In the NAR, short estuarine residence results in a much
979 lower removal of riverine carbon by degassing compared to the MAR. Laruelle et al. (2015)
980 suggested that this process could contribute to the weaker continental shelf carbon sink adjacent to
981 the NAR, compared to the MAR. In the SAR, most estuaries remove between 40% and 65% of the
982 carbon inputs. The high temperatures observed and resulting accelerated biogeochemical process
983 rates in this region favor the degradation of organic matter and contribute to increase the estuarine
984 filtering capacity for carbon. However, in the SAR, a large fraction of the OC loads is derived from
985 adjacent salt marshes located along the estuarine salinity gradients, thereby reducing the overall
986 residence time of OC within the systems. The filtering capacity of the riverine OC alone, which
987 transits through the entire estuary, would thus be higher than the one calculated here. As a
988 consequence, highest C retention rates are expected in warm tidal estuaries devoid of salt marshes
989 or mangroves (Cai, 2011).

Deleted: 8b

990 **3.2 Seasonal variability of estuarine carbon dynamics**

991 Carbon dynamics in estuaries of the US East coast not only show a marked spatial variability, but also
992 vary on the seasonal timescale. Table 5 presents the seasonal distribution of NEM and FCO_2 for each
993 sub-region. In the NAR, a strong seasonality is simulated for the NEM and the summer period
994 contributes more than a third to the annually integrated value. The outgassing reveals a lower

997 seasonal variability and is only slightly higher than summer outgassing during fall and lower during
998 spring. In the MAR, summer contributes more to the *NEM* (>28% of the yearly total) than any other
999 season, but seasonality is less pronounced than in the NAR. Here, FCO_2 is largest in winter and
1000 particularly low during summer. In the SAR, summer accounts for 30 % of the *NEM*, while spring
1001 contributes 21 %. FCO_2 is relatively constant throughout the year suggesting that seasonal variations
1002 in carbon processing decrease towards the lower latitudes in the SAR. This is partly related to the
1003 low variability in river discharge throughout the year in lower latitudes (Tab. S1). In riverine
1004 dominated systems with low residence times, such as, for instance, the Altamaha River estuary, the
1005 CO_2 exchange at the air-water interface is mainly controlled by the river discharge because the time
1006 required to degrade the entire riverine organic matter flux exceeds the transit time of OC through
1007 the estuary. Therefore, the riverine sustained outgassing is highest during the spring peak discharge
1008 periods. In contrast, the seasonal variability in FCO_2 in long-residence, marine-dominated systems
1009 with large marsh areas (e.g. Sapelo and Doboy Sound) is essentially controlled by seasonal
1010 temperature variations. Its maximum is reached during summer when marsh plants are dying and
1011 decomposing, as opposed to spring when marshes are in their productive stage (Jiang et al., 2008).
1012 These contrasting seasonal trends have already been reported for different estuarine systems in
1013 Georgia, such as the Altamaha Sound, the Sapelo Sound and the Doboy Sound (Cai, 2011). At the
1014 scale of the entire East coast of the US, the seasonal trends in *NEM* reveal a clear maximum in
1015 summer and minimal values during autumn and winter. The seasonality of FCO_2 is much less
1016 pronounced because the outgassing of oversaturated riverine waters throughout the year
1017 contributes to a large fraction of the FCO_2 and dampens the effect of the temperature dependent
1018 processes (*NEM* and denitrification). In our simulations, the competition between temperature and
1019 river discharge is the main driver of the seasonal estuarine carbon dynamics is. When discharge
1020 increases, the carbon loads increase proportionally and the residence time within the system
1021 decreases, consequently limiting an efficient degradation of organic carbon input fluxes. In warm

Deleted: Table

1023 regions like the SAR, the temperature is sufficiently high all year round to sustain high C processing
1024 rates and this explains the reduced seasonal variability in NEM.

1025

1026 3.3 Regional carbon budget: a comparative analysis

1027 The annual carbon budget for the entire East coast of the US is summarized in [Fig. 11a](#). The total
1028 carbon input to estuaries along the East coast of the US is 4.6 Tg C y^{-1} , of which 42% arrives in
1029 organic form and 58% in inorganic form. Of this total input, saltmarshes contribute 0.6 Tg C yr^{-1} ,
1030 which corresponds to about 14% of the total carbon loads and 32% of the organic loads in the
1031 region. The relative contribution of the saltmarshes to the total carbon input increases towards low
1032 latitudes and is as high as 60% in the SAR region. Model results suggest that 2.7 Tg C y^{-1} is exported
1033 to the continental shelf (25% as TOC and 75% as DIC), while 1.9 Tg C y^{-1} is emitted to the
1034 atmosphere. The overall carbon filtering capacity of the region thus equals 41% of the total carbon

Deleted: fig

Deleted: 9a

1035 entering the [43](#) estuarine systems (river + saltmarshes). Because of the current lack of a benthic
1036 module in C-GEM, the water column carbon removal occurs entirely in the form of CO_2 outgassing
1037 and does not account for the potential contribution of carbon burial in sediments. The estimated
1038 estuarine carbon retention presented here is thus likely a lower bound estimate. Reported to the
1039 modeled surface area of the region, the total FCO_2 of 1.9 Tg C y^{-1} translates into a mean air water
1040 CO_2 flux of about 14 mol C $\text{m}^{-2} \text{y}^{-1}$. This value is slightly higher than the estimate of 10.8 mol C $\text{m}^{-2} \text{y}^{-1}$
1041 calculated by Laruelle et al., (2013) on the basis of local $\overline{\text{FCO}_2}$ estimates assumed to be
1042 representative of yearly averaged conditions (see section 2.1). The latter was calculated as the

Deleted: 47

1043 average of 13 annual $\overline{\text{FCO}_2}$ values reported in the literature ([Tab. 2](#)), irrespective of the size of the
1044 systems. This approach is useful and widely used to derive regional and global carbon budgets
1045 (Borges et al., 2005; Laruelle et al., 2010; Chen et al., 2013). However, it may lead to potentially
1046 significant errors (Volta et al., 2016a) due to the uncertainty introduced by the spatial interpolation

Deleted: table

Deleted: 3

1052 of local measurements to large regional surface areas, while useful and widely used to derive
1053 regional and global carbon budgets.

1054 Regional C budgets are sparse. To our knowledge, the only other published regional assessment of
1055 the estuarine carbon and CO₂ dynamics comes from a relatively well studied region: the estuaries
1056 flowing into the North Sea in Western Europe (Fig. [11b](#)). This budget was calculated using a similar
1057 approach (Volta 2016a) and thus provides an ideal opportunity for a comparative assessment of C
1058 cycling in these regions. However, it is important to note that there are also important differences in
1059 the applied model approaches and those differences should be taken into account when comparing
1060 the derived budgets. In particular, the NW European study is based on a simulation of the 6 largest
1061 systems only (Elbe, Scheldt, Thames, Ems, Humber and Weser), accounting for about 40% for the
1062 riverine carbon loads of the region. It assumes that the intensity of carbon processing and evasion in
1063 all other smaller estuaries discharging into the North Sea (16 % of the carbon loads) can be
1064 represented by the average of the 6 largest system simulation results. In addition, the Rhine-Meuse
1065 system, which alone accounts for 44% of the carbon riverine inputs of the region, was treated as a
1066 passive conduit with respect to carbon due to its very short freshwater residence time (Abril et al.,
1067 2002). The contribution of saltmarshes to the regional carbon budget was also ignored because their
1068 total surface area is much smaller than along the US East coast (Regnier et al., 2013b). Another
1069 important difference is the inclusion of seasonality in the present study while the budget calculated
1070 for the North Sea is derived from yearly average conditions (Volta et al., 2016a).

1071 Overall, although both regions receive similar amounts of C from rivers (4.6 Tg C y⁻¹ and 5.9 Tg C y⁻¹
1072 for the East coast of the US and the North Sea, respectively), they reveal significantly different C
1073 filtering capacities. While the estuaries of the East coast of the US filter 41% of the riverine TC loads,
1074 those from the North Sea only remove 8% of the terrestrial-derived material. This is partly due to the
1075 large amounts of carbon transiting through the 'passive' Rhine-Meuse system. The regional filtering
1076 capacity is higher (15%) when this system is excluded from the analysis. However, even when

Deleted: 9b

1078 neglecting this system, significant differences in filtering efficiencies between both regions remain.
1079 FCO_2 from the North Sea estuaries (0.5 Tg C y^{-1}) is significantly lower than the 1.9 Tg C y^{-1} computed
1080 for the East coast of the US. The reason for the lower evasion rate in NW European estuaries is
1081 essentially twofold. First, the total cumulative surface area available for gas exchange is significantly
1082 lower along the North Sea, in spite of comparable flux densities calculated using the entire estuarine
1083 surface areas of both regions ($14 \text{ mol C m}^{-2} \text{ y}^{-1}$ and $23 \text{ mol C m}^{-2} \text{ y}^{-1}$ for the East coast of the US and
1084 the North Sea, respectively). Second, although the overall riverine carbon loads are comparable in
1085 both regions (Fig. [11](#)), the ratio of organic to inorganic matter input is much lower in the North Sea
1086 area because of the regional lithology is dominated by carbonate rocks and mixed sediments that
1087 contain carbonates (Dürr et al., 2005; Hartmann et al., 2012). As a consequence, TOC represents less
1088 than 20% of the riverine loads and only 10% of the carbon exported to the North Sea. In both
1089 regions, however, the increase of the inorganic to organic carbon ratio between input and output is
1090 sustained by a negative NEM (Fig. [11](#)). Although the ratios themselves may significantly vary from a
1091 region of the world to the other as evidenced by these two studies, a NEM driven increase of the
1092 inorganic fraction within carbon load along the estuarine axis is consistent with the global estuarine
1093 carbon budget proposed by Bauer et al. (2013). In the East coast of the US, the respiration of riverine
1094 OC within the estuarine filter is partly compensated by OC inputs from marshes and mangroves in
1095 such a way that the input and export IC/OC ratios are closer than in the North Sea region.

Deleted: 9

Deleted: 9

1096 **3.4 Scope of applicability and model limitations**

1097 Complex multidimensional models are now increasingly applied to quantitatively explore carbon and
1098 nutrient dynamics along the land-ocean transition zone over seasonal and even annual timescales
1099 (Garnier et al., 2001; Arndt et al., 2007, 2009; Arndt and Regnier, 2007; Mateus et al., 2012).
1100 However, the application of such complex models remains limited to individual, well-constrained
1101 systems due their high data requirements and computational demand resulting from the need to
1102 resolve important physical, biogeochemical and geological processes on relevant temporal and

1105 spatial scales. The one-dimensional, computationally efficient model C-GEM has been specifically
1106 designed to reduce data requirements and computational demand and to enable regional/global
1107 scale applications (Volta et al., 2014, 2016a). However, such a low data demand and computational
1108 efficiency inevitably requires simplification. The following paragraphs critically discuss these
1109 simplifications and their implications.

1110 *Spatial resolution*

1111 Here, C-GEM is used with a 0.5° spatial resolution. While this resolution captures the features of
1112 large systems, it is still very coarse for relatively small watershed, such as those of the St. Francis
1113 River, Piscataqua River, May River or the Sapelo River. For instance, the 5 estuaries reported by Hunt
1114 et al. (2010, 2011, see section 2.6) are all small systems contained by the same watershed at a 0.5°
1115 resolution. Only watersheds whose area spans several grid cells can be properly identified and
1116 represented (i.e. Merrimack or Penobscot with 6 and 9 cells, respectively).

1118 *Hydrodynamic and Transport Model*

1119 C-GEM is based on a theoretical framework that uses idealized geometries and significantly reduces
1120 data requirements. These idealized geometries are fully described by three, easily obtainable
1121 geometrical parameters (B , b_0 , H). The model thus approximates the variability of estuarine width
1122 and cross-section along the longitudinal axis through a set of exponential functions. A
1123 comprehensive sensitivity study (Volta et al., 2014) has shown that integrated process rates are
1124 generally sensitive to changes in these geometrical parameters because of their control on estuarine
1125 residence times. For instance, Volta et al. (2014) demonstrated that the NEM, is particularly sensitive
1126 to the convergence length. Similarly, the use of constant depth profile may lead to variations of
1127 about 10% in NEM (Volta et al., 2014). Nevertheless, geometrical parameters are generally easy to
1128 constrain, especially well-monitored regions such as the US east coast. Here, all geometrical
1129 parameters are constrained on the basis of observed estuarine surface areas and average water

1130 depths. In addition, the model also accounts for the slope of the estuarine channel. This approach
1131 ensures that simulated estuarine surface areas, volumes and, thus, residence times are in good
1132 agreement with those of the real systems and minimizes uncertainties associated to the physical set-
1133 up.

1134 In addition, the one-dimensional representation of the idealized estuarine systems does not resolve
1135 two- or three-dimensional circulation features induced by complex topography and density driven
1136 circulation. While C-GEM performs well in representing the dominant longitudinal gradients, its
1137 applicability to branched systems or those with aspect ratios for which a dominant axis is difficult to
1138 identify (e.g. Blackwater estuary, UK; Pearl River estuary, China; Tagus estuary, Portugal; Bay of
1139 Brest, France) is limited.

1140 *Biogeochemical Model*

1141 Although the reaction network of C-GEM accounts for all processes that control estuarine FCO_2
1142 (Borges and Abril, 2012; Cai, 2011), several, potentially important processes, such as benthic-pelagic
1143 exchange processes, phosphorous sorption/desorption and mineral precipitation, a more complex
1144 representation of the local phytoplankton community, grazing by higher trophic levels, or multiple
1145 reactive organic carbon pools are not included. Although these processes are difficult to constrain
1146 and their importance for FCO_2 is uncertain, the lack of their explicit representations induces
1147 uncertainties in C_{filt} . In particular, the exclusion of benthic processes such as organic matter
1148 degradation and burial in estuarine sediments could result in an underestimation of C_{filt} . However,
1149 because very little is known on the long term fate of organic carbon in estuarine sediments, setting
1150 up and calibrating a benthic module proves a difficult task. Furthermore, to a certain degree model
1151 parameters (such as organic matter degradation and denitrification rate constant) implicitly account
1152 for benthic dynamics. We nonetheless acknowledge that, by ignoring benthic processes and burial in
1153 particular, our estimates for the estuarine carbon filtering may be underestimated, particularly in
1154 the shallow systems of the SAR.

1155 Biogeochemical model parameters for regional and global applications are notoriously difficult to
1156 constrain (Volta et al., 2016b). Model parameters implicitly account for processes that are not
1157 explicitly resolved and their transferability between systems is thus limited. In addition, published
1158 parameter values are generally biased towards temperate regions in industrialized countries (Volta
1159 et al., 2016b). A first order estimation of the parameter uncertainty associated to the estuarine
1160 carbon removal efficiency (C_{filt}) can be extrapolated from the extensive parameter sensitivity
1161 analyses carried out by Volta et al. (2014, 2016b). These comprehensive sensitivity studies on end-
1162 member systems have shown that the relative variation in C_{filt} when a number of key
1163 biogeochemical parameters are varied by two orders of magnitude varies by is ±15 % in prismatic
1164 (short residence time on order of days) to ±25 % in funnel-shaped (long residence time) systems.
1165 Thus, assuming that uncertainty increases linearly between those bounds as a function of residence
1166 time, an uncertainty estimate can be obtained for each of our modelled estuary. With this simple
1167 method, the simulated regional C_{filt} of 1.9 Tg C yr⁻¹ would be associated with an uncertainty range
1168 comprised between 1.5 and 2.2 Tg C yr⁻¹. Our regional estuarine CO₂ evasion estimate is thus
1169 reported with moderate confidence. Furthermore, in the future, this uncertainty range could be
1170 further constrained using statistical methods such as Monte Carlo simulations (e.g. Lauerwald et al.,
1171 2015).

1172 Boundary Conditions and Forcings

1173 In addition, simulations are only performed for climatological means over the period 1990-2010
1174 without resolving interannual and secular variability. Boundary conditions and forcings are critical as
1175 they place the modelled system in its environmental context and drive transient dynamics. However,
1176 for regional applications, temporally resolved boundary conditions and forcings are difficult to
1177 constrain. C-GEM places the lower boundary condition 20 km from the estuarine mouth into the
1178 coastal ocean and the influence of this boundary condition on simulated biogeochemical dynamics is
1179 thus limited. At the lower boundary condition, direct observations for nutrients and oxygen are

1180 extracted from databases such as the World Ocean Atlas (Antonov et al., 2014). However, lower
1181 boundary conditions for OC and pCO₂ (zero concentration for OC and assumption of pCO₂
1182 equilibrium at the sea side) are simplified. This approach does not allow addressing the additional
1183 complexity introduced by biogeochemical dynamics in the estuarine plume (see Arndt et al., 2011).
1184 Yet, these dynamics only play a secondary role in the presented study that focuses on the role of the
1185 estuarine transition zone in processing terrestrial-derived carbon.

1186 Constraining upper boundary conditions and forcings is thus more critical. Here, C-GEM is forced by
1187 seasonally-averaged conditions for Q, T, and radiation. To date, GlobalNEWS only provide yearly-
1188 averaged conditions for a number of upper boundary conditions (Seitzinger et al., 2005; Mayorga et
1189 al., 2010), representative of the year 2000. Simulations are thus only partly transient (induced by
1190 seasonality in Q, T and radiation) and do not resolve short-lived events such as storms or extreme
1191 drought conditions. In addition, direct observations of upper boundary conditions are rarely
1192 available- in particular over seasonal or annual timescales. For the US East Coast estuaries, direct
1193 observations are only available for O₂, chlorophyll a, DIC and Alk. For DIC and alkalinity and boundary
1194 conditions are constrained by calculating the average concentration over a period of about three
1195 decades. In addition, observational data is extracted at the station closest to the model's upper
1196 boundary, which might be still located several kilometres upstream or downstream of the model
1197 boundary. Upper boundary conditions of POC, DOC, DIN, DIP, DSi are extracted from GlobalNews
1198 and thus model-derived. As a consequence, our results are thus intimately dependent on the
1199 robustness of the GlobalNEWS predictions. These values are usually only considered robust
1200 estimates for watersheds larger than ~10 cells (Beusen et al., 2005), which only correspond to 13 of
1201 the 43 estuaries modelled in this study.

1202 *Model-data comparison*

1203 The generic nature of the applied model approach and, in particular the application of
1204 seasonally/annually averaged or model-deduced boundary conditions renders a direct validation of

1205 model results on the basis of local and instantaneous observational data (e.g. longitudinal profiles),
1206 which is likely not representative of these long-term average conditions, difficult. Therefore, model
1207 performance is evaluated on the basis of spatially aggregated estimates (e.g. regional FCO_2 estimates
1208 based on local measurements) rather than system-to-system comparisons with longitudinal profile
1209 from specific days. However, note that the performance of C-GEM has been intensively tested by
1210 specific model-data comparisons for a number of different systems (e.g. Volta et al., 2014, 2016a)
1211 and we are thus confident of its predictive capabilities.

1212 Despite the numerous simplifying assumptions inevitably required for such a regional assessment of
1213 carbon fluxes along the land-ocean continuum, the presented approach does nevertheless provide
1214 an important step forward in evaluating the role of land-ocean transition systems in the global
1215 carbon cycle. It provides a first robust estimate of carbon dynamics based on a theoretically well-
1216 founded and carefully tested, spatially and temporally resolved model approach. This approach
1217 provides novel insights that go beyond those gained through traditionally applied zero-salinity
1218 method or box model approaches. In addition, it also highlights critical variables and data gaps and
1219 thus helps guide efficient monitoring strategies.

1220 **3.5 Towards predictors of the estuarine carbon processing**

Deleted: 4

1221 The mutual dependence between geometry and transport in tidal estuaries and, ultimately, their
1222 biogeochemical functioning (Savenije, 1992; Volta et al., 2014) allows relating easily extractable
1223 parameters linked to their shape or their hydraulic properties to biogeochemical indicators. In this
1224 section, we explore the relationships between such simple physical parameters and indicators of the
1225 estuarine carbon processing \overline{NEM} , $\overline{FCO_2}$ and $CFilt$. In order to account for the effect of temperature
1226 on C dynamics, $-\overline{NEM}$ and $\overline{FCO_2}$ are also normalized to the same temperature (arbitrarily chosen to
1227 be 0 degree). These normalized values are obtained by dividing $-\overline{NEM}$ and $\overline{FCO_2}$ by a Q_{10} function
1228 $f(T)$ (see Volta et al., 2014). This procedure allows accounting for the exponential increase in the rate
1229 of several temperature dependent processes contributing to the NEM (i.e. photosynthesis, organic

Deleted:

1232 carbon degradation...). Applying the same normalization to \overline{NEM} and $\overline{FCO_2}$ is a way of testing how
1233 intimately linked \overline{NEM} and $\overline{FCO_2}$ are in estuarine systems. Indeed linear relationships relating one to
1234 the other have been reported (Mayer and Eyre, 2012). The three indicators are then investigated as
1235 a function of the ratio between the estuarine surface S and the seasonal river discharge Q . The
1236 surface area is calculated from the estuarine width and length, as described by equation 2, in order
1237 to use a parameter which is potentially applicable to other regions for which direct estimates of the
1238 real estuarine surface area is not available. Since the fresh water residence time of a system is
1239 obtained by dividing volume by river discharge, the S/Q ratio is also intimately linked to residence
1240 time. Here, we choose to exclude the estuarine depth from the analysis because this variable cannot
1241 be easily quantified from maps or remote sensing images and would thus compromise the
1242 applicability of a predictive relationship on the global scale. However, from dimensional analysis, S/Q
1243 can be viewed as a water residence time normalized to meter depth of water. As shown by equation
1244 3, S only requires constraining BO and width convergence length b , two parameters that can readily
1245 be extracted from the Google Earth engine. Global database of river discharges, as for instance
1246 RivDIS (Vörösmarty et al., 1996) are also available in such a way that the S/Q ratio can potentially be
1247 extracted for all estuaries around the globe.

Formatted: Font: Italic

Formatted: Font: Italic

Formatted: Font: Italic, Subscript

1248 Figure [12a](#) reveals that small values of S/Q are associated with the most negative $\overline{NEM} / f(T)$. The
1249 magnitude of the \overline{NEM} then exponentially decreases with increasing values of S/Q . Estuaries
1250 characterized by small values of S/Q are mainly located in the NAR sub-region and correspond to
1251 small surface area, and thus short residence time systems. It is possible to quantitatively relate -
1252 $\overline{NEM} / f(T)$ and S/Q through a power law function ($y = 25.85 x^{-0.64}$ with a $r^2 = 0.82$). The coefficient
1253 of determination remains the same when excluding estuaries from the NAR region and the equation
1254 itself is not significantly different, although those estuaries on their own do not display any
1255 statistically significant trend ([Tab. 6](#)). The decrease in the intensity of the net ecosystem metabolism
1256 in larger estuaries (Fig [8](#)), characterized by high S/Q ratios, can be related to the extensive

Deleted: 10a

Deleted: table

Deleted: 6

1260 consumption of the organic matter pool during its transit through the estuarine filter. However,
1261 when reported to the entire surface area of the estuary, larger systems (with high values of S/Q) still
1262 reveal the most negative surface integrated NEM (Fig. 12b). It can also be noted that some estuaries
1263 from the NAR region display very low values of $-NEM$. These data points correspond to fall and
1264 winter simulations for which the temperature was relatively cold (<5 °C) and biogeochemical
1265 processing was very low.

Deleted: fig

Deleted: 10b

1266 The overall response of $\overline{FCO_2}/f(T)$ to S/Q is comparable to that of $-\overline{NEM}/f(T)$ (Fig. 12c), with
1267 lower values of $\overline{FCO_2}$ observed for high values of S/Q. However, for $S/Q < 3$ days m^{-1} , the $\overline{FCO_2}$
1268 values are very heterogeneous and contain many, low $\overline{FCO_2}$ outliers from the NAR region. These
1269 data points generally correspond to low water temperature conditions which keep pCO_2 low, even if
1270 the system generates enough CO_2 internally via NEM. Thus, the well-documented correlation
1271 between \overline{NEM} and $\overline{FCO_2}$ (Maher and Eyre, 2012) does not seem to hold for systems with very short
1272 residence times. For systems with $S/Q > 3$ days m^{-1} , we obtain a regression $FCO_2 = -0.64 \times NEM + 5.96$
1273 with a r^2 of 0.46, which compares well with the relation $FCO_2 = -0.42 \times NEM + 12$ proposed by Maher
1274 and Eyre (2012) who used 24 seasonal estimates from small Australian estuaries. However, our
1275 results suggest that this relationship cannot be extrapolated to small systems such as those located
1276 in the NAR. Figure 12d, which reports non-normalized FCO_2 reveals a monotonous increase of FCO_2
1277 with S/Q. This suggests that, unlike the NEM for which the normalization by a temperature function
1278 allowed explaining most of the variability; FCO_2 is mostly controlled by the water residence time
1279 within the system. Discharge is the main FCO_2 driver in riverine dominated systems, while
1280 interactions with marshes are driving the outgassing in marine dominated systems surrounded by
1281 marshes. Net aquatic biological production (NEM being negative or near 0) in large estuaries (with
1282 large S/Q) is another important reason for low FCO_2 in such systems. For example, despite the higher
1283 CO_2 degassing flux in the upper estuary of the Delaware, strong biological CO_2 uptake in the mid-bay
1284 and near zero NEM in the lower bay result in a much lower FCO_2 for the entire estuary (Joesoef et al.

Deleted: 10c

Deleted: m

Formatted: Font: Italic

1289 2015). In systems with $S/Q < 3 \text{ days m}^{-1}$, the short residence time prevents the excess CO_2 of
1290 oversaturated water from being entirely exchanged with the atmosphere and simulations reveal that
1291 the estuarine waters are still oversaturated in CO_2 at the estuarine mouth. Thus, the inorganic
1292 carbon, produced by the decomposition of organic matter, is not outgassed within the estuary but
1293 exported to the adjacent continental shelf waters. This result is consistent with the observation-
1294 based hypothesis of Laruelle et al. (2015) for the NAR estuaries. As a consequence of the distinct
1295 behavior of short residence time systems, the coefficient of determination of the best-fitted power
1296 law function relating $\overline{FCO_2}$ and S/Q is only significant if NAR systems are excluded ($y = 31.64 x^{-0.58}$

1297 with a $r^2 = 0.70$). This thus suggest that such relationships (as well as that proposed by Maher and
1298 Eyre, 2012) cannot be applied to any system but only those for which $S/Q > 3 \text{ day m}^{-1}$.

Formatted: Superscript

1299 Finally, Fig. 12e reports the simulated mean seasonal carbon filtering capacities as a function of the
1300 depth normalized residence time. Not surprisingly, and in overall agreement with previous studies
1301 on nutrient dynamics in estuaries (Nixon et al., 1996), the carbon filtering capacity increases with
1302 S/Q . The best statistical relation between $CFilt$ and S/Q is obtained when including all 3 regions,
1303 resulting in $r^2 = 0.70$ ($y = 40.64 \log_{10}(x) + 11.84$). Very little C removal occurs in systems with $S/Q < 1$
1304 day m^{-1} . For systems characterized by longer depth-normalized residence times, $CFilt$ increases
1305 regularly, and reaches 100% for $S/Q > 100 \text{ day m}^{-1}$. Such high values are only observed for very large
1306 estuaries from the MAR region (Delaware and Chesapeake Bays); the majority of our systems had an
1307 S/Q range between 1 and 100 day m^{-1} . The quantitative assessment of estuarine filtering capacities
1308 is further complicated by the complex interplay of estuarine and coastal processes. Episodically,
1309 marked spatial variability in concentration gradients near the estuarine mouth may lead to a reversal
1310 of net material fluxes from coastal waters into the estuary (Regnier et al., 1998; Arndt et al. 2011).
1311 Our results show that this feature is particularly significant for estuaries with a large width at the
1312 mouth and short convergence length (funnel shaped or 'Bay type' systems). These coastal nutrient
1313 and carbon inputs influence the internal estuarine C dynamics and lead to filtering capacities that

Deleted: Figure

Deleted: 10e

1316 can exceed 100%. This feature is particularly significant in summer, when riverine inputs are low and
1317 the marine material is intensively processed inside the estuary.

1318 Previous work investigated the relationship between fresh water residence time and nutrient
1319 retention (Nixon et al., 1996; Arndt et al., 2011; Laruelle, 2009). These studies, however, were
1320 constrained by the scarcity of data. For instance, the pioneering work of Nixon et al. (1996) only
1321 relied on a very limited number (<10) of quite heterogeneous coastal systems, all located along the
1322 North Atlantic. Here, our modeling approach allows us to generate 172 (43 x 4) data points, each
1323 representing a system-scale biogeochemical behavior. Together, this database spans the entire
1324 spectrum of estuarine settings and climatic conditions found along the East coast of the US. In
1325 addition, the ratio S/Q used as master variable for predicting temperature normalized $\overline{-NEM}$, $\overline{FCO_2}$
1326 and $CFilt$ only requires a few easily accessible geometric parameters ($B0$, b and L) and an estimate of
1327 the river discharge. While it is difficult to accurately predict $\overline{FCO_2}$ for small systems such as those
1328 located in the NAR region, the relationships found are quite robust for systems in which $S/Q > 3$ days
1329 m^{-1} . Most interestingly, $CFilt$ values reveal a significant correlation with S/Q and could be used in
1330 combination with global riverine carbon delivery estimates such as GlobalNews 2 (Mayorga et al.,
1331 2010) to constrain the estuarine CO_2 evasion and the carbon export to the coastal ocean at the
1332 continental and global scales.

1333 **4. Conclusions**

1334 This study presents the first complete estuarine carbon budget for the East coast of the US using a
1335 modeling approach. The structure of the model C-GEM relies on a restricted number of readily
1336 available global datasets to constrain boundary conditions and limits the number of geometrical and
1337 physical parameters to be constrained. Our simulations predict a total CO_2 outgassing of $1.9 \text{ Tg C } \gamma^{-1}$
1338 for all tidal estuaries of the East coast of the US. This quantification accounts for the seasonality in
1339 estuarine carbon processing as well as for distinct individual behaviors among estuarine types
1340 (marine or river dominated). The total carbon output to the coastal ocean is estimated at $2.7 \text{ TgC } \gamma^{-1}$,

1341 and the carbon filtering capacity with respect to riverine, marshes and mangrove inputs is thus on
1342 the order of 40%. This value is significantly higher than the recently estimated C filtering capacity for
1343 estuaries surrounding the North Sea using a similar approach (Volta et al., 2016a), mainly because
1344 the surface area available for gas exchange and the draining lithology limits the CO₂ evasion in the
1345 NW European systems. At the regional scale of the US East coast estuaries, net heterotrophy is the
1346 main driver (50%) of the CO₂ outgassing, followed by the ventilation of riverine supersaturated
1347 waters entering the estuarine systems (32%) and nitrification (18%). The dominant mechanisms for
1348 the gas exchange and the resulting carbon filtering capacities nevertheless reveal a clear latitudinal
1349 pattern, which reflects the shapes of estuarine systems, climatic conditions and dominant land-use
1350 characteristics.

1351 Our model results are used to derive predictive relationships relating the intensity of the area-based
1352 Net Ecosystem Metabolism (\overline{NEM}), air-water CO₂ exchange ($\overline{FCO_2}$) and the carbon filtering capacity
1353 ($CFilt$) to the depth normalized residence time, expressed as the ratio of the estuarine surface area
1354 to the river discharge. In the future, such simple relationships relying on readily available geometric
1355 and hydraulic parameters could be used to quantify carbon processing in areas of the world devoid
1356 of direct measurements. However, it is important to note that such simple relationships are only
1357 valid over the range of boundary conditions and forcings explored and may not be applicable to
1358 conditions that fall outside of this range. In regions with better data coverage, such as the one
1359 investigated here, our study highlights that the regional-scale quantification, attribution, and
1360 projection of estuarine biogeochemical cycling are now at reach.

Formatted: Font: Not Bold, Not Italic,
No underline

Deleted: prediction

1361 5. Acknowledgements

1362 G. G. Laruelle is Chargé de recherches du F.R.S.-FNRS at the Université Libre de Bruxelles. The
1363 research leading to these results has received funding from the European Union's Horizon 2020
1364 research and innovation programme under the Marie Skłodowska-Curie grant agreement No 643052

1366 (C-CASCADES project). The authors thank V. L. Mulder for her thorough reading of the manuscript
1367 upon submission.

1368 |

1369 **References:**

- 1370 Abril, G., Nogueira, M., Etcheber, H., Cabeçadas, G., Lemaire, E., and Brogueira, M.J.: Behaviour of
1371 organic carbon in nine contrasting European estuaries. *Estuar. Coast. Shelf Sci.*, 54, 241-262,
1372 2002.
- 1373 Antonov, J.I., Seidov, D., Boyer, T.P., Locarnini, R.A., Mishonov, A.V., Garcia, H.E., Baranova, O.K.,
1374 Zweng, M.M., and Johnson, D.R.: *World Ocean Atlas 2009, Volume 2: Salinity*. S., 2010.
- 1375 Arndt, S., Vanderborght, J.P., and Regnier, P.: Diatom growth response to physical forcing in a
1376 macrotidal estuary: Coupling hydrodynamics, sediment transport, and biogeochemistry.
1377 *Journal of Geophysical Research C: Oceans*, 112(5), 2007.
- 1378 Arndt, S. and Regnier, P.: A model for the benthic-pelagic coupling of silica in estuarine ecosystems:
1379 sensitivity analysis and system scale simulation, *Biogeosciences*, 4, 331-352, doi:10.5194/bg-
1380 4-331-2007, 2007.
- 1381 Arndt, S., Regnier, P., and Vanderborght, J.P.: Seasonally-resolved nutrient export fluxes and filtering
1382 capacities in a macrotidal estuary. *Journal of Marine Systems*, 78(1), 42-58, 2009.
- 1383 Arndt, S., Lacroix, G., Gypens, N., Regnier, P., and Lancelot, C.: Nutrient dynamics and phytoplankton
1384 development along an estuary-coastal zone continuum: A model study. *Journal of Marine
1385 Systems*, 84(3-4), 49-66, 2011.
- 1386 Atlas, R., Hoffman, R.N., Ardizzone, J., Leidner, S.M., Jusem, J.C., Smith, D.K. and Gombos, D.: A
1387 cross-calibrated, multiplatform ocean surface wind velocity product for meteorological and
1388 oceanographic applications. *Bulletin of the American Meteorological Society*, 92(2), 157-174,
1389 2011.
- 1390 Baklouti, M., Chevalier, C., Bouvy, M., Corbin, D., Pagano, M., Troussellier, M., and Arfi, R.: A study of
1391 plankton dynamics under osmotic stress in the Senegal River Estuary, West Africa, using a 3D
1392 mechanistic model, *Ecol. Model.*, 222, 2704-2721, 2011.
- 1393 Bauer, J.E., Cai, W.J., Raymond, P.A., Bianchi, T.S., Hopkinson, C.S., and Regnier, P.A.G.: The changing
1394 carbon cycle of the coastal ocean. *Nature*, 504(7478), 61-70, 2013.
- 1395 Beusen, A. H.W., Dekkers, A. L. M., Bouwman, A. F., Ludwig, W., and Harrison, J.: Estimation of global
1396 river transport of sediments and associated particulate C, N, and P, *Global Biogeochem. Cy.*,
1397 19, GB4S05, doi:10.1029/2005GB002453, 2005.
- 1398 Beusen, A.H.W., Bouwman, A.F., Dürr, H.H., Dekkers, A.L.M., and Hartmann, J.: Global patterns of
1399 dissolved silica export to the coastal zone: Results from a spatially explicit global model.
1400 *Global Biogeochemical Cycles*, 23, GB0A02, doi:10.1029/2008GB003281, 2009.
- 1401 Billen, G., Thieu, V., Garnier, J., and Silvestre, M.: Modelling the N cascade in regional waters: The
1402 case study of the Seine, Somme and Scheldt rivers, *Agr. Ecosyst. Environ.*, 133, 234-246,
1403 2009.
- 1404 Borges, A.V., Delille, B., and Frankignoulle, M.: Budgeting sinks and sources of CO₂ in the coastal
1405 ocean: Diversity of ecosystems counts. *Geophys. Res. Lett.*, 32(14), L14601, 2005.
- 1406 Borges, A.V., and Abril, G.: Carbon Dioxide and Methane Dynamics in Estuaries. In: E. Wolanski and
1407 D.S. McLusky (Editors), *Treatise on Estuarine and Coastal Science*. Academic Press, Waltham,
1408 pp. 119-161, 2012.
- 1409 Bricker, S., Longstaff, B., Dennison, W., Jones, A., Boicourt, K., Wicks, C., and Woerner, J.: *Effects of
1410 Nutrient Enrichment In the Nation's Estuaries: A Decade of Change*, NOAA, MD, 2007.
- 1411 Brock, T.D.: Calculating solar radiation for ecological studies. *Ecological Modelling*, 14(1-2), 1-19,
1412 1981.
- 1413 Caffrey, J.: Factors controlling net ecosystem metabolism in U.S. estuaries. *Estuaries*, 27(1), 90-101,
1414 2004.
- 1415 Cai, W.J., and Wang, Y.: The chemistry, fluxes, and sources of carbon dioxide in the estuarine waters
1416 of the Satilla and Altamaha Rivers, Georgia. *Limnology and Oceanography*, 43(4), 657-668,
1417 1998.
- 1418 Cai, W.J., Wang, Y., and Hodson, R. E.: Acid-base properties of dissolved organic matter in the
1419 estuarine waters of Georgia, USA. *Geochimica et Cosmochimica Acta*, 62(3), 473-483, 1998.

Deleted: ¶

Formatted: English (U.K.)

Formatted: English (U.K.)

Deleted: ¶

Formatted: English (U.K.)

Formatted: English (U.K.)

1422 Cai, W.J., Pomeroy, L.R., Moran, M.A., and Wang, Y.: Oxygen and carbon dioxide mass balance for
1423 the estuarine-intertidal marsh complex of five rivers in the southeastern U.S. *Limnology and*
1424 *Oceanography*, 44, 639-649, 1999.

1425 Cai, W.J.: Estuarine and coastal ocean carbon paradox: CO₂ sinks or sites of terrestrial carbon
1426 incineration? *Ann. Rev. Mar. Sci.*, 3, 123-145, 2011.

1427 [Cerco, C., Kim, S.-C., and Noel, M.: The 2010 Chesapeake Bay eutrophication model. US](#)
1428 [Environmental Protection Agency Chesapeake Bay Program, Annapolis, MD, 2010.](#)

1429 Chen, C.-T.A., Huang, T.-H., Fu, Y.-H., Bai, Y., and He, X.: Strong sources of CO₂ in upper estuaries
1430 become sinks of CO₂ in large river plumes. *Current Opinion in Environmental Sustainability*,
1431 4(2), 179-185, 2012.

1432 Chen, C.-T. A., Huang, T.-H., Chen, Y.-C., Bai, Y., He, X., and Kang, Y.: Air-sea exchanges of CO₂ in the
1433 world's coastal seas, *Biogeosciences*, 10, 6509–6544, doi:10.5194/bg-10-6509-2013, 2013.

1434 Dai, T., and Wiegert, R.G.: Estimation of the primary productivity of *Spartina alterniflora* using a
1435 canopy model. *Ecography*, 19(4), 410-423, 1996.

1436 Dufore, C. M.: Spatial and Temporal Variations in the Air-Sea Carbon Dioxide Fluxes of Florida Bay,
1437 Graduate School Thesis, University of South Florida, 2012.

1438 Dürr, H.H., Meybeck, M., and Dürr, S.H.: Lithological composition of the Earth's continental surfaces
1439 derived from a new digital map emphasizing riverine material transfer. *Glob. Biogeochem.*
1440 *Cycles* 19 (4), GB4S10, 2005.

1441 Dürr, H.H., Laruelle, G.G., van Kempen, C.M., Slomp, C.P., Meybeck, M., and Middelkoop, H.:
1442 Worldwide Typology of Nearshore Coastal Systems: Defining the Estuarine Filter of River
1443 Inputs to the Oceans. *Estuaries and Coasts*, 34(3), 441-458, 2011.

1444 EPA (2009). "1970 - 2008 Average annual emissions, all criteria pollutants in MS Excel." National
1445 Emissions Inventory (NEI) Air Pollutant Emissions Trends Data. Office of Air Quality Planning
1446 and Standards. Available online at <<http://www.epa.gov/ttn/chieftrends/index.html>>

1447 Fekete, B.M., Vörösmarty, C.J., and Grabs, W.: High-resolution fields of global runoff combining
1448 observed river discharge and simulated water balances. *Global Biogeochemical Cycles*, 16(3),
1449 15-1, 2002.

1450 Fischer, H. B.: Mixing and Dispersion in Estuaries, *Annu. Rev. Fluid Mech.*, 8, 107–133,
1451 1976. Friedrichs, M.A.M., and Hofmann, E.E.: Physical control of biological processes in the
1452 central equatorial Pacific Ocean. *Deep-Sea Research Part I: Oceanographic Research Papers*,
1453 48(4), 1023-1069, 2001.

1454 Garcia, H.E., Locarnini, R.A., Boyer, E.W., Antonov, A., Baranova, O.K., Zweng, M.M., and Johnson,
1455 D.R.: *World Ocean Atlas 2009, Volume 3: Dissolved Oxygen, Apparent Oxygen Utilization,*
1456 *and Oxygen Saturation, 2010a.*

1457 Garcia, H.E., Locarnini, R.A., Boyer, E.W., Antonov, J.I., Baranova, O.K., Zweng, M.M., and Johnson,
1458 D.R.: *World Ocean Atlas 2009, Volume 4: Nutrients (phosphate, nitrate, silicate), 2010b.*

1459 [Garnier, J., Servais, P., Billen, G., Akopian, M., and Brion, N.: Lower Seine River and Estuary \(France\)](#)
1460 [Carbon and Oxygen Budgets During Low Flow, *Estuaries*, 24, 964–976, 2001.](#)

1461 Harrison, J.A., Caraco, N., and Seitzinger, S.P.: Global patterns and sources of dissolved organic
1462 matter export to the coastal zone: Results from a spatially explicit, global model. *Global*
1463 *Biogeochemical Cycles*, 19(4), GB4S03, doi:10.1029/2004GB002357, 2005.

1464 Hartmann, J., Jansen, N., Dürr, H.H., Kempe, S., and Köhler, P.: Global CO₂ consumption by chemical
1465 weathering: What is the contribution of highly active weathering regions? *Global Planet.*
1466 *Change*, 69(4), 185-194, 2009.

1467 Hartmann, J., Dürr, H.H., Moosdorf, N., Meybeck, M., and Kempe, S.: The geochemical composition
1468 of the terrestrial surface (without soils) and comparison with the upper continental crust.
1469 *Int. J. Earth Sci.* 101, 365-376, 2012.

1470 Herrmann, M., Najjar, R.G., Kemp, W.M., Alexander, R.B., Boyer, E.W., Cai, W.-J., Griffith, P.C.,
1471 Kroeger, K.D., McCallister, S.L., and Smith, R.A.: Net ecosystem production and organic

Deleted: F

1473 carbon balance of U.S. East Coast estuaries: A synthesis approach, *Global Biogeochem.*
1474 *Cycles*, 29, doi:10.1002/2013GB004736, 2015.

1475 Hofmann, A.F., Soetaert, K., and Middelburg, J.J.: Present nitrogen and carbon dynamics in the
1476 Scheldt estuary using a novel 1-D model. *Biogeosciences*, 5(4), 981-1006, 2008.

1477 [Hofmann, E.E., Cahill, B., Fennel, K., Friedrichs, M.A.M., Hyde, K., Lee, C., Mannino, A., Najjar, R.G.,
1478 O'Reilly, J.E., Wilkin, J., and Xue, J.: Modeling the dynamics of continental shelf carbon. *Ann
1479 Rev Mar Sci.* 3, 93-122, 2011.](#)

1480 Hunt, C. W., Salisbury, J. E., Vandemark, D., and McGillis, W.: Contrasting Carbon Dioxide Inputs and
1481 Exchange in Three Adjacent New England Estuaries. *Estuar. Coast.*, 34, 68–77,
1482 doi:10.1007/s12237-010-9299-9, 2010.

1483 Hunt, C.W., Salisbury, J.E., Vandemark, D., and McGillis, W.: Contrasting Carbon Dioxide Inputs and
1484 Exchange in Three Adjacent New England Estuaries. *Estuaries and Coasts*, 34(1), 68-77, 2011.

1485 Ippen, A.T., and Harleman, D.R.F.: One-dimensional Analysis of Salinity Intrusion in Estuaries,
1486 Technical Bulletin No. 5, Committee on Tidal Hydraulics, Corps of Engineers, US Army,
1487 Vicksburg, 1961.

1488 Jiang, L.Q., Cai, W.J., and Wang, Y.: A comparative study of carbon dioxide degassing in river- and
1489 marine-dominated estuaries. *Limnology and Oceanography*, 53(6), 2603-2615, 2008.

1490 Jiang, L.-Q., Cai, W.-J., Wang, Y., and Bauer, J. E.: Influence of terrestrial inputs on continental shelf
1491 carbon dioxide, *Biogeosciences*, 10, 839–849, doi:10.5194/bg-10-839-2013, 2013.

1492 Joesoef, A., Huang, W.-J., Gao, Y., and Cai, W.-J.: Air–water fluxes and sources of carbon dioxide in
1493 the Delaware Estuary: spatial and seasonal variability, *Biogeosciences*, 12, 6085-6101,
1494 doi:10.5194/bg-12-6085-2015, 2015.

1495 Kent, B.H.: Turbulent diffusion in a Sectionally Homogeneous Estuary, Technical Report 16,
1496 Chesapeake Bay Institute, John Hopkins, University, Baltimore, 1958.

1497 Key, R.M., Kozyr, A., Sabine, C.L., Lee, K., Wanninkhof, R., Bullister, J.L., Feely, R.A., Millero, F.J.,
1498 Mordy, C., and Peng, T.H.: A global ocean carbon climatology: Results from Global Data
1499 Analysis Project (GLODAP). *Global Biogeochemical Cycles*, 18(4), 1-23, 2004.

1500 Laruelle, G.G.: Quantifying nutrient cycling and retention in coastal waters at the global scale, Ph D
1501 dissertation, Utrecht University, 2009.

1502 Laruelle, G. G., Regnier, P., Ragueneau, O., Kempa, M., Moriceau, B., Ni Longphuiert, S., Leynaert, A.,
1503 Thouzeau, G., and Chauvaud, L.: Benthic-pelagic coupling and the seasonal silica cycle in the
1504 Bay of Brest (France): new insights from a coupled physical-biological model, *Mar. Ecol.-
1505 Prog. Ser.*, 385, 15–32, 2009.

1506 Laruelle, G.G., Dürr, H.H., Slomp, C.P., and Borges, A.V.: Evaluation of sinks and sources of CO₂ in the
1507 global coastal ocean using a spatially-explicit typology of estuaries and continental shelves.
1508 *Geophys. Res. Lett.*, 37(15), L15607, doi:10.1029/2010GL043691, 2010.

1509 Laruelle, G.G., Dürr, H.H., Lauerwald, R., Hartmann, J., Slomp, C.P., Goossens, N., and Regnier, P.A.G.:
1510 Global multi-scale segmentation of continental and coastal waters from the watersheds to
1511 the continental margins. *Hydrol. Earth Syst. Sci.*, 17(5), 2029-2051, 2013.

1512 Laruelle, G.G., Lauerwald, R., Rotschi, J. Raymond, P.A., and Regnier, P.: Seasonal response of air-
1513 water CO₂ exchange along the land-ocean aquatic continuum of the northeast North
1514 American coast. *Biogeosci.* 12, 1447-1458, 2015.

1515 Lauerwald, R., Hartmann, J., Moosdorf, N., Kempe, S., and Raymond, P.A.: What controls the spatial
1516 patterns of the riverine carbonate system? — A case study for North America. *Chemical
1517 Geology*, 337–338, 114-127, 2013.

1518 [Lauerwald, R., Laruelle, G. G., Hartmann, J., Clais, P., and Regnier, P. A. G.: Spatial patterns in CO₂
1519 evasion from the global river network, *Global Biogeochem. Cy.*, 29, 534–554,
1520 doi:10.1002/2014GB004941, 2015.](#)

1521 Leonard, B.: Third-Order Upwinding as a Rational Basis for Computational Fluid Dynamics, in:
1522 *Computational Techniques and Applications: CTAC-83*, edited by: Noye J. and Fletcher C. A.
1523 J., Elsevier, North-Holland, 1984.

- 1524 Le Quéré, C., Peters, G. P., Andres, R. J., Andrew, R. M., Boden, T. A., Ciais, P., Friedlingstein, P.,
 1525 Houghton, R. A., Marland, G., Moriarty, R., Sitch, S., Tans, P., Arneeth, A., Arvanitis, A., Bakker,
 1526 D. C. E., Bopp, L., Canadell, J. G., Chini, L. P., Doney, S. C., Harper, A., Harris, I., House, J. I.,
 1527 Jain, A. K., Jones, S. D., Kato, E., Keeling, R. F., Klein Goldewijk, K., Körtzinger, A., Koven, C.,
 1528 Lefèvre, N., Maignan, F., Omar, A., Ono, T., Park, G.-H., Pfeil, B., Poulter, B., Raupach, M. R.,
 1529 Regnier, P., Rödenbeck, C., Saito, S., Schwinger, J., Segschneider, J., Stocker, B. D., Takahashi,
 1530 T., Tilbrook, B., van Heuven, S., Viovy, N., Wanninkhof, R., Wiltshire, A., and Zaehle, S.:
 1531 Global carbon budget 2013, *Earth Syst. Sci. Data*, 6, 235-263, doi:10.5194/essd-6-235-2014,
 1532 2014.
- 1533 Le Quéré, C., Moriarty, R., Andrew, R. M., Canadell, J. G., Sitch, S., Korsbakken, J. I., Friedlingstein, P.,
 1534 Peters, G. P., Andres, R. J., Boden, T. A., Houghton, R. A., House, J. I., Keeling, R. F., Tans, P.,
 1535 Arneeth, A., Bakker, D. C. E., Barbero, L., Bopp, L., Chang, J., Chevallier, F., Chini, L. P., Ciais, P.,
 1536 Fader, M., Feely, R. A., Gkritzalis, T., Harris, I., Hauck, J., Ilyina, T., Jain, A. K., Kato, E., Kitidis,
 1537 V., Klein Goldewijk, K., Koven, C., Landschützer, P., Lauvset, S. K., Lefèvre, N., Lenton, A.,
 1538 Lima, I. D., Metzl, N., Millero, F., Munro, D. R., Murata, A., Nabel, J. E. M. S., Nakaoka, S.,
 1539 Nojiri, Y., O'Brien, K., Olsen, A., Ono, T., Pérez, F. F., Pfeil, B., Pierrot, D., Poulter, B., Rehder,
 1540 G., Rödenbeck, C., Saito, S., Schuster, U., Schwinger, J., Séférian, R., Steinhoff, T., Stocker, B.
 1541 D., Sutton, A. J., Takahashi, T., Tilbrook, B., van der Laan-Luijkx, I. T., van der Werf, G. R., van
 1542 Heuven, S., Vandemark, D., Viovy, N., Wiltshire, A., Zaehle, S., and Zeng, N.: Global Carbon
 1543 Budget 2015, *Earth Syst. Sci. Data*, 7, 349-396, doi:10.5194/essd-7-349-2015, 2015.
- 1544 [Lin, J., Xie, L., Pietrafesa, L. J., Ramus, J. S., and Paerl, H.W.: Water Quality Gradients across](#)
 1545 [Albemarle-Pamlico Estuarine System: Seasonal Variations and Model Applications, *J. Coast.*](#)
 1546 [Res., 23, 213–229, 2007.](#)
- 1547 Locarnini, R.A., Mishonov, A.V., Antonov, J.I., Boyer, T.P., Garcia, H.E., Baranova, O.K., Zweng, M.M.,
 1548 and Johnson, D.R.: World Ocean Atlas 2009, Volume 1: Temperature, 2010.
- 1549 Ludwig, W., Probst, J. L., and Kempe, S.: predicting the oceanic input of organic carbon by
 1550 continental erosion, *Global Biogeochem. Cy.*, 10, 23–41, 1996.
- 1551 Maher, D.T., and Eyre, B.D.: Carbon budgets for three autotrophic Australian estuaries: Implications
 1552 for global estimates of the coastal air-water CO₂ flux. *Global Biogeochem. Cycles*, 26(1),
 1553 GB1032, 2012.
- 1554 [Mateus, M., Vaz, N., and Neves, R.: A process-oriented model of pelagic biogeochemistry for marine](#)
 1555 [systems. Part II: Application to a mesotidal estuary, *J. Mar. Syst.*, 94, 90–101, 2012.](#)
- 1556 Mayorga, E., Seitzinger, S.P., Harrison, J.A., Dumont, E., Beusen, A.H.W., Bouwman, A.F., Fekete,
 1557 B.M., Kroeze, C., and Van Drecht, G.: Global Nutrient Export from WaterSheds 2 (NEWS 2):
 1558 Model development and implementation. *Environmental Modelling and Software*, 25(7),
 1559 837-853, 2010.
- 1560 Meybeck, M.: Carbon, nitrogen, and phosphorus transport by world rivers. *Am. J. Sci.*, 282(4), 401-
 1561 450, 1982.
- 1562 Meybeck, M., Dürr, H. H., and Vörosmary, C. J.: Global coastal segmentation and its river catchment
 1563 contributors: A new look at land-ocean linkage, *Global Biogeochem. Cy.*, 20, GB1S90,
 1564 doi:10.1029/2005GB002540, 2006.
- 1565 Middelburg, J.J., Klaver, G., Nieuwenhuize, J., Wielemaker, A., De Haas, W., Vlug, T., and Van Der
 1566 Nat, J.F.W.A.: Organic matter mineralization in intertidal sediments along an estuarine
 1567 gradient. *Marine Ecology Progress Series*, 132(1-3), 157-168, 1996.
- 1568 NASA/NGA: SRTM Water Body Data Product Specific Guidance, Version 2.0, 2003.
- 1569 Najjar, R.G., Friedrichs, M., and Cai, W.-J. (Editors): Report of The U.S. East Coast Carbon Cycle
 1570 Synthesis Workshop, January 19-20, 2012. Ocean Carbon and Biogeochemistry Program and
 1571 North American Carbon Program, 34 pp, 2012.
- 1572 Nihoul, J. C. J., and Runday, F.: Modèles d'estuaires partiellement stratifiés, *Projet Mer*, Vol. 10,
 1573 Service de la Programmation Scientifique, Bruxelles, Belgium, 71–98, 1976.

- 1574 Nixon, S.W., J.W. Ammerman, L.P. Atkinson, V.M. Berounsky, G. Billen, W.C. Boicourt, W.R. Boynton,
 1575 T.M. Church, D.M. Ditoro, R. Elmgren, J.H. Garber, A.E. Giblin, R.A. Jahnke, N.J. P. Owens,
 1576 M.E.Q. Pilson, and Seitzinger, S.P.: The fate of nitrogen and phosphorus at the land–sea
 1577 margin of the North Atlantic Ocean. *Biogeochemistry* 3, 141–180, 1996.
- 1578 NOAA: National Estuarine Inventory Data Atlas, Volume 1: Physical and Hydrologic Characteristics,
 1579 National Oceanic and Atmospheric Administration, MD, 1985.
- 1580 Odum, H.T.: Primary Production in Flowing Waters. *Limnol. Oceanogr.*, 1, 102-117, 1956.
- 1581 O'Kane, J. P.: Estuarine Water Quality Management. Pitman, London, U.K, 1980.
- 1582 Paerl, H.W., Valdes, L.M., Peierls, B.L., Adolf, J.E., and Harding Jr, L.W.: Anthropogenic and climatic
 1583 influences on the eutrophication of large estuarine ecosystems. *Limnology and*
 1584 *Oceanography*, 51(1 II), 448-462, 2006.
- 1585 Platt, T., Gallegos, C. L., and Harrison, W. G.: Photoinhibition of photosynthesis in natural
 1586 assemblages of marine phytoplankton. *J. Mar. Res.*, 38, 687-701, 1980.
- 1587 Preddy, W. S.: The mixing and movement of water in the estuary of the Thames, *J. Mar. biol. Ass. UK*,
 1588 33, 645–662, 1954.
- 1589 Press, W. H., Teukolosky, S. A., Vetterling, W. T., and Flannery, B.P.: Numerical Recipes in C: The Art
 1590 of Scientific Programming, 2nd Edn., Cambridge University Press, USA, 1992.
- 1591 Pritchard, D. W.: The Equations of Mass Continuity and Salt Continuity in Estuaries, *J. Marine Res.*,
 1592 15, 33–42, 1958.
- 1593 Raymond, P.A., Caraco, N.F., and Cole, J.J.: Carbon dioxide concentration and atmospheric flux in the
 1594 Hudson River. *Estuaries*, 20(2), 381-390, 1997.
- 1595 Raymond, P.A., Bauer, J.E., and Cole, J.J.: Atmospheric CO2 evasion, dissolved inorganic carbon
 1596 production, and net heterotrophy in the York River estuary. *Limnology and Oceanography*,
 1597 45(8), 1707-1717, 2000.
- 1598 Raymond, P.A., and Hopkinson, C.S.: Ecosystem Modulation of Dissolved Carbon Age in a Temperate
 1599 Marsh-Dominated Estuary. *Ecosystems*, 6(7), 694-705, 2003.
- 1600 Raymond, P.A., Hartmann, J., Lauerwald, R., Sobek, S., McDonald, C., Hoover, M., Butman, D., Striegl,
 1601 R., Mayorga, E., Humborg, C., Kortelainen, P., Dürr, H., Meybeck, M., Ciais, P., and Guth, P.:
 1602 Global carbon dioxide emissions from inland waters. *Nature*, 503(7476), 355-359, 2013.
- 1603 Regnier, P., Wollast, R., and Steefel, C.I.: Long-term fluxes of reactive species in macrotidal estuaries:
 1604 Estimates from a fully transient, multicomponent reaction-transport model. *Marine*
 1605 *Chemistry*, 58(1-2), 127-145, 1997.
- 1606 Regnier, P., Mouchet, A., Wollast, R., and Ronday, F.: A discussion of methods for estimating residual
 1607 fluxes in strong tidal estuaries, *Cont. Shelf Res.*, 18, 1543–1571, 1998.
- 1608 Regnier, P., and Steefel, C.I.: A high resolution estimate of the inorganic nitrogen flux from the
 1609 Scheldt estuary to the coastal North Sea during a nitrogen-limited algal bloom, spring 1995.
 1610 *Geochimica et Cosmochimica Acta*, 63(9), 1359-1374, 1999.
- 1611 Regnier, P., Vanderborght, J. P., Steefel, C. I., and O'Kane, J. P.: Modeling complex multi-component
 1612 reactive-transport systems: Towards a simulation environment based on the concept of a
 1613 Knowledge Base, *Appl. Math. Model.*, 26, 913–927, 2002.
- 1614 Regnier, P., Friedlingstein, P., Ciais, P., Mackenzie, F.T., Gruber, N., Janssens, I.A., Laruelle, G.G.,
 1615 Lauerwald, R., Luyssaert, S., Andersson, A.J., Arndt, S., Arnosti, C., Borges, A.V., Dale, A.W.,
 1616 Gallego-Sala, A., Godderis, Y., Goossens, N., Hartmann, J., Heinze, C., Ilyina, T., Joos, F.,
 1617 LaRowe, D.E., Leifeld, J., Meysman, F.J.R., Munhoven, G., Raymond, P.A., Spahni, R.,
 1618 Suntharalingam, P., and Thullner, M.: Anthropogenic perturbation of the carbon fluxes from
 1619 land to ocean. *Nature Geosci*, 6(8), 597-607, 2013a.
- 1620 Regnier, P., Arndt, S., Goossens, N., Volta, C., Laruelle, G.G., Lauerwald, R., and Hartmann, J.:
 1621 Modelling Estuarine Biogeochemical Dynamics: From the Local to the Global Scale. *Aquatic*
 1622 *Geochemistry*, 19(5-6), 591-626, 2013b.
- 1623 Riemann, B., Simonsen, P., and Stensgaard, L.: The carbon and chlorophyll content of phytoplankton
 1624 from various nutrient regimes. *Journal of Plankton Research*, 11 (5), 1037-1045, 1989.

Deleted: .

1626 [Rossow, W.B., and Schiffer, R.A.: Advances in understanding clouds from ISCCP. Bull. Amer.](#)
1627 [Meteorol. Soc., 80, 2261-2288, doi:10.1175/1520-0477\(1999\)080<2261:AIUCFI>2.0.CO;2,](#)
1628 [1999.](#)

1629 Sarma, V.V.S.S., Viswanadham, R., Rao, G.D., Prasad, V.R., Kumar, B.S.K., Naidu, S.A., Kumar, N.A.,
1630 Rao, D.B., Sridevi, T., Krishna, M.S., Reddy, N.P.C., Sadhuram, Y., and Murty, T.V.R.: Carbon
1631 dioxide emissions from Indian monsoonal estuaries. *Geophysical Research Letters*, 39(3),
1632 L03602, 2012.

1633 Savenije, H.H.G.: A one-dimensional model for salinity intrusion in alluvial estuaries. *Journal of*
1634 *Hydrology*, 85(1-2), 87-109, 1986.

1635 Savenije, H.H.G.: Lagrangian solution of St. Venant's equations for alluvial estuary. *Journal of*
1636 *Hydraulic Engineering*, 118(8), 1153-1163, 1992.

1637 Savenije, H. H. G. (Ed.): *Salinity and Tides in Alluvial Estuaries*, 1st Edn., Elsevier, Amsterdam, 2005.

1638 Savenije, H. H. G. (Ed.): *Salinity and Tides in Alluvial Estuaries*, 2nd Edn., available at:
1639 <http://salinityandtides.com> (last access: 8 March 2015), 2012.

1640 [Seitzinger, S. P., Harrison, J. A., Dumont, E., Beusen, A. H. W., and Bouwman, A. F.: Sources and](#)
1641 [delivery of carbon, nitrogen, and phosphorus to the coastal zone: An overview of Global](#)
1642 [Nutrient Export from Watersheds \(NEWS\) models and their application, *Global Biogeochem.*](#)
1643 [Cycles, 19, GB4S01, doi:10.1029/2005GB002606, 2005.](#)

1644 [Schwarz, G.E., Hoos, A.B., Alexander, R.B., and Smith, R.A.: The SPARROW Surface Water-Quality](#)
1645 [Model: Theory, Application and User Documentation. U.S. Geological Survey, Techniques](#)
1646 [and Methods Report, Book 6, Chapter B3, Reston, Virginia, 2006](#)

1647 [Sharp, J. H., Yoshiyama, K., Parker, Schwartz, M. C., Curless, S. E., Beaugard, A. Y., Ossolinski, J. E.,](#)
1648 [and Davis, A. R.: A Biogeochemical View of Estuarine Eutrophication: Seasonal and Spatial](#)
1649 [Trends and Correlations in the Delaware Estuary. *Estuaries and Coasts*, 32, 1023-1043.,](#)
1650 [doi:10.1007/s12237-009-9210-8, 2009.](#)

1651 [Sharp, J. H.: Estuarine oxygen dynamics: What can we learn about hypoxia from long-time records in](#)
1652 [the Delaware Estuary? *Limnol. Oceanogr.*, 55\(2\), 2010, 535-548, 2010.](#)

1653 Shih, J.-S., Alexander, R.B., Smith, R.A., Boyer, E.W., Schwarz, G.E., and Chung, S.: An initial SPARROW
1654 model of land use and in-stream controls on total organic carbon in streams of the
1655 conterminous United States, U. S. Geological Survey, Reston, Virginia, 2010.

1656 Signorini, S.R., Mannino, A., Najjar Jr, R.G., Friedrichs, M.A.M., Cai, W.J., Salisbury, J., Wang, Z.A.,
1657 Thomas, H., and Shadwick, E.: Surface ocean pCO₂ seasonality and sea-air CO₂ flux
1658 estimates for the North American east coast. *Journal of Geophysical Research C: Oceans*,
1659 118(10), 5439-5460, 2013.

1660 [Simmons, H. B.: Some effects of inland discharge on estuarine hydraulics, *Proc. Am. Soc. Civ. Eng.-*](#)
1661 [ASCE, 81, 792, 1955.](#)

1662 Soetaert, K., and Herman, P.M.J.: Nitrogen dynamics in the Westerschelde estuary (SW Netherlands)
1663 estimated by means of the ecosystem model MOSES. *Hydrobiologia*, 311(1-3), 225-246,
1664 1995.

1665 Stets, E.G., and Strieg, R.G.: Carbon export by rivers draining the conterminous united states. *Inland*
1666 *Waters*, 2(4), 177-184, 2012.

1667 Stigter, C., and Siemons, J.: Calculation of longitudinal salt distribution in estuaries as function of
1668 time, Publication Delft Hydraulics Laboratory, 52, The Netherlands, 1967.

1669 Thieu, V., Mayorga, E., Billen, G., and Garnier, J.: Subregional and downscaled global scenarios of
1670 nutrient transfer in river basins: Seine-Somme-Scheldt case study. *Global Biogeochemical*
1671 *Cycles*, 24(2) , 2010.

1672 Tian, H., Chen, G., Liu, M., Zhang, C., Sun, G., Lu, C., Xu, X., Ren, W., Pan, S., and Chappelka, A.: Model
1673 estimates of net primary productivity, evapotranspiration, and water use efficiency in the
1674 terrestrial ecosystems of the southern United States during 1895-2007. *Forest Ecology and*
1675 *Management*, 259(7), 1311-1327, 2010.

1676 Tian, H., Chen, G., Zhang, C., Liu, M., Sun, G., Chappelka, A., Ren, W., Xu, X., Lu, C., Pan, S., Chen, H.,
1677 Hui, D., McNulty, S., Lockaby, G., and Vance, E.: Century-Scale Responses of Ecosystem
1678 Carbon Storage and Flux to Multiple Environmental Changes in the Southern United States.
1679 *Ecosystems*, 15(4), 674-694, 2012.

1680 U. S. Fish and Wildlife Service. 2014. National Wetlands Inventory website. U.S. Department of the
1681 Interior, Fish and Wildlife Service, Washington, D.C. <http://www.fws.gov/wetlands/>, last
1682 accessed: February 2015.

1683 Vanderborght, J.P., Wollast, R., Loijens, M., and Regnier, P.: Application of a transport-reaction
1684 model to the estimation of biogas fluxes in the Scheldt Estuary. *Biogeochemistry*, 59(1-2),
1685 207-237, 2002.

1686 Vanderborght, J.P., Folmer, I., Aguilera, D.R., Uhrenholdt, T., and Regnier, P.: Reactive-transport
1687 modelling of a river-estuarine-coastal zone system: application to the Scheldt estuary. *Mar.*
1688 *Chem.* 106, 92-110, 2007.

1689 Van der Burgh, P.: Ontwikkeling van een methode voor het voorspellen van zoutverdelingen in
1690 estuaria, kanalen and zeeen, Rijkswaterstaat Rapport, The Netherlands, 1972.

1691 Volta, C., Arndt, S., Savenije, H.H.G., Laruelle, G.G., and Regnier, P.: C-GEM (v 1.0): a new, cost-
1692 efficient biogeochemical model for estuaries and its application to a funnel-shaped system.
1693 *Geosci. Model Dev.*, [7, 1271-1295, doi:10.5194/gmd-7-1271-2014](#), 2014.

1694 Volta, C., Laruelle, G. G., and Regnier, P.: Regional carbon and CO₂ budgets of North Sea tidal
1695 estuaries, *Estuarine, Coastal and Shelf Science*, 176, 76-90, 2016a.

1696 Volta, C., Laruelle, G. G., Arndt, S., and Regnier, P.: Linking biogeochemistry to hydro-geometrical
1697 variability in tidal estuaries: a generic modeling approach, *Hydrol. Earth Syst. Sci.*, 20, 991-
1698 1030, doi:10.5194/hess-20-991-2016, 2016b.

1699 Vörösmarty, C.J., Fekete, B., and Tucker, B.A.: River Discharge Database, Version 1.0 (RivDIS v1.0),
1700 Volumes 0 through 6. A contribution to IHP-V Theme 1. Technical Documents in Hydrology
1701 Series. UNESCO, Paris, 1996.

1702 Wang, Z.A., and Cai, W.J.: Carbon dioxide degassing and inorganic carbon export from a marsh-
1703 dominated estuary (the Duplin River): A marsh CO₂ pump. *Limnology and Oceanography*,
1704 49(2), 341-354, 2004.

Deleted: 6(4), 5645-5709,

Deleted: ¶

1705

1708 **Table 1:** Estimates of total annual riverine input from watersheds to estuaries (Tg C yr⁻¹). The ranges
 1709 are based on Stets and Striegl (2012), Global NEWS (Mayorga et al. 2010), Hartmann et al. (2009),
 1710 SPARROW (Shih et al. 2010) and DLEM (Tian et al. 2010, 2012). Modified from Najjar et al. 2012.

	DIC	DOC	POC	TOTAL
NAR	0.2-0.8	0.3-2.1	0.1-0.2	0.6-3.1
MAR	1.4-1.8	0.5-2.3	0.1-0.3	2.0-4.4
SAR	0.4-1.4	0.9-1.6	0.1-0.2	1.4-3.2
TOTAL	2.0-4.0	1.7-6.0	0.3-0.7	4.0-10.7

1711

1712

1713

1714
1715

Table 2: Published local annually averaged estimates of $\overline{FCO_2}$ in mol C m⁻² yr⁻¹ for estuaries along the East coast of the US.”

Name	Lon	Lat	$\overline{FCO_2}$		Reference
			Observed.	Modeled	
Altamaha Sound	-81.3	31.3	32.4	72.7	Jiang et al. (2008)
Bellamy	-70.9	43.2	3.6	3.9	Hunt et al. (2010)
Cocheco	-70.9	43.2	3.1	3.9	Hunt et al. (2010)
Doboy Sound	-81.3	31.4	13.9	25.7	Jiang et al. (2008)
Great Bay	-70.9	43.1	3.6	3.9	Hunt et al. (2011)
Little Bay	-70.9	43.1	2.4	3.9	Hunt et al. (2011)
Oyster Bay	-70.9	43.1	4	3.9	Hunt et al. (2011)
Parker River estuary	-70.8	42.8	1.1	3.9	Raymond and Hopkinson (2003)
Sapelo Sound	-81.3	31.6	13.5	20.6	Jiang et al. (2008)
Satilla River	-81.5	31	42.5	25.7	Cai and Wang (1998)
York River	-76.4	37.2	6.2	8.1	Raymond et al. (2000)
Hudson River	-74	40.6	13.5	15.5	Raymond et al. (1997)
Florida Bay	-80.68	24.96	1.4	n.a.	Dufore (2012)

1716

1717

1718

Table 3: State variables and processes explicitly implemented in CGEM.


Deleted: 2

State variables		
Name	Symbol	Unit
Suspended Particulate Mater	SPM	g L^{-1}
Total Organic Carbon	TOC	$\mu\text{M C}$
Nitrate	NO_3	$\mu\text{M N}$
Ammonium	NH_4	$\mu\text{M N}$
Phosphate	DIP	$\mu\text{M P}$
Dissolved Oxygen	DO	$\mu\text{M O}_2$
Phytoplankton	Phy	$\mu\text{M C}$
Dissolved Silica	dSi	$\mu\text{M Si}$
Dissolved Inorganic Carbon	DIC	$\mu\text{M C}$
Biogeochemical reactions		
Name	Symbol	Unit
Gross primary production	GPP	$\mu\text{M C s}^{-1}$
Net primary production	NPP	$\mu\text{M C s}^{-1}$
Phytoplankton mortality	M	$\mu\text{M C s}^{-1}$
Aerobic degradation	R	$\mu\text{M C s}^{-1}$
Denitrification	D	$\mu\text{M C s}^{-1}$
Nitrification	N	$\mu\text{M N s}^{-1}$
O_2 exchange with the atmosphere	FO_2	$\mu\text{M O}_2 \text{ s}^{-1}$
CO_2 exchange with the atmosphere	FCO_2	$\mu\text{M C s}^{-1}$
SPM erosion	E_{SPM}	$\text{g L}^{-1} \text{ s}^{-1}$
SPM deposition	D_{SPM}	$\text{g L}^{-1} \text{ s}^{-1}$

1719

1720

1723 **Table 4:** Yearly averaged surface area (*S*), fresh water discharge (*Q*), residence time (*Rt*), *FCO₂* and
 1724 *NEM* of all simulated estuaries.

Deleted: Table 3: Published local annually averaged estimates of *FCO₂* for estuaries along the East coast of the US. 

long degrees	lat degrees	<i>S</i> km ²	<i>Q</i> m ³ s ⁻¹	<i>Rt</i> days	$\overline{FCO_2}$ mol C m ⁻² yr ⁻¹	\overline{NEM} mol C m ⁻² yr ⁻¹	<i>FCO₂</i> 10 ⁶ mol C yr ⁻¹	<i>NEM</i> 10 ⁶ mol C yr ⁻¹
NAR								
-67.25	44.75	7	38.5	15	3.7	-37.4	27	-270
-67.25	45.25	12	73.6	15	6.0	-56.7	71	-666
-67.25	45.25	12	73.6	15	13.8	-56.6	162	-666
-67.75	44.75	3	68.5	4	6.7	-63.5	23	-221
-68.25	44.75	14	69.5	19	4.1	-56.2	58	-791
-68.75	44.75	89	309.9	23	27.4	-58.2	2431	-5163
-69.75	44.25	50	626.6	5	32.3	-74.4	1607	-3703
-70.25	43.75	3	25.8	10	2.1	-21.0	7	-71
-70.75	41.75	288	103.6	958	5.0	-4.0	1428	-1146
-70.75	42.25	63	210.7	40	16.2	-32.9	1025	-2081
-70.75	42.75	17	105.8	3	56.3	-69.0	943	-1155
MAR								
-70.75	43.25	31	29.9	11	21.6	-37.4	662	-1146
-71.25	41.75	257	28.2	808	3.9	-2.5	997	-650
-71.75	41.25	21	112.4	4	35.2	-32.6	726	-672
-72.75	40.75	20	25.4	62	30.7	-21.1	623	-430
-72.75	41.25	10	142.5	2	150.8	-36.9	1578	-386
-72.75	41.75	55	476.6	3	55.9	-45.7	3088	-2523
-73.25	40.75	19	26.8	56	31.4	-28.4	608	-550
-74.25	40.75	1192	608.2	126	15.5	-11.8	18432	-14047
-75.25	38.25	399	80.5	172	13.9	-5.0	5558	-2016
-75.25	38.75	354	31.8	357	7.5	-3.0	2659	-1076
-75.25	39.75	1716	499.0	221	10.0	-7.8	17072	-13439
-75.75	39.25	224	18.3	434	7.5	-2.9	1685	-640
-76.25	39.25	3427	717.1	352	8.1	-5.1	27646	-17352
-76.75	37.25	586	272.3	74	15.0	-10.4	8810	-6084
-76.75	37.75	154	36.3	163	10.7	-6.6	1654	-1023
-76.75	39.25	59	71.2	29	48.6	-34.6	2862	-2038
-77.25	38.25	206	30.2	268	6.1	-3.3	1265	-676
-77.25	38.75	568	259.2	118	16.7	-10.8	9488	-6134
SAR								
-78.25	34.25	48	167.4	7	122.5	-62.4	5916	-3015
-79.25	33.25	47	56.3	42	43.4	-36.5	2056	-1728
-79.25	33.75	45	291.4	8	85.1	-78.7	3843	-3551
-79.75	33.25	25	33.8	15	37.9	-32.8	956	-828
-80.25	32.75	25	31.0	50	48.8	-42.5	1214	-1057
-80.25	33.25	92	75.5	61	62.7	-61.2	5769	-5625
-80.75	32.25	71	21.1	182	12.9	-7.0	918	-501
-80.75	32.75	164	63.1	95	20.6	-11.5	3372	-1879
-81.25	31.75	92	71.7	45	25.7	-20.9	2361	-1926
-81.25	32.25	130	379.8	11	51.7	-39.2	6732	-5097
-81.75	30.75	34	18.7	61	17.5	-14.7	602	-505
-81.75	31.25	130	17.7	294	5.5	-4.0	713	-523
-81.75	31.75	56	350.5	4	72.7	-67.4	4068	-3770

1725

1730 **Table 5:** Seasonal contribution to FCO_2 and NEM in each the sub-region. The seasons displaying the
 1731 highest percentages are indicated in bold. [Winter is defined as January, February and March, Spring](#)
 1732 [as April, May and June and so on...](#)

Region	NEM mol C y^{-1}	winter %	spring %	summer %	fall %	FCO_2 mol C y^{-1}	winter %	spring %	summer %	fall %
NAR	$-16.3 \cdot 10^9$	14.7	21.2	37.0	27.2	$7.2 \cdot 10^9$	26.3	18.9	26.5	28.3
MAR	$-72.2 \cdot 10^9$	21.9	25.9	28.8	23.4	$108.3 \cdot 10^9$	29.8	23.3	20.7	26.2
SAR	$-30.5 \cdot 10^9$	24.6	20.9	30.3	24.2	$39.2 \cdot 10^9$	26	23.4	27	23.6

1733

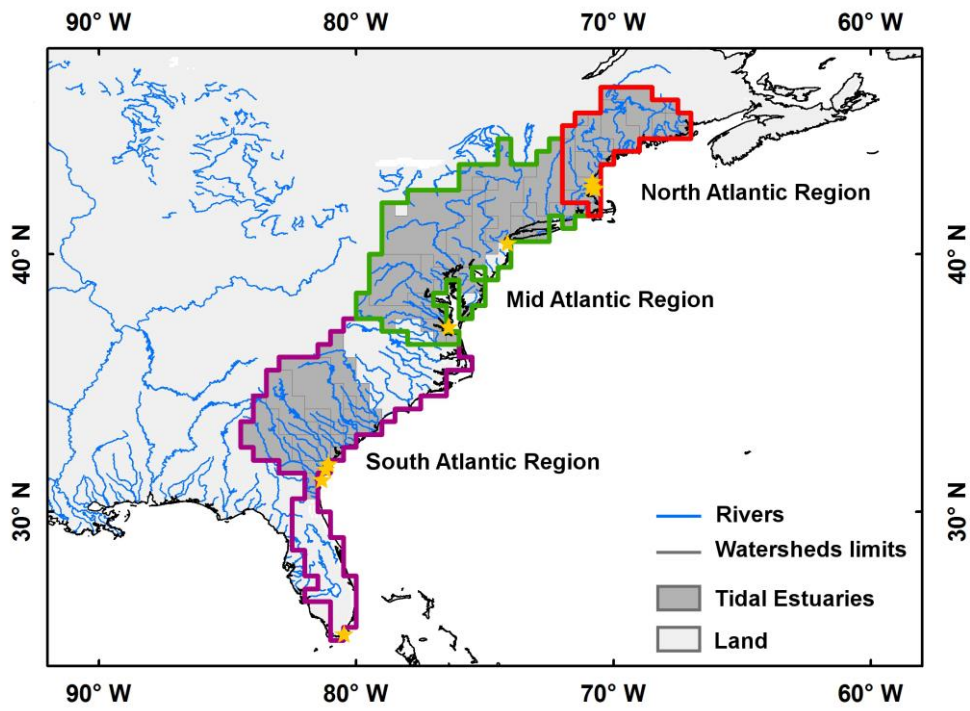
1734

1735 **Table 6:** Regressions and associated coefficient of determination between the depth normalized
 1736 residence time (S/Q) and $\overline{-NEM}/f(T)$, $\overline{FCO_2}/f(T)$ and $CFilt$.

Region	$\overline{-NEM}/f(T)$	$\overline{FCO_2}/f(T)$	$CFilt$
NAR	$y = 27.84 x^{-0.17}$ $r^2 = 0.11$	$y = 6.07 x^{0.00}$ $r^2 = 0.00$	$y = 15.08 \log_{10}(x) + 4.86$ $r^2 = 0.40$
MAR	$y = 26.03 x^{-0.63}$ $r^2 = 0.86$	$y = 34.36 x^{-0.58}$ $r^2 = 0.68$	$y = 40.46 \log_{10}(x) + 9.60$ $r^2 = 0.70$
SAR	$y = 28.36 x^{-0.71}$ $r^2 = 0.76$	$y = 32.82 x^{-0.66}$ $r^2 = 0.80$	$y = 23.19 \log_{10}(x) + 43.71$ $r^2 = 0.46$
MAR + SAR	$y = 25.85 x^{-0.64}$ $r^2 = 0.82$	$y = 31.64 x^{-0.58}$ $r^2 = 0.70$	$y = 33.30 \log_{10}(x) + 24.88$ $r^2 = 0.57$
NAR + MAR + SAR	$y = 28.98 x^{-0.66}$ $r^2 = 0.82$	$y = 12.98 x^{-0.33}$ $r^2 = 0.30$	$y = 40.64 \log_{10}(x) + 11.84$ $r^2 = 0.70$

1737

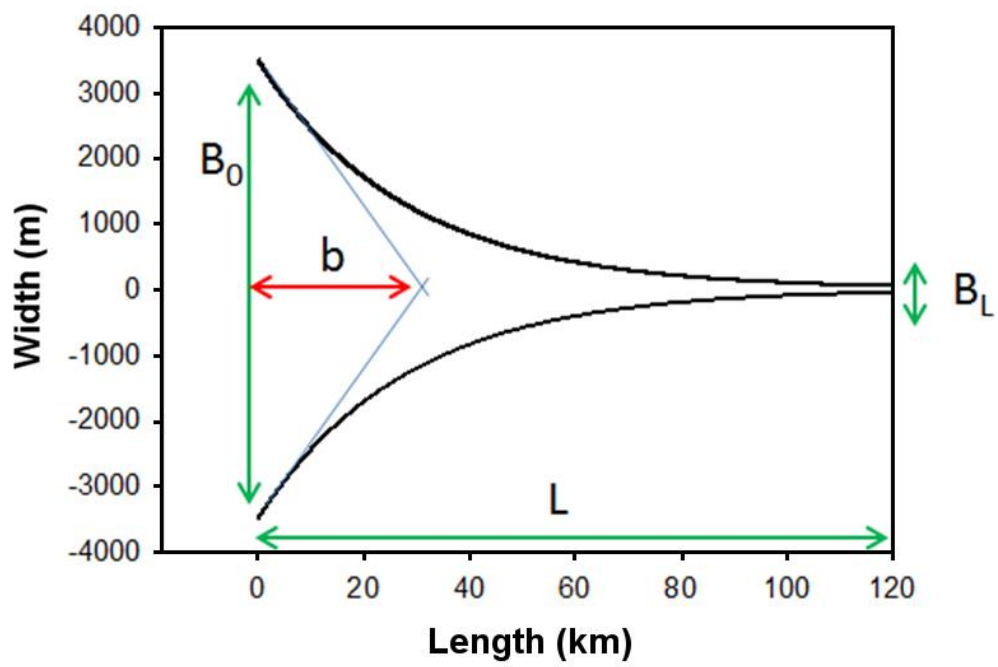
1738



1739

1740 **Figure 1:** Limits of the 0.5 degrees resolution watersheds corresponding to tidal estuaries of the East
 1741 coast of the US. 3 sub-regions are delimited with colors and orange stars represent the location of
 1742 previous studies.

1743

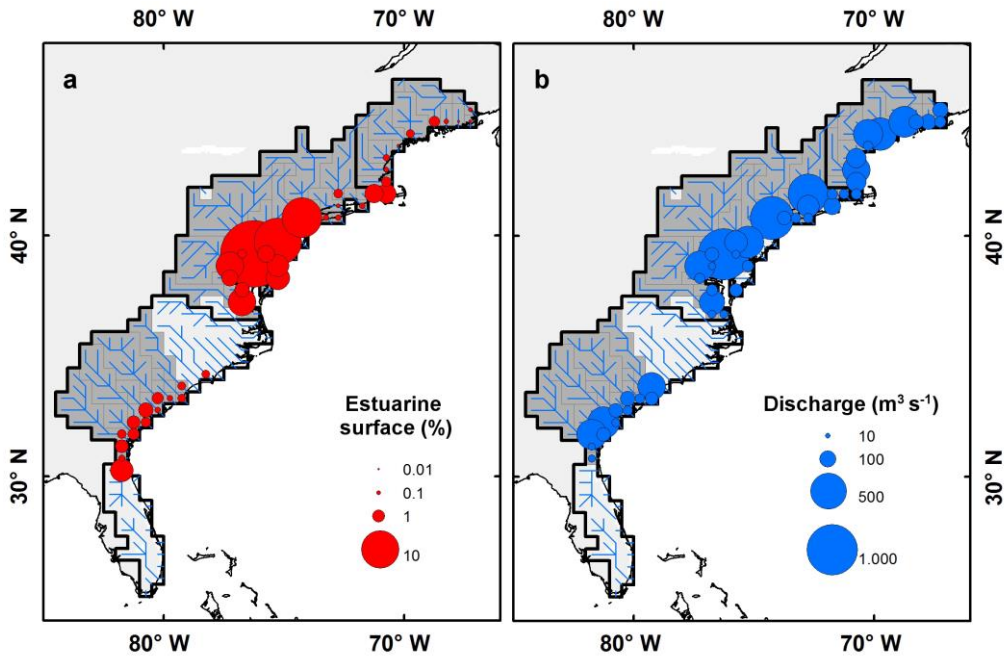


1744

1745 **Figure 2:** Idealized estuarine geometry and main parameters. Parameters indicated by green arrows
 1746 are measured, b is calculated. See section 2.3.1 for further details.

1747

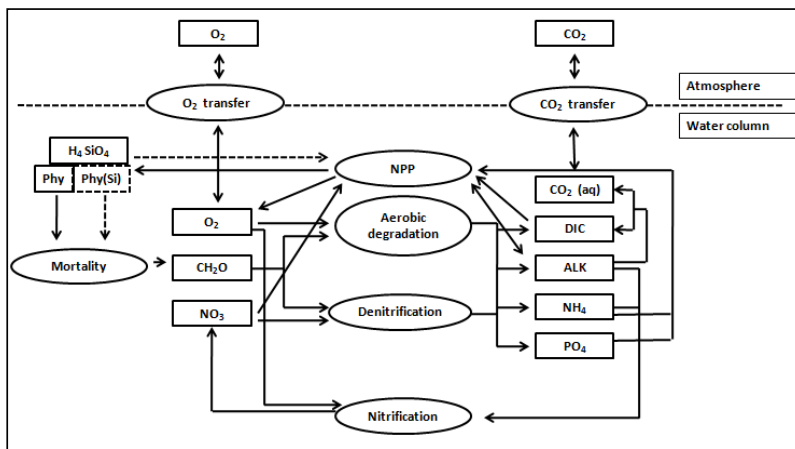
1748



1749

1750 **Figure 3:** Estuarine surface area (a) and mean annual freshwater discharge (b) for each tidal estuary
1751 of the East coast of the US. Estuarine surface area are expressed as percentage of the entire surface
1752 area of the region (19830 km²)

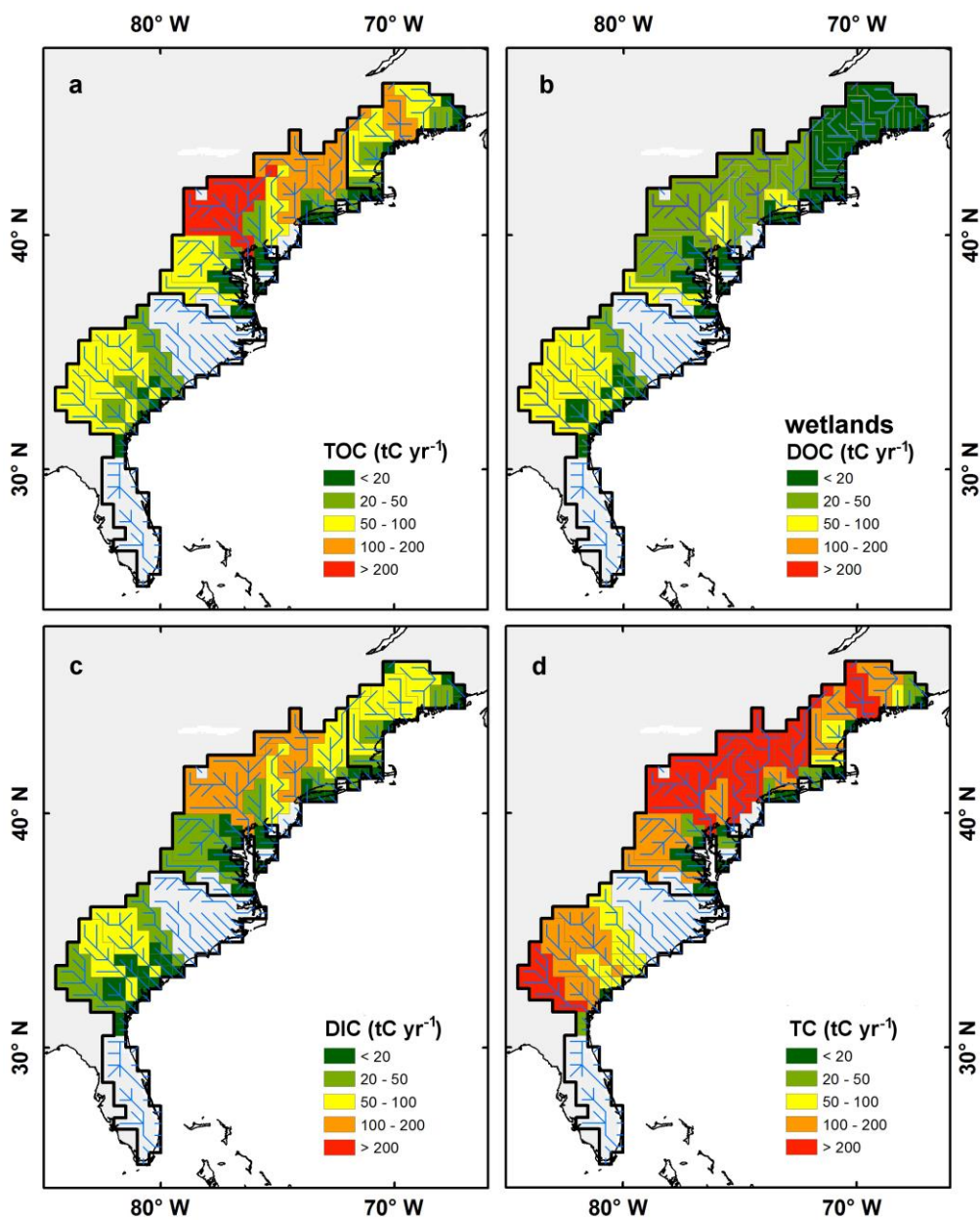
1753



1754

1755 **Figure 4:** Conceptual scheme of the biogeochemical module of C-GEM used in this study. State-
 1756 variables and processes are represented by boxes and oval shapes, respectively. Modified from Volta
 1757 et al., 2014.

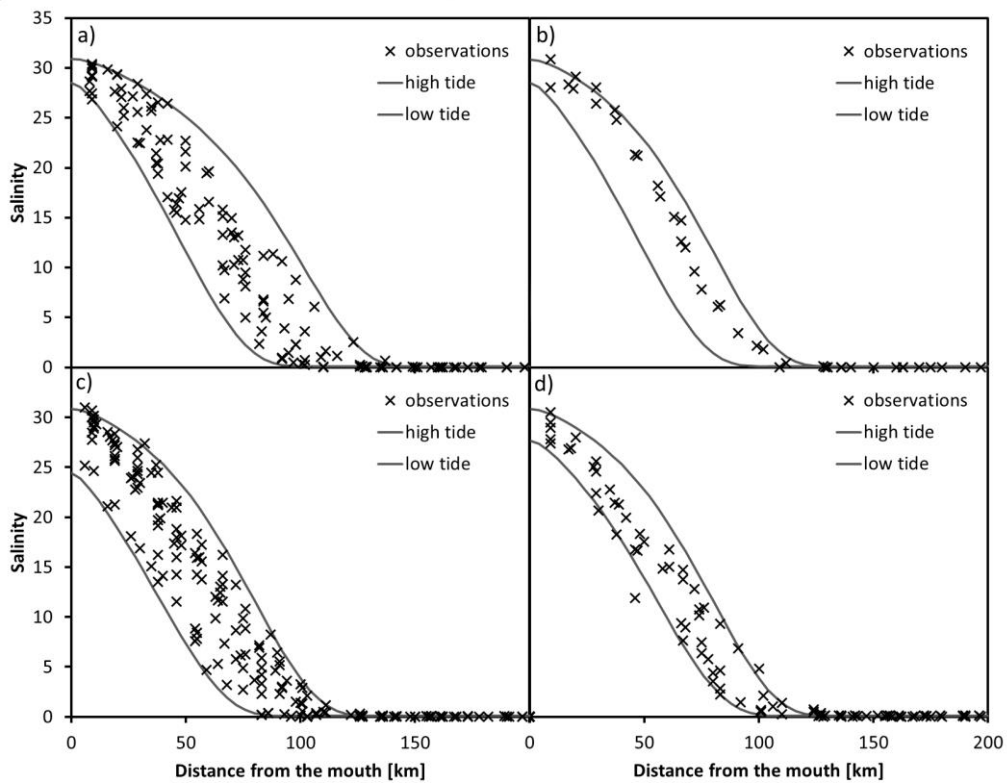
1758



1759

1760 **Figure 5:** Annual river carbon loads of TOC (a), annual DOC fluxes from wetlands (b), annual river
 1761 carbon loads of DIC (c) and annual TC fluxes (d). All fluxes are indicated per watershed.

1762



Formatted: Font color: Blue

1763

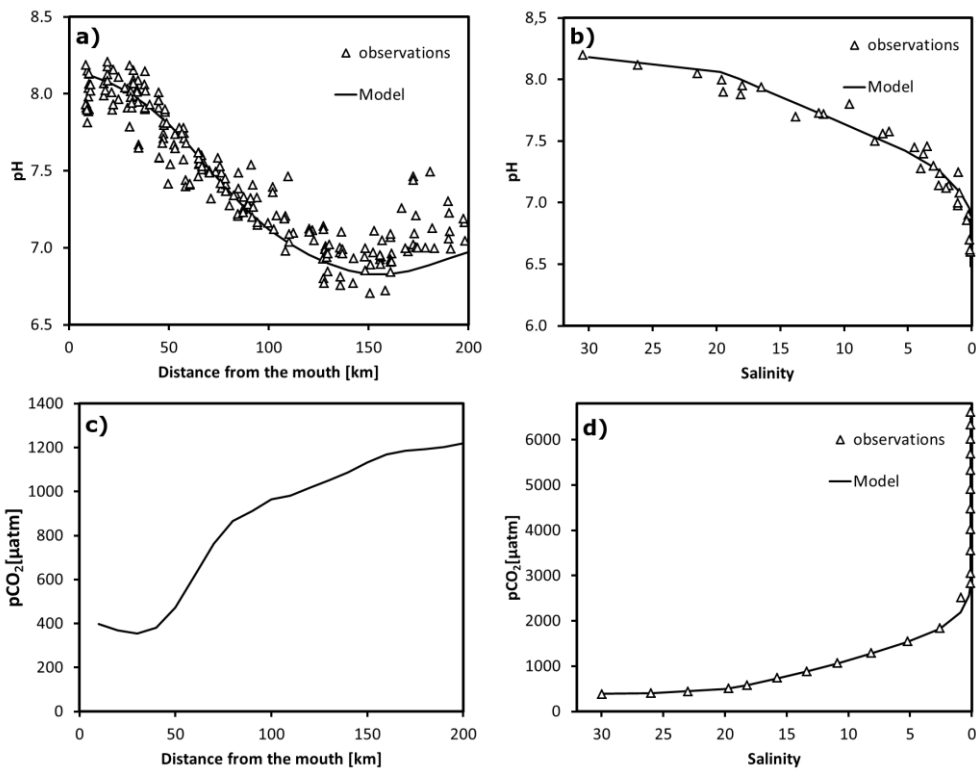
1764 **Figure 6. Modeled (lines) and measured (crosses) salinities in the Delaware Bay estuary for January**

Formatted: Font: Bold, Not Italic

1765 **(a), February (b), May (c), June (d). The two lines correspond to high and low tides.**

Formatted: Font: Not Italic

1766



Formatted: Font: Bold, Font color: Blue

1767

1768 Figure 7. Longitudinal profiles of pH (top) and pCO₂ (bottom) for the Delaware Bay (left) and
 1769 Altamaha river estuary (right).

1770

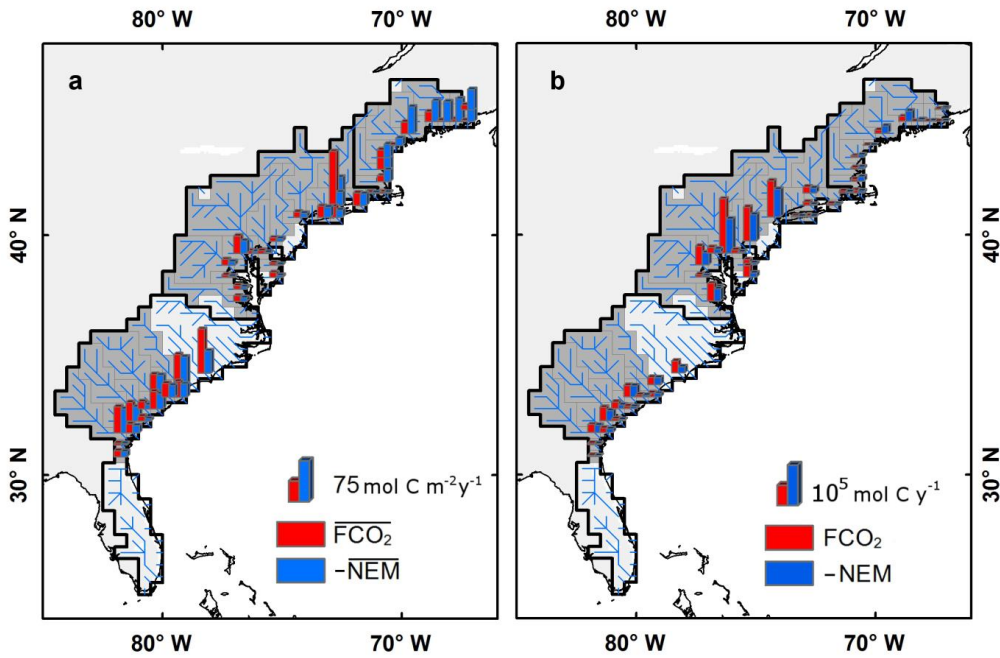
Formatted: Font: Not Italic, No underline

Formatted: Font: Not Italic, No underline

Formatted: Font: Not Bold, Not Italic, No underline

Formatted: Font: Not Italic, No underline

1771



1772

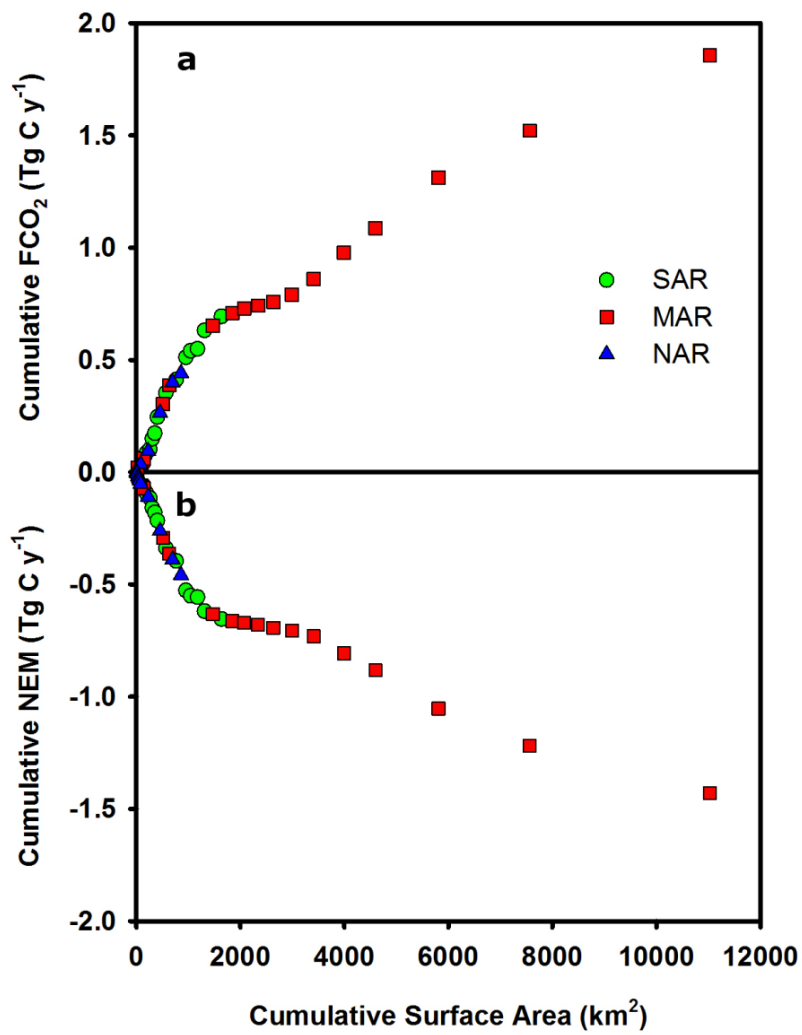
1773 | **Figure 8:** Spatial distribution of spatially averaged value (a) and integrated value (b) of mean annual
1774 $\overline{FCO_2}$ (red) and $-\overline{NEM}$ (blue) along the East coast of the US. On panel a, the notation with overbars
1775 ($\overline{FCO_2}$ and $-\overline{NEM}$) represents rates per unit surface. For the sake of the comparison with $\overline{FCO_2}$, **Fig.**
1776 **8** displays $-\overline{NEM}$ because the model predicts that all estuaries in this region are net heterotrophic.

Deleted: 6

Deleted: figure

Deleted: 6

1777

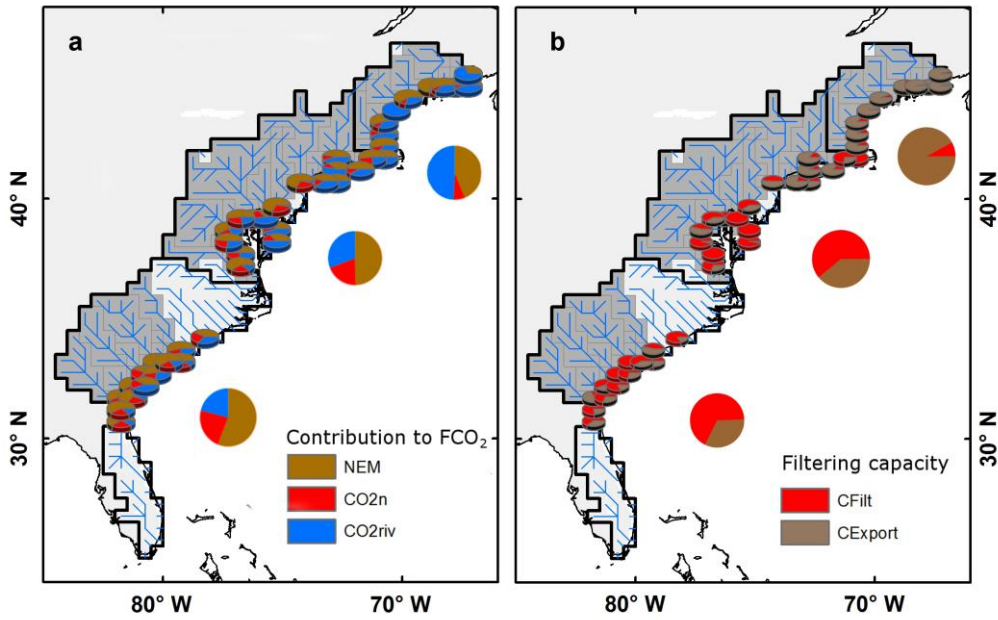


1781

1782 | **Figure 9:** The Cumulative FCO_2 (a) and NEM (b) as functions of the cumulative estuarine surface area.
 1783 Systems are sorted by increasing surface area.

Deleted: 7

1784



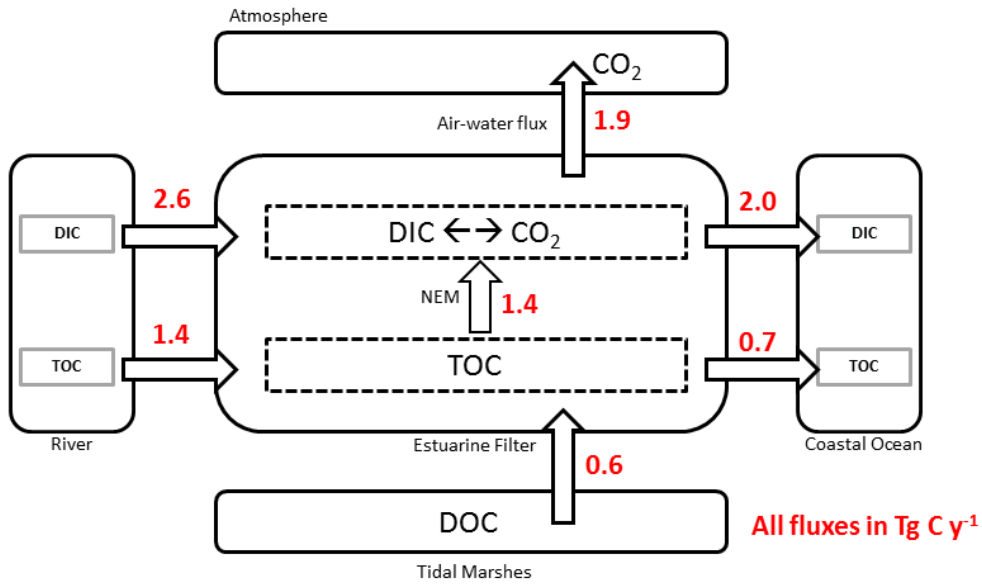
1786

1787 | **Figure 10:** Contribution of *NEM*, nitrification and riverine waters super-saturated waters to the mean
 1788 annual FCO_2 (a). Spatial distribution of mean annual carbon filtration capacities ($CFilt$) and export
 1789 ($CExport$) along the East coast of the US (b).

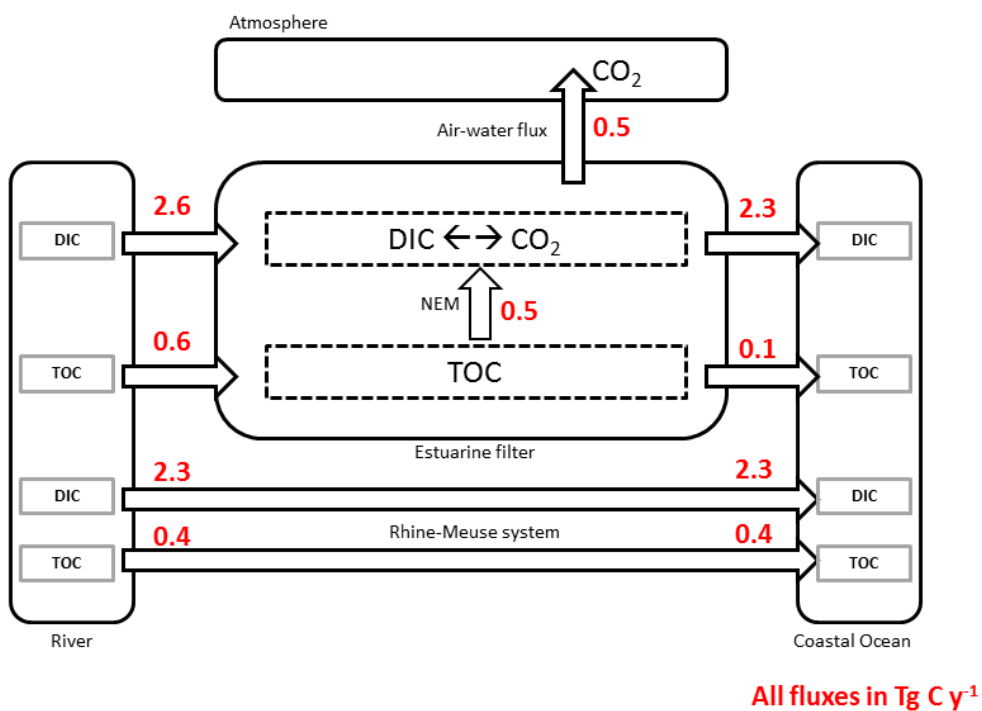
Deleted: 8

1790

a) Eastern US coast



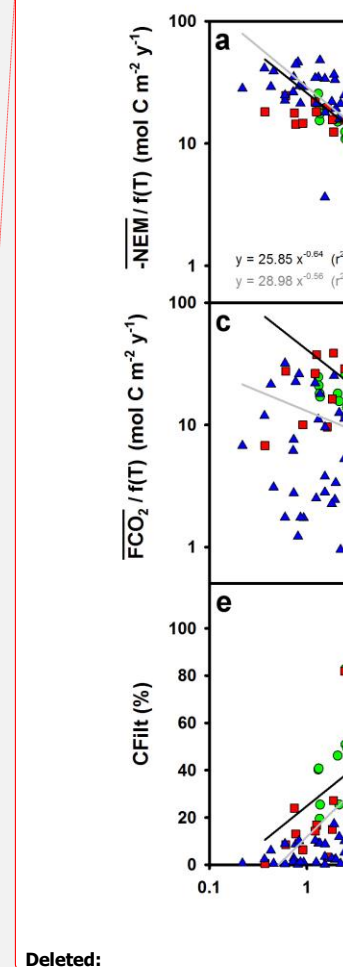
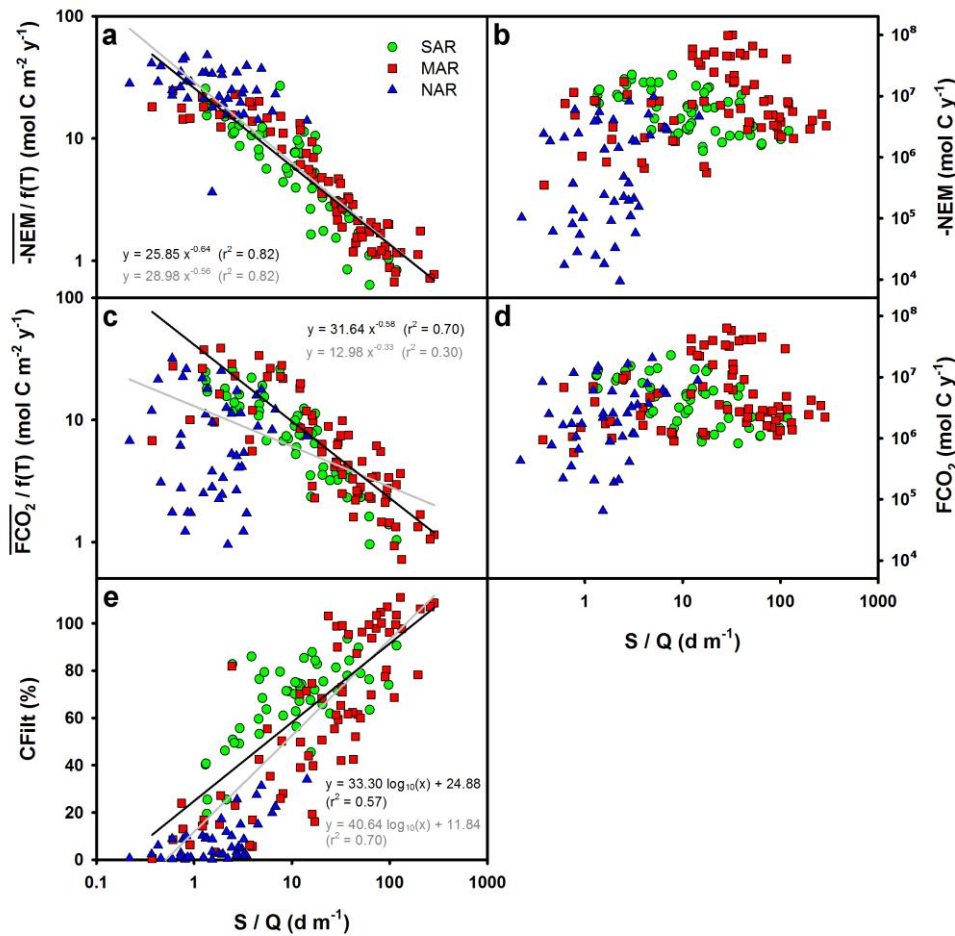
b) North Sea coast



1792

1793 | **Figure 11:** Annual carbon budget of the estuaries of the East coast of the US (a) and of the coast of
 1794 the North Sea (b, modified from Volta et al., 2016a).

Deleted: 9



1796

1797

1798

1799

1800

1801

1802

1803

Figure 12: System scale integrated biogeochemical indicators expressed as functions of the depth normalized residence time expressed as the ratio of the estuarine surface S and the river discharge Q for all seasons. Panels b, d and e represent NEM, $-FCO_2$ and CFilt, respectively. Panels a and c represent NEM, $-FCO_2$ normalized by a temperature Q_{10} function. Black lines are the best fitted linear regressions obtained using all the point. Grey lines are best fit using only the estuaries from the MAR and SAR regions.

- Deleted:** 10
- Deleted:** $-NEM/f(T)$ (a), $-NEM$ (b), $FCO_2/f(T)$ (c), FCO_2 (d) and CFilt (e)
- Formatted:** Font: Not Bold, Not Italic, No underline
- Formatted:** Font: Not Bold, Not Italic, No underline
- Formatted:** Font: Not Bold, Not Italic, No underline
- Formatted:** Font: Not Bold, Not Italic, No underline
- Formatted:** Font: Not Bold, Not Italic, No underline
- Formatted:** Font: Not Bold, Not Italic, No underline
- Deleted:** The grey and black lines are the best fitted regressions obtained using all the point or only the estuaries from the MAR and SAR regions, respectively.